Electron-positron pairs in physics, astrophysics and cosmology

Contents

1. Topics

- The three fundamental contributions to the electron-positron pair creation and annihilation and the concept of critical electric field
- Nonlinear electrodynamics and rate of pair creation
- Pair production and annihilation in QED
- Phenomenology of electron-positron pair creation and annihilation
- Plasma oscillations and radiation in uniform or nonuniform electric fields, and thermalization of the mildly relativistic pair plasma
- The energy extraction from a black hole by pair productions, and Einstein-Euler-Heisenberg theory and charged black holes
- Dyadophere of electron-positron pairs and photons formation in gravitational collapses
- Polarization of strong electromagnetic fields and its applications in polarizations of laser fields, GRBs and CMB photons, as well as neutrinos
- Pair production and interactions of fields and matter in the cosmology within the framework of quantum Einstein-Cartan-Maxwell theory
- Semiclassical approach to pair production rate for strong time-dependent electrical fields with more than one component
- Pair production, ultra-high energy particles, gravitational and electromagnetic energies in gravitational collapse or accretion processes
- Pulsating or static strong electromagnetic fields in gravitational collapse cores and heavy atoms
- The Breit-Wheeler cutoff in high-energy γ-rays and cosmic absorption (opacity) of ultra high energy particles

2. Participants

2.1. ICRANet participants

- C. L. Bianco (ICRANet, University of Rome, Italy)
- C. Cherubini (ICRANet, Univ. Campus Biomedico, Rome, Italy)
- H. Kleinert (ICRANet, Free University of Berlin , Germany)
- J. Rueda (ICRANet, University of Rome, Italy)
- R. Ruffini (ICRANet, University of Rome, Italy)
- G. Vereshchagin (ICRANet, University of Rome, Italy)
- S.-S. Xue (ICRANet, Sapienza University of Rome, Italy)
- Yu Wang (ICRANet, Sapienza Univ., Italy)
- Rahim Moradi (ICRANet, Sapienza Univ., Italy)
- Li Liang (ICRANet, Sapienza Univ., Italy)
- Soroush Shakeri (Isfahan ICRANet, Isfahan University of Technology, Iran)

2.2. Past collaborators

- D. Bini (ICRANet, CNR, Rome, Italy)
- A. Benedetti (Max Planck Institute, Heidelberg, Germany)
- T. Damour (ICRANet, IHES, Bures sur Yvette, France)
- F. Fraschetti (CEA Saclay, France)

- R. Klippert (ICRANet, Brazile)
- G. Preparata* (INFN, University of Milan, Italy)
- V. Popov (ITEP, Moscow, Russia)
- G. t'Hooft (Institute for Theoretical Physics Universiteit Utrecht)
- M. Rotondo (University of Rome, Italy)
- J. Rafelski (University of Arizona, USA)
- J. Wilson* (Livemore National Lab., University of California, USA)
- J. Salmonson (Livemore National Lab., University of California, USA)
- L. Stella (Rome Astronomical Observatory, Italy)
- L. Vitagliano (University of Salerno, Italy)

2.3. On going collaborations

- P. Chen (Physics Department, Taiwan University, Taiwan, China)
- C.H. Keitel (Max Planck Inst, Germany)
- A. Di Piazza (Max Planck Inst, Germany)
- Yuanbin Wu (Max Planck Institute, Heidelberg, Germany)
- S. P. Kim (University of Sogang, South Korea)
- H. W. Lee (University of Pusan, South Korea)
- W.-B. Han (Shanghai Astronomical Observatory, China)
- G. Mathews (Center for Astrophysics, University of Notre Dame, USA)
- N. Mavromatos (King's college London, England)
- R. Mohammadi (Research Institute of Advance Study, Iran)

- E. Bavarsad (Department of Physics, University of Kashan, Kashan, Iran)
- M. Abdi (Isfahan University of Technology, Iran)
- M. Haghighat (Shiraz University, Shiraz, Iran)
- Carlos Argulles (University of Argentina, Argentina)
- Xin Zhang (Northeastern University, Shenyang, China)
- Daniele Gregoris (Jiangsu University of Science and Technology, China)
- Fazlollah Hajkarim (University of Padova, INFN, Italy)
- Orlando Panella (University of Perugia, INFN, Italy)
- Hao Sun (Institute of Theoretical Physics, School of Physics, Dalian University of Technology, China)
- Francesco Romeo (Vanderbilt University, USA)
- A. Gurrola (Vanderbilt University, USA)

2.4. Young researcher, Ph.D. and M.S. Students

- Stefano Campion (ICRANet, Sapienza Univ., Italy)
- Clement Stahl (Pontificia Universidad Católica de Valparaíso, Valparaíso (PUCV), Chile)
- XiaoFeng Yang (Xing Jian Astronomy Observatory, CAS, China)
- David Melon Fukson (Sapienza, Italy)
- Seddigheh Tizchang (IPM, Isfahan University of Technology, Iran)
- Somayye Mahmoudi (Shiraz University, Shiraz, Iran)
- Yu Ling Chang (Shanghai Jiaotong Univ., China)
- Takahiro Hayashinaka, (Toyko University, Japan)

- Cheng-Jun Xia (ITP, CAS, and Zhejiang Univ., China)
- Li-Yang Gao (Northeastern University, Shenyang, China)
- Ze-Wei Zhao (Northeastern University, Shenyang, China)
- Sehar Ajmal (University of Perugia, INFN, Italy)
- Roberto Leonardi (University of Perugia, INFN, Italy)
- Matteo Presilla (University of Perugia, INFN, Italy)
- Jethro t Gaglione (Vanderbilt University, USA)
- Sareh Eslamzadeh Askestani (University of Mazandaran, Iran)
- YunLong Zheng (University of USTC, Hehui, China)

* passed away

3. Brief description

3.1. Abstract

Due to the interaction of physics and astrophysics we are witnessing in these years a splendid synthesis of theoretical, experimental and observational results originating from three fundamental physical processes. They were originally proposed by Dirac, by Breit and Wheeler and by Sauter, Heisenberg, Euler and Schwinger. For almost seventy years they have all three been followed by a continued effort of experimental verification on Earth-based experiments. The Dirac process, $e^+e^- \rightarrow 2\gamma$, has been by far the most successful. It has obtained extremely accurate experimental verification and has led as well to an enormous number of new physics in possibly one of the most fruitful experimental avenues by introduction of storage rings in Frascati and followed by the largest accelerators worldwide: DESY, SLAC etc. The Breit–Wheeler process, $2\gamma \rightarrow e^+e^-$, although conceptually simple, being the inverse process of the Dirac one, has been by far one of the most difficult to be verified experimentally. Only recently, through the technology based on free electron X-ray laser and its numerous applications in Earth-based experiments, some first indications of its possible verification have been reached. The vacuum polarization process in strong electromagnetic field, pioneered by Sauter, Heisenberg, Euler and Schwinger, introduced the concept of critical electric field $E_c = m_e^2c^3/(e\hbar)$. It has been searched without success for more than forty years by heavy-ion collisions in many of the leading particle accelerators worldwide.

The novel situation today is that these same processes can be studied on a much more grandiose scale during the gravitational collapse leading to the formation of a black hole being observed in Gamma Ray Bursts (GRBs). This report is dedicated to the scientific race. The theoretical and experimental work developed in Earth-based laboratories is confronted with the theoretical interpretation of space-based observations of phenomena originating on cosmological scales. What has become clear in the last ten years is that all the

three above mentioned processes, duly extended in the general relativistic framework, are necessary for the understanding of the physics of the gravitational collapse to a black hole. Vice versa, the natural arena where these processes can be observed in mutual interaction and on an unprecedented scale, is indeed the realm of relativistic astrophysics.

We systematically analyze the conceptual developments which have followed the basic work of Dirac and Breit–Wheeler. We also recall how the seminal work of Born and Infeld inspired the work by Sauter, Heisenberg and Euler on effective Lagrangian leading to the estimate of the rate for the process of electron–positron production in a constant electric field. In addition of reviewing the intuitive semi-classical treatment of quantum mechanical tunneling for describing the process of electron–positron production, we recall the calculations in *Quantum Electro-Dynamics* of the Schwinger rate and effective Lagrangian for constant electromagnetic fields. We also review the electron–positron production in both time-alternating electromagnetic fields, studied by Brezin, Itzykson, Popov, Nikishov and Narozhny, and the corresponding processes relevant for pair production at the focus of coherent laser beams as well as electron beam–laser collision. We finally report some current developments based on the general JWKB approach which allows to compute the Schwinger rate in spatially varying and time varying electromagnetic fields.

We also recall the pioneering work of Landau and Lifshitz, and Racah on the collision of charged particles as well as experimental success of AdA and ADONE in the production of electron–positron pairs.

We then turn to the possible experimental verification of these phenomena. We review: (A) the experimental verification of the $e^+e^- \to 2\gamma$ process studied by Dirac. We also briefly recall the very successful experiments of e^+e^- annihilation to hadronic channels, in addition to the Dirac electromagnetic channel; (B) ongoing Earth based experiments to detect electron–positron production in strong fields by focusing coherent laser beams and by electron beam–laser collisions; and (C) the multiyear attempts to detect electron–positron production in Coulomb fields for a large atomic number $Z > 137$ in heavy ion collisions. These attempts follow the classical theoretical work of Popov and Zeldovich, and Greiner and their schools.

We then turn to astrophysics. We first review the basic work on the energetics and electrodynamical properties of an electromagnetic black hole and the application of the Schwinger formula around Kerr–Newman black holes as pioneered by Damour and Ruffini. We only focus on black hole masses

larger than the critical mass of neutron stars, for convenience assumed to coincide with the Rhoades and Ruffini upper limit of 3.2 $M_{\odot}$. In this case the electron Compton wavelength is much smaller than the spacetime curvature and all previous results invariantly expressed can be applied following well established rules of the equivalence principle. We derive the corresponding rate of electron–positron pair production and introduce the concept of dyadosphere. We review recent progress in describing the evolution of optically thick electron–positron plasma in presence of supercritical electric field, which is relevant both in astrophysics as well as ongoing laser beam experiments. In particular we review recent progress based on the Vlasov-Boltzmann-Maxwell equations to study the feedback of the created electron–positron pairs on the original constant electric field. We evidence the existence of plasma oscillations and its interaction with photons leading to energy and number equipartition of photons, electrons and positrons. We finally review the recent progress obtained by using the Boltzmann equations to study the evolution of an electron–positron-photon plasma towards thermal equilibrium and determination of its characteristic timescales. The crucial difference introduced by the correct evaluation of the role of two and three body collisions, direct and inverse, is especially evidenced. We then present some general conclusions.

The results reviewed in this report are going to be submitted to decisive tests in the forthcoming years both in physics and astrophysics. To mention only a few of the fundamental steps in testing in physics we recall the starting of experimental facilities at the National Ignition Facility at the Lawrence Livermore National Laboratory as well as corresponding French Laser the Mega Joule project. In astrophysics these results will be tested in galactic and extragalactic black holes observed in binary X-ray sources, active galactic nuclei, microquasars and in the process of gravitational collapse to a neutron star and also of two neutron stars to a black hole giving origin to GRBs. The astrophysical description of the stellar precursors and the initial physical conditions leading to a gravitational collapse process will be the subject of a forthcoming report. As of today no theoretical description has yet been found to explain either the emission of the remnant for supernova or the formation of a charged black hole for GRBs. Important current progress toward the understanding of such phenomena as well as of the electrodynamical structure of neutron stars, the supernova explosion and the theories of GRBs will be discussed in the above mentioned forthcoming report. What is important to recall at this stage is only that both the supernovae and GRBs processes

are among the most energetic and transient phenomena ever observed in the Universe: a supernova can reach energy of $\sim 10^{54}$ ergs on a time scale of a few months and GRBs can have emission of up to $\sim 10^{54}$ ergs in a time scale as short as of a few seconds. The central role of neutron stars in the description of supernovae, as well as of black holes and the electron–positron plasma, in the description of GRBs, pioneered by one of us (RR) in 1975, are widely recognized. Only the theoretical basis to address these topics are discussed in the present report.

3.2. The three fundamental contributions to the electron-positron pair creation and annihilation and the concept of critical electric field

The annihilation of electron–positron pair into two photons, and its inverse process – the production of electron–positron pair by the collision of two photons were first studied in the framework of quantum mechanics by P.A.M. Dirac and by G. Breit and J.A. Wheeler in the 1930s (Dirac (1930); Breit and Wheeler (1934)).

A third fundamental process was pioneered by the work of Fritz Sauter and Oscar Klein, pointing to the possibility of creating an electron–positron pair from the vacuum in a constant electromagnetic field. This became known as the 'Klein paradox' and such a process named as *vacuum polarization*. It would occur for an electric field stronger than the critical value

$$E_c \equiv \frac{m_e^2 c^3}{e\hbar} \simeq 1.3 \cdot 10^{16}\,\mathrm{V/cm}. \tag{3.2.1}$$

where m_e, e, c and $\hbar$ are respectively the electron mass and charge, the speed of light and the Planck's constant.

The experimental difficulties to verify the existence of such three processes became immediately clear. While the process studied by Dirac was almost immediately observed Klemperer (1934) and the electron–positron collisions became possibly the best tested and prolific phenomenon ever observed in physics. The Breit–Wheeler process, on the contrary, is still today waiting a direct observational verification. Similarly the vacuum polarization process

defied dedicated attempts for almost fifty years in experiments in nuclear physics laboratories and accelerators all over the world, see Section 7 in the following article.

From the theoretical point of view the conceptual changes implied by these processes became immediately clear. They were by vastness and depth only comparable to the modifications of the linear gravitational theory of Newton introduced by the nonlinear general relativistic equations of Einstein. In the work of Euler, Oppenheimer and Debye, Born and his school it became clear that the existence of the Breit–Wheeler process was conceptually modifying the linearity of the Maxwell theory. In fact the creation of the electron–positron pair out of the two photons modifies the concept of superposition of the linear electromagnetic Maxwell equations and impose the necessity to transit to a nonlinear theory of electrodynamics. In a certain sense the Breit–Wheeler process was having for electrodynamics the same fundamental role of Gedankenexperiment that the equivalence principle had for gravitation. Two different attempts to study these nonlinearities in the electrodynamics were made: one by Born and Infeld Born (1933, 1934); Born and Infeld (1934) and one by Euler and Heisenberg Heisenberg and Euler (1936). These works prepared the even greater revolution of Quantum Electro-Dynamics by Tomonaga Tomonaga (1946), Feynman Feynman (1948, 1949b,a), Schwinger Schwinger (1948, 1949a,b) and Dyson Dyson (1949a,b).

In Section 3 in the following article we review the fundamental contributions to the electron–positron pair creation and annihilation and to the concept of the critical electric field. In Section 3.1 of the following article we review the Dirac derivation Dirac (1930) of the electron–positron annihilation process obtained within the perturbation theory in the framework of relativistic quantum mechanics and his derivation of the classical formula for the cross-section $\sigma^{\rm lab}_{e^+e^-}$ in the rest frame of the electron

$$\sigma^{\rm lab}_{e^+e^-} = \pi \left(\frac{\alpha\hbar}{m_e\, c}\right)^2 (\hat{\gamma}-1)^{-1} \left\{ \frac{\hat{\gamma}^2+4\hat{\gamma}+1}{\hat{\gamma}^2-1} \ln[\hat{\gamma}+(\hat{\gamma}^2-1)^{1/2}] - \frac{\hat{\gamma}+3}{(\hat{\gamma}^2-1)^{1/2}} \right\},$$

where $\hat{\gamma} \equiv \mathcal{E}_+/m_e\, c^2 \geq 1$ is the energy of the positron and $\alpha = e^2/(\hbar c)$ is as usual the fine structure constant, and we recall the corresponding formula for the center of mass reference frame. In article Section 3.2 we recall the main steps in the classical Breit–Wheeler work Breit and Wheeler (1934) on the production of a real electron–positron pair in the collision of two photons,

following the same method used by Dirac and leading to the evaluation of the total cross-section $\sigma_{\gamma\gamma}$ in the center of mass of the system

$$\sigma_{\gamma\gamma} = \frac{\pi}{2}\left(\frac{\alpha\hbar}{m_e c}\right)^2 (1-\hat{\beta}^2)\Big[2\hat{\beta}(\hat{\beta}^2-2) + (3-\hat{\beta}^4)\ln\big(\frac{1+\hat{\beta}}{1-\hat{\beta}}\big)\Big], \quad \text{with} \quad \hat{\beta} = \frac{c|\mathbf{p}|}{\mathcal{E}},$$

where $\hat{\beta}$ is the reduced velocity of the electron or the positron. In Section 3.3 of the article we recall the basic higher order processes, compared to the Dirac and Breit–Wheeler ones, leading to pair creation. In Section 3.4 in the following review we recall the famous Klein paradox Klein (1929); Sauter (1931) and the possible tunneling between the positive and negative energy states leading to the concept of level crossing and pair creation by analogy to the Gamow tunneling Gamow (1931) in the nuclear potential barrier. We then turn to the celebrated Sauter work Sauter (1931) showing the possibility of creating a pair in a uniform electric field E. We recover in Section 3.5.1 of the review a JWKB approximation in order to reproduce and improve on the Sauter result by obtaining the classical Sauter exponential term as well as the prefactor

$$\frac{\Gamma_{\text{JWKB}}}{V} \simeq D_s \frac{\alpha E^2}{2\pi^2\hbar} e^{-\pi E_c/E},$$

where $D_s = 2$ for a spin-1/2 particle and $D_s = 1$ for spin-0, V is the volume. Finally, in review Section 3.5.2 the case of a simultaneous presence of an electric and a magnetic field B is presented leading to the estimate of pair production rate

$$\frac{\Gamma_{\text{JWKB}}}{V} \simeq \frac{\alpha\beta\varepsilon}{\pi\hbar}\coth\left(\frac{\pi\beta}{\varepsilon}\right)\exp\left(-\frac{\pi E_c}{\varepsilon}\right), \quad \text{spin}-1/2 \ \text{particle}$$

and

$$\frac{\Gamma_{\text{JWKB}}}{V} \simeq \frac{\alpha\beta\varepsilon}{2\pi\hbar}\sinh^{-1}\left(\frac{\pi\beta}{\varepsilon}\right)\exp\left(-\frac{\pi E_c}{\varepsilon}\right), \quad \text{spin}-0 \ \text{particle},$$

where

$$\begin{aligned}\varepsilon &\equiv \sqrt{(S^2+P^2)^{1/2}+S},\\ \beta &\equiv \sqrt{(S^2+P^2)^{1/2}-S},\end{aligned}$$

where the scalar S and the pseudoscalar P are

$$S \equiv \frac{1}{4} F_{\mu\nu} F^{\mu\nu} = \frac{1}{2}(\mathbf{E}^2 - \mathbf{B}^2); \quad P \equiv \frac{1}{4} F_{\mu\nu} \tilde{F}^{\mu\nu} = \mathbf{E} \cdot \mathbf{B},$$

where $\tilde{F}^{\mu\nu} \equiv \epsilon^{\mu\nu\lambda\kappa} F_{\lambda\kappa}$ is the dual field tensor.

3.3. Nonlinear electrodynamics and rate of pair creation

In article Section 4 we first recall the seminal work of Hans Euler Euler (1936) pointing out for the first time the necessity of nonlinear character of electromagnetism introducing the classical Euler Lagrangian

$$\mathcal{L} = \frac{\mathbf{E}^2 - \mathbf{B}^2}{8\pi} + \frac{1}{\alpha} \frac{1}{E_0^2} \left[a_E \left(\mathbf{E}^2 - \mathbf{B}^2 \right)^2 + b_E \left(\mathbf{E} \cdot \mathbf{B} \right)^2 \right],$$

where

$$a_E = -1/(360\pi^2), \quad b_E = -7/(360\pi^2),$$

a first order perturbation to the Maxwell Lagrangian. In review article Section 4.2 we review the alternative theoretical approach of nonlinear electrodynamics by Max Born Born (1934) and his collaborators, to the more ambitious attempt to obtain the correct nonlinear Lagrangian of Electro-Dynamics. The motivation of Born was to attempt a theory free of divergences in the observable properties of an elementary particle, what has become known as 'unitarian' standpoint versus the 'dualistic' standpoint in description of elementary particles and fields. We recall how the Born Lagrangian was formulated

$$\mathcal{L} = \sqrt{1 + 2S - P^2} - 1,$$

and one of the first solutions derived by Born and Infeld Born and Infeld (1934). We also recall one of the interesting aspects of the courageous approach of Born had been to formulate this Lagrangian within a unified theory of gravitation and electromagnetism following Einstein program. Indeed, we also recall the very interesting solution within the Born theory obtained by Hoffmann Hoffmann (1935); Hoffmann and Infeld (1937). Still in the work of Born Born (1934) the seminal idea of describing the nonlinear vacuum prop-

erties of this novel electrodynamics by an effective dielectric constant and magnetic permeability functions of the field arisen. We then review in Section 4.3.1 of the article the work of Heisenberg and Euler Heisenberg and Euler (1936) adopting the general approach of Born and generalizing to the presence of a real and imaginary part of the electric permittivity and magnetic permeability. They obtain an integral expression of the effective Lagrangian given by

$$\begin{aligned}\Delta\mathcal{L}_{\text{eff}} &= \frac{e^2}{16\pi^2\hbar c}\int_0^\infty e^{-s}\frac{ds}{s^3}\Big[is^2\,\bar{E}\bar{B}\frac{\cos(s[\bar{E}^2-\bar{B}^2+2i(\bar{E}\bar{B})]^{1/2})+\text{c.c.}}{\cos(s[\bar{E}^2-\bar{B}^2+2i(\bar{E}\bar{B})]^{1/2})-\text{c.c.}} \\ &\quad + \left(\frac{m_e^2c^3}{e\hbar}\right)^2+\frac{s^2}{3}(|\bar{B}|^2-|\bar{E}|^2)\Big],\end{aligned}$$

where $\bar{E}, \bar{B}$ are the dimensionless reduced fields in the unit of the critical field E_c,

$$\bar{E}=\frac{|\mathbf{E}|}{E_c},\quad \bar{B}=\frac{|\mathbf{B}|}{E_c}.$$

obtaining the real part and the crucial imaginary term which relates to the pair production in a given electric field. It is shown how these results give as a special case the previous result obtained by Euler (Eq. (4.1.3) in the review). In Section 4.3.2 of the following article the work by Weisskopf Weisskopf (1936) working on a spin-0 field fulfilling the Klein–Gordon equation, in contrast to the spin 1/2 field studied by Heisenberg and Euler, confirms the Euler-Heisenberg result. Weisskopf obtains explicit expression of pair creation in an arbitrary strong magnetic field and in an electric field described by $\bar{E}$ and $\bar{B}$ expansion.

For the first time Heisenberg and Euler provided a description of the vacuum properties by the characteristic scale of strong field E_c and the effective Lagrangian of nonlinear electromagnetic fields. In 1951, Schwinger Schwinger (1951, 1954a,b) made an elegant quantum field theoretic reformulation of this discovery in the QED framework. This played an important role in understanding the properties of the QED theory in strong electromagnetic fields. The QED theory in strong coupling regime, i.e., in the regime of strong electromagnetic fields, is still a vast arena awaiting for experimental verification as well as of further theoretical understanding.

3.4. Pair production and annihilation in QED

In the review article in Section 5 after recalling some general properties of QED in Section 5.1 and some basic processes in Section 5.2 we proceed to the consideration of the Dirac and the Breit–Wheeler processes in QED in Secton 5.3. Then we discuss some higher order processes, namely double pair production in Section 5.4, electron-nucleus bremsstrahlung and pair production by a photon in the field of a nucleus in Section 5.5, and finally pair production by two ions in Section 5.6. In Section 5.7 the classical result for the vacuum to vacuum decay via pair creation in uniform electric field by Schwinger is recalled

$$\frac{\Gamma}{V} = \frac{\alpha E^2}{\pi^2} \sum_{n=1}^{\infty} \frac{1}{n^2} \exp\left(-\frac{n\pi E_c}{E}\right).$$

This formula generalizes and encompasses the previous results reviewed in our report: the JWKB results, discussed in Section 3.5, and the Sauter exponential factor (Eq. (3.5.11) in the review), and the Heisenberg-Euler imaginary part of the effective Lagrangian. We then recall the generalization of this formula to the case of a constant electromagnetic fields. Such results were further generalized to spatially nonuniform and time-dependent electromagnetic fields by Nikishov (1970), Vanyashin and Terent'ev (1965), Popov (1971, 1972b, 2001a), Narozhnyi and Nikishov (1970) and Batalin and Fradkin (1970a). We then conclude this argument by giving the real and imaginary parts for the effective Lagrangian for arbitrary constant electromagnetic field recently published by Ruffini and Xue (2006). This result generalizes the previous result obtained by Weisskopf in strong fields. In weak field it gives the Euler-Heisenberg effective Lagrangian. As we will see in the Section 7.2 of the review much attention has been given experimentally to the creation of pairs in the rapidly changing electric fields. A fundamental contribution in this field studying pair production rates in an oscillating electric field was given by Brezin and Itzykson (1970) and we recover in review Section 5.8 their main results which apply both to the case of bosons and fermions. We recall how similar results were independently obtained two years later by Popov Popov (1972a). In Section 5.10 of the article we recall an alternative physical process considering the quantum theory of the interaction of free electron with the field of a strong electromagnetic waves: an ultrarelativistic electron absorbs multiple photons and emits only a single photon in the reaction Bula et al.

(1996):

$$e + n\omega \to e' + \gamma.$$

This process appears to be of the great relevance as we will see in the next Section for the nonlinear effects originating from laser beam experiments. Particularly important appears to be the possibility outlined by Burke et al. (1997) that the high-energy photon γ created in the first process propagates through the laser field, it interacts with laser photons $n\omega$ to produce an electron–positron pair

$$\gamma + n\omega \to e^+ + e^-.$$

We also refer to the papers by Nikishov and Ritus (1964a,b, 1965, 1967, 1979); Narozhnyĭ et al. (1965) studying the dependence of this process on the status of the polarization of the photons.

We point out the great relevance of departing from the case of the uniform electromagnetic field originally considered by Sauter, Heisenberg and Euler, and Schwinger. We also recall some of the classical works of Brezin and Itzykson and Popov on time varying fields. The space variation of the field was also considered in the classical papers of Nikishov and Narozhny as well as in the work of Wang and Wong. Finally, we recall the work of Khriplovich Khriplovich (2000) studying the vacuum polarization around a Reissner–Nordström black hole. A more recent approach using the worldline formalism, sometimes called the string-inspired formalism, was advanced by Dunne and Schubert Schubert (2001); Dunne and Schubert (2005a).

3.5. Phenomenology of electron-positron pair creation and annihilation

In Section 7 of the review we focus on the phenomenology of electron–positron pair creation and annihilation experiments. There are three different aspects which are examined: the verification of the process (3.0.1) initially studied by Dirac, the process (3.14.1) studied by Breit and Wheeler, and then the classical work of vacuum polarization process around a supercritical nucleus, following the Sauter, Euler, Heisenberg and Schwinger work. We first recall in Section 7.1 how the process (3.0.1) predicted by Dirac was almost immediately discovered by Klemperer Klemperer (1934). Following this discovery the electron–positron collisions have become possibly the most prolific

field of research in the domain of particle physics. The crucial step experimentally was the creation of the first electron–positron collider the "Anello d'Accumulazione" (AdA) was built by the theoretical proposal of Bruno Touschek in Frascati (Rome) in 1960 Bernardini (2004). Following the success of AdA (luminosity $\sim 10^{25}/(\text{cm}^2$ sec), beam energy $\sim$0.25GeV), it was decided to build in the Frascati National Laboratory a storage ring of the same kind, Adone. Electron-positron colliders have been built and proposed for this purpose all over the world (CERN, SLAC, INP, DESY, KEK and IHEP). The aim here is just to recall the existence of this enormous field of research which appeared following the original Dirac idea. In the review the main cross-sections (7.1.1) and (7.1.2) are recalled and the diagram (Fig. 7.1) summarizing this very great success of particle physics is presented. While the Dirac process (3.0.1) has been by far one of the most prolific in physics, the Breit–Wheeler process (3.14.1) has been one of the most elusive for direct observations. In Earth-bound experiments the major effort today is directed to evidence this phenomenon in very strong and coherent electromagnetic field in lasers. In this process collision of many photons may lead in the future to pair creation. This topic is discussed in Section 7.2. Alternative evidence for the Breit–Wheeler process can come from optically thick electron–positron plasma which may be created either in the future in Earth-bound experiments, or currently observed in astrophysics, see Section 10. One additional way to probe the existence of the Breit–Wheeler process is by establishing in astrophysics an upper limits to observable high-energy photons, as a function of distance, propagating in the Universe as pioneered by Nikishov Nikishov (1961), see Section 7.4. We then recall in Section 7.3 how the crucial experimental breakthrough came from the idea of John Madey Deacon et al. (1977) of self-amplified spontaneous emission in an undulator, which results when charges interact with the synchrotron radiation they emit (Tremaine et al. (2002)). Such X-ray free electron lasers have been constructed among others at DESY and SLAC and focus energy onto a small spot hopefully with the size of the X-ray laser wavelength $\lambda \simeq O(0.1)$nm (Nuhn and Pellegrini (2000)), and obtain a very large electric field $E \sim 1/\lambda$, much larger than those obtainable with any optical laser of the same power. This technique can be used to achieve a very strong electric field near to its critical value for observable electron–positron pair production in vacuum. No pair can be created by a single laser beam. It is then assumed that each X-ray laser pulse is split into two equal parts and recombined to form a standing wave with a frequency ω. We then recall how for a laser pulse with wavelength λ about $1\mu m$ and

the theoretical diffraction limit $\sigma_{\text{laser}} \simeq \lambda$ being reached, the critical intensity laser beam would be

$$I^c_{\text{laser}} = \frac{c}{4\pi} E_c^2 \simeq 4.6 \cdot 10^{29} W/\text{cm}^2.$$

In review Section 7.2.1 we recall the theoretical formula for the probability of pair production in time-alternating electric field in two limiting cases of large frequency and small frequency. It is interesting that in the limit of large field and small frequency the production rate approach the one of the Sauter, Heisenberg, Euler and Schwinger, discussed in Section 5. In the following Section 7.2.2 we recall the actually reached experimental limits quoted by Ringwald Ringwald (2001) for a X-ray laser and give a reference to the relevant literature. In Section 7.2.3 we summarize some of the most recent theoretical estimates for pair production by a circularly polarized laser beam by Narozhny, Popov and their collaborators. In this case the field invariants (3.5.23) are not vanishing and pair creation can be achieved by a single laser beam. They computed the total number of electron–positron pairs produced as a function of intensity and focusing parameter of the laser. Particularly interesting is their analysis of the case of two counter-propagating focused laser pulses with circular polarizations, pair production becomes experimentally observable when the laser intensity $I_{\text{laser}} \sim 10^{26} W/\text{cm}^2$ for each beam, which is about $1 \sim 2$ orders of magnitude lower than for a single focused laser pulse, and more than 3 orders of magnitude lower than the critical intensity (7.2.4). Equally interesting are the considerations which first appear in treating this problem that the back reaction of the pairs created on the field has to be taken into due account. We give the essential references and we will see in Section 9 how indeed this feature becomes of paramount importance in the field of astrophysics. We finally review in Section 7.2.4 the technological situation attempting to increase both the frequency and the intensity of laser beams.

The difficulty of evidencing the Breit–Wheeler process even when the high-energy photon beams have a center of mass energy larger than the energy-threshold $2m_e c^2 = 1.02$ MeV was clearly recognized since the early days. We discuss the crucial role of the effective nonlinear terms originating in strong electromagnetic laser fields: the interaction needs not to be limited to initial states of two photons Reiss (1962, 1971). A collective state of many interacting laser photons occurs. We turn then in Section 7.3 of the review to an even more complex and interesting procedure: the interaction of an ultrarelativis-

tic electron beam with a terawatt laser pulse, performed at SLAC Kotseroglou et al. (1996), when strong electromagnetic fields are involved. A first nonlinear Compton scattering process occurs in which the ultrarelativistic electrons absorb multiple photons from the laser field and emit a single photon via the process (5.9.1). The theory of this process has been given in Section 5.10. The second is a drastically improved Breit–Wheeler process (5.9.2) by which the high-energy photon γ, created in the first process, propagates through the laser field and interacts with laser photons $n\omega$ to produce an electron–positron pair Burke et al. (1997). In Section 7.3.1 we describe the status of this very exciting experiments which give the first evidence for the observation in the laboratory of the Breit–Wheeler process although in a somewhat indirect form. Having determined the theoretical basis as well as attempts to verify experimentally the Breit–Wheeler formula we turn in Section 7.4 to a most important application of the Breit–Wheeler process in the framework of cosmology. As pointed out by Nikishov Nikishov (1961) the existence of background photons in cosmology puts a stringent cutoff on the maximum trajectory of the high-energy photons in cosmology.

Having reviewed both the theoretical and observational evidence of the Dirac and Breit–Wheeler processes of creation and annihilation of electron–positron pairs we turn then to one of the most conspicuous field of theoretical and experimental physics dealing with the process of electron–positron pair creation by vacuum polarization in the field of a heavy nuclei. This topic has originated one of the vastest experimental and theoretical physics activities in the last forty years, especially by the process of collisions of heavy ions. We first review in Section 7.5 of the article the $Z = 137$ catastrophe, a collapse to the center, in semi-classical approach, following the Pomeranchuk work Pomeranchuk and Smorodinskii (1945) based on the imposing the quantum conditions on the classical treatment of the motion of two relativistic particles in circular orbits. We then proceed showing in Section 7.5.3 how the introduction of the finite size of the nucleus, following the classical work of Popov and Zeldovich Zeldovich and Popov (1971), leads to the critical charge of a nucleus of $Z_{cr} = 173$ above which a bare nucleus would lead to the level crossing between the bound state and negative energy states of electrons in the field of a bare nucleus. We then review in Section 7.5.5 the recent theoretical progress in analyzing the pair creation process in a Coulomb field, taking into account radial dependence and time variability of electric field. We finally recall in Section 7.6 the attempt to use heavy-ion collisions to form transient superheavy "quasimolecules": a long-lived metastable nuclear complex

with $Z > Z_{cr}$. It was expected that the two heavy ions of charges respectively Z_1 and Z_2 with $Z_1 + Z_2 > Z_{cr}$ would reach small inter-nuclear distances well within the electron's orbiting radii. The electrons would not distinguish between the two nuclear centers and they would evolve as if they were bounded by nuclear "quasimolecules" with nuclear charge $Z_1 + Z_2$. Therefore, it was expected that electrons would evolve quasi-statically through a series of well defined nuclear "quasimolecules" states in the two-center field of the nuclei as the inter-nuclear separation decreases and then increases again. When heavy-ion collision occurs the two nuclei come into contact and some deep inelastic reaction occurs determining the duration Δt_s of this contact. Such "sticking time" is expected to depend on the nuclei involved in the reaction and on the beam energy. Theoretical attempts have been proposed to study the nuclear aspects of heavy-ion collisions at energies very close to the Coulomb barrier and search for conditions, which would serve as a trigger for prolonged nuclear reaction times, to enhance the amplitude of pair production. The sticking time Δt_s should be larger than $1 \sim 2 \cdot 10^{-21}$ sec Greiner and Reinhardt (1999) in order to have significant pair production. Up to now no success has been achieved in justifying theoretically such a long sticking time. In reality the characteristic sticking time has been found of the order of $\Delta t \sim 10^{-23}$ sec, hundred times shorter than the needed to activate the pair creation process. We finally recall in Section 7.6.2 of the review the Darmstadt-Brookhaven dialogue between the Orange and the Epos groups and the Apex group at Argonne in which the claim for discovery of electron–positron pair creation by vacuum polarization in heavy-ion collisions was finally retracted. Out of the three fundamental processes addressed in this report, the Dirac electron–positron annihilation and the Breit–Wheeler electron–positron creation from two photons have found complete theoretical descriptions within Quantum Electro-Dynamics. The first one is very likely the best tested process in physical science, while the second has finally obtained the first indirect experimental evidence. The third process, the one of the vacuum polarization studied by Sauter, Euler, Heisenberg and Schwinger, presents in Earth-bound experiments presents a situation "terra incognita".

3.6. Plasma oscillations and radiation in uniform or nonuniform electric fields, and thermalization of the mildly relativistic pair plasma

The conditions encountered in the vacuum polarization process around black holes lead to a number of electron–positron pairs created of the order of 10^{60} confined in the dyadosphere volume, of the order of a few hundred times to the horizon of the black hole. Under these conditions the plasma is expected to be optically thick and is very different from the nuclear collisions and laser case where pairs are very few and therefore optically thin. We turn then in Section 9, to discuss a new phenomenon: the plasma oscillations, following the dynamical evolution of pair production in an external electric field close to the critical value. In particular, we will examine: (i) the back reaction of pair production on the external electric field; (ii) the screening effect of pairs on the electric field; (iii) the motion of pairs and their interactions with the created photon fields. In review Secs. 9.1 and 9.2, we review semi-classical and kinetic theories describing the plasma oscillations using respectively the Dirac-Maxwell equations and the Boltzmann-Vlasov equations. The electron–positron pairs, after they are created, coherently oscillate back and forth giving origin to an oscillating electric field. The oscillations last for at least a few hundred Compton times. We review the damping due to the quantum decoherence. The energy from collective motion of the classical electric field and pairs flows to the quantum fluctuations of these fields. This process is quantitatively discussed by using the quantum Boltzmann-Vlasov equation in Sections 9.4 and 9.5. The damping due to collision decoherence is quantitatively discussed in Sections 9.6 and 9.7 by using Boltzmann-Vlasov equation with particle collisions terms. This damping determines the energy flows from collective motion of the classical electric field and pairs to the kinetic energy of non-collective motion of particles of these fields due to collisions. In Section 9.7, we particularly address the study of the influence of the collision processes $e^+e^- \rightleftarrows \gamma\gamma$ on the plasma oscillations in supercritical electric field Ruffini et al. (2003b). It is shown that the plasma oscillation is mildly affected by a small number of photons creation in the early evolution during a few hundred Compton times (see Fig. 9.4 of the review). In the later evolution of 10^{3-4} Compton times, the oscillating electric field is damped to its critical value with a large number of photons created. An equipartition of number and energy between electron–positron pairs and photons is reached

(see Fig. 9.4). In Section 9.8, we introduce an approach based on the following three equations: the number density continuity equation, the energy-momentum conservation equation and the Maxwell equations. We describe the plasma oscillation for both overcritical electric field $E > E_c$ and undercritical electric field $E < E_c$ Ruffini et al. (2007b). In additional of reviewing the result well known in the literature for $E > E_c$ we review some novel result for the case $E < E_c$. It was traditionally assumed that electron–positron pairs, created by the vacuum polarization process, move as charged particles in external uniform electric field reaching arbitrary large Lorentz factors. It is reviewed how recent computations show the existence of plasma oscillations of the electron–positron pairs also for $E \lesssim E_c$. For both cases we quote the maximum Lorentz factors $\gamma_{\max}$ reached by the electrons and positrons as well as the length of oscillations. Two specific cases are given. For $E_0 = 10E_c$ the length of oscillations 10 $\hbar/(m_e c)$, and $E_0 = 0.15E_c$ the length of oscillations 10^7 $\hbar/(m_e c)$. We also review the asymptotic behavior in time, $t \to \infty$, of the plasma oscillations by the phase portrait technique. Finally we review some recent results which differentiate the case $E > E_c$ from the one $E < E_c$ with respect to the creation of the rest mass of the pair versus their kinetic energy. For $E > E_c$ the vacuum polarization process transforms the electromagnetic energy of the field mainly in the rest mass of pairs, with moderate contribution to their kinetic energy.

Plasma oscillations and radiation in nonuniform electric fields

We also study electron-positron pair oscillation in spatially inhomogeneous and bound electric fields by integrating the equations of energy-momentum and particle-number conservations and Maxwell equations. The space and time evolutions of the pair-induced electric field, electric charge- and current-densities are calculated. The results show non-vanishing electric charge-density and the propagation of pair-induced electric fields, that are different from the case of homogeneous and unbound electric fields. The space and time variations of pair-induced electric charges and currents emit an electromagnetic radiation. We obtain the narrow spectrum and intensity of this radiation, whose peak ω_{peak} locates in the region around 4 keV for electric field strength $\sim E_c$. We discuss their relevances to both the laboratory experiments for electron and positron pair-productions and the astrophysical observations of compact stars with an electromagnetic structure.

The origin of electron-positron pairs being created strong electric field and

their oscillations has been considered in Ruffini et al. (2007b). There it was shown that plasma oscillations occur not only for overcritical electric field, but also for undercritical electric field, provided the electric field is maintained on spatial distances larger than the distance of oscillations determined explicitly in Ruffini et al. (2007b).

In the paper by Han et al. (2010) the spectrum of electromagnetic radiation seen by far observer for initial phase of oscillations has been computed. It was shown there that the spectrum contain a narrow feature which corresponds to the frequency of plasma oscillations. We revisited the approach of Ruffini et al. (2007b) and showed that for the case of uniform external electric field it is possible to reduce the system of four first order ordinary differential equations governing the dynamics of particle number density, energy density, momentum and electric field to just one second order equation.

Then in the paper by Han et al. (2010); Benedetti et al. (2011) we analyzed the frequency of oscillations, and found that the frequency of oscillations coincides up to a factor close to unity with the plasma frequency, which is strongly time dependent due to pair creation process. Analytical arguments suggest that the frequency of oscillations should asymptotically reach the plasma frequency, and this fact has been demonstrated. The results of this work allow simple estimation of the frequency of plasma oscillations, and then of the spectrum of electromagnetic radiation generated by these oscillations. For the details of this parts, see Appendex B.

Thermalization of the mildly relativistic pair plasma

We then turn in Section 10 of the review to the last physical process needed in ascertaining the reaching of equilibrium of an optically thick electron–positron plasma. The average energy of electrons and positrons we illustrate is $0.1 < \epsilon < 10$ MeV. These bounds are necessary from the one hand to have significant amount of electron–positron pairs to make the plasma optically thick, and from the other hand to avoid production of other particles such as muons. As we will see in the next report these are indeed the relevant parameters for the creation of ultrarelativistic regimes to be encountered in pair creation process during the formation phase of a black hole. We then review the problem of evolution of optically thick, nonequilibrium electron–positron plasma, towards an equilibrium state, following Aksenov et al. (2007, 2008). These results have been mainly obtained by two of us (RR and GV) in recent publications and all relevant previous results are also

reviewed in this Section 10. We have integrated directly relativistic Boltzmann equations with all binary and triple interactions between electrons, positrons and photons two kinds of equilibrium are found: kinetic and thermal ones. Kinetic equilibrium is obtained on a timescale of few $(\sigma_T n_{\pm} c)^{-1}$, where σ_T and $n_{\pm}$ are Thomson's cross-section and electron–positron concentrations respectively, when detailed balance is established between all binary interactions in plasma. Thermal equilibrium is reached on a timescale of few $(\alpha \sigma_T n_{\pm} c)^{-1}$, when all binary and triple, direct and inverse interactions are balanced. In Section 10.1 basic plasma parameters are illustrated. The computational scheme as well as the discretization procedure are discussed in Section 10.2. Relevant conservation laws are given in Section 10.3. Details on binary interactions, consisting of Compton, Møller and Bhabha scatterings, Dirac pair annihilation and Breit–Wheeler pair creation processes, and triple interactions, consisting of relativistic bremsstrahlung, double Compton process, radiative pair production and three photon annihilation process, are presented in Section 10.5 and 10.6, respectively. In Section 10.5 collisional integrals with binary interactions are computed from first principles, using QED matrix elements. In Section 10.7 Coulomb scattering and the corresponding cutoff in collisional integrals are discussed. Numerical results are presented in Section 10.8 where the time dependence of energy and number densities as well as chemical potential and temperature of electron–positron-photon plasma is shown, together with particle spectra. The most interesting result of this analysis is to have differentiate the role of binary and triple interactions. The detailed balance in binary interactions following the classical work of Ehlers Ehlers (1973) leads to a distribution function of the form of the Fermi-Dirac for electron–positron pairs or of the Bose-Einstein for the photons. This is the reason we refer in the text to such conditions as the Ehlers equilibrium conditions. The crucial role of the direct and inverse three-body interactions is well summarized in fig. 10.1, panel A from which it is clear that the inverse three-body interactions are essential in reaching thermal equilibrium. If the latter are neglected, the system deflates to the creation of electron–positron pairs all the way down to the threshold of 0.5MeV. This last result which is referred as the Cavallo–Rees scenario Cavallo and Rees (1978) is simply due to improper neglection of the inverse triple reaction terms (see Appendix 10).

3.7. The energy extraction from a black hole by pair-productions, and Einstein-Euler-Heisenberg theory and charged black holes

We turn then to astrophysics, where, in the process of gravitational collapse to a black hole and in its outcomes these three processes will be for the first time verified on a much larger scale, involving particle numbers of the order of 10^{60}, seeing both the Dirac process and the Breit–Wheeler process at work in symbiotic form and electron–positron plasma created from the "blackholic energy" during the process of gravitational collapse. It is becoming more and more clear that the gravitational collapse process to a Kerr–Newman black hole is possibly the most complex problem ever addressed in physics and astrophysics. What is most important for this report is that it gives for the first time the opportunity to see the above three processes simultaneously at work under ultrarelativistic special and general relativistic regimes. The process of gravitational collapse is characterized by the timescale $\Delta t_g = GM/c^3 \simeq 5 \cdot 10^{-6} M/M_\odot$ sec and the energy involved are of the order of $\Delta E = 10^{54} M/M_\odot$ ergs. It is clear that this is one of the most energetic and most transient phenomena in physics and astrophysics and needs for its correct description such a highly time varying treatment. Our approach in Section 8 is to gain understanding of this process by separating the different components and describing 1) the basic energetic process of an already formed black hole, 2) the vacuum polarization process of an already formed black hole, 3) the basic formula of the gravitational collapse recovering the Tolman-Oppenheimer-Snyder solutions and evolving to the gravitational collapse of charged and uncharged shells. This will allow among others to obtain a better understanding of the role of irreducible mass of the black hole and the maximum blackholic energy extractable from the gravitational collapse. We will as well address some conceptual issues between general relativity and thermodynamics which have been of interest to theoretical physicists in the last forty years. Of course in these brief chapter we will be only recalling some of these essential themes and refer to the literature where in-depth analysis can be found. In Section 8.1 we recall the Kerr–Newman metric and the associated electromagnetic field. We then recall the classical work of Carter Carter (1968) integrating the Hamilton-Jacobi

equations for charged particle motions in the above given metric and electromagnetic field. We then recall in Section 8.2 the introduction of the effective potential techniques in order to obtain explicit expression for the trajectory of a particle in a Kerr–Newman geometry, and especially the introduction of the reversible–irreversible transformations which lead then to the Christodoulou-Ruffini mass formula of the black hole

$$M^2c^4 = \left(M_{\rm ir}c^2 + \frac{c^2Q^2}{4GM_{\rm ir}}\right)^2 + \frac{L^2c^8}{4G^2M_{\rm ir}^2},$$

where $M_{\rm ir}$ is the irreducible mass of a black hole, Q and L are its charge and angular momentum. We then recall in article Section 8.3 the positive and negative root states of the Hamilton–Jacobi equations as well as their quantum limit. We finally introduce in Section 8.4 the vacuum polarization process in the Kerr–Newman geometry as derived by Damour and Ruffini Damour and Ruffini (1975) by using a spatially orthonormal tetrad which made the application of the Schwinger formalism in this general relativistic treatment almost straightforward. We then recall in Section 8.5 the definition of a dyadosphere in a Reissner–Nordström geometry, a region extending from the horizon radius

$$r_+ \;=\; 1.47\cdot 10^5\mu(1+\sqrt{1-\xi^2})\ {\rm cm}$$

out to an outer radius

$$r^\star = \left(\frac{\hbar}{m_ec}\right)^{1/2}\left(\frac{GM}{c^2}\right)^{1/2}\left(\frac{m_{\rm p}}{m_e}\right)^{1/2}\left(\frac{e}{q_{\rm p}}\right)^{1/2}\left(\frac{Q}{\sqrt{GM}}\right)^{1/2} = \\ = 1.12\cdot 10^8\sqrt{\mu\xi}\ {\rm cm},$$

where the dimensionless mass and charge parameters $\mu = \frac{M}{M_\odot}$, $\xi = \frac{Q}{(M\sqrt{G})} \leq 1$. In Section 8.6 of the review the definition of a dyadotorus in a Kerr–Newman metric is recalled. We have focused on the theoretically well defined problem of pair creation in the electric field of an already formed black hole. Having set the background for the blackholic energy we recall some fundamental features of the dynamical process of the gravitational collapse. In Section 8.7 we address some specific issues on the dynamical formation of the black hole, recalling first the Oppenheimer-Snyder solution Oppenheimer

and Snyder (1939) and then considering its generalization to the charged non-rotating case using the classical work of W. Israel and V. de la Cruz Israel (1966); De la Cruz and Israel (1967). In Section 8.7.1 we recover the classical Tolman-Oppenheimer-Snyder solution in a more transparent way than it is usually done in the literature. In the Section 8.7.2 we are studying using the Israel-de la Cruz formalism the collapse of a charged shell to a black hole for selected cases of a charged shell collapsing on itself or collapsing in an already formed Reissner–Nordström black hole. Such elegant and powerful formalism has allowed to obtain for the first time all the analytic equations for such large variety of possibilities of the process of the gravitational collapse. The theoretical analysis of the collapsing shell considered in the previous section allows to reach a deeper understanding of the mass formula of black holes at least in the case of a Reissner–Nordström black hole. This allows as well to give in Section 8.8 of the review an expression of the irreducible mass of the black hole only in terms of its kinetic energy of the initial rest mass undergoing gravitational collapse and its gravitational energy and kinetic energy T_+ at the crossing of the black hole horizon r_+

$$M_{\rm ir} = M_0 - \frac{M_0^2}{2r_+} + T_+.$$

Similarly strong, in view of their generality, are the considerations in Section 8.8.2 which indicate a sharp difference between the vacuum polarization process in an overcritical $E \gg E_c$ and undercritical $E \ll E_c$ black hole. For $E \gg E_c$ the electron–positron plasma created will be optically thick with average particle energy 10 MeV. For $E \ll E_c$ the process of the radiation will be optically thin and the characteristic energy will be of the order of 10^{21} eV. This argument will be further developed in a forthcoming report. In Section 8.9 we show how the expression of the irreducible mass obtained in the previous Section leads to a theorem establishing an upper limit to 50% of the total mass energy initially at rest at infinity which can be extracted from any process of gravitational collapse independent of the details. These results also lead to some general considerations which have been sometimes claimed in reconciling general relativity and thermodynamics.

Einstein-Euler-Heisenberg theory and charged black holes

Taking into account the Euler-Heisenberg effective Lagrangian of one-loop nonperturbative quantum electrodynamics (QED) contributions, we formu-

late the Einstein-Euler-Heisenberg theory and study the solutions of nonrotating black holes with electric and magnetic charges in spherical geometry. In the limit of strong and weak electromagnetic fields of black holes, we calculate the black hole horizon radius, area, and total energy up to the leading order of QED corrections and discuss the black hole irreducible mass, entropy, and maximally extractable energy as well as the Christodoulou-Ruffini mass formula. We find that these black hole quantities receive the QED corrections, in comparison with their counterparts in the Reissner-Nordström solution. The QED corrections show the screening effect on black hole electric charges and the paramagnetic effect on black hole magnetic charges. As a result, the black hole horizon area, irreducible mass, and entropy increase; however, the black hole total energy and maximally extractable energy decrease, compared with the Reissner-Nordström solution. In addition, we show that the condition for extremely charged black holes is modified due to the QED correction. The reason is that the QED vacuum polarization gives rise to the screening effect on the black hole electric charge and the paramagnetic effect on the black hole magnetic charge. It is mentioned that in the Einstein-Euler-Heisenberg theory, it is worthwhile to study Kerr-Newman black holes, whose electric field **E** and magnetic field **B** are determined by the black hole mass M, charge Q, and angular momentum a Newman et al. (1965). In addition, it will be interesting to study the QED corrections in black hole physics by taking into account the one-loop photon-graviton amplitudes of the effective Lagrangian (E.3.11) Drummond and Hathrell (1980) and its generalizations Gilkey (1975); Bastianelli et al. (2000); Barvinsky and Vilkovisky (1985); Gusev (2009); Bastianelli et al. (2009). We leave these studies for future work. For the details of this part, see Appendix E.

3.8. Dyadosphere of electron-positron pairs and photons formed in gravitational collapses

In Refs. Ruffini et al. (2003b,a), first initiating with supercritical electric fields on the core surface, we study electron-positron pair production and oscillation together with gravitational collapse. We use the exact solution of Einstein–Maxwell equations describing the gravitational collapse of a thin charged shell. Recall that the region of space–time external to the core is Reissner–

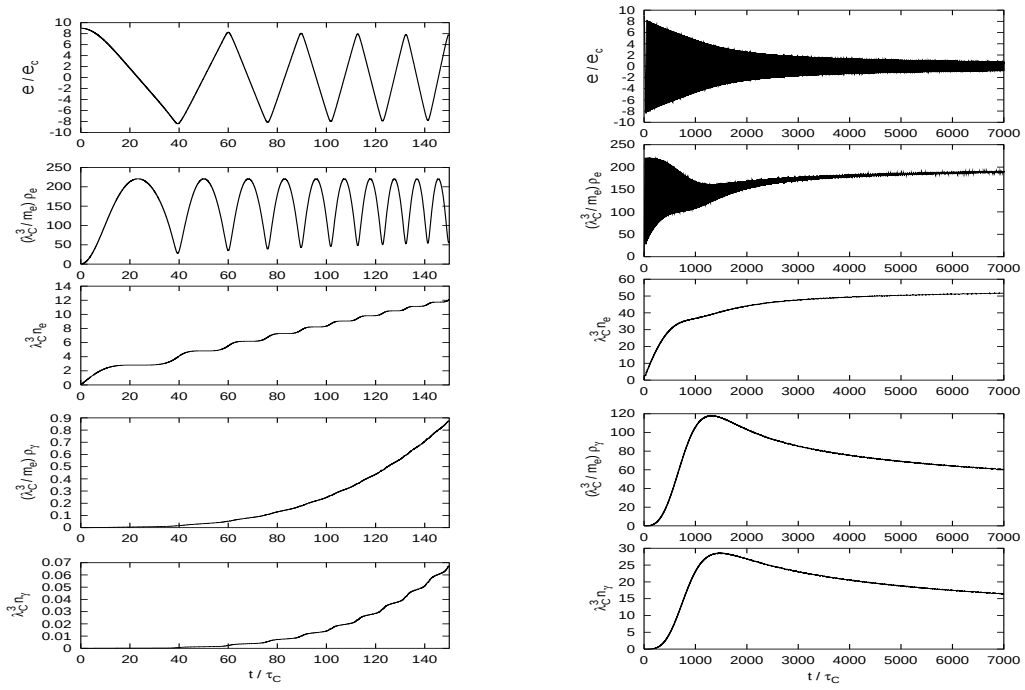

Figure 3.1.: In left figure: We plot for $t < 150\tau_C$, from the top to the bottom panel: a) electromagnetic field strength; b) electrons energy density; c) electrons number density; d) photons energy density; e) photons number density as functions of time. The right figure: We plot for $t < 7000\tau_C$ as the same quantities as in left.

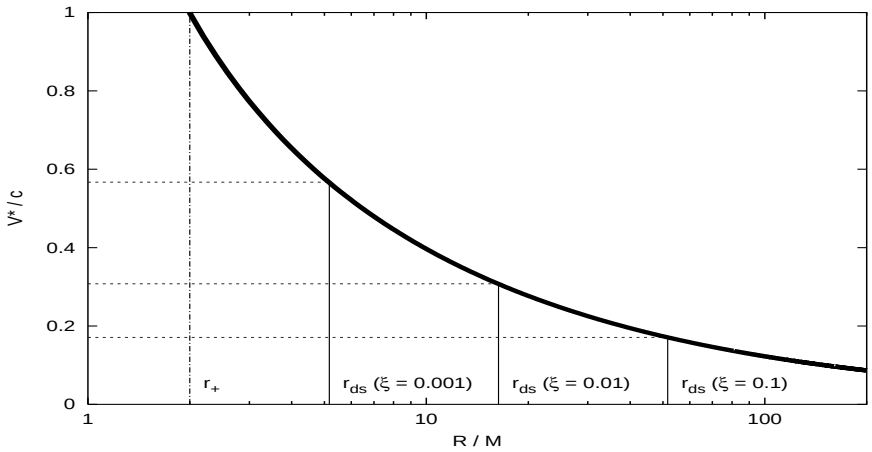

Figure 3.2.: Collapse velocity of a charged stellar core of mass $M_0 = 20M_\odot$ as measured by static observers as a function of the radial coordinate of the core surface. Dyadosphere radii for different charge to mass ratios ($\xi = 10^{-3}, 10^{-2}, 10^{-1}$) are indicated in the plot together with the corresponding velocity.

Nordström with line element

$$ds^2 = -\alpha^2 dt^2 + \alpha^{-2} dr^2 + r^2 d\Omega^2 \tag{3.8.1}$$

in Schwarzschild like coordinate (t, r, θ, ϕ), where $\alpha^2 = 1 - 2M/r + Q^2/r^2$; M is the total energy of the core as measured at infinity and Q is its total charge. Let us label with r_0 and t_0 the radial and time–like coordinate of the core surface, and the equation of motion of the core is Israel (1966); De la Cruz and Israel (1967); Bekenstein (1971):

$$\frac{dr_0}{dt_0} = -\frac{\alpha^2(r_0)}{\Omega(r_0)}\sqrt{\Omega^2(r_0) - \alpha^2(r_0)}, \quad \Omega(r_0) = \frac{M}{M_0} - \frac{M_0^2+Q^2}{2M_0 r_0}; \tag{3.8.2}$$

M_0 being the rest mass of the shell. The analytical solutions of Eq. (3.8.2) were found $t_0 = t_0(r_0)$, and the core collapse speed $V^*(r_0)$ as a function of r_0 is plotted in Fig. 3.2, where we indicate $V^*_{\rm ds} \equiv V^*|_{r_0=r_{\rm ds}}$ as the velocity of the core at the Dyadosphere radius $r_{\rm ds}$.

We now turn to the pair creation and plasma oscillation taking place in the classical electric and gravitational fields during the gravitational collapse of

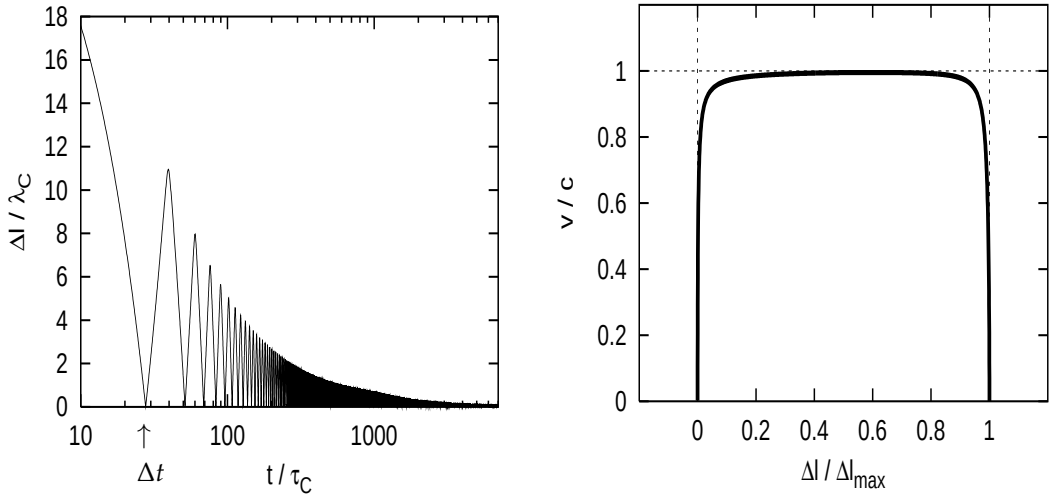

Figure 3.3.: In left figure: Electrons elongation as function of time in the case $r = r_{\rm ds}/3$. The oscillations are damped in a time of the order of $10^3 - 10^4\tau_{\rm C}$. The right figure: Electrons mean velocity as a function of the elongation during the first half oscillation. The plot summarize the oscillatory behaviour: as the electrons move, the mean velocity grows up from 0 to the speed of light and then falls down at 0 again.

a charged overcritical stellar core. As already show in Fig. 3.1, (i) the electric field oscillates with lower and lower amplitude around 0; (ii) electrons and positrons oscillates back and forth in the radial direction with ultra relativistic velocity, as result the oscillating charges are confined in a thin shell whose radial dimension is given by the elongation Δl of the oscillations. In Fig. 3.3, we plot the elongation Δl as a function of time and electron mean velocity v as a function of the elongation during the first half period Δt of oscillation. This shows precisely the characteristic time Δt and size Δl of charge confinement due to plasma oscillation.

In the time Δt the charge oscillations prevent a macroscopic current from flowing through the surface of the core. Namely in the time Δt the core moves inwards of

$$\Delta r^* = V^* \Delta t \gg \Delta l. \tag{3.8.3}$$

Since the plasma charges are confined within a region of thickness Δl, due to Eq. (3.8.3) no charge "reaches" the surface of the core which can neutralize it

and the initial charge of the core remains untouched. For example in the case $M = 20M_{\odot}, \xi = 0.1$, and $r = \frac{1}{3}r_{\rm ds}$, we have

$$\Delta l \lesssim 30\lambda_{\rm C}, \quad \Delta t \sim 10^3\tau_{\rm C}, \quad V^* \sim 0.3c, \tag{3.8.4}$$

and $\Delta r^* \gg \Delta l$. We conclude that the core is not discharged or, in other words, the electric charge of the core is stable against vacuum polarization and electric field $E = Q/r_0^2$ is amplified during the gravitational collapse. As a consequence, an enormous amount ($N \sim Qr_{\rm ds}/e\lambda_{\rm C}$ as claimed in Refs. Preparata et al. (1998, 2003); Ruffini and Xue (2008b,a)) of pairs is left behind the collapsing core and Dyadosphere Ruffini and Xue (2008a); Preparata et al. (1998, 2003) is formed.

Recently, we study this pair-production process in a neutral collapsing core, rather than a charged collapsing core, as described above. Neutral stellar cores at or over nuclear densities are described by positive charged baryon cores and negative charged electron gas since they possess different masses and interactions (equations of state). In static case, the equilibrium configuration of positive charged baryon cores and negative charged electron gas described by Thomas-Fermi equation shows an overcritical electric field on the surface of baryon core. Based on such an initial configuration and a simplified model of spherically collapsing cores, we approximately integrate the Einstein-Maxwell equations and the equations for the particle number and energy-momentum conservations. It is shown that in gravitational core-collapse, such an electric field dynamically evolves in the space-time and electron-positron pairs are produced and gravitational energy is converted to electron-positron energy. This important result has been published in Physics Review D. The details on this topic can be found in Appendix C.

The e^+e^- pairs generated by the vacuum polarization process around the core are entangled in the electromagnetic field Ruffini et al. (2003a), and thermalize in an electron–positron–photon plasma on a time scale $\sim 10^4\tau_C$ Ruffini et al. (2003b) (see Fig. 3.1). As soon as the thermalization has occurred, the hydrodynamic expansion of this electrically neutral plasma starts Ruffini et al. (1999, 2000). While the temporal evolution of the $e^+e^-\gamma$ plasma takes place, the gravitationally collapsing core moves inwards, giving rise to a further amplified supercritical field, which in turn generates a larger amount of e^+e^- pairs leading to a yet higher temperature in the newly formed $e^+e^-\gamma$ plasma. We report progress in this theoretically challenging process which is marked by distinctive and precise quantum and general relativistic effects. As pre-

sented in Ref. Ruffini et al. (2003a): we follow the dynamical phase of the formation of Dyadosphere and of the asymptotic approach to the horizon by examining the time varying process at the surface of the gravitationally collapsing core. The details on this topic can be found in Appendix A

Recently, we study the homologous collapse of stellar nuclear core, the virial theorem for hadron collisional relaxations, and photon productions from hadron collisions. We thus show the gravo-thermal dynamical process that transforms gravitational energy to photon energy. The process is energetically and entropically favourable. The total baryon number conservation, Euler equation for energy-momentum conservation and Poisson's equation for gravitational potential are adopted to describe homologous core collapses. The virial theorem determines the hadron collision energy gain from gravitational potential. The hadronic photon production rate determines the photon energy density. The time scales of macroscopic and microscopic processes are studied to verify approximations. As a result, we show the formation of opaque photon-pair spheres, whose total energy, size, temperature and number density, accounting for the main energetic features of Gamma-Ray Burst progenitors. We obtain the intrinsic correlations of these quantities. They depend only on the averaged thermal index of the stellar core. We discuss the possibility to confront them with observational data. For details, see JCAP07 (2021) 044, https://arxiv.org/abs/2104.03021

3.9. Polarization of strong electromagnetic fields and its applications in polarizations of laser fields, GRBs and CMB photons, as well as neutrinos

Euler-Heisenberg Lagrangian and CMB photon circular polarization

Considering the effective Euler-Heisenberg Lagrangian, i.e., non-linear photon-photon interactions, we study the circular polarization of electromagnetic radiation based on the time-evolution of Stokes parameters. To the leading order, we solve the Quantum Boltzmann Equation for the density matrix describing an ensemble of photons in the space of energy-momentum and polarization states, and calculate the intensity of circular polarizations. Applying these results to a linear polarized thermal radiation, we calculate the

circular polarization intensity, and discuss its possible relevance to the circular polarization intensity of the Cosmic Microwave Background radiation. For the details of this part, see I. Motie, S.-S. Xue, European Physics Letter, 100, 17006, (2012)

To probe the nonlinear effects of photon-photon interaction in the quantum electrodynamics, we study the generation of circular polarized photons by the collision of two linearly polarized laser beams. In the framework of the Euler-Heisenberg effective Lagrangian and the Quantum Boltzmann equation for the time evolution of the density matrix of polarization, we calculate the intensity of circular polarization generated by the collision of two linearly polarized laser beams and estimate the rate of generation that is proportional to α^2. As a result, we show that the generated circular polarization can be experimentally measured by two head-on colliding optical laser beams of the cross-sectional area $\lesssim 0.01\,\mathrm{cm}^2$ and the laser pulse energy $\sim$ mJ. which are currently available in laboratories. Our study presents a valuable supplement to other theoretical and experimental frameworks to study and measure the nonlinear effects of photon-photon interaction in the quantum electrodynamics. For the details of this part, see "Circular polarization from linearly polarized laser beam collisions", I. Motie, R. Mohammadi, and S.-S. Xue, Physics Review A377 (2013) 2450.

In addition, we have studied the following case. Nonlinear QED interactions induce different polarization properties on a given probe beam. We consider the polarization effects caused by the photon-photon interaction in laser experiments, when a laser beam propagates through a constant magnetic field or collides with another laser beam. We solve the quantum Boltzmann equation within the framework of the Euler-Heisenberg Lagrangian for both time-dependent and constant background field to explore the time evolution of the Stokes parameters Q, U, and V describing polarization. Assuming an initially linearly polarized probe laser beam, we also calculate the induced ellipticity and rotation of the polarization plane. For details see "Polarization of a probe laser beam due to nonlinear QED effects", S. Shakeri, S. Z. Kalantari, and S.-S. Xue, Physical Review A 95, 012108 (2017).

CMB or laser photon circular polarization via interaction with neutrino beam or cosmic background

We study the phenomenon that laser photons acquire circular polarization by interacting with a Dirac or Majorana neutrino beam. It is shown that for

the reason of neutrinos being left-handed and their gauge-couplings being parity-violated, linearly polarized photons acquire their circular polarization by interacting with neutrinos. Calculating the ratio of linear and circular polarizations of laser photons interacting with either Dirac or Majorana neutrino beam, we obtain this ratio for the Dirac neutrino case, which is about twice less than the ratio for the Majorana neutrino case. Based on this ratio, we discuss the possibility of using advanced laser facilities and the T2K neutrino experiment to measure the circular polarization of laser beams interacting with neutrino beams in ground laboratories. This could be an additional and useful way to gain some insight into the physics of neutrinos, for instance their Dirac or Majorana nature. For the details of this part, see R. Mohammadi and S.-S. Xue Physics Letters B731 272–278, (2014).

Recently, the similar idea has been used to study the Lorentz violation effects via a laser beam interacting with a high-energy charged lepton beam. The conversion of linear polarization of a laser beam to circular one through its forward scattering by a TeV order charged lepton beam in the presence of Lorentz violation correction is explored. We calculate the ratio of circular polarization to linear one (Faraday Conversion phase) of the laser beam interacting with either electron or the muon beam in the framework of the quantum Boltzmann equation. Regarding the experimentally available sensitivity to the Faraday conversion, we show that the scattering of a linearly polarized laser beam with energy 0.1 eV and an electron/muon beam with available flux places an upper bound on the combination of lepton sector Lorentz violation coefficients c components (cTT+1.4 c(TZ)+0.25(cXX+cYY+2 cZZ)). The obtained bound on the combination for the electron beam is at the 10^{15} level and for the muon beam at the 3.910^{13} level. It should be mentioned that the laser and charged lepton beams considered here to reach the experimentally measurable Faraday Conversion phase are currently available or will be accessible in the near future. This study provides a valuable supplementary to other theoretical and experimental frameworks for measuring and constraining Lorentz violation coefficients. For the details of this part, see Seddigheh Tizchang, R. Mohammadi and S.-S. Xue, Eur. Phys. J. C (2019) 79: 224 https://arxiv.org/abs/1811.00486.

We propose a novel scheme for distinguishing between the Dirac and Majorana nature of neutrinos via interaction of a neutrino beam with microwave photons inside a cavity. We study the effective photon-photon polarization exchange induced by the photon-neutrino scattering. The quantum field theoretical studies of such effective picture are presented for both Dirac and Ma-

jorana neutrinos. Our phenomenological analyses show that the difference between Dirac and Majorana neutrinos can manifest itself in scattering rate of the photons. To enhance the effect a cavity scheme is employed. An experimental setup based on microwave cavities is then designed and simulated by finite element method to measure the scattering rate. Our results suggest that an experiment based on the current state-of-the-art technology will be able to probe the difference in about one year. However, it can be done in a few days by enhancing the neutrino beam flux or implementing with the near future equipments. Therefore, our work provides the possibility for solving the long lasting puzzle of Dirac or Majorana nature of neutrinos. For details see the article by Mehdi Abdi (IUT), Roohollah Mohammadi (INMOST and SoA-IPM), She-Sheng Xue (ICRANet), Moslem Zarei (IUT) https://arxiv.org/abs/1909.01536

In this approch of measuring scatted photon's polarization, another goal is to probe axion or axion-like particles in light-by-light forward scattering process. We consider the polarization effects caused by on-shell axions in the photon-photon scattering process. We show that the circular polarization signal generated in light-by-light scattering in the current/future laser experiments can shed more light on different aspects of these mysterious particles. Our results show a large enhancement in the conversion rate between circular and linear polarizations at the domain close to the resonance point of inter-mediating axions. This signal enhancement can be used in order to discriminate between the ALP contribution to photon-photon scattering and one originates from the virtual electron-positron pairs in the pure QED framework. This work is in preparation by Soroush Shakeri, Rohollah Mohammadi, She-Sheng Xue " Light by Light Scattering as a Probe for Axion Dark Matter".

Photon-neutrino scattering and the B-mode spectrum of CMB photons

On the basis of the quantum Boltzmann equation governing the time-evolution of the density matrix of polarized CMB photons in the primordial scalar perturbations of metric, we calculate the B-mode spectrum of polarized CMB photons contributed from the scattering of CMB photons and CNB neutrinos (Cosmic Neutrino Background). We show that such contribution to the B-mode spectrum is negligible for small ℓ, however is significantly large for $50 < \ell < 200$ by plotting our results together with the BICEP2 data. Our study and results imply that in order to theoretically better understand the origin of the observed B-mode spectrum of polarized

CMB photons (r-parameter), it should be necessary to study the relevant and dominate processes in both tensor and scalar perturbations. For the details of this part, see the Rapid communication section of Physics Review D 90, 091301(R) (2014), J. Khodagholizadeh, R. Mohammadi and S.-S. Xue.

In addition, we study the cosmic microwave background polarization, especially the B-mode due to the weak interaction of the cosmic neutrino background and cosmic microwave background, in addition to the Compton scattering in both cases of scalar and tensor metric perturbations. It is shown that the power spectrum C_{Bl} of the B-mode polarization receives some contributions from scalar and tensor modes, which have effects on the value of the r-parameter. We also show that the B-mode polarization power spectrum can be used as an indirect probe into the cosmic neutrino background. B-mode polarization receives some contributions from scalar and tensor modes, which have effects on the value of the r-parameter. We also show that the B-mode polarization power spectrum can be used as an indirect probe into the cosmic neutrino background. For the details of this part, see Physics Review D 93, 091301 (2016), R. Mohammadi, J. Khodagholizadeh, M. Sadegh, and She-Sheng Xue.

Recently, we explore the possibility of the polarization conversion of a wide energy range of cosmic photons to the circular polarization through their interaction with Sterile neutrino as a dark matter candidate. By considering the Sterile neutrino in the seesaw mechanism framework and right-handed current model, we estimate the Faraday conversion $\Delta\phi_{\rm FC}$ of gamma ray burst (GRB) photons interacting with the Sterile neutrinos at both the prompt and afterglow emission levels. We show that for active-Sterile neutrino with mixing angle $\theta^2 \lesssim 10^{-2}$ motivated by models with a hidden sector coupled to the sterile neutrino, the Faraday conversion can be estimated as $\Delta\phi_{\rm FC} \lesssim 10^{-2} - 10^{-17}$ rad. We also examine the V-mode power spectrum C_{Vl} of the cosmic microwave background (CMB) at the last scattering surface. We show that the circular polarization power spectrum at the leading order is proportional to the linear polarization power spectrum C_{pl} and the mixing angle where for $\theta^2 \lesssim 10^{-2}$ leads to $C_{Vl} \lesssim 0.01$ Nano-Kelvin squared. For details see the recent article by M. Haghighat, S. Mahmoudi, R.Mohammadi, S. Tizchang and S.S. Xue, Circular polarization of cosmic photons due to their interactions with Sterile neutrino dark matter, Phys. Rev. D 101, 123016 (2020) https://arxiv.org/abs/1909.03883.

Generation of circular polarization of gamma ray bursts

We study the generation of the circular polarization of gamma ray burst (GRB) photons via their interactions with astroparticles in the presence or absence of background fields such as magnetic fields. Solving the quantum Boltzmann equation for GRB photons as a photon ensemble, we discuss the generation of circular polarization (as Faraday conversion phase shift $\Delta\varphi_{FC}$ of GRBs in the following cases: (i)

intermediate interactions, i.e., the Compton scattering of GRBs in the galaxy cluster magnetic field, and the scattering of GRBs in the cosmic neutrino background (CNB), as well as cosmic microwave background (CMB); (ii) interactions with particles and fields in shockwaves, i.e., the Compton scattering of GRBs with accelerated charged particles in the presence of magnetic fields. We found that (i) after shockwave crossing, the greatest contribution of $\Delta\varphi_{FC}$ for energetic GRBs (of the order of GeV and larger) comes from GRB-CMB interactions, but for low-energy GRBs the contributions of the Compton scattering of GRBs in the galaxy cluster magnetic field dominate; (ii) in shockwave crossing, the magnetic field has significant effects on converting a GRB's linear polarization to a circular one, and this effect can be used to better understand the magnetic profile in shockwaves. The main aim of this work is to study and measure the circular polarization of GRBs for a better understanding of the physics and mechanism of the generation of GRBs and their interactions before reaching us. For the details of this part, see the reference Phys. Rev. D 94, 065033 – Published 22 September 2016 S. Batebi, R. Mohammadi, R. Ruffini, S. Tizchang, and S.-S. Xue. This work is also presented in the conference MG14, Rome, Italy 2015, see the conference proceeding of MG14, World Scientific, Singapore, 2017.

We have also studied the following case. In the presence of strong magnetic fields near pulsars, the QED vacuum becomes a birefringent medium due to nonlinear QED interactions. Here, we explore the impact of the effective photon-photon interaction on the polarization evolution of photons propagating through the magnetized QED vacuum of a pulsar. We solve the quantum Boltzmann equation within the framework of the Euler-Heisenberg Lagrangian to find the evolution of the Stokes parameters. We find that linearly polarized X-ray photons propagating outward in the magnetosphere of a rotating neutron star can acquire high values for the circular polarization parameter. Meanwhile, it is shown that the polarization characteristics of photons besides photon energy depend strongly on parameters of the pulsars such as magnetic field strength, inclination angle and rotational period. Our results are clear predictions of QED vacuum polarization effects in the near vicinity of magnetic stars which can be tested with the upcoming X-ray polarimetric observations. For details see "Nonlinear QED effects in X-ray emission of pulsars" , S. Shakeri, M. Haghighat, S.-S. Xue, JCAP 10, 014 (2017).

3.10. Pair production and interactions of fields and matter in the cosmology within the framework of quantum Einstein-Cartan-Maxwell theory

Fermionic and bosonic current and Schwinger effect in de Sitter spacetime

Semiclassical fermion pair creation in de Sitter spacetime is studied, we present a method to semiclassically compute the pair creation rate of bosons and fermions in de Sitter spacetime. The results in the bosonic case agree with the ones in the literature. We find that for the constant electric field the fermionic and bosonic pair creation rate are the same. This analogy of bosons and fermions in the semiclassical limit is known from several flat spacetime examples.

We study the fermionic Schwinger effect in two dimensional de Sitter spacetime. To do so we first present a method to semiclassically compute the number of pairs created per momentum mode for general time dependent fields. In addition the constant electric field is studied in depth. In this case solutions for the Dirac equation can be found and the number of pairs can be computed using the standard Bogoliubov method. This result is shown to agree with the semiclassical one in the appropriate limit. The solutions are also used to compute the expectation value of the induced current. Comparing these results to similar studies for bosons we find that while the results agree in the semiclassical limit they do not generally. Especially there is no occurrence of a strong current for small electric fields.

We present a method to semiclassically compute the pair creation rate of bosons and fermions in de Sitter spacetime. The results in the bosonic case agree with the ones in the literature. We find that for the constant electric field the fermionic and bosonic pair creation rate are the same. This analogy of bosons and fermions in the semiclassical limit is known from several flat spacetime examples.

For the details of this part, see C. Stahl, E. Strobel, and S.-S. Xue, "Fermionic current and Schwinger effect in de Sitter spacetime", for the details, see the reference Physics Review D **93**,025004 (2016), and AIP Conf. Proc. 1693, 050005 (2015), arXiv:1507.01401 [hep-th].

In a further study, we consider a charged scalar field in a D dimensional de Sitter spacetime and investigate pair creation by Schwinger mechanism in a constant electric field background. Using a semiclassical approximation the current of the created pairs has been estimated. We find that, the semiclassical current of the created pairs in the strong electric field limit responds as $E^{\frac{D}{2}}$. Going further but restricting to

$D = 3$ dimensional de Sitter spacetime, the quantum expectation value of the spacelike component of the induced current has been computed in the in-vacuum state by applying an adiabatic subtraction scheme. We find that, in the strong electric field limit, the current responds as $E^{\frac{3}{2}}$. In the weak electric field limit the current has a linear response in E and an inverse dependence on the mass of the scalar field. In the case of a massless scalar field, the current varies with E^{-1} which leads to a phenomenon of infrared hyperconductivity. A new relation between infrared hyperconductivity, tachyons and conformality is discussed and a scheme to avoid an infrared hyperconductivity regime is proposed. In D dimension, we eventually presented some first estimates of the backreaction of the Schwinger pairs to the gravitational field, we find a decrease of the Hubble constant due to the pair creation. For more details, see the reference "Scalar current of created pairs by Schwinger mechanism in de Sitter spacetime", Ehsan Bavarsad, Clément Stahl and She-Sheng Xue, Phys. Rev. D 94, 104011 (2016), as well as E. Bavarsad, S. P. Kim, C. Stahl, S.-S. Xue, "Effect of a magnetic field on Schwinger mechanism in de Sitter spacetime", Phys. Rev. D 97, 025017 (2018).

In addition, we considered a new renormalization condition for the vacuum expectation values of the scalar and spinor currents induced by a homogeneous and constant electric field background in de Sitter spacetime. Following a semiclassical argument, the condition named maximal subtraction imposes the exponential suppression on the massive charged particle limit of the renormalized currents. The maximal subtraction changes the behaviors of the induced currents previously obtained by the conventional minimal subtraction scheme. The maximal subtraction is favored for a couple of physically decent predictions including the identical asymptotic behavior of the scalar and spinor currents, the removal of the infrared (IR) hyperconductivity from the scalar current, and the finite current for the massless fermion. For details see the article by Takahiro Hayashinaka, She-Sheng Xue, "Physical renormalization condition for de Sitter QED", published in Phys. Rev. D 97, 105010 (2018).

Recently we consider a massive charged scalar field in a uniform electric field background in a de Sitter spacetime (dS). We compute the in-vacuum expectation value of the trace of the energy-momentum tensor for the created Schwinger pairs, and using adiabatic subtraction scheme the trace is regularized. The effect of the Schwinger pair creation on the evolution of the Hubble constant is investigated. We find that the production of the semiclassical pairs leads to a decay of the Hubble constant. Whereas, the production of a light scalar field in the weak electric field regime leads to a superacceleration phenomenon. For details see the article by E. Bavarsad, S. P. Kim, C. Stahl, S.-S. Xue, https://arxiv.org/abs/1909.09319, will appear soon in the proceeding of MG15 and regular scientific journal.

An overall review has been made on this subject. Recent observations of gravi-

tational waves from binary mergers of black holes or neu- tron stars and the rapid development of ultrahigh intensity laser pulses lead strong field physics to a frontier of new physics in the 21st century. Strong gravity phenomena are most precisely described by general relativity, and lasers that are described by another most precisely tested quantum electrodynamics (QED) can be focused into a tiny area in a short period through the chirped pulse amplification (CPA) and generate extremely high intensity electromagnetic (EM) fields beyond the conventional methods. It is physically interesting to study QED phenomena in curved spacetimes, in which both strong gravitational and electromagnetic fields play important roles. There are many sources for strong gravitational and electromagnetic fields in the sky or universe, such highly magnetized neutron stars, magnetized black holes, and the early universe. We review quantum field theoretical frameworks for QED both in the Minkowski spacetime and curved spacetimes, in particular, charged black holes and the early universe, and discuss QED physics in strong EM fields, such as the vacuum polarization and Schwinger pair production and their implications to astrophysics and cosmology. For details see Sang Pyo Kim https://arxiv.org/abs/1905.13439, the review article will appear soon in the proceeding of MG15 and regular scientific journal IJMPD.

We explore the enhancement of an electromagnetic field in an inflationary background with an anti-conductive plasma of scalar particles. The scalar particles are created by Schwinger effect in curved spacetime and backreact to the electromagnetic field. The possibility of a negative conductivity was recently put forward in the context of the renormalization of the Schwinger induced current in de Sitter spacetime. While a negative conductivity enhances the produced magnetic field, we find that it is too weak to seed the observed intergalactic magnetic field today. This results on pair creation in inflationary scenario is however important for primordial scenarios of magnetogenesis as the presence of a conductivity alters the spectral index of the magnetic field. This also shows on a specific example that backreaction can increase the electromagnetic field and not only suppress it. For details see Clement Stahl, Nucl. Phys. B12, 017, 2018, https://arxiv.org/abs/1806.06692

We currently consider that particles creation under the influence of both an electromagnetic field and a de Sitter (dS) spacetime is an interesting topic to probe quantum electrodynamics (QED) and quantum gravitational effects. By applying the gamma-function regularization to the in-out formulation, we find the exact one-loop effective action in the proper-time integral representation for a charged scalar field in a uniform electric field and a parallel magnetic field in a dS space, which reduces to Weisskofp-Schwinger scalar QED action in the limit of Minkowski spacetime and the one-loop action in the pure dS space. We find the consistency of the effective action with the vacuum persistence amplitude and the Schwinger effect of Phys. Rev. D 97, 025017. The effective action is analyzed for the pure dS space and QED actions in the

pure electric field in dS space and in both electric and magnetic fields. The effective action in the pure dS space consists of a series of the scalar curvature starting with the quadratic order. We explore the effect of curvature on the QED vacuum polarization and find consistency of the effective action with the perturbative expansion from the worldline formalism. The article is in preparation by E. Bavarsad, S. P. Kim, C. Stahl, S.-S. Xue.

Schwinger effect and backreaction in de Sitter spacetime

For the backreaction of created pairs on external fields, we first consider the particle-antiparticle pairs produced by both a strong electric field and de Sitter curvature. We investigate in 1 + 1 D the backreaction of the pairs on the electromagnetic field. To do so we describe the canonical quantization of an electromagnetic field in de Sitter space and add in the Einstein-Maxwell equation the fermionic current induced by the pairs. After solving this equation, we find that the electric field gets either damped or unaffected depending on the value of the pair mass and the gauge coupling. No enhancement of the electromagnetic field to support a magnetogenesis scenario is found. The physical picture is that the Schwinger pairs locally created screen the production and amplification of the electromagnetic field. However, if one considers light bosons created by the Schwinger mechanism, we report a solution to the Einstein-Maxwell equation with an enhancement of the electromagnetic field. This solution could be a new path to primordial magnetogenesis. For more details, see the reference Clement Stahl and She-Sheng Xue Physics Letters B, Volume 760, p. 288-292.

In addition, we also study the pair creation in the early universe, and present a short review in the conference proceeding of the the MG14 meeting. In the very early universe, a generalized Schwinger effect can create pairs from both electrical and gravitational fields. The expectation value of fermionic current induced by these newly created pairs has been recently computed in de Sitter spacetime. I will discuss different limiting cases of this result and some of its possible physical interpretations. See the conference proceeding of MG14, World scientific, Stahl Clément Strobel Eckhard and Xue She-Sheng

Quantum Regge calculus of Einstein-Cartan theory and its phase and critical point

We study the Quantum Regge Calculus of Einstein-Cartan theory to describe quantum dynamics of Euclidean space-time discretized as a 4-simplices complex. Tetrad field $e_\mu(x)$ and spin-connection field $\omega_\mu(x)$ are assigned to each 1-simplex. Applying the torsion-free Cartan structure equation to each 2-simplex, we discuss paral-

lel transports and construct a diffeomorphism and *local* gauge-invariant Quantum Regge Calculus of Einstein-Cartan action. Invariant holonomies of field $\omega_\mu(x)$ along large loops are also given. Quantization is defined by a bounded partition function with the measure of $SO(4)$-group valued $\omega_\mu(x)$ fields and Dirac-matrix valued $e_\mu(x)$ fields over 4-simplices complex.

We present detailed discussions and calculations of the Quantum Regge calculus of Einstein-Cartan theory. The Euclidean space-time is discretized by a four-dimensional simplicial complex. We adopt basic tetrad and spin-connection fields to describe the simplicial complex. By introducing diffeomorphism and local Lorentz invariant holonomy fields, we construct a regularized Einstein-Cartan theory for studying the quantum dynamics of the simplicial complex and fermion fields. This regularized Einstein-Cartan action is shown to properly approach to its continuum counterpart in the continuum limit. Based on the local Lorentz invariance, we derive the dynamical equations satisfied by invariant holonomy fields. In the mean-field approximation, we show that the averaged size of 4-simplex, the element of the simplicial complex, is larger than the Planck length. This formulation provides a theoretical framework for analytical calculations and numerical simulations to study the quantum Einstein-Cartan theory.

On the basis of strong coupling expansion, mean-field approximation and dynamical equations satisfied by holonomy fields, we present calculations and discussions to show the phase structure of the quantum Einstein-Cartan gravity, (i) the order phase: long-range condensations of holonomy fields in strong gauge couplings; (ii) the disorder phase: short-range fluctuations of holonomy fields in weak gauge couplings. According to the competition of the activation energy of holonomy fields and their entropy, we give a simple estimate of the possible ultra-violet critical point and correlation length for the second-order phase transition from the order phase to disorder one. At this critical point, we discuss whether the continuum field theory of quantum Einstein-Cartan gravity can be possibly approached when the macroscopic correlation length of holonomy field condensations is much larger than the Planck length. For the details of this part, see Physical Review D 82, 064039 (2010), Physics Letters B665 54 (2008), B682 (2009) 300 and B711 (2012) 404.

How universe evolves with cosmological and gravitational constants in the field theory of quantum Einstein-Cartan gravity

With a basic varying space-time cutoff $\tilde{\ell}$, we study a regularized and quantized Einstein-Cartan gravitational field theory and its domains of ultraviolet-unstable fixed point $g_{\rm ir} \gtrsim 0$ and ultraviolet-stable fixed point $g_{\rm uv} \approx 4/3$ of the gravitational gauge coupling $g = (4/3)G/G_{\rm Newton}$. Because the fundamental operators of quantum gravitational field theory are dimension-2 area operators, the cosmological con-

stant is inversely proportional to the squared correlation length $\Lambda \propto \xi^{-2}$. The correlation length ξ characterizes an infrared size of a causally correlate patch of the universe. The cosmological constant Λ and the gravitational constant G are related by a generalized Bianchi identity. As the basic space-time cutoff $\tilde{\ell}$ decreases and approaches to the Planck length $\ell_{\rm pl}$, the universe undergoes inflation in the domain of the ultraviolet-unstable fixed point $g_{\rm ir}$, then evolves to the low-redshift universe in the domain of ultraviolet-stable fixed point $g_{\rm uv}$. We give the quantitative description of the low-redshift universe in the scaling-invariant domain of the ultraviolet-stable fixed point $g_{\rm uv}$, and its deviation from the ΛCDM can be examined by low-redshift $(z \lesssim 1)$ cosmological observations, such as supernova Type Ia. For the details of this part, see Nuclear Physics B897 (2015) 326–345.

Based on above framework that Einstein equation and Hawking radiation govern Universe evolution, we present a possible understanding to the issues of cosmological constant, inflation, matter and coincidence problems based on the Einstein equation and Hawking pair production of particles and antiparticles. In this scenario, the cosmological constant is attributed to the spacetime horizon that generates matter via pair productions, in turn the matter contributes to the RHS of the Einstein equation, conversely governing the spacetime horizon. In such a way, the cosmological and matter terms are interacting via the spacetime horizon in their evolutions. As a result, the inflation naturally appears and results agree to observations. The CMB large-scale anomaly can be explained and the dark-matter acoustic wave is speculated. The cosmological term $\Omega_{_\Lambda}$ tracks down the matter term $\Omega_{_M}$ from the reheating to the radiation-matter equilibrium, then it varies very slowly, $\Omega_{_\Lambda} \propto$ constant. Thus the cosmic coincidence problem can be possibly avoided. The relation between $\Omega_{_\Lambda}$ and $\Omega_{_M}$ is obtained and can be examined at large redshifts. The details can be found in Modern Physics Letters A, (2020) 2050123 https://arxiv.org/abs/2004.10859

In details we study Cosmological Λ driven inflation and produced particles. Suppose that the early Universe starts with a quantum spacetime originated cosmological Λ-term at the Planck scale $M_{\rm pl}$. The cosmological energy density $\rho_{_\Lambda}$ drives inflation and simultaneously reduces its value to create the matter-energy density $\rho_{_M}$ via the continuous pair productions of massive fermions and antifermions. The decreasing $\rho_{_\Lambda}$ and increasing $\rho_{_M}$, in turn, slows down the inflation to its end when the pair production rate Γ_M is larger than the Hubble rate H of inflation. Such back-reaction evolutions of the density $\rho_{_\Lambda}$ and Hubble rate H are uniquely determined by two independent equations from the Einstein equation and energy conservation law, in addition, the $\rho_{_M}$ and its equation of state as functions of H are determined by continuous massive pair productions. For very massive and dense pairs $m \gg H$, $\rho_{_M} \propto m^2H^2$ and $\rho_{_\Lambda} \propto M_{\rm pl}^2H^2 > \rho_{_M}$. As a result, inflation naturally appears and theoretical results agree to Planck 2018 observations. The CMB large-scale anomaly can be possibly explained and the dark-matter acoustic wave is speculated. Suppose that the reheating

efficiently converts the cosmological energy density ρ_Λ to the matter-energy density $\rho_M \gg \rho_\Lambda$ accounting for the most relevant Universe mass, and some massive pairs decay to relativistic particles of energy density ρ_R starting the hot Big Bang. Since then, the energy density ρ_R produced at the reheating predominately governs the decreasing Hubble rate $H^2 \propto \rho_R$, and massive pair productions are small and unimportant. However, the aforementioned back reaction $\rho_M \leftrightarrow H \leftrightarrow \rho_\Lambda$ is weak but continues in standard cosmological evolution. As a consequence, the cosmological energy density ρ_Λ closely tracks down the energy density ρ_R from the reheating end up to the radiation-matter equilibrium, then it varies very slowly, $\rho_\Lambda \propto$ constant, due to the transition from radiation dominate to matter dominate epoch. Therefore the cosmic coincidence problem can be possibly avoided. The relation between ρ_Λ and radiation and matter-energy densities is obtained and can be examined at large redshifts. For more details, see https://arxiv.org/abs/1910.03938

In addition, we study Cosmological Λ converts to reheating energy and cold dark matter. Suppose that the early Universe starts with a quantum spacetime originated cosmological Λ-term at the Planck scale $M_{\rm pl}$. The cosmological energy density ρ_Λ drives inflation and simultaneously reduces its value to create the pair-energy density ρ_M via the continuous pair productions of massive fermions and antifermions. The decreasing ρ_Λ and increasing ρ_M, in turn, slows down the inflation to its end when the pair production rate Γ_M is larger than the Hubble rate H of inflation. A large number of massive pairs is produced and reheating epoch starts. In addition to Einstein equation and energy-conservation law, we introduce the Boltzmann-type rate equation describing the number of pairs produced from (annihilating to) the spacetime, and reheating equation describing massive unstable pairs decay to relativistic particles and thermodynamic laws. This forms a close set of four independent differential equations uniquely determining H, ρ_Λ, ρ_M and radiation-energy density ρ_R, given the initial conditions at inflation end. Numerical solutions demonstrate three episodes of preheating, massive pairs dominate and genuine reheating. Results show that ρ_Λ can efficiently convert to ρ_M by producing massive pairs, whose decay accounts for reheating ρ_R, temperature and entropy of the Big-Bang Universe. The stable massive pairs instead account for cold dark matter. Using CMB and baryon number-to-entropy ratio measurements, we constrain effective mass of pairs, Yukawa coupling and degeneracies of relativistic particles. As a result, the obtained inflation e-folding number, reheating scale, temperature and entropy are in terms of the tensor-to-scalar ratio in the theoretically predicated range $0.042 \lesssim r \lesssim 0.048$, consistently with current observations. For details, see https://arxiv.org/abs/2006.15622

Moreover, we study Horizon crossing causes baryogenesis, magnetogenesis and dark-matter acoustic wave. Sapcetime $\mathcal{S}$ produces massive particle-antiparticle pairs $\bar{F}F$ that in turn annihilate to spacetime. Such back and forth gravitational process

$S \Leftrightarrow \bar{F}F$ is described by Boltzmann-type cosmic rate equation of pair-number conservation. This cosmic rate equation, Einstein equation, and the reheating equation of pairs decay to relativistic particles completely determine the horizon H, cosmological energy density, massive pair and radiation energy densities in reheating epoch. Moreover, oscillating $S \Leftrightarrow \bar{F}F$ process leads to the acoustic perturbations of massive particle-antiparticle symmetric and asymmetric densities. We derive wave equations for these perturbations and find frequencies of lowest lying modes. Comparing their wavelengths with horizon variation, we show their subhorion crossing at preheating, and superhorizon crossing at reheating. The superhorizon crossing of particle-antiparticle asymmetric perturbations accounts for the baryogenesis of net baryon numbers, whose electric currents lead to magnetogenesis. The baryon number-to-entropy ratio, upper and lower limits of primeval magnetic fields are computed in accordance with observations. Given a pivot comoving wavelength, it is shown that these perturbations, as dark-matter acoustic waves, originate in pre-inflation and return back to the horizon after the recombination, possibly leaving imprints on the matter power spectrum at large length scales. Due to the Jeans instability, tiny pair-density acoustic perturbations in superhorizon can be amplified to the order of unity. Thus their amplitudes at reentry horizon become non-linear and maintain approximately constant physical sizes, and have physical influences on the formation of large scale structure and galaxies. For details, see https://arxiv.org/abs/2007.03464

Using this model, we compare supernovae and Baryon Acoustic Oscillations data to the predictions of a cosmological model of interacting dark matter and dark energy. This theoretical model can be derived from the effective field theory of Einstein-Cartan gravity with two scaling exponents δ_G and δ_Λ, related to the interaction between dark matter and dark energy. We perform a χ^2 fit to the data to compare and contrast it with the standard ΛCDM model. We then explore the range of parameter of the model which gives a better χ^2 than the standard cosmological model. All those results lead to tight constraints on the scaling exponents of the model. Our conclusion is that this class of models, provides a decent alternative to the ΛCDM model. For details see Damien Bégué, Clément Stahl and She-Sheng Xue "A model of interacting dark fluids tested with supernovae and Baryon Acoustic Oscillations data" Nuclear Physics, Section B, Volume 940, p. 312-320

Recently, with Chinese colleagues Li-Yang Gao and Xin Zhang, we study the problem of H_0 tension by using this cosmological model, shedding light on cosmological model from H_0 tension. It is a recent important issue in cosmology that the standard model ΛCDM resultant H_0 value has a 4.2σ tension with the local measurement $H_0 = (74.03 \pm 1.42)$ km s^{-1}Mpc^{-1}. We analyse the variant model of ΛCDM by scaling the matter term $\rho_{M,R}(1+z)^{-\delta_G}$ and cosmological term $\rho_\Lambda(1+z)^{\delta_\Lambda}$, which is motivated by the asymptotic safety of gravity theory, due to Weinberg. Separately using the CMB, BAO and SN with and without the H_0 data sets to constrain the

model parameters $|\delta_G| \ll 1$ and $|\delta_\Lambda| \ll 1$, we study how the H_0 tension is alleviated to 0.59σ, compare and contrast it to ΛCDM, wCDM, $\Lambda(t)$CDM and CPL models. Our results show the model is the probably best approximation to the data sets according to AIC and BIC criteria. We discuss the possible reasons for the H_0 tension and why the model can relieve the tension. For details, see Reference JCAP 07 (2021) 005, https://arxiv.org/abs/2101.10714.

In the recent progress on massive particle pair production and oscillation in Friedman Universe: its consequence on inflation, we study the Friedman equation for the time-varying cosmological term and Hubble function H, and quantised field equation for massive modes $M \gg H$. Classical slow components $\mathcal{O}(H^{-1})$ and quantum fast components $\mathcal{O}(M^{-1})$ are coupled. Numerically solving these equations, we show the production of particle-antiparticle pairs and the oscillation of pair density and pressure. Their quantum-time averages effectively modify the classical equation. We present resultant impacts and consequences on inflation. The obtained relation of spectral index and tensor-to-scalar ratio agrees with recent observations.

Quantum Einstein-Cartan theory with four-fermion interactions and its resulted particle mass spectra for matter and dark matter

In the fermion content and gauge symmetry of the standard model (SM), we study the four-fermion operators in the torsion-free quantum Einstein-Cartan theory. The collider signatures of irrelevant operators are suppressed by the high-energy cutoff (torsion-field mass) Λ, and cannot be experimentally accessible at TeV scales. Whereas the dynamics of relevant operators accounts for (i) the SM symmetry-breaking in the domain of infrared-stable fixed point with the energy scale $v \approx 239.5$ GeV and (ii) composite Dirac particles restoring the SM symmetry in the domain of ultraviolet-stable fixed point with the energy scale $\mathcal{E} \gtrsim 5$ TeV. To search for the resonant phenomena of composite Dirac particles with peculiar kinematic distributions in final states, we discuss possible high-energy processes: multi-jets and dilepton Drell-Yan process in LHC $p\,p$ collisions, the resonant cross-section in e^-e^+ collisions annihilating to hadrons and deep inelastic lepton-hadron $e^-\,p$ scatterings. To search for the nonresonant phenomena due to the form-factor of Higgs boson, we calculate the variation of Higgs-boson production and decay rate with the CM energy in LHC. We also present the discussions on four-fermion operators in the lepton sector and the mass-squared differences for neutrino and sterile neutrinos, as well as its resulted particle spectra for matter and the candidates for dark matter. We also present the discussions on the fermion-mass generation and vectorlike gauge-boson coupling due to the four-fermion operators in Quantum Einstein-Cartan theory For the details this part, see " Resonant and nonresonant phenomena as well as fermion-mass generations due to the four-fermion operators in quantum Einstein-Cartan theory"

Physics Letters B744 88–94 (2015), B737 (2014) 172, B727, 308 (2013), B721 (2013) 347, and Physics Review D 93, 073001 (2016), JHEP 11, 027 (2016), JHEP 05, 146 (2017). Also, we study the LHC phenomenology, see the European Physical Journal C volume 80, Article number: 309 (2020), https://arxiv.org/abs/1810.11420.

Recently, we explain the phenomenology of Xenon1T experiment in terms of sterile neutrinos of dark matter candidates, The XENON1T collaboration recently reported the excess of events from recoil electrons, possibly giving an insight into new area beyond the Standard Model (SM) of particle physics. We try to explain this excess by considering effective interactions between the sterile neutrinos and the SM particles. In this paper, we present an effective model based on one-particle-irreducible interaction vertices at low energies that are induced from the SM gauge symmetric four-fermion operators at high energies. The effective interaction strength is constrained by the SM precision measurements, astrophysical and cosmological observations. We introduce a novel effective electromagnetic interaction between sterile neutrinos and SM neutrinos, which can successfully explain the XENON1T event rate through inelastic scattering of the sterile neutrino dark matter from Xenon electrons. We find that sterile neutrinos with masses around 90 keV and specific effective coupling can fit well with the XENON1T data where the best fit points preserving DM constraints and possibly describe the anomalies in other experiments. For details, see Soroush Shakeri, Fazlollah Hajkarim, She-Sheng Xue "Shedding New Light on Sterile Neutrinos from XENON1T Experiment ", JHEP12 (2020) 194, https://arxiv.org/abs/2008.0

In addition, in this theoretical framework, we study the Peccei-Quinn (PQ) symmetry of sterile right-handed neutrino sector and the gauge symmetries of the Standard Model (SM). Due to four-fermion interactions, spontaneous breaking of these symmetries at the electroweak scale generates top-quark Dirac mass and sterile-neutrino Majorana mass. The top quark channels yields massive Higgs, $W^{\pm}$ and Z^0 bosons. The sterile neutrino channel yields the heaviest sterile neutrino Majorana mass, sterile Nambu-Goldstone axion (or majoron) and massive scalar χboson ($m_\chi \sim 10^2$ GeV). Their tiny couplings to SM particles are effectively induced by four-fermion operators. We show that such sterile axion is the PQ solution to the strong CP problem. The lightest sterile neutrino ($m_N^e \sim 10^2$ keV), sterile QCD axion ($m_a < 10^{-6}$ eV, $g_{a\gamma} < 10^{-13}\text{GeV}^{-1}$)and χboson can be dark matter particle candidates, for their tiny couplings and long lifetimes inferred from the Xenon1T experiment. The axion and χboson couplings to SM particles are below the values reached by current laboratory experiments and astrophysical observations for directly or indirectly detecting dark matter particles. For details, see https://arxiv.org/abs/2012.04648

In addition, we have also generalized our study to the solid state physics. Our goal is to understand the phenomena arising in optical lattice fermions at low temperature in an external magnetic field. Varying the field, the attraction between any two fermions can be made arbitrarily strong, where composite bosons form via so-

called Feshbach resonances. By setting up strong-coupling equations for fermions, we find that in spatial dimension they couple to bosons which dress up fermions and lead to new massive composite fermions. At low enough temperature, we obtain the critical temperature at which composite bosons undergo the Bose–Einstein condensate (BEC), leading to BEC-dressing massive fermions. These form tightly bound pair states which are new bosonic quasi-particles producing a BEC-type condensate. A quantum critical point is found and the formation of condensates of complex quasi-particles is speculated over. For details, see Hagen Kleinert, She-Sheng Xue, "Composite fermions and their pair states in a strongly-coupled Fermi liquid", Nuclear Physics B. Volume 936, November 2018, Pages 352-363.

Fractal matter distribution and supernovae

Recently, we report here a work on a simple inhomogeneous cosmological model within the Lemaître-Tolman-Bondi (LTB) metric. The mass-scale function of the LTB model is taken to be $M(r) \propto r^d$ and would correspond to a fractal distribution for $0 < d < 3$. The luminosity distance for this model is computed and then compared to supernovae data. Unlike LTB models which have in the most general case two free functions, our model has only two free parameters as the flat standard model of cosmology. The best fit obtained is a matter distribution with an exponent of $d = 3.44$. Finally by adding an upper cutoff on the scale $r = 2300$ Mpc, we find a better fit than the simple fractal model with an exponent $d = 3.36$. For some details, see the reference, C. Stahl, R. Ruffini, the conference proceedings of the 15th Italian and Korean meeting, Pescara Italy July, 2015, World scientific, Singapore. The proceeding is published together with the MG XIV proceedings.

Testing the cosmological parameters and isotropy principle by use of gamma-ray bursts data

We perform a model independent analysis to study the constraints on the cosmological parameter by use of gamma-ray bursts data. Most gamma-ray bursts have higher redshifts than the traditional probes, such as SNe Ia. We employ 118 long gamma-ray bursts to constrain the cosmological parameter in model independent manner. We find the best value indicates $\Omega_{m0} = 0.32$, which is consistent with other latest observations, like Planck CMB 2015 released result.

A cosmological preferred direction was reported from the type Ia supernovae (SNe Ia) data in recent years. Most gamma-ray bursts have higher redshifts than SNe Ia. We use the long gamma-ray bursts data to give a simple classification of such studies for the first time. Because the maximum anisotropic direction is independent of isotropic cosmological models, we adopt two cosmological models (ΛCDM,

wCDM) for the hemisphere comparison analysis and ΛCDM model for dipole fit approach. In hemisphere comparison method, the matter density and the equation of state of dark energy are adopted as the diagnostic qualities in the ΛCDM model and wCDM model, respectively. In dipole fit approach, we fit the fluctuation of distance modulus. We find that there is a null signal for the hemisphere comparison method, while a preferred direction ($b = -14.3^\circ \pm 10.1^\circ, l = 307.1^\circ \pm 16.2^\circ$) for the dipole fit method. This result indicates that the dipole fit is more sensitive than the hemisphere comparison method. Y. Wang, X. F. Yang, C. Stahl, R. Ruffini .

In addition, we study that the cosmological black holes are black holes living not in an asymptotically flat universe but in an expanding spacetime. They have a rich dynamics in particular for their mass and horizon. In this article we perform a natural step in investigating this new type of black hole: we consider the possibility of a charged cosmological black hole. We derive the general equations of motion governing its dynamics and report a new analytic solution for the special case of the charged Lemaitre-Tolman-Bondi equations of motion that describe a charged cosmological black hole. We then study various relevant quantities for the characterization of the black hole such as the C-function, the effect of the charge on the black hole flux and the nature of the singularity. We also perform numerical investigations to strengthen our results. Finally we challenge a model of gamma ray burst within our framework. For details, see R. Moradi, C. Stahl, J. Firouzjaee, S.-S. Xue, "Charged cosmological black hole" Phys. Rev. D 96, 104007 (2017).

3.11. Semiclassical approach to pair production rate for strong time-dependent electrical fields with more than one component

Semi-classical description of pair production in a general electric field

In review Section 6, after recalling studies of pair production in inhomogeneous electromagnetic fields in the literature by Dunne and Schubert (2005a); Dunne et al. (2006); Dunne and Wang (2006); Kim and Page (2002, 2006, 2007), we present a brief review of our recent work Kleinert et al. (2008) where the general formulas for pair production rate as functions of either crossing energy level or classical turning point, and total production rate are obtained in external electromagnetic fields which vary either in one space direction $E(z)$ or in time $E(t)$. In Sections 6.1 and 6.2, these formulas are explicitly derived in the JWKB approximation and generalized to the case of three-dimensional electromagnetic configurations. We apply these formulas to several cases of such inhomogeneous electric field configurations, which are classified

into two categories. In the first category, we study two cases: a semi-confined field $E(z) \neq 0$ for $z \lesssim \ell$ and the Sauter field

$$E(z) = E_0/\cosh^2(z/\ell), \quad V(z) = -\sigma_s m_e c^2 \tanh(z/\ell),$$

where ℓ is width in the z-direction, and

$$\sigma_s \equiv eE_0\ell/m_e c^2 = (\ell/\lambda_C)(E_0/E_c).$$

In these two cases the pairs produced are not confined by the electric potential and can reach an infinite distance. The resultant pair production rate varies as a function of space coordinate. The result we obtained is drastically different from the Schwinger rate in homogeneous electric fields without any boundary. We clearly show that the approximate application of the Schwinger rate to electric fields limited within finite size of space overestimates the total number of pairs produced, particularly when the finite size is comparable with the Compton wavelength λ_C, see article Figs. 6.2 and 6.3 where it is clearly shown how the rate of pair creation far from being constant goes to zero at both boundaries. The same situation is also found for the case of the semi-confined field $z(z) \neq 0$ for $|z| \lesssim \ell$, see Eq. (6.3.34). In the second category, we study a linearly rising electric field $E(z) \sim z$, corresponding to a harmonic potential $V(z) \sim z^2$, see Figs. 6.1. In this case the energy spectra of bound states are discrete and thus energy crossing levels for tunneling are discrete. To obtain the total number of pairs created, using the general formulas for pair production rate, we need to sum over all discrete energy crossing levels, see Eq. (6.4.11), provided these energy levels are not occupied. Otherwise, the pair production would stop due to the Pauli principle.

Semiclassical approach to pair production rate for strong time-dependent electrical fields with more than one component

Since Sauter in 1931 Sauter (1931) and Heisenberg and Euler Heisenberg and Euler (1936) four years later gave a first description of the vacuum properties of QED, there have been a lot of investigations of the pair creation rate in strong electric fields. In particular, Schwinger Schwinger (1951, 1954a,b) reformulated their result in an elegant way using quantum-field theoretic methods (see also Nikishov (1970); Batalin and Fradkin (1970b)).
The formulation was extended to space-time-dependent fields using different methods, e.g. the imaginary time method Brezin and Itzykson (1970); Popov (1972d,c, 1973b); Marinov and Popov (1977); Popov (2001b) and a tunneling picture Kleinert (2008); Kleinert and Xue (2013), both using WKB-approximations or the world-line instanton method Dunne and Schubert (2005b); Dunne et al. (2006).

By comparing numerical with analytic results it was found that for more complicated field configurations, i.e. for those which have more than one distinct pair of semiclassical turning points, interference effects arise. This was already discussed as a resonance effect for oscillating fields in Popov (1973). Interference effects were recently studied in Dumlu and Dunne (2010, 2011b) for the WKB-method and in Dumlu and Dunne (2011a) for the world-line instanton approach. In this study we consider only fields with one dominant pair of turning points where interference effects are negligible. This enables us to use scalar quantum-electrodynamics, since it is known to give the same results as spinor quantum electrodynamics at the leading non-perturbative order if there are no interference effects Dumlu and Dunne (2011b). All the analytic methods mentioned above give the same results for electric fields with only one component depending on either space or time. A more general case, namely electric fields with two or three components depending on space was discussed in Dunne and Wang (2006) in the world-line instanton approach.
A special case namely a (two component) rotating electrical field was discussed in Popov (1973b). Recently pair production in rotating fields has been studied numerically in Blinne and Gies (2013) using the Wigner formalism. These results can be used to calculate the pair creation rate of a plane wave in a plasma as shown in Bulanov et al. (2003).
So far, electron-positron pair production has not been directly observed in experiments due to the necessity of high field strengths which are out of the range reached by nowadays laser systems. However recent theoretical investigations have shown that less strong fields are needed if one uses carefully-shaped multi-component laser pulses Schützhold et al. (2008); Dunne et al. (2009); Bell and Kirk (2008); Di Piazza et al. (2009); Monin and Voloshin (2010a,b); Heinzl et al. (2010); Bulanov et al. (2010). For this reason, we generalize the above mentioned analytic methods to compute the pair creation rate for a general time-dependent periodic electrical field which is characterized by the potential

$$A_\mu(t) = [0, A_1(t), A_2(t), A_3(t)] = \frac{1}{e\,c}[0, V_1(t), V_2(t), V_3(t)]. \tag{3.11.1}$$

To do so we use the WKB-approximation as well as the world-line instanton method of Dunne et al. (2006).
As is well known, the WKB approach the pair creation rate per volume V takes the general form (see, e.g., Kleinert (2008); Kleinert and Xue (2013))

$$\frac{\Gamma_{\mathrm{WKB}}}{V} \sim \int \frac{d^3P}{(2\pi\hbar)^3} \exp\left(-\pi \frac{E_c}{E_0} G(\vec{P})\right). \tag{3.11.2}$$

where the integral over $\vec{P}$ is over the momentum modes of the produced pairs. We introduce the critical electrical field

$$E_c = \frac{m^2 c^3}{e\hbar}. \tag{3.11.3}$$

In Eq. (3.11.2) E_0 is a characteristic electric field strength and $G(\vec{P})$ is a function depending on the explicit form of the electric field, which is straightforwardly generalized to more than one component.
We find that if the momentum spectrum $\exp(-\pi E_c / E_0 G(\vec{P}))$ is peaked around zero canonical momentum $\vec{P} = 0$ it can be approximated by expanding around this point and it is possible to simplify the result via Gaussian integration.
In the world-line instanton framework of Dunne et al. (2006) the momentum, arising as an integration constant, was implicitly taken to vanish with a Gaussian momentum integration producing the prefactors, as discussed in Dumlu and Dunne (2011a). We argue that this is a *de facto* expansion around $\vec{P} = 0$. We generalize this method to the case of electric fields with more than one component and show that the result agrees with the WKB result expanded around $\vec{P} = 0$.
The momentum spectrum is usually peaked around $\vec{P} = 0$ for the examples of one-component fields studied in the literature (see, e.g., Dunne et al. (2006)). Thus the expansion around $\vec{P} = 0$ presents a good approximation. However this situation changes if one goes to the case of two-component fields. By looking at rotating electric fields we find that their momentum spectra are not peaked around $\vec{P} = 0$.
If the momentum spectrum is not peaked around $\vec{P} = 0$ one can not use the expanded WKB result since it does not present a good approximation. Also the world-line instanton method of Dunne et al. (2006) and the generalized form presented here implicitly require the momentum spectrum to be peaked around $\vec{P} = 0$. This implies that it is not appropriate to calculate the pair production rate for cases where the momentum spectrum is not peaked around $\vec{P} = 0$ in the form discussed here.
Rotating field configurations such as the one studied here are of interest since they are related to circularly-polarized laser waves. A circularly-polarized wave in medium can be described by a rotating electric field, since it is possible to make a transformation into the co-moving Lorentz frame (see, e.g., Bulanov et al. (2003)).
Recently it has become obvious that the pair production rate of lasers depends sensitively on the pulse shape Schützhold et al. (2008); Dunne et al. (2009); Bell and Kirk (2008); Di Piazza et al. (2009); Monin and Voloshin (2010a,b); Heinzl et al. (2010); Bulanov et al. (2010). For the design of feasible experiments to directly measure pair production it is therefore of interest to find a pulse profile which enhances this process. Obviously for complicated laser pulse profiles the calculation has to be done numerically. The development of semiclassical analytical methods discussed in this study certainly helps to provide some physical intuition for these numerical simula-

tions. For the details of this part, see E. Strobel and S.-S. Xue, Nuclear Physics B 886, 1153 (2014).

Using semiclassical WKB-methods, we calculate the rate of electron- positron pair-production from the vacuum in the presence of two external fields, a strong (space- or time-dependent) classical field and a monochromatic electromagnetic wave. We discuss the possible medium effects on the rate in the presence of thermal electrons, bosons, and neutral plasma of electrons and protons at a given temperature and chemical potential. Using our rate formula, we calculate the rate enhancement due to a laser beam, and discuss the possibility that a significant enhancement may appear in a plasma of electrons and protons with self-focusing properties. For details of this part, see H. Kleinert and S.-S. Xue, "Vacuum pair-production in a classical electric field and an electromagnetic wave", Annals of Physics 333 (2013) 104.

By using this approach, we semiclassically investigate Schwinger pair production for pulsed rotating electric fields depending on time. To do so we solve the Dirac equation for two-component fields in a WKB-like approximation. The result shows that for two-component fields the spin distribution of produced pairs is generally not 1:1. As a result the pair creation rates of spinor and scalar quantum electro dynamics (QED) are different even for one pair of turning points. For rotating electric fields the pair creation rate is dominated by particles with a specific spin depending on the sense of rotation for a certain range of pulse lengths and frequencies. We present an analytical solution for the momentum spectrum of the constant rotating field. We find interference effects not only in the momentum spectrum but also in the total particle number of rotating electric fields. For the details of this part, see E. Strobel and S.-S. Xue Physics Review D 91, 045016 (2015).

Nonlinear Breit-Wheeler process in the collision of a photon with two plane waves

Electron-positron pair creation by the collision of two real photons (Breit-Wheeler process [Breit and Wheeler, Phys. Rev. 46, 1087 (1934)]) is one of most relevant elementary processes in high-energy astrophysics. It can lead to observable effects such as cutoff in the high-energy Gamma spectra. In order to access the observations of this fundamental phenomenon in the earth-based experiments, the generalization of the Breit-Wheeler process to the nonlinear Breit-Wheeler process of pair production in the collision a photon with an intensive monochromatic plane wave has been fully analyzed and discussed in the past few decades [e.g., Reiss, J. Math. Phys. 3, 59 (1962) and Ritus, J. Sov. Laser Res. 6, 497 (1985)]. Such a nonlinear Breit-Wheeler process has been detected in the SLAC-E-144 experiment [Burke et al., Phys. Rev. Lett. 79, 1626 (1997)]. In this article, we analyzed the nonlinear Breit-Wheeler process of pair production off a probe photon colliding with a bifrequent field. The

bifrequent field is composed of a low-frequency and a high-frequency electromagnetic wave that propagate in the same direction. We calculate the pair-production probability and the spectra of created pairs in the nonlinear Breit-Wheeler processes of pair production off a probe photon colliding with two plane waves or one of these two plane waves. The differences of these two cases are discussed. We evidently show, in the two-wave case, the possibility of Breit-Wheeler pair production with simultaneous photon emission into the low-frequency wave and the high multiphoton phenomena: (i) Breit-Wheeler pair production by absorption of the probe photon and a large number of photons from the low-frequency wave, in addition to the absorption of one photon from the high-frequency wave; (ii) Breit-Wheeler pair production by absorption of the probe photon and one photon from the high-frequency wave with simultaneous emission of a large number of photons into the low-frequency wave. The phenomenon of photon emission into the wave cannot happen in the one-wave case. Compared with the one-wave case, the contributions from high multiphoton processes are largely enhanced in the two-wave case. A multipeak structure of the spectra (multipeak structure) of created e^- e^+ pairs in the two-wave process is shown, as a result of the effects of the phenomenon of pair production with simultaneous photon emission into the low-frequency wave and high multiphoton (absorption and emission) phenomenon. The results presented in this article show a possible way to access the observations of the phenomenon of photon emission into the wave and high multiphoton phenomenon in Breit-Wheeler pair production even with the laser-beam intensity of order 10^{18} W/cm^2. For the details of this part, see Yuan-Bin Wu and S.-S. Xue, Physics Review D 90, 013009 (2014).

Fractional Effective Action at strong electromagnetic fields

In 1931 Sauter Sauter (1931) and four years later Heisenberg and Euler Heisenberg and Euler (1936) provided a first description of the vacuum properties of QED. They identified a characteristic scale of strong field $E_c = m_e^2 c^3/e\hbar$, at which the field energy is sufficient to create electron positron pairs from the vacuum, and calculated an effective Lagrangian that will replace the Maxwell Lagrangian at strong fields. In 1951, Schwinger Schwinger (1951, 1954a,b) gave an elegant quantum-field theoretic reformulation of their result in the spinor and scalar QED framework (see also Nikishov (1970); Batalin and Fradkin (1970b)). The description was further extended to space-time dependent electromagnetic fields in Refs. Popov (1972d,c, 2001b); Narozhnyi and Nikishov (1970); Schubert (2001); Dunne and Schubert (2005b); Kleinert and Xue (2013). The monographs Itzykson and Zuber (2006); Kleinert (2008); Greiner et al. (1985); Grib et al. (1980); Fradkin et al. (1991) and the recent review articles Dunne and Schubert (2000); Dunne (2005); Ruffini et al. (2010) can be consulted for more detailed calculations, discussions and bibliographies. Since then, the properties of

QED in strong electromagnetic fields have become vast arena of theoretical research, awaiting experimental verification as well as further theoretical understanding.

An interesting aspect of effective field theories in the strong-field limit has recently been emphasized in a completely different class of quantum field theories. These have the property of developing in the strong-field limit an anomalous power behavior. It is experimentally observable at the critical point in second-order phase transitions, and for this reason such a power behavior is also called *critical behavior*. Such a behavior arises if the the so-called beta function (also called the Stueckelberg–Petermann function or the Gell-Mann–Low function) Stueckelberg and Petermann (1953); Gell-Mann and Low (1954), which governs the logarithmic growth of the coupling strength for varying energy scale, has a fixed point in the infrared. In such theories, it is possible to take the theory to the limit of infinite coupling strength. The effective action can usually be calculated in perturbation theory as a power series in the fields. The coefficients are the one-particle irreducible n-point vertex functions of the theory. In the limit of large field strength, this power series can be shown to develop an anomalous power behavior with irrational exponents Kleinert and Frohlinde (2001); Kleinert. Also the gradient terms in this effective action show anomalous powers Kleinert (2012).

In QED such a fixed point is presently believed to be absent Suslov (2001), even though many authors have in the past argued that it may exist Johnson et al. (1963, 1964); Maris et al. (1964, 1965); Frishman (1965) and could ultimately explain the numerical value of the fine structure constant. In this study we shall not assume the existence of such a fixed point, but point out that at strong fields, the effective action exhibits nevertheless a power behavior that is typical for critical phenomena.

We conclude that in the strong fields expansion, the leading order behavior of the Euler-Heisenberg effective Lagrangian is logarithmic, and can be formulated as a power law for three different cases:

1. $|S/P| \gg 1$,
2. ϵ, $\beta \gg E_c$ and $\epsilon/\beta \sim \mathcal{O}(1)$,
3. $|P/S| \gg 1$.

The the general form is the same for scalar and spinor QED. The only difference is a factor of four in the anomalous power δ.

We have not been able to conclude a result for $S, P \gg E_c^2$. This case is equivalent to $|\vec{E}| \gg |\vec{B}| \gg E_c$ or $|\vec{B}| \gg |\vec{E}| \gg E_c$ while the fields are almost parallel. If we combine the result

$$\mathcal{L}^{\Re} = \frac{1}{2} E_c^{-\delta} (\vec{E}^2 - \vec{B}^2) |\vec{E}^2 - \vec{B}^2|^{\delta/2} + \ldots, \tag{3.11.4}$$

for the cases 1. and the result

$$\mathcal{L}^{\Re} = \frac{1}{2} E_c^{-\delta} (\vec{E}^2 - \vec{B}^2) |\vec{E} \cdot \vec{B}|^{\delta/2} + \ldots, \tag{3.11.5}$$

for the cases 3. with the anomalous power $\delta := e^2/12\pi$, we can conjecture the more general result:

$$\mathcal{L}_{\text{eff}} = \frac{1}{2} E_c^{-2\delta} (\vec{E}^2 - \vec{B}^2) \left(|\vec{E}^2 - \vec{B}^2| |\vec{E} \cdot \vec{B}| \right)^{\delta/2} + \ldots. \tag{3.11.6}$$

This correctly reduces to the cases 1. and 3. in the respective limits and thus is more general. As a result, Eq. (3.11.6) defines a fractional formulation for the QED in the regime of strong fields. Thus our finding exhibits an interesting similarity to the fractional quantum field theory discussed in Kleinert (2012).

The Euler-Heisenberg-Lagrangian is obtained in the configuration of constant electromagnetic fields. Nevertheless, for the case of smooth and slow variations of electromagnetic fields in space and time, it can be approximately used to study interesting effects like light-by-light scattering, photon splitting or electron-positron pair production (for reviews see Dunne (2005); Ruffini et al. (2010)). This implies that the fractional QED obtained in this article could find some applications in the regime of strong electromagnetic fields. This is particularly important for the recent rapid developments of experimental facilities using novel strong laser sources to reach the field strength and intensity of theoretical interest. Such facilities include the Extreme Light Infrastructure (ELI)[1], the Exawatt Center for Extreme Light studies (XCELS)[2], or the High Power laser Energy Research (HiPER)[3] facility, which are planned to exceed powers of 100 PW. Both theoretical and experimental studies of the QED of strong electromagnetical fields at the Sauter-Euler-Heisenberg scale E_c promise to become increasingly fascinating in the coming years. For the details of this part, see H. Kleinert, E. Strobel and S.-S. Xue, "Fractional Effective Action at strong electromagnetic fields", Physics Review D88, 025049 (2013).

[1] http://www.extreme-light-infrastructure.eu/
[2] http://www.xcels.iapras.ru/
[3] http://www.hiper-laser.org/

3.12. Pair-production, ultra-high energy particles, gravitational and electromagnetic energies in gravitational collapse and accretion processes

Electron and positron pair-production in gravitational collapses

We attempt to study possible electric processes in the dynamical perturbations of neutral stellar cores. These dynamical perturbations can be caused by either the gravitational collapse or pulsation of neutral stellar cores. The basic equations are the Einstein-Maxwell equations and those governing the particle number and energy-momentum conservation

$$\begin{aligned}(\bar{n}_{e,B}U^{\nu}_{e,B})_{;\nu} &= 0,\\ G_{\mu\nu} &= -8\pi G(T_{\mu\nu}+T^{\rm em}_{\mu\nu}),\\ (T^{\nu}_{\ \mu})_{;\nu} &= -F_{\mu\nu}J^{\nu},\\ F^{\mu\nu}_{\ \ ;\nu} &= 4\pi J^{\mu},\end{aligned} \tag{3.12.1}$$

in which the Einstein tensor $G_{\mu\nu}$, the electromagnetic field $F^{\mu\nu}$ (satisfying $F_{[\alpha\beta,\gamma]}=0$) and its energy-momentum tensor $T^{\rm em}_{\mu\nu}$ appear; $U^{\nu}_{e,B}$ and $\bar{n}_{e,B}$ are, respectively, the four velocities and proper number-densities of the electrons and baryons. The electric current density is

$$J^{\mu}=e\bar{n}_{p}U^{\mu}_{B}-e\bar{n}_{e}U^{\mu}_{e}, \tag{3.12.2}$$

where $\bar{n}_{p}$ is the proper number-density of the positively charged baryons. The energy-momentum tensor $T^{\mu\nu}=T^{\mu\nu}_{e}+T^{\mu\nu}_{B}$ is taken to be that of two simple perfect fluids representing the electrons and the baryons, each of the form

$$T^{\mu\nu}_{e,B} = \bar{p}_{e,B}g^{\mu\nu}+(\bar{p}_{e,B}+\bar{\rho}_{e,B})U^{\mu}_{e,B}U^{\nu}_{e,B}, \tag{3.12.3}$$

where $\bar{\rho}_{e,B}(r,t)$ and $\bar{p}_{e,B}(r,t)$ are the respective proper energy densities and pressures. Baryon fluid and electron fluid are separately described for the reason that in addition to baryons being much more massive than electrons, the EOS of baryons $\bar{p}_{B}=\bar{p}_{B}(\bar{\rho}_{B})$ is very different from the electron one $\bar{p}_{e}=\bar{p}_{e}(\bar{\rho}_{e})$ due to the strong interaction. Therefore, in the dynamical perturbations of neutral stellar cores, one should not expect that the space-time evolution of number density, energy density, four velocity, and pressure of baryon fluid be identical to the space-time evolution of counterparts of electron fluid. The difference of space-time evolutions of two fluids results in the electric current J^{μ} and field $F^{\mu\nu}$, possibly leading to some electric pro-

cesses. In a simplified model for the dynamical perturbations of neutral stellar cores, we approximately study possible electric processes by assuming that the equilibrium configurations of neutral stellar cores are initial configurations.

As a result, we find that total electric field, electron number density, energy density, and pressure oscillate around their equilibrium configurations. These oscillations with frequency $\omega = \tau_{\rm osci}^{-1} \sim 1.5m_e$ around the equilibrium configuration take place in a thin layer of a few Compton lengths around the boundary of baryon core, which undergo the dynamical perturbations caused by the gravitational collapse or pulsation. Suppose that the dynamical perturbation of the baryon core is caused by either the gravitational collapse or pulsation of the baryon core, that gains the gravitational energy. Then, in this oscillating process, energy transforms from the dynamical perturbation of the baryon core to the electron fluid via an oscillating electric field. This can been seen from the energy conservation along a flow line of the electron fluid for $v_e \neq v_p$

$$U_e^\mu (T^\nu{}_\mu)_{;\nu} = e\bar{n}_p F_{\mu\nu} U_e^\mu U_B^\nu = e\bar{n}_p \gamma_e \gamma_B (v_p - v_e) g_{rr} E. \tag{3.12.4}$$

The energy densities of the oscillating electric field and electron fluid are converted from one to another in the oscillating process with frequencies $\omega \sim \tau_{\rm osci}^{-1} \sim 1.5m_e$ around the equilibrium configuration. Oscillating electric fields $E(r,t) > E_{\rm eq}(r)$, this leads to electron-positron pair production in strong electric fields and converts electric energy into the energy of electron-positron pairs, provided the pair-production rate $\tau_{\rm pair}^{-1} \approx 6.6m_e$ is faster than the oscillating frequency $\omega = \tau_{\rm osci}^{-1}$.

It is an assumption that the gravitationally collapsing process is represented by the sequence of events: the baryon core starts to collapse from rest by gaining gravitational energy, the increasing Coulomb energy results in decreasing kinetic energy and slowing down the collapse process, the electric processes mentioned above convert the Coulomb energy into the radiative energy of electron-positron pairs, and as a result the baryon core restarts to accelerate the collapse process by further gaining gravitational energy. This indicates that in the gravitationally collapsing process, the gravitational energy must be partly converted into the radiative energy of electron-positron pairs. By summing over all events in the sequence of the gravitationally collapsing process, we approximately estimate the total number and energy of electron-positron pairs produced in the range $R_c \sim 5 \times 10^5 - 10^7$cm: from 10^{56}–10^{57} and 10^{52}–10^{53} erg to 10^{55}–10^{56} and 10^{51}–10^{52} erg for different ratios of charged and neutral baryon numbers. These electron-positron pairs undergo the plasma oscillation in strong electric fields and annihilate to photons to form a neutral plasma of photons and electron-positron pairs Ruffini et al. (2003b,a). This is reminiscent of the vacuum polarization of a charged black hole Damour and Ruffini (1975); Cherubini et al. (2009) and the Dyadosphere supposed to be dynamically created during

gravitational collapse in Refs. Ruffini and Xue (2008a); Preparata et al. (1998, 2003). For the details of this part, see Appendix C.

Gravitational and electric energies in gravitational collapses

In our previous work "Electron and positron pair-production in gravitational collapses" (PHYSICAL REVIEW D 86, 084004 (2012)), we present a study of strong oscillating electric fields and electron-positron pair-production in gravitational collapse of a neutral stellar core at or over nuclear densities. In order to understand the back-reaction of such electric energy building and radiating on collapse, we adopt a simplified model describing the collapse of a spherically thin capacitor to give an analytical description how gravitational energy is converted to both kinetic and electric energies in collapse. It is shown that (i) averaged kinetic and electric energies are the same order, about an half of gravitational energy of spherically thin capacitor in collapse; (ii) caused by radiating and rebuilding electric energy, gravitational collapse undergoes a sequence of "on and off" hopping steps in the microscopic Compton scale. Although such a collapse process is still continuous in terms of macroscopic scales, it is slowed down as kinetic energy is reduced and collapsing time is about an order of magnitude larger than that of collapse process eliminating electric processes. These results indicate that it is essential to take into account, rather than ignore, electric processes in more realistic models for studying gravitational collapse of neutral stellar core at or over the nuclear density. For the details of this part, see Appendix D.

Electromagnetic field generated by neutral plasma Accretion into a Kerr Black hole

Recently, we have exploited Ruffini-Wilson model to describe strong electromagnetic fields generated by neutral plasma Accretion into a Kerr Black hole, which can be account for a possible engine for GRBs and AGNs. In this work we study the accretion of magnetized plasma to an extremely rotating $(a = M)$ Kerr black hole. Using infinite conductivity condition $(FU = 0)$ and Carter solutions as geodesics of falling plasma components we have plotted the electromagnetic field configuration and current density lines around Kerr black hole. The total amount of electromagnetic energy which can be extracted from such an engine has been discussed. We have concluded that the total charge which is induced on the Kerr black hole can be around $Q/M\ 10^{-4}$, which is quite significant.

The first part of the work "On Perfect Relativistic magnetohydrodynamics around black holes in horizon penetrating coordinates", C. Cherubini, S. Filippi, A. Loppini, R. Ruffini, R. Moradi, Y. Wang, and S.-S. Xue, published in Phys. Rev. D 97, 064038

(2018) is: Plasma accreting processes on black holes represent a central problem for Relativistic Astrophysics. In this context, here we specifically revisit the classical Ruffini-Wilson work developed for analytically modelling via analytical solutions for geodesic equations the accretion of perfect magnetized plasma on a rotating Kerr black hole. Introducing the horizon penetrating coordinates found by Doran twenty five years later, we revisit the entire approach studying Maxwell invariants, electric and magnetic fields, volumetric charge density and electromagnetic total energy. We finally discuss the physical implications of this analysis.

It has been shown that a rotating Black Hole (BH hereafter) immersed in a test background magnetic field, of initial strength B_0 and aligned parallel to the BH rotation axis, generates an induced electric field, which strength is proportional to the background magnetic field. We consider the configuration of crossed fields: $\mathbf{B} = B\hat{z}$ and $\mathbf{E} = E\hat{y}$. In this system, a huge number of e^+e^- pairs can be emitted and start to be accelerated to high energies, by means of the induced electric field, and emit synchrotron photons. These photons interact with the magnetic field via the magnetic pair production process (MPP hereafter), $\gamma + B \rightarrow e^+ + e^-$. The motion of all these pairs around the magnetic field lines generates also an induced magnetic field oriented in the opposite direction to the background one. This implies a reduction of the background magnetic field. The purpose of this study is to show if this reduction occurs, which implies a decreases the MPP efficiency and, consequently, the enhancement of the probability for the synchrotron photons to escape from the region and be detected. For details, see S. Campion, J. A.Rueda, S. S. Xue, R. Ruffini "On the magnetic field screening in strong crossed electromagnetic fields", Astronomy Reports, 2021, Vol. 98, No. 1, and Physics Letters B Volume 820, 10 September 2021, 136562 .

3.13. Strong and pulsating electromagnetic field in gravitational collapse core or heavy atoms

Surface tension for heavy atoms

Based on the relativistic mean field theory and the Thomas-Fermi approximation, we study the surface properties of giant-nucleus compressed atoms; a giant-nucleus compressed atom has a giant nuclear core (giant nucleus) and degenerate electrons some of which have penetrated into the giant nucleus. Taking into account the strong, weak, and electromagnetic interactions, we numerically study the structure of giant-nucleus compressed atoms and calculate the nuclear surface tension and Coulomb energy. We analyze the influence of the electron component and the background matter on the nuclear surface tension and Coulomb energy of giant-nucleus

compressed atoms. We also compare and contrast these results in the case of giant-nucleus compressed atoms with phenomenological results in nuclear physics and the results of the core-crust interface of neutron stars with global charge neutrality. Based on the numerical results we study the instability against Bohr-Wheeler surface deformations in the case of giant-nucleus compressed atoms. The results in this article provide the evidence of strong effects of the electromagnetic interaction and electrons on the structure of giant-nucleus compressed atoms. For details of this part, see J. Rueda, R. Ruffini, Y.-B. Wu and S.-S. Xue, "Surface tension for heavy atoms", to submitted to Physics Review C.

On the other hand, with Chinese collaborators Cheng-Jun Xia, Ren-Xin Xu, Shan-Gui Zhou, We investigate the stability and e^+e^- pair creation of supercritically charged superheavy nuclei, *ud*QM nuggets, strangelets, and strangeon nuggets based on the Thomas-Fermi approximation. The model parameters are fixed by reproducing masses and charge properties of these supercritically charged objects reported in earlier publications. It is found that *ud*QM nuggets, strangelets, and strangeon nuggets may be more stable than ^{56}Fe at the baryon number $A \gtrsim 315$, 5×10^4, and 1.2×10^8, respectively. For those stable against neutron emission, the most massive superheavy element has a baryon number $\sim$965, while *ud*QM nuggets, strangelets, and strangeon nuggets need to have baryon numbers larger than 39, 433, and 2.7×10^5. The e^+e^- pair creation will inevitably start for superheavy nuclei with charge numbers $Z \geq 177$, for *ud*QM nuggets with $Z \geq 163$, for strangelets with $Z \geq 192$, and for strangeon nuggets with $Z \geq 212$. A universal relation $Q/R_e = (m_e - \bar{\mu}_e)/\alpha$ is obtained at a given electron chemical potential $\bar{\mu}_e$, where Q is the total charge and R_e the radius of electron cloud. The maximum number of Q without causing e^+e^- pair creation is then fixed by taking $\bar{\mu}_e = -m_e$. For supercritically charged objects with $\bar{\mu}_e < -m_e$, the decay rate for e^+e^- pair production is estimated based on the Jeffreys-Wentzel-Kramers-Brillouin (JWKB) approximation. It is found that most positrons are emitted at $t \lesssim 10^{-15}$ s, while a long lasting positron emission can be observed for large objects with $R \gtrsim 1000$ fm. The emission of positrons and electron-positron annihilation from supercritically charged objects may be partially responsible for the short γ-ray burst during the merger of binary compact stars, the 511 keV continuum emission, as well as the narrow faint emission lines in X-ray spectra from galaxies and galaxy clusters. For details see "Supercritically charged objects and electron-positron pair creation ", published in Phys. Rev. D 101, 103031 (2020), for details see, https://arxiv.org/abs/2001.03531 .

Critical fermion density for restoring spontaneously broken symmetry

We show how the phenomenon of spontaneous symmetry breakdown is affected by the presence of a sea of fermions in the system. When its density exceeds a criti-

cal value, the broken symmetry can be restored. We calculate the critical value and discuss the consequences for three different physical systems: First, for the standard model of particle physics, where the spontaneous symmetry breakdown leads nonzero masses of intermediate gauge bosons and fermions. The symmetry restoration will greatly enhance various processes with dramatic consequences for the early universe. Second, for the Gell-Mann–Lèvy σ-model of nuclear physics, where the symmetry breakdown gives rise to the nucleon and meson masses. The symmetry restoration may have important consequences for formation or collapse of stellar cores. Third, for the superconductive phase of condensed-matter, where the BCS condensate at low-temperature may be destroyed by a too large electron density. For the details of this part, see H. Kleinert and S.-S. Xue, Mod. Phys. Lett. A, Vol. 30, No. 24 (2015) 1550122.

Strong and pulsating electromagnetic field in gravitational collapse core or heavy atoms

Then we study collective electronic pulsation of compressed atoms in Thomas-Fermi model. Based on the Thomas-Fermi solution for compressed electron gas around a giant nucleus, we study electric pulsations of electron number-density, pressure and electric fields, which could be caused by an external perturbations acting on the nucleus or the electrons themselves. We numerically obtain the eigen-frequencies and eigen-functions for stationary pulsation modes that fulfill the boundary-value problem established by electron-number and energy-momentum conservation, equation of state, and Maxwell's equations, as well as physical boundary conditions, and assume the nucleons in β-equilibrium at nuclear density. We particularly study the configuration of ultra-relativistic electrons with a large fraction contained within the nucleus. Such configurations can be realized for a giant nucleus or high external compression on the electrons. The lowest modes turn out to be heavily influenced by the relativistic plasma frequency induced by the positive charge background in the nucleus. Our results can be applied to heavy nuclei in the neutron star crust, as well as to the whole core of a neutron star. We discuss the possibility to apply our results to dynamic nuclei using the spectral method. For the details of this part, see L. Hendrik, R. Ruffini, and S.-S. Xue, "Collective electronic pulsation of compressed atoms in Thomas-Fermi model", Nuclear Physics A 941, 1–15 (2015).

We are proceeding to further study the phenomenon of pulsating electromagnetic field and electron-positron pair-production in gravitational collapse process of neutral core, and its astrophysics applications, GRBs etc.

R. Moradi, R. Ruffini, S. Shakeri, Y. Wang, and S.-S. Xue, The work is in progress.

3.14. The Breit-Wheeler cutoff in high-energy γ-rays and cosmic absorption (opacity) of ultra high energy particles

The Breit-Wheeler process for the photon-photon pair production is one of most relevant elementary processes in high energy astrophysics (see review Sec. 7.4). In addition to the importance of this process in dense radiation fields of compact objects (Bonometto and Rees, 1971), the essential role of this process in the context of intergalactic absorption of high-energy γ-rays was first pointed out by Nikishov (Nikishov, 1961; Gould and Schréder, 1967). The spectra of TeV radiation observed from distant ($d > 100$ Mpc) extragalactic objects suffer essential deformation during the passage through the intergalactic medium, caused by energy-dependent absorption of primary γ-rays at interactions with the diffuse extragalactic background radiation, for the optical depth $\tau_{\gamma\gamma}$ most likely significantly exceeding one (Gould and Schréder, 1967; Stecker et al., 1992; Vassiliev, 2000; Coppi and Aharonian, 1999). A relevant broad-band information about the cosmic background radiation (CBR) is important for the interpretation of the observed high-energy γ spectra (Aharonian et al., 2000; Kneiske et al., 2002; Dwek and Krennrich, 2005; Aharonian et al., 2006). For details see Hauser and Dwek (2001); Aharonian (2003). In this section, we are particularly interested in such absorption effect of high-energy γ-ray, originated from cosmological sources, interacting with the Cosmic Microwave Background (CMB) photons. Fazio and Stecker (Fazio and Stecker, 1970; Stecker et al., 1977) were the first who calculated the cutoff energy versus redshift for cosmological γ-rays. This calculation was applied to further study of the optical depth of the Universe to high-energy γ-rays (MacMinn and Primack, 1996; Kneiske et al., 2004; Stecker et al., 2006). With the Fermi telescope, such study turns out to be important to understand the spectrum of high-energy γ-ray originated from GRBs' sources at cosmological distance, we therefore offer the details of theoretical analysis as follow.

Breit-Wheeler cross-section in arbitrary frame

Breit and Wheeler (1934) studied the process

$$\gamma_1 + \gamma_2 \to e^+ + e^-, \tag{3.14.1}$$

in the center of mass of the system, the momenta of the electron and positron are equal and opposite $\mathbf{p}_1 = -\mathbf{p}_2$. The same thing holds for the momenta of the photons in the initial state: $\mathbf{k}_1 = -\mathbf{k}_2$. As a consequence, the energies of electron and positron are equal: $\mathcal{E}_1 = \mathcal{E}_2 = \mathcal{E}$, and so are the energies of the photons: $\hbar\omega_1 = \hbar\omega_2 = \mathcal{E}_\gamma = \mathcal{E}$.

They found the total cross-section in the center of mass of the system:

$$\sigma_{\gamma\gamma} = \frac{\pi}{2}\left(\frac{\alpha\hbar}{m\,c}\right)^2 (1-\hat{\beta}^2)\left[2\hat{\beta}(\hat{\beta}^2-2) + (3-\hat{\beta}^4)\ln\left(\frac{1+\hat{\beta}}{1-\hat{\beta}}\right)\right], \quad \text{with} \quad \hat{\beta} = \frac{c|\mathbf{p}|}{\mathcal{E}}, \tag{3.14.2}$$

where $\mathbf{p}$ and $\hat{\beta}$ are respectively momentum and the reduced velocity of an electron or positron. The necessary kinematic condition in order for the process (3.14.1) taking place is that the energy of two colliding photons is larger than the energetic threshold $2m_ec^2$, i.e.,

$$\mathcal{E}_\gamma > m_ec^2. \tag{3.14.3}$$

The cross-section in line (3.14.2) can be easily generalized to an arbitrary reference frame $\mathcal{K}$, in which the two photons k_1 and k_2 are moving in opposite directions; for Lorentz invariance of $(k_1 \cdot k_2)$, one has $\omega_1\omega_2 = \mathcal{E}_\gamma^2$. Since

$$\mathcal{E}_\gamma = \mathcal{E} = m_ec^2/\sqrt{1-\hat{\beta}^2}, \tag{3.14.4}$$

to obtain the total cross-section in the arbitrary frame $\mathcal{K}$, we must therefore make the following substitution (Landau and Lifshitz, 1975),

$$\hat{\beta} \to \sqrt{1 - m_e^2c^4/(\omega_1\omega_2)}, \tag{3.14.5}$$

in Eq. (3.14.2). For $\mathcal{E} \gg m_ec^2$, the total effective cross-section is approximately proportional to

$$\sigma_{\gamma\gamma} \simeq \pi\left(\frac{\alpha\hbar}{m_ec}\right)^2\left(\frac{m_ec^2}{\mathcal{E}}\right)^2 = \pi r_e^2\left(\frac{m_ec^2}{\mathcal{E}}\right)^2, \tag{3.14.6}$$

where $r_e = \left(\frac{\alpha\hbar}{m_ec}\right)$ is the electron classical radius and $\pi r_e^2 \simeq 2.5\cdot 10^{-25}\text{cm}^2$.

Opacity of high-energy GRB photons colliding with CMB photons

We study the Breit-Wheeler process (3.14.1) to the case that high-energy GRB photons ω_1, originated from GRBs sources at cosmological distance z, on their way traveling to us, collide with CMB photons ω_2 in the rest frame of CMB photons, leading to electron-positron pair production. We calculate the opacity and mean free-path of these high-energy GRB photons, find the energy-range of absorption as a function of the cosmological red-shift z.

In general, a high-energy GRB photon with a give energy ω_1, collides with background photons in all possible energies ω_2. We assume that i-type background photons have the spectrum distribution $f_i(\omega_2/T_i)$, where T_i is the characteristic energy

scale of the distribution, the opacity is then given by

$$\tau^{i}_{\gamma\gamma}(\omega_1, z) = \int dr \int_{m_e^2c^4/\omega_1}^{\infty} \frac{\omega_2^2 d\omega_2}{\pi^2} f_i(\omega_2/T_i)\sigma_{\gamma\gamma}(\frac{\omega_1\omega_2}{m_e^2c^4}), \tag{3.14.7}$$

where $m_e^2c^4/\omega_1$ is the energy-threshold (3.14.3) above which the Breit-Wheeler process (3.14.1) can occurs and the cross-section $\sigma_{\gamma\gamma}(x)$ is given by Eqs. (3.14.2), depending only on $x = \frac{\omega_1\omega_2}{m_e^2c^4}$. The total opacity is then given by

$$\tau^{\text{total}}_{\gamma\gamma}(\omega_1, z) = \sum_i \tau^{i}_{\gamma\gamma}(\omega_1, z), \tag{3.14.8}$$

which the sum is over all types of photon background in the Universe. The high-energy photons traveling path $\int dr$ is given by ,

$$\int_t^{t_0} \frac{dt'}{R(t')} = \int_0^{r(t)} \frac{dr}{(1-kr^2)^{1/2}} = \int_0^{r(t)} dr, \tag{3.14.9}$$

where $R(t)$ is the scalar factor, t_0 is the present time and t corresponds to epoch of the red-shift z for a flat $(k = 0)$ Freemann Universe. Using the relationship $z + 1 = R_0/R(t)$, we change integrand variable from t' to the red-shift z,

$$dt' = -\frac{dz}{(z'+1)H(z')}, \tag{3.14.10}$$

so that we have

$$\int_0^{r(t)} dr = \int_t^{t_0} \frac{dt'}{R(t')} = \frac{1}{R_0}\int_0^{z} \frac{dz}{H(z)}, \tag{3.14.11}$$

where $H(z) = \dot{R}(t)/R(t_0)$ is the Hubble function, obeyed the Friedmann equation

$$H(z) = H_0[\Omega_M(z+1)^3 + \Omega_\Lambda]^{1/2}, \quad \Omega_M + \Omega_\Lambda = 1, \tag{3.14.12}$$

$\Omega_M \simeq 0.3$ and $\Omega_M \simeq 0.7$.

In the case of CMB photons in a black-body distribution $1/(e^{\omega_2/T} - 1)$ with the temperature T, the opacity is given by

$$\tau_{\gamma\gamma}(\omega_1, z) = \int dr \int_{m_e^2c^4/\omega_1}^{\infty} \frac{d\omega_2}{\pi^2} \frac{\omega_2^2}{e^{\omega_2/T} - 1} \sigma_{\gamma\gamma}(\frac{\omega_1\omega_2}{m_e^2c^4}), \tag{3.14.13}$$

where the Boltzmann constant $k_B = 1$. To simply Eq. (3.14.13), we set $x = \frac{\omega_1\omega_2}{m_e^2c^4}$,

$$\tau_{\gamma\gamma}(\omega_1, z) = \int dr \left(\frac{m_e^2c^4}{\omega_1}\right)^3 \int_1^\infty \frac{dx}{\pi^2} \frac{x^2}{\exp\frac{xm_e^2c^4}{\omega_1 T} - 1} \sigma_{\gamma\gamma}(x). \tag{3.14.14}$$

In terms of CMB temperature and GRB-photons energy at the present time,

$$T = (z+1)T^0; \quad \omega_{1,2} = (z+1)\omega_{1,2}^0, \tag{3.14.15}$$

we obtain,

$$\tau_{\gamma\gamma}(\omega_1^0, z) = \frac{1}{R_0}\int_0^z \frac{dz'}{H(z')} \frac{}{(z+1)^3} \left(\frac{m_e^2c^4}{\omega_1^0}\right)^3 \int_1^\infty \frac{dx}{\pi^2} \frac{x^2}{\exp(x/\theta) - 1} \sigma_{\gamma\gamma}(x), \tag{3.14.16}$$

where

$$\theta = x^0(z+1)^2; \quad x^0 = \frac{\omega_1^0 T^0}{m_e^2c^4}, \tag{3.14.17}$$

and x^0 is the energy ω_1^0 in unit of $m_ec^2(m_ec^2/T^0) = 1.15 \cdot 10^{15}$eV. For the purpose of numerical calculations, we rewrite the expression,

$$\begin{aligned}
\tau_{\gamma\gamma}(x^0, z) &= \frac{\pi r_e^2}{R_0 H_0/c} \left(\frac{T^0}{x^0}\right)^3 \int_0^z \frac{dz'}{[\Omega_M(z'+1)^3 + \Omega_\Lambda]^{1/2}} \frac{1}{(z'+1)^3} \times \\
&\times \int_1^\infty \frac{dx}{2\pi^2} \frac{x^2 f_{\gamma\gamma}(x)}{\exp(x/\theta) - 1} = \\
&= \frac{23.8}{R_0 h} \left(\frac{1}{x^0}\right)^3 \int_0^z \frac{dz'}{[\Omega_M(z'+1)^3 + \Omega_\Lambda]^{1/2}} \frac{1}{(z'+1)^3} \times \\
&\times \int_1^\infty \frac{dx}{2\pi^2} \frac{x^2 f_{\gamma\gamma}(x)}{\exp(x/\theta) - 1},
\end{aligned} \tag{3.14.18}$$

where $R_0 = 1$, present Hubble constant $h = H_0/100\text{km}/sec/\text{Mpc}$ and

$$f_{\gamma\gamma}(x) \quad = \quad (1-\hat{\beta}^2)\Big[2\hat{\beta}(\hat{\beta}^2 - 2) + (3 - \hat{\beta}^4)\ln\big(\frac{1+\hat{\beta}}{1-\hat{\beta}}\big)\Big], \quad \hat{\beta} = \sqrt{1 - 1/x}.$$

The $\tau_{\gamma\gamma}(\omega_1^0, z) = 1$ give the relationship $\omega_1^0 = \omega_1^0(z)$ that separates the absorbed regime $\tau_{\gamma\gamma}(\omega_1^0, z) > 1$ and transparent regime $\tau_{\gamma\gamma}(\omega_1^0, z) < 1$ in the $\omega_1^0 - z$ plane.

The numerical result is shown in Fig. 3.4. It clearly shows the following properties:

1. for the redshift z smaller than a critical value $z_c \simeq 0.1$ ($z < z_c$), the CMB photons are transparent $\tau_{\gamma\gamma}(\omega_1^0, z) < 1$ to GRB photons in any energy bands,

this indicates a minimal mean-free path of photons traveling in CMB photons background;

2. for the redshift z larger than the value ($z > z_c$), there are two branches of solutions for $\tau_{\gamma\gamma}(\omega_1^0, z) = 1$, respectively corresponding to the different energy-dependence of the cross-section (3.14.2): the cross-section increases with the center-mass-energy $x = \mathcal{E}_\gamma^2/(m_e c^2)^2$ from the energy-threshold $x = 1$ to $x \simeq 1.99$, and decreases (3.14.6) from $x \simeq 1.99$ to $x \to \infty$. The turn point ($z \simeq 0.1, \omega_1^0 \simeq 1.15 \cdot 10^{15}$eV) from one solution to another is determined by the maximal cross-section at $x \simeq 1.99$. Due to these two solutions, CMB photons are transparent to GRB photons of large and small energies, opaque to those GRB photons in an intermediate energy-range large for a given finite z-value;

3. CMB photons are transparent to very low-energy GRB photons $\omega_1^0 < 10^{12}$eV, i.e., $x^0 < 10^{-3}$, due to their energies are below the energetic threshold for the Breit-Wheeler process (3.14.1). In addition, CMB photons are transparent to very large-energy GRB photons $\omega_1^0 > 10^{18}$eV, i.e., $x^0 > 10^3$, due to the cross-section of Breit-Wheeler process (3.14.1) is very small for extremely high-energy photons. For very large $z \sim 10^3$, the Universe becomes completely opaque and photon distribution cannot be described by the black body spectrum, we disregard this regime.

Due to the fact that there are other radiation backgrounds (3.14.7), the background of CMB photons gives the lowest bound of opacity, absorption limit, to GRB photons with respect to the Breit-Wheeler process (3.14.1). Finally, we point out that Fazio and Stecker (Fazio and Stecker, 1970; Stecker et al., 1977) gave only asymptotic form of small-energy solution indicated in Fig. (3.4).

Cosmic absorption of ultra high energy particles

We summarize the limits on propagation of ultra high energy particles in the Universe, set up by their interactions with cosmic background of photons and neutrinos. By taking into account cosmic evolution of these backgrounds and considering appropriate interactions we derive the mean free path for ultra high energy photons, protons and neutrinos. For photons the relevant processes are the Breit-Wheeler process as well as the double pair production process. For protons the relevant reactions are the photopion production and the Bethe-Heitler process. We discuss the interplay between the energy loss length and mean free path for the Bethe-Heitler process. Neutrino opacity is determined by its scattering off the cosmic background neutrino. We compute for the first time the high energy neutrino horizon as a function of its energy. For the details of this part, see R. Ruffini, G. Vereshchagin and S.-S.

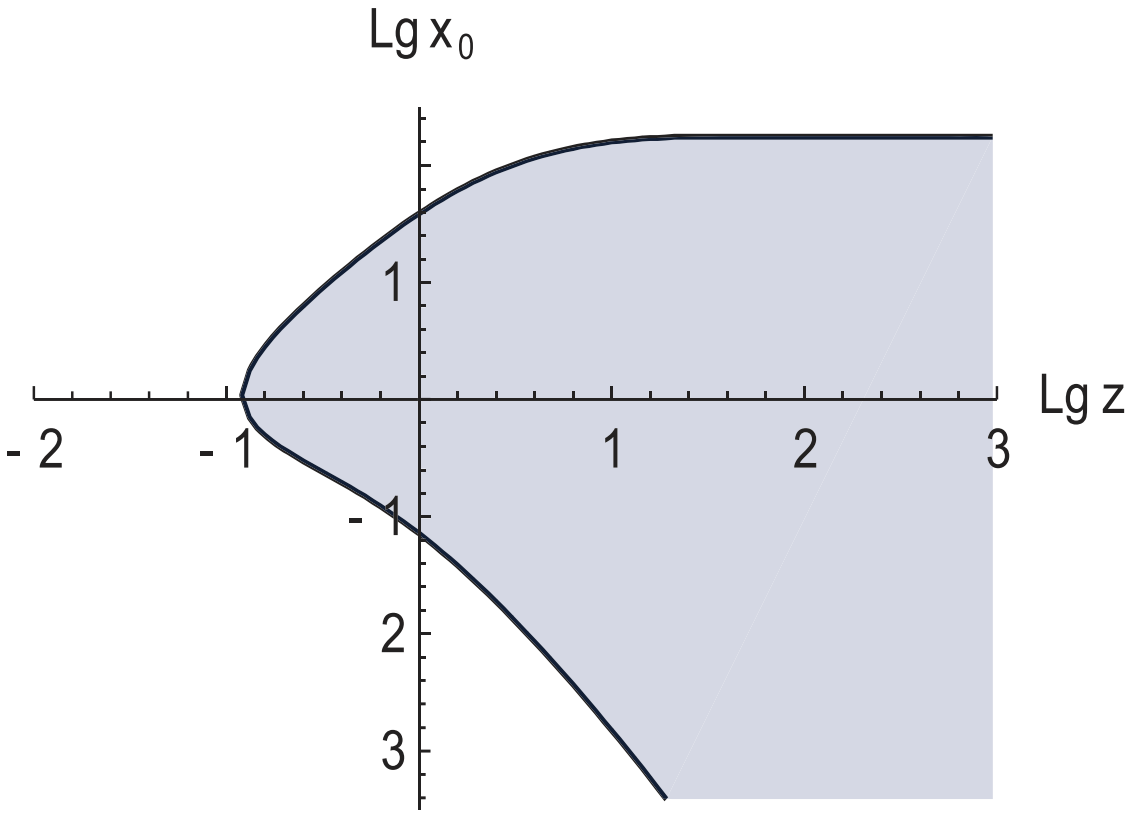

Figure 3.4.: This is a Log-Log plot for GRB photon energy x^0 (in unit of $1.11 \cdot 10^{15}$) vs redshift z. For $z > z_c \simeq 0.1$, the line that bounds shadow area indicates two solutions for the opacity $\tau_{\gamma\gamma} = 1$: (i) large-energy solution for $\omega_1^0 > 1.15 \cdot 10^{15}$eV; (ii) small-energy solution for $\omega_1^0 < 1.15 \cdot 10^{15}$eV, which separate the optically thick regime (shadow area) $\tau_{\gamma\gamma}(\omega_1^0, z) > 1$ and optically thin regime $\tau_{\gamma\gamma}(\omega_1^0, z) < 1$.

Xue, "Cosmic absorption of ultra high energy particles", Astrophysics and Space Science, Volume 361, article id.82, 2016 11 pp.

In addition, we study the high energy photon interaction with cosmic microwave background (CMB) and calculate the optical depth due to Euler-Heisenberg photon-photon scattering at cosmological redshift. According to our results the photon-photon scattering is predominant with respect to the Breit-Wheeler pair production at energies below 1 GeV. However, it is relevant for sources of high energy photons at high redshift $z > 100$. We also discuss implications of our results for two astrophysical observations of gamma-ray bursts and blazars. Tizchang, Seddigheh; Batebi, Saghar; Mohammadi, Rohollah; Ruffini, Remo; Vereshchagin, Gregory; S.-S. Xue, the conference proceeding of MG14, Rome, Italy 2015.

4. Publications (before 2005)

1. R. Ruffini and J. A. Wheeler, "Introducing the black hole ", Phys. Today, January (1971) 178.

   This article proved to be popular and was written with the intention of communicating some of the major processes made in understanding the final configurations of collapsed stars to the largest possible audience. In this article, the authors summarized the results of their students' work with particular emphasis on the work of D. Christodoulou (graduate student of R. Ruffini's at that time) together with some of their most significant new results. Moreover, it was emphasized that of all the procedures for identifying a collapsed object in space at a great distance, the most promising consisted of analyzing a close binary system in which one member is a normal star and the other a black hole. The X–ray emission associated with the transfer of material from the normal star to the collapsed object would then be of greatest importance in determining the properties of the collapsed object. This article has been reprinted many times and has been translated into many languages (Japanese, Russian, and Greek, among others). It has created much interest in the final configuration of stars after the endpoint of their thermonuclear evolution. The analysis of the possible processes leading to the formation of a black hole, via either a one–step process of a multistep process, was also presented for the first time in this article.

2. D. Christodoulou and R. Ruffini, "Reversible Transformations of a Charged Black Hole", Phys. Rev. D4 (1971) 3552.

   A formula is derived for the mass of a black hole as a function of its "irreducible mass," its angular momentum, and its charge. It is shown that 50% of the mass of an extreme charged black hole can be converted into energy as contrasted with 29% for an extreme rotating black hole.

3. T. Damour and R. Ruffini, "Quantum electrodynamical effects in Kerr-Newman geometries", Phys. Rev. Lett. 35 (1975) 463.

   Following the classical approach of Sauter, of Heisenberg and Euler and of Schwinger the process of vacuum polarization in the field of a "bare" Kerr-Newman geometry is studied. The value of the critical strength of the elec-

tromagnetic fields is given together with an analysis of the feedback of the discharge on the geometry. The relevance of this analysis for current astrophysical observations is mentioned.

4. J. Ferreirinho, R. Ruffini and L. Stella, "On the relativistic Thomas-Fermi model", Phys. Lett. B 91, (1980) 314. The relativistic generalization of the Thomas-Fermi model of the atom is derived. It approaches the usual nonrelativistic equation in the limit $Z \ll Z_{\rm crit}$, where Z is the total number of electrons of the atom and $Z_{\rm crit} = (3\pi/4)^{1/2}\alpha^{-3/2}$ and α is the fine structure constant. The new equation leads to the breakdown of scaling laws and to the appearance of a critical charge, purely as a consequence of relativistic effects. These results are compared and contrasted with those corresponding to N self-gravitating degenerate relativistic fermions, which for $N \approx N_{\rm crit} = (3\pi/4)^{1/2}(m/m_p)^3$ give rise to the concept of a critical mass against gravitational collapse. Here m is the mass of the fermion and $m_p = (\hbar c/G)^{1/2}$ is the Planck mass.

5. R. Ruffini and L. Stella,"Some comments on the relativistic Thomas-Fermi model and the Vallarta-Rosen equation", Phys. Lett. B 102 (1981) 442. Some basic differences between the screening of the nuclear charge due to a relativistic cloud of electrons in a neutral atom and the screening due to vacuum polarization effects induced by a superheavy ion are discussed.

6. G. Preparata, R. Ruffini and S.-S. Xue, "The dyadosphere of black holes and gamma-ray bursts", Astron. Astroph. Lett. 337 (1998) L3.

   The "dyadosphere" has been defined (Ruffini, Preparata et al.) as the region outside the horizon of a black hole endowed with an electromagnetic field (abbreviated to EMBH for "electromagnetic black hole") where the electromagnetic field exceeds the critical value, predicted by Heisenberg & Euler for e^+e^- pair production. In a very short time ($\sim O(\hbar/(mc^2))$), a very large number of pairs is created there. We here give limits on the EMBH parameters leading to a Dyadosphere for $10M_\odot$ and $10^5M_\odot$ EMBH's, and give as well the pair densities as functions of the radial coordinate. We here assume that the pairs reach thermodynamic equilibrium with a photon gas and estimate the average energy per pair as a function of the EMBH mass. These data give the initial conditions for the analysis of an enormous pair-electromagnetic-pulse or "P.E.M. pulse" which naturally leads to relativistic expansion. Basic energy requirements for gamma ray bursts (GRB), including GRB971214 recently observed at $z = 3.4$, can be accounted for by processes occurring in the dyadosphere. In this letter we do not address the problem of forming either the EMBH or the dyadosphere: we establish some inequalities which must be satisfied during their formation process.

7. R. Ruffini, "On the dyadosphere of black holes", at the XLIXth Yamada Conference on "Black Holes and High-Energy Astrophysics", H. Sato Ed., Univ. Acad. Press, Tokyo, 1998.

   The "dyadosphere" (from the Greek word "duas-duados" for pairs) is here defined as the region outside the horizon of a black hole endowed with an electromagnetic field (abbreviated to EMBH for "electromagnetic black hole") where the electromagnetic field exceeds the critical value, predicted by Heisenberg and Euler for electron-positron pair production. In a very short time, a very large number of pairs is created there. I give limits on the EMBH parameters leading to a Dyadosphere for 10 solar mass and 100000 solar mass EMBH's, and give as well the pair densities as functions of the radial coordinate. These data give the initial conditions for the analysis of an enormous pair-electromagnetic-pulse or "PEM-pulse" which naturally leads to relativistic expansion. Basic energy requirements for gamma ray bursts (GRB), including GRB971214 recently observed at z=3.4, can be accounted for by processes occurring in the dyadosphere.

8. R. Ruffini, J. D. Salmonson, J. R. Wilson and S.-S. Xue, "On the Pair Electromagnetic Pulse of a Black Hole with Electromagnetic Structure", Astron. Astroph. 350 (1999) 334.

   Starting from a nonequilibrium configuration we analyse the essential role of the direct and the inverse binary and triple interactions in reaching an asymptotic thermal equilibrium in a homogeneous isotropic electron-positron-photon plasma. We focus on energies in the range 0.1–10 MeV. We numerically integrate the integro-partial differential relativistic Boltzmann equation with the exact QED collisional integrals taking into account all binary and triple interactions in the plasma. We show that first, when detailed balance is reached for all binary interactions on a timescale $t_k \lesssim 10^{-14}$sec, photons and electron-positron pairs establish kinetic equilibrium. Successively, when triple interactions fulfill the detailed balance on a timescale $t_{eq} \lesssim 10^{-12}$sec, the plasma reaches thermal equilibrium. It is shown that neglecting the inverse triple interactions prevents reaching thermal equilibrium. Our results obtained in the theoretical physics domain also find application in astrophysics and cosmology.

9. R. Ruffini, J. D. Salmonson, J. R. Wilson and S.-S. Xue, "On Evolution of the Pair-Electromagnetic Pulse of a Charge Black Hole ", Astron. Astrophys. Suppl. Ser. 138 (1999) 511.

   Using hydrodynamic computer codes, we study the possible patterns of relativistic expansion of an enormous pair-electromagnetic-pulse (P.E.M. pulse);

a hot, high density plasma composed of photons, electron-positron pairs and baryons deposited near a charged black hole (EMBH). On the bases of baryon-loading and energy conservation, we study the bulk Lorentz factor of expansion of the P.E.M. pulse by both numerical and analytical methods.

10. R. Ruffini, J. D. Salmonson, J. R. Wilson and S.-S. Xue, "On the pair-electromagnetic pulse from an electromagnetic Black Hole surrounded by a Baryonic Remnant ", Astron. Astrophys 359, 855-864 (2000).

    The interaction of an expanding Pair-Electromagnetic pulse (PEM pulse) with a shell of baryonic matter surrounding a Black Hole with electromagnetic structure (EMBH) is analyzed for selected values of the baryonic mass at selected distances well outside the dyadosphere of an EMBH. The dyadosphere, the region in which a super critical field exists for the creation of electron-positron pairs, is here considered in the special case of a Reissner-Nordstrom geometry. The interaction of the PEM pulse with the baryonic matter is described using a simplified model of a slab of constant thickness in the laboratory frame (constant-thickness approximation) as well as performing the integration of the general relativistic hydrodynamical equations. The validation of the constant-thickness approximation, already presented in a previous paper Ruffini, et al.(1999) for a PEM pulse in vacuum, is here generalized to the presence of baryonic matter. It is found that for a baryonic shell of mass-energy less than 1% of the total energy of the dyadosphere, the constant-thickness approximation is in excellent agreement with full general relativistic computations. The approximation breaks down for larger values of the baryonic shell mass, however such cases are of less interest for observed Gamma Ray Bursts (GRBs). On the basis of numerical computations of the slab model for PEM pulses, we describe (i) the properties of relativistic evolution of a PEM pulse colliding with a baryonic shell; (ii) the details of the expected emission energy and observed temperature of the associated GRBs for a given value of the EMBH mass; 10^3 solar masses, and for baryonic mass-energies in the range 10^{-8} to 10^{-2} the total energy of the dyadosphere.

11. G. Preparata, R. Ruffini and S.-S. Xue,"The role of the screen factor in GRBs ", Il Nuovo Cimento B115 (2000) 915.

    We derive the screen factor for the radiation flux from an optically thick plasma of electron-positron pairs and photons, created by vacuum polarization process around a black hole endowed with electromagnetic structure.

12. C. L. Bianco, R. Ruffini and S.-S. Xue, "The elementary spike produced by a pure e^+e^- pair-electromagnetic pulse from a Black Hole: The PEM Pulse ", Astron. Astrophys. 368 (2001) 377.

In the framework of the model that uses black holes endowed with electromagnetic structure (EMBH) as the energy source, we study how an elementary spike appears to the detectors. We consider the simplest possible case of a pulse produced by a pure e^+e^- pair-electro-magnetic plasma, the PEM pulse, in the absence of any baryonic matter. The resulting time profiles show a *Fast-Rise-Exponential-Decay* shape, followed by a power-law tail. This is obtained without any special fitting procedure, but only by fixing the energetics of the process taking place in a given EMBH of selected mass, varying in the range from 10 to 10^3 $M_\odot$ and considering the relativistic effects to be expected in an electron-positron plasma gradually reaching transparency. Special attention is given to the contributions from all regimes with Lorentz γ factor varying from $\gamma = 1$ to $\gamma = 10^4$ in a few hundreds of the PEM pulse travel time. Although the main goal of this paper is to obtain the elementary spike intensity as a function of the arrival time, and its observed duration, some qualitative considerations are also presented regarding the expected spectrum and on its departure from the thermal one. The results of this paper will be comparable, when data will become available, with a subfamily of particularly short GRBs not followed by any afterglow. They can also be propedeutical to the study of longer bursts in presence of baryonic matter currently observed in GRBs.

13. R. Ruffini and L. Vitagliano, "Irreducible mass and energetics of an electromagnetic black hole ", Phys. Lett. B545 (2002) 233.

    The mass-energy formula for a black hole endowed with electromagnetic structure (EMBH) is clarified for the nonrotating case. The irreducible mass $M_{\rm irr}$ is found to be independent of the electromagnetic field and explicitly expressable as a function of the rest mass, the gravitational energy and the kinetic energy of the collapsing matter at the horizon. The electromagnetic energy is distributed throughout the entire region extending from the horizon of the EMBH to infinity. We discuss two conceptually different mechanisms of energy extraction occurring respectively in an EMBH with electromagnetic fields smaller and larger than the critical field for vacuum polarization. For a subcritical EMBH the energy extraction mechanism involves a sequence of discrete elementary processes implying the decay of a particle into two oppositely charged particles. For a supercritical EMBH an alternative mechanism is at work involving an electron-positron plasma created by vacuum polarization. The energetics of these mechanisms as well as the definition of the spatial regions in which thay can occur are given. The physical implementations of these ideas are outlined for ultrahigh energy cosmic rays UHECR) and gamma ray bursts (GRBs).

14. C. Cherubini, R. Ruffini and L. Vitagliano, "On the electromagnetic field of a charged collapsing spherical shell in general relativity ", Phys. Lett. B545

(2002) 226.

A new exact solution of the Einstein-Maxwell equations for the gravitational collapse of a shell of matter in an already formed black hole is given. Both the shell and the black hole are endowed with electromagnetic structure and are assumed spherically symmetric. Implications for current research are outlined.

15. R. Ruffini, L. Vitagliano and S.-S. Xue, "On Plasma Oscillations in Strong Electric Fields ", Phys. Lett. B559 (2003) 12.

    We describe the creation and evolution of electron-positron pairs in a strong electric field as well as the pairs annihilation into photons. The formalism is based on generalized Vlasov equations, which are numerically integrated. We recover previous results about the oscillations of the charges, discuss the electric field screening and the relaxation of the system to a thermal equilibrium configuration. The timescale of the thermalization is estimated to be $\sim 10^3 - 10^4 \hbar/m_e c^2$.

16. R. Ruffini, L. Vitagliano and S.-S. Xue, "Electron-positron-photon plasma around a collapsing star ", (invited talk) in Proc. of the 28^{th} Joint ICFA Conference on Quantum Aspects of Beam Physics and Other Critical Issues of Beams in Physics and Astrophysics, January 7–11, 2003, Hiroshima University, Higashi–Hiroshima, Japan, Pisin Chen Ed., World Scientific, Singapore.

    We describe electron-positron pairs creation around an electrically charged star core collapsing to an electromagnetic black hole (EMBH), as well as pairs annihilation into photons. We use the kinetic Vlasov equation formalism for the pairs and photons and show that a regime of plasma oscillations is established around the core. As a byproduct of our analysis we can provide an estimate for the thermalization time scale.

17. G. Preparata, R. Ruffini and S.-S. Xue, "On the Dyadosphere of Black Hole", J. Korean Phys.Soc. 42 (2003) S99-S104 (astro-ph/0204080).

    Basic energy requirements of Gamma Ray Burst(GRB) sources can be easily accounted for by a pair creation process occurring in the "Dyadosphere" of a Black Hole endowed with an electromagnetic field (abbreviated to EMBH for "electromagnetic Black Hole"). This includes the recent observations of GRB971214 by Kulkarni et al. The "Dyadosphere" is defined as the region outside the horizon of an EMBH where the electromagnetic field exceeds the critical value for e^+e^- pair production. In a very short time $\sim O(\hbar mc^2)$, very large numbers of pairs are created there. Further evolution then leads naturally to a relativistically expanding pair-electromagnetic-pulse (PEM-pulse).

Specific examples of Dyadosphere parameters are given for 10 and 10^5 solar mass EMBH's. This process does occur for EMBH with charge-to-mass ratio larger than 2.210^{-5} and strictly smaller than one. From a fundamental point of view, this process represents the first mechanism proved capable of extracting large amounts of energy from a Black Hole with an extremely high efficiency (close to 100%).

18. R. Ruffini and L. Vitagliano, "Energy Extraction From Gravitational Collapse to Static Black Holes ", Int. J. Mod. Phys. D12 (2003) 121.

    The mass–energy formula of black holes implies that up to 50% of the energy can be extracted from a static black hole. Such a result is reexamined using the recently established analytic formulas for the collapse of a shell and expression for the irreducible mass of a static black hole. It is shown that the efficiency of energy extraction process during the formation of the black hole is linked in an essential way to the gravitational binding energy, the formation of the horizon and the reduction of the kinetic energy of implosion. Here a maximum efficiency of 50% in the extraction of the mass energy is shown to be generally attainable in the collapse of a spherically symmetric shell: surprisingly this result holds as well in the two limiting cases of the Schwarzschild and extreme Reissner-Nordström space-times. Moreover, the analytic expression recently found for the implosion of a spherical shell onto an already formed black hole leads to a new exact analytic expression for the energy extraction which results in an efficiency strictly less than 100% for any physical implementable process. There appears to be no incompatibility between General Relativity and Thermodynamics at this classical level.

5. Publications (2005-2022)

1. R. Ruffini, F. Fraschetti, L. Vitagliano and S.-S. Xue,"Observational signatures of an electromagnetic overcritical gravitational collapse ", Int. Journ. Mod. Phys. D14 (2005) 131.

   We present theoretical predictions for the spectral, temporal and intensity signatures of the electromagnetic radiation emitted during the process of the gravitational collapse of a stellar core to a black hole, during which electromagnetic field strengths rise over the critical value for e^+e^- pair creation. The last phases of this gravitational collapse are studied, leading to the formation of a black hole with a subcritical electromagnetic field, likely with zero charge, and an outgoing pulse of initially optically thick e^+e^--photon plasma. Such a pulse reaches transparency at Lorentz gamma factors of 10^2–10^4. We find a clear signature in the outgoing electromagnetic signal, drifting from a soft to a hard spectrum, on very precise time-scales and with a very specific intensity modulation. The relevance of these theoretical results for the understanding of short gamma-ray bursts is outlined.

2. Federico Fraschetti, Remo Ruffini, Luca Vitagliano, and She-Sheng Xue, "Theoretical predictions of spectral evolution of short GRBs ", in Venice (Italy), June 5-9, 2006, IL NUOVO CIMENTO Vol. 121 (2006) 1477.

   We present the properties of spectrum of radiation emitted during gravitational collapse in which electromagnetic field strengths rise over the critical value for e^+e^- pair creation. A drift from soft to a hard energy and a high energy cut off have been found; a comparison with a pure black body spectrum is outlined.

3. R. Ruffini and S.-S. Xue, "Effective Lagrangian of QED", Journal of the Korean physical society, Vol. 49, No. 2, august 2006, pp. 715.

   From the Euler-Heisenberg formula we calculate the exact real part of the one-loop effective Lagrangian of Quantum Electrodynamics in a constant electromagnetic field, and determine its strong-field limit.

4. C. Cherubini, A. Geralico, J. Rueda and R. Ruffini, "On the "Dyadotorus" of Kerr-Newman space time ", Phys. Rev. D 79 124002 (2009).

We present the geometrical properties of the region where vacuum polarization precess occur int he Kerr-Newman space time. We find that the shape of the region can be ellipsoid-like or torus-like depending on the charge of the black hole.

5. H. Kleinert, R. Ruffini and S.-S. Xue, "Electron-positron pair-production in nonuniform electric fields", Phys. Rev. D 78 (2008) 025011.

   Treating the production of electron and positron pairs in vacuum as quantum tunneling, at the semiclassical level $O(\hbar)$, we derive a general expression, both exponential and pre-exponential factors, of the pair-production rate in nonuniform electric fields varying only in one direction. In particularly we discuss the expression for the case when produced electrons (or positrons) fill into bound states of electric potentials with discrete spectra of energy-level crossings. This expression is applied to the examples of the confined field $E(z) \neq 0, |z| \lesssim \ell$, half-confined field $E(z) \neq 0, z \gtrsim 0$, and linear increasing field $E(z) \sim z$, as well as the Coulomb field $E(r) = eZ/r^2$ for a nucleus with finite size $r_{\rm n}$ and large $Z \gg 1$.

6. R. Ruffini, G. V. Vereshchagin and S.-S. Xue, "Vacuum polarization and plasma oscillations", Phys. Lett. A 371(2007) 399 (arXiv:0706.4363).

   We evidence the existence of plasma oscillations of electrons-positron pairs created by the vacuum polarization in an uniform electric field with $E < E_c$. Our general treatment, encompassing also the traditional, well studied case of $E > E_c$, shows the existence in both cases of a maximum Lorentz factor acquired by electrons and positrons and allows determination of the a maximal length of oscillation. We quantitatively estimate how plasma oscillations reduce the rate of pair creation and increase the time scale of the pair production. These results are particularly relevant in view of the experimental progress in approaching the field strengths $E < E_c$.

7. A. G. Aksenov, R. Ruffini, and G. V. Vereshchagin, "Thermalization of a nonequilibrium electron-positron-photon plasma ", Phys.Rev.Lett. 99 (2007) 125003 .

   Starting from a nonequilibrium configuration we analyse the essential role of the direct and the inverse binary and triple interactions in reaching an asymptotic thermal equilibrium in a homogeneous isotropic electron-positron-photon plasma. We focus on energies in the range 0.1–10 MeV. We numerically integrate the integro-partial differential relativistic Boltzmann equation with the exact QED collisional integrals taking into account all binary and triple interactions in the plasma. We show that first, when detailed balance is reached

for all binary interactions on a timescale $t_k \lesssim 10^{-14}$sec, photons and electron-positron pairs establish kinetic equilibrium. Successively, when triple interactions fulfill the detailed balance on a timescale $t_{eq} \lesssim 10^{-12}$sec, the plasma reaches thermal equilibrium. It is shown that neglecting the inverse triple interactions prevents reaching thermal equilibrium. Our results obtained in the theoretical physics domain also find application in astrophysics and cosmology.

8. S.-S. Xue, "Gravitational Instanton and Cosmological term ", Int. Journ. Mod. Phys. A Vol. 24, Nos. 20 & 21 (2009) 3865–3891.

   Quantum fluctuation of unstable modes about gravitational instantons causes the instability of flat space at finite temperature, leading to the spontaneous process of nucleating quantum black holes. The energy-density of quantum black holes, depending on the initial temperature, gives the cosmological term, which naturally accounts for the inflationary phase of the early universe. The reheating phase is attributed to the Hawking radiation and annihilation of these quantum black holes. Then, the radiation energy-density dominates over the energy-density of quantum black holes, the universe started the standard cosmology phase. In this phase the energy-density of quantum black holes depends on the reheating temperature. It asymptotically approaches to the cosmological constant in matter domination phase, consistently with current observations.

9. R. Ruffini, M. Rotondo and S.-S. Xue, "Electrodynamics for Nuclear Matter in Bulk ", Int. Journ. Mod. Phys. D Vol. 16, No. 1 (2007) 1-9.

   A general approach to analyze the electrodynamics of nuclear matter in bulk is presented using the relativistic Thomas-Fermi equation generalizing to the case of $N \simeq (m_{\rm Planck}/m_n)^3$ nucleons of mass m_n the approach well tested in very heavy nuclei ($Z \simeq 10^6$). Particular attention is given to implement the condition of charge neutrality globally on the entire configuration, versus the one usually adopted on a microscopic scale. As the limit $N \simeq (m_{\rm Planck}/m_n)^3$ is approached the penetration of electrons inside the core increases and a relatively small tail of electrons persists leading to a significant electron density outside the core. Within a region of 10^2 electron Compton wavelength near the core surface electric fields close to the critical value for pair creation by vacuum polarization effect develop. These results can have important consequences on the understanding of physical process in neutron stars structures as well as on the initial conditions leading to the process of gravitational collapse to a black hole.

10. V. Popov, M. Rotondo, R. Ruffini and S.-S. Xue, "Analytic treatment of the

electrodynamics for nuclear matter in bulk", Int. Journal of Modern Physics D 20 (2011) 1995.

Using the relativistic Thomas-Fermi equation, we present an analytic treatment of the electrodynamic properties of nuclear matter in bulk. Following the works of Migdal and Popov we generalize to the case of a massive core with the mass number $A \sim 10^{57}$ the analytic approach well tested in very heavy nuclei with $A \sim 10^6$. Attention is given to implement the condition of charge neutrality globally on the entire configuration, versus the one usually adopted on a microscopic scale. It is confirmed that also in this limit A, an electric field develops near the core surface of magnitude close to the critical value of vacuum polarization. It is shown that such a configuration is energetically favorable with respect to the one which obeys local charge neutrality. These results can have important consequences on the understanding of the physical process in neutron stars as well as on the initial conditions leading to the process of gravitational collapse to a black hole.

11. R. Ruffini, M. Rotondo and S.-S. Xue, "Neutral nuclear core vs super charged one ", in Proceedings of the Eleventh Marcel Grossmann Meeting, R. Jantzen, H. Kleinert, R. Ruffini (eds.), (World Scientific, Singapore, 2008).

    Based on the Thomas-Fermi approach, we describe and distinguish the electron distributions around extended nuclear cores: (i) in the case that cores are neutral for electrons bound by protons inside cores and proton and electron numbers are the same; (ii) in the case that super charged cores are bare, electrons (positrons) produced by vacuum polarization are bound by (fly into) cores (infinity).

12. R. Ruffini and S.-S. Xue, "Dyadosphere formed in gravitational collapse ", AIP Conf. Proc. 1059 (2008) 72.

    We first recall the concept of Dyadosphere (electron-positron-photon plasma around a formed black holes) and its motivation, and recall on (i) the Dirac process: annihilation of electron-positron pairs to photons; (ii) the Breit-Wheeler process: production of electron-positron pairs by photons with the energy larger than electron-positron mass threshold; the Sauter-Euler-Heisenberg effective Lagrangian and rate for the process of electron-positron production in a constant electric field. We present a general formula for the pair-production rate in the semi-classical treatment of quantum mechanical tunneling. We also present in the *Quantum Electro-Dynamics* framework, the calculations of the Schwinger rate and effective Lagrangian for constant electromagnetic fields. We give a review on the electron-positron plasma oscillation in constant electric fields, and its interaction with photons leading to energy and number

equipartition of photons, electrons and positrons. The possibility of creating an overcritical field in astrophysical condition is pointed out. We present the discussions and calculations on (i) energy extraction from gravitational collapse; (ii) the formation of Dyadosphere in gravitational collapsing process, and (iii) its hydrodynamical expansion in Reissner Nordström geometry. We calculate the spectrum and flux of photon radiation at the point of transparency, and make predictions for short Gamma-Ray Bursts.

13. Jorge A. Rueda, Remo Ruffini, and S.-S. Xue, "On the electrostatic structure of neutron stars", AIP Conference Proceedings Volume 1205, page 143 (2009), International Conference in Honor of Ya.B. Zeldovich's 95th Anniversary, Minsk, (Belarus), 20-23 April 2009.

    We consider neutron stars composed by, (1) a core of degenerate neutrons, protons, and electrons above nuclear density; (2) an inner crust of nuclei in a gas of neutrons and electrons; and (3) an outer crust of nuclei in a gas of electrons. We use for the strong interaction model for the baryonic matter in the core an equation of state based on the phenomenological Weizsacker mass formula, and to determine the properties of the inner and the outer crust below nuclear saturation density we adopt the well–known equation of state of Baym–Bethe–Pethick. The integration of the Einstein–Maxwell equations is carried out under the constraints of β–equilibrium and global charge neutrality. We obtain baryon densities that sharply go to zero at nuclear density and electron densities matching smoothly the electron component of the crust. We show that a family of equilibrium configurations exists fulfilling overall neutrality and characterized by a non–trivial electrodynamical structure at the interface between the core and the crust. We find that the electric field is overcritical and that the thickness of the transition surface–shell separating core and crust is of the order of the electron Compton wavelength.

14. Jorge A. Rueda H., B. Patricelli, M. Rotondo, R. Ruffini, and S. S. Xue, "The Extended Nuclear Matter Model with Smooth Transition Surface", in the Proceedings of The 3rd Stueckelberg Workshop on Relativistic Field Theories, Pescara-Italy (2008).

    The existence of electric fields close to their critical value $E_c = m_e^2 c^3/(e\hbar)$ has been proved for massive cores of 10^7 up to 10^{57} nucleons using a proton distribution of constant density and a sharp step function at its boundary. We explore the modifications of this effect by considering a smoother density profile with a proton distribution fulfilling a Woods-Saxon dependence. The occurrence of a critical field has been confirmed. We discuss how the location of the maximum of the electric field as well as its magnitude is modified by the

smoother distribution.

15. B. Patricelli, M. Rotondo and R. Ruffini, "On the Charge to Mass Ratio of Neutron Cores and Heavy Nuclei", AIP Conference Proceedings, Vol. 966 (2008), pp. 143-146.

    We determine theoretically the relation between the total number of protons N_p and the mass number A (the charge to mass ratio) of nuclei and neutron cores with the model recently proposed by Ruffini et al. (2007) and we compare it with other N_p versus A relations: the empirical one, related to the Periodic Table, and the semi-empirical relation, obtained by minimizing the Weizsäcker mass formula. We find that there is a very good agreement between all the relations for values of A typical of nuclei, with differences of the order of per cent. Our relation and the semi-empirical one are in agreement up to $A \approx 10^4$ for higher values, we find that the two relations differ. We interpret the different behavior of our theoretical relation as a result of the penetration of electrons (initially confined in an external shell) inside the core, that becomes more and more important by increasing A; these effects are not taken into account in the semi-empirical mass-formula.

16. M. Rotondo, R. Ruffini and S.-S Xue, "On the Electrodynamical properties of Nuclear matter in bulk", AIP Conference Proceedings, Vol. 966 (2008), pp. 147-152.

    We analyze the properties of solutions of the relativistic Thomas-Fermi equation for globally neutral cores with radius of the order of $R \approx 10$ Km, at constant densities around the nuclear density. By using numerical tecniques as well as well tested analytic procedures developed in the study of heavy ions, we confirm the existence of an electric field close to the critical value $E_c = m_e^2 c^3 / e\hbar$ in a shell $\Delta R \approx 10^4 \hbar / m_\pi c$ near the core surface. For a core of ≈ 10 Km the difference in binding energy reaches 10^{49} ergs. These results can be of interest for the understanding of very heavy nuclei as well as physics of neutron stars, their formation processes and further gravitational collapse to a black hole.

17. B. Patricelli, M. Rotondo, J. A. Rueda H. and R. Ruffini, "The Electrodynamics of the Core and the Crust components in Neutron Stars", AIP Conference Proceedings, Vol. 1059 (2008), pp. 68-71.

    We study the possibility of having a strong electric field (E) in Neutron Stars. We consider a system composed by a core of degenerate relativistic electrons, protons and neutrons, surrounded by an oppositely charged leptonic component and show that at the core surface it is possible to have values of E of the

order of the critical value for electron-positron pair creation, depending on the mass density of the system. We also describe Neutron Stars in general relativity, considering a system composed by the core and an additional component: a crust of white dwarf - like material. We study the characteristics of the crust, in particular we calculate its mass M_{crust}. We propose that, when the mass density of the star increases, the core undergoes the process of gravitational collapse to a black hole, leaving the crust as a remnant; we compare M_{crust} with the mass of the baryonic remnant considered in the fireshell model of GRBs and find that their values are compatible.

18. Iman Motie and She-Sheng Xue, "High energy neutrino oscillation at the presence of the Lorentz Invariance Violation ", International Journal of Modern Physics A Vol. 27, No. 19 (2012) 1250104.

    Due to quantum gravity fluctuations at the Planck scale, the space-time manifold is no longer continuous, but discretized. As a result the Lorentz symmetry is broken at very high energies. In this article, we study the neutrino oscillation pattern due to the Lorentz Invariance Violation (LIV), and compare it with the normal neutrino oscillation pattern due to neutrino masses. We find that at very high energies, neutrino oscillation pattern is very different from the normal one. This could provide an possibility to study the Lorentz Invariance Violation by measuring the oscillation pattern of very high energy neutrinos from a cosmological distance.

19. R. Ruffini, "The Role of Thomas-Fermi approach in Neutron Star Matter", in the Proceedings of the 9^{th} International Conference "Path Integrals - New trends and perspectives", Max Planck Institute for the Physics of Complex Systems, Dresden, Germany, Semptember 23 - 28 2007, World Scientific 207 - 218 (2008), eds. W. Janke and A. Pelster

    The role of the Thomas-Fermi approach in Neutron Star matter cores is presented and discussed with special attention to solutions globally neutral and not fulfilling the traditional condition of local charge neutrality. A new stable and energetically favorable configuration is found. This new solution can be of relevance in understanding unsolved issues of the gravitational collapse processes and their energetics.

20. S.-S. Xue, "The phase structure of Einstein-Cartan theory ", Physics Letters B665 54 (2008).

    In the Einstein–Cartan theory of torsion-free gravity coupling to massless fermions, the four-fermion interaction is induced and its strength is a function of the gravitational and gauge couplings, as well as the Immirzi parameter. We

study the dynamics of the four-fermion interaction to determine whether effective bilinear terms of massive fermion fields are generated. Calculating one-particle-irreducible two point functions of fermion fields, we identify three different phases and two critical points for phase transitions characterized by the strength of four-fermion interaction: (1) chiral symmetric phase for massive fermions in strong coupling regime; (2) chiral symmetric broken phase for massive fermions in intermediate coupling regime; (3) chiral symmetric phase for massless fermions in weak coupling regime. We discuss the scaling-invariant region for an effective theory of massive fermions coupled to torsion-free gravity in the low-energy limit.

21. S.-S. Xue, "Quantum Regge calculus of Einstein-Cartan theory and its phase and critical point", Physics Letters B682 (2009) 300.

    We study the Quantum Regge Calculus of Einstein-Cartan theory to describe quantum dynamics of Euclidean space-time discretized as a 4-simplices complex. Tetrad field $e_\mu(x)$ and spin-connection field $\omega_\mu(x)$ are assigned to each 1-simplex. Applying the torsion-free Cartan structure equation to each 2-simplex, we discuss parallel transports and construct a diffeomorphism and *local* gauge-invariant Einstein-Cartan action. Invariant holonomies of tetrad and spin-connection fields along large loops are also given. Quantization is defined by a bounded partition function with the measure of $SO(4)$-group valued $\omega_\mu(x)$ fields and Dirac-matrix valued $e_\mu(x)$ fields over 4-simplices complex.

22. S.-S. Xue, "Quantum Regge calculus of Einstein-Cartan theory", Physical Review D 82, 064039 (2010),

    We then present detailed discussions and calculations of Quantum Regge calculus of Einstein-Cartan theory. The Euclidean space-time is discretized by a four-dimensional simplicial complex. We adopt basic tetrad and spin-connection fields to describe the simplicial complex. By introducing diffeomorphism and local Lorentz invariant holonomy fields, we construct a regularized Einstein-Cartan theory for studying the quantum dynamics of the simplicial complex and fermion fields. This regularized Einstein-Cartan action is shown to properly approach to its continuum counterpart in the continuum limit. Based on the local Lorentz invariance, we derive the dynamical equations satisfied by invariant holonomy fields. In the mean-field approximation, we show that the averaged size of 4-simplex, the element of the simplicial complex, is larger than the Planck length. This formulation provides a theoretical framework for analytical calculations and numerical simulations to study the quantum Einstein-Cartan theory.

23. S.-S. Xue, "The phase and critical point of quantum Einstein-Cartan gravity ",

Physics Letters B711 (2012) 404.

By introducing diffeomorphism and local Lorentz gauge invariant holonomy fields, we study the quantum Einstein-Cartan gravity in the framework of Regge calculus. On the basis of strong coupling expansion, mean-field approximation and dynamical equations satisfied by holonomy fields, we present in this Letter calculations and discussions to show the phase structure of the quantum Einstein-Cartan gravity, (i) the order phase: long-range condensations of holonomy fields in strong gauge couplings; (ii) the disorder phase: short-range fluctuations of holonomy fields in weak gauge couplings. According to the competition of the activation energy of holonomy fields and their entropy, we give a simple estimate of the possible ultra-violet critical point and correlation length for the second-order phase transition from the order phase to disorder one. At this critical point, we discuss whether the continuum field theory of quantum Einstein-Cartan gravity can be possibly approached when the macroscopic correlation length of holonomy field condensations is much larger than the Planck length.

24. R. Ruffini and S.-S. Xue, "Electron-positron pairs production in a macroscopic charged core", Phys. Lett. B 696 (2011) 416.

    Classical and semi-classical energy states of relativistic electrons bounded by a massive and charged core with the charge-mass-radio Q/M and macroscopic radius R_c are discussed. We show that the energies of semi-classical (bound) states can be much smaller than the negative electron mass-energy ($-mc^2$), and energy-level crossing to negative energy continuum occurs. Electron-positron pair production takes place by quantum tunneling, if these bound states are not occupied. Electrons fill into these bound states and positrons go to infinity. We explicitly calculate the rate of pair-production, and compare it with the rates of electron-positron production by the Sauter-Euler-Heisenberg-Schwinger in a constant electric field. In addition, the pair-production rate for the electro-gravitational balance ratio $Q/M = 10^{-19}$ is much larger than the pair-production rate due to the Hawking processes.

25. W.-B. Han, R. Ruffini and S.-S. Xue, "Electron-positron pair oscillation in spatially inhomogeneous electric fields and radiation ", Physics Letters B, Vol. 691 (2010), pp. 99-104.

    It is known that strong electric fields produce electron and positron pairs from the vacuum, and due to the back-reaction these pairs oscillate back and forth coherently with the alternating electric fields in time. We study this phenomenon in spatially inhomogeneous and bound electric fields by integrating the equations of energy-momentum and particle-number conservations and

Maxwell equations. The space and time evolutions of the pair-induced electric field, electric charge- and current-densities are calculated. The results show non-vanishing electric charge-density and the propagation of pair-induced electric fields, that are different from the case of homogeneous and unbound electric fields. The space and time variations of pair-induced electric charges and currents emit an electromagnetic radiation. We obtain the narrow spectrum and intensity of this radiation, whose peak $\omega_{\rm peak}$ locates in the region around 4 keV for electric field strength $\sim E_c$. We discuss their relevances to both the laboratory experiments for electron and positron pair-productions and the astrophysical observations of compact stars with an electromagnetic structure.

26. A. Benedetti, W.-B. Han, R. Ruffini, G. V. Vereshchagin, "On the frequency of oscillations in the pair plasma generated by a strong electric field ", Phys. Lett. B698:75-79,2011.

    We study the frequency of the plasma oscillations of electron-positron pairs created by the vacuum polarization in an uniform electric field with strength E in the range $0.2E_c < E < 10E_c$. Following the approach adopted in [1] we work out one second order ordinary differential equation for a variable related to the velocity from which we can recover the classical plasma oscillation equation when $E \to 0$. Thereby, we focus our attention on its evolution in time studying how this oscillation frequency approaches the plasma frequency. The time-scale needed to approach to the plasma frequency and the power spectrum of these oscillations are computed. The characteristic frequency of the power spectrum is determined uniquely from the initial value of the electric field strength. The effects of plasma degeneracy and pair annihilation are discussed.

27. M. Rotondo, Jorge A. Rueda, R. Ruffini, S.-S. Xue, "The self-consistent general relativistic solution for a system of degenerate neutrons, protons and electrons in beta-equilibrium ", Physics Letters B, Volume 701, Issue 5, p. 667-671 (2011).

    We present the self-consistent treatment of the simplest, nontrivial, self-gravitating system of degenerate neutrons, protons and electrons in β-equilibrium within relativistic quantum statistics and the Einstein-Maxwell equations. The impossibility of imposing the condition of local charge neutrality on such systems is proved, consequently overcoming the traditional Tolman-Oppenheimer-Volkoff treatment. We emphasize the crucial role of imposing the constancy of the generalized Fermi energies. A new approach based on the coupled system of the general relativistic Thomas-Fermi-Einstein-Maxwell equations is presented and solved. We obtain an explicit solution fulfilling global and not local charge neutrality by solving a sophisticated eigenvalue problem of the general

relativistic Thomas-Fermi equation. The value of the Coulomb potential at the center of the configuration is $eV(0) \simeq m_\pi c^2$ and the system is intrinsically stable against Coulomb repulsion in the proton component. This approach is necessary, but not sufficient, when strong interactions are introduced.

28. M. Rotondo, Jorge A. Rueda, R. Ruffini, S.-S. Xue, "On Compressed Nuclear Matter: from Nuclei to Neutron Stars ", International Journal of Modern Physics D, Volume 20, Issue 10, pp. 1789-1796 (2011).

    We address the description of neutron-proton-electron degenerate matter in beta equilibrium subjected to compression both in the case of confined nucleons into a nucleus as well as in the case of deconfined nucleons. We follow a step-by-step generalization of the classical Thomas-Fermi model to special and general relativistic regimes, which leads to a unified treatment of beta equilibrated neutron-proton-electron degenerate matter applicable from the case of nuclei all the way up to the case of white-dwarfs and neutron stars. New gravito-electrodynamical effects, missed in the traditional approach for the description of neutron star configurations, are found as a consequence of the new set of general relativistic equilibrium equations.

29. M. Rotondo, Jorge A. Rueda, R. Ruffini, S.-S. Xue, "The relativistic Feynman-Metropolis-Teller theory for white-dwarfs in general relativity ", Physical Review D, vol. 84, Issue 8, 084007 (2011).

    The recent formulation of the relativistic Thomas-Fermi model within the Feynman-Metropolis-Teller theory for compressed atoms is applied to the study of general relativistic white dwarf equilibrium configurations. The equation of state, which takes into account the β-equilibrium, the nuclear and the Coulomb interactions between the nuclei and the surrounding electrons, is obtained as a function of the compression by considering each atom constrained in a Wigner-Seitz cell. The contribution of quantum statistics, weak, nuclear, and electromagnetic interactions is obtained by the determination of the chemical potential of the Wigner-Seitz cell. The further contribution of the general relativistic equilibrium of white dwarf matter is expressed by the simple formula $\sqrt{g_{00}}\mu_{\rm ws}$= constant, which links the chemical potential of the Wigner-Seitz cell $\mu_{\rm ws}$ with the general relativistic gravitational potential g_{00} at each point of the configuration. The configuration outside each Wigner-Seitz cell is strictly neutral and therefore no global electric field is necessary to warranty the equilibrium of the white dwarf. These equations modify the ones used by Chandrasekhar by taking into due account the Coulomb interaction between the nuclei and the electrons as well as inverse β-decay. They also generalize the work of Salpeter by considering a unified self-consistent approach to the Coulomb

interaction in each Wigner-Seitz cell. The consequences on the numerical value of the Chandrasekhar-Landau mass limit as well as on the mass-radius relation of ^{4}He, ^{12}C, ^{16}O and ^{56}Fe white dwarfs are presented. All these effects should be taken into account in processes requiring a precision knowledge of the white dwarf parameters.

30. M. Rotondo, Jorge A. Rueda, R. Ruffini, S.-S. Xue, "On the relativistic Thomas-Fermi treatment of compressed atoms and compressed nuclear matter cores of stellar dimensions ", Physics Review C83, 045805 (2011).

    The Feynman, Metropolis and Teller treatment of compressed atoms is extended to the relativistic regimes. Each atomic configuration is confined by a Wigner-Seitz cell and is characterized by a positive electron Fermi energy. The non-relativistic treatment assumes a point-like nucleus and infinite values of the electron Fermi energy can be attained. In the relativistic treatment there exists a limiting configuration, reached when the Wigner-Seitz cell radius equals the radius of the nucleus, with a maximum value of the electron Fermi energy $(E_e^F)_{max}$, here expressed analytically in the ultra-relativistic approximation. The corrections given by the relativistic Thomas-Fermi-Dirac exchange term are also evaluated and shown to be generally small and negligible in the relativistic high density regime. The dependence of the relativistic electron Fermi energies by compression for selected nuclei are compared and contrasted to the non-relativistic ones and to the ones obtained in the uniform approximation. The relativistic Feynman, Metropolis, Teller approach here presented overcomes some difficulties in the Salpeter approximation generally adopted for compressed matter in physics and astrophysics. The treatment is then extrapolated to compressed nuclear matter cores of stellar dimensions with $A \simeq (m_{\rm Planck}/m_n)^3 \sim 10^{57}$ or $M_{core} \sim M_\odot$. A new family of equilibrium configurations exists for selected values of the electron Fermi energy varying in the range $0 < E_e^F \leq (E_e^F)_{max}$. Such configurations fulfill global but not local charge neutrality. They have electric fields on the core surface, increasing for decreasing values of the electron Fermi energy reaching values much larger than the critical value $E_c = m_e^2 c^3/(e\hbar)$, for $E_e^F = 0$. We compare and contrast our results with the ones of Thomas-Fermi model in strange stars.

31. Belvedere, Riccardo; Pugliese, Daniela; Rueda, Jorge A.; Ruffini, Remo; Xue, She-Sheng, "Neutron star equilibrium configurations within a fully relativistic theory with strong, weak, electromagnetic, and gravitational interactions ", Nuclear Physics A, Volume 883, p. 1-24, 2012.

    We formulate the equations of equilibrium of neutron stars taking into account strong, weak, electromagnetic, and gravitational interactions within the

framework of general relativity. The nuclear interactions are described by the exchange of the sigma, omega, and rho virtual mesons. The equilibrium conditions are given by our recently developed theoretical framework based on the Einstein-Maxwell-Thomas-Fermi equations along with the constancy of the general relativistic Fermi energies of particles, the "Klein potentials", throughout the configuration. The equations are solved numerically in the case of zero temperatures and for selected parametrization of the nuclear models. The solutions lead to a new structure of the star: a positively charged core at supranuclear densities surrounded by an electronic distribution of thickness $\sim \hbar/(m_e c)$ of opposite charge, as well as a neutral crust at lower densities. Inside the core there is a Coulomb potential well of depth $\sim m_\pi c^2/e$. The constancy of the Klein potentials in the transition from the core to the crust, impose the presence of an overcritical electric field $\sim (m_\pi/m_e)^2 E_c$, the critical field being $E_c = m_e^2 c^3/(e\hbar)$. The electron chemical potential and the density decrease, in the boundary interface, until values $\mu_e^{\rm crust} < \mu_e^{\rm core}$ and $\rho_{\rm crust} < \rho_{\rm core}$. For each central density, an entire family of core-crust interface boundaries and, correspondingly, an entire family of crusts with different mass and thickness, exist. The configuration with $\rho_{\rm crust} = \rho_{\rm drip} \sim 4.3 \times 10^{11}$ g/cm^3 separates neutron stars with and without inner crust. We present here the novel neutron star mass-radius for the case $\rho_{\rm crust} = \rho_{\rm drip}$ and compare and contrast it with the one obtained from the Tolman-Oppenheimer-Volkoff treatment.

32. H. Kleinert and S.-S. Xue, "Vacuum pair-production in a classical electric field and an electromagnetic wave ", Annals of Physics 333 (2013) 104.

    Using semiclassical WKB-methods, we calculate the rate of electron- positron pair-production from the vacuum in the presence of two external fields, a strong (space- or time-dependent) classical field and a monochromatic electromagnetic wave. We discuss the possible medium effects on the rate in the presence of thermal electrons, bosons, and neutral plasma of electrons and protons at a given temperature and chemical potential. Using our rate formula, we calculate the rate enhancement due to a laser beam, and discuss the possibility that a significant enhancement may appear in a plasma of electrons and protons with self-focusing properties.

33. Jorge A. Rueda, R. Ruffini, S.-S. Xue, "The Klein first integrals in an equilibrium system with electromagnetic, weak, strong and gravitational interactions ", Nuclear Physics A, Volume 872, Issue 1, 286-295 (2011).

    The isothermal Tolman condition and the constancy of the Klein potentials originally expressed for the sole gravitational interaction in a single fluid are here generalized to the case of a three quantum fermion fluid duly taking into

account the strong, electromagnetic, weak and gravitational interactions. The set of constitutive equations including the Einstein-Maxwell-Thomas-Fermi equations as well as the ones corresponding to the strong interaction description are here presented in the most general relativistic isothermal case. This treatment represents an essential step to correctly formulate a self-consistent relativistic field theoretical approach of neutron stars.

34. H. Kleinert, E. Strobel and S.-S. Xue, "Fractional Effective Action at strong electromagnetic fields ", Physics Review D88, 025049 (2013).

    In 1936, Weisskopf showed that for vanishing electric or magnetic fields the strong-field behavior of the one loop Euler-Heisenberg effective Lagrangian of quantum electro dynamics (QED) is logarithmic. Here we generalize this result for different limits of the Lorentz invariants $(\vec{E}^2 - \vec{B}^2)$ and $(\vec{B} \cdot \vec{E})$. The logarithmic dependence can be interpreted as a lowest-order manifestation of an anomalous power behavior of the effective Lagrangian of QED, with critical exponents $(\delta = e^2/(12\pi))$ for spinor QED, and $(\delta_S = \delta/4)$ for scalar QED.

35. A. Benedetti, R. Ruffini and G. Vereshchagin, "Phase space evolution of pairs created in strong electric fields ", Phys. Lett. A377, 206-215 (2013).

    We study the process of energy conversion from overcritical electric field into electron-positron-photon plasma. We solve numerically Vlasov-Boltzmann equations for pairs and photons assuming the system to be homogeneous and anisotropic. All the 2-particle QED interactions between pairs and photons are described by collision terms. We evidence several epochs of this energy conversion, each of them associated to a specific physical process. Firstly pair creation occurs, secondly back reaction results in plasma oscillations. Thirdly photons are produced by electron-positron annihilation. Finally particle interactions lead to completely equilibrated thermal electron-positron-photon plasma.

36. W.-B. Han, R. Ruffini and S.-S. Xue, "Electron and positron pair production in gravitational collapse ", Physics Review D86, 084004 (2012).

    Neutral stellar core at or over nuclear densities is described by a positive charged baryon core and negative charged electron fluid since they possess different masses and interactions. Based on a simplified model of a gravitationally collapsing or pulsating baryon core, we approximately integrate the Einstein-Maxwell equations and the equations for the number and energy-momentum conservation of complete degenerate electron fluid. We show possible electric processes that lead to the production of electron-positron pairs in the boundary of a baryon core and calculate the number and energy of electron-positron

pairs. This can be relevant for understanding the energetic sources of supernovae and gamma-ray bursts.

37. S.-P. Kim, H. W. Lee and R. Ruffini, "Schwinger Pair Production in Pulsed Electric Fields ", arXiv:1207.5213 (2012).

    We numerically investigate the temporal behavior and the structure of longitudinal momentum spectrum and the field polarity effect on pair production in pulsed electric fields in scalar quantum electrodynamics (QED). Using the evolution operator expressed in terms of the particle and antiparticle operators, we find the exact quantum states under the influence of electric pulses and measure the number of pairs of the Minkowski particle and antiparticle. The number of pairs, depending on the configuration of electric pulses, exhibits rich structures in the longitudinal momentum spectrum and undergoes diverse dynamical behaviors at the onset of the interaction but always either converges to a momentum-dependent constant or oscillates around a momentum-dependent time average after the completion of fields.

38. R. Ruffini, Y.-B. Wu and S.-S. Xue, "Einstein-Euler-Heisenberg theory and charged black holes ", Physics Review D88, 085004 (2013).

    Taking into account the Euler-Heisenberg effective Lagrangian of one-loop nonperturbative quantum electrodynamics (QED) contributions, we formulate the Einstein-Euler-Heisenberg theory and study the solutions of nonrotating black holes with electric and magnetic charges in spherical geometry. In the limit of strong and weak electromagnetic fields of black holes, we calculate the black hole horizon radius, area, and total energy up to the leading order of QED corrections and discuss the black hole irreducible mass, entropy, and maximally extractable energy as well as the Christodoulou-Ruffini mass formula. We find that these black hole quantities receive the QED corrections, in comparison with their counterparts in the Reissner-Nordström solution. The QED corrections show the screening effect on black hole electric charges and the paramagnetic effect on black hole magnetic charges. As a result, the black hole horizon area, irreducible mass, and entropy increase; however, the black hole total energy and maximally extractable energy decrease, compared with the Reissner-Nordström solution. In addition, we show that the condition for extremely charged black holes is modified due to the QED correction.

39. I. Motie and S.-S. Xue, "Euler-Heisenberg Lagrangian and CMB photon circular polarization", European Physics Letter, 100, 17006, (2012).

    Considering the effective Euler-Heisenberg Lagrangian, i.e., non-linear photon-photon interactions, we study the circular polarization of electromagnetic radiation based on the time-evolution of Stokes parameters. To the leading order,

we solve the Quantum Boltzmann Equation for the density matrix describing an ensemble of photons in the space of energy-momentum and polarization states, and calculate the intensity of circular polarizations. Applying these results to a linear polarized thermal radiation, we calculate the circular polarization intensity, and discuss its possible relevance to the circular polarization intensity of the Cosmic Microwave Background radiation.

40. R. Mohammadi, I. Motie and S.-S. Xue, "Circular polarization from linearly polarized laser beam collisions ", Physics Review A377 (2013) 2450.

    To probe the nonlinear effects of photon-photon interaction in the quantum electrodynamics, we study the generation of circular polarized photons by the collision of two linearly polarized laser beams. In the framework of the Euler-Heisenberg effective Lagrangian and the Quantum Boltzmann equation for the time evolution of the density matrix of polarization, we calculate the intensity of circular polarization generated by the collision of two linearly polarized laser beams and estimate the rate of generation that is proportional to α^2. As a result, we show that the generated circular polarization can be experimentally measured by two head-on colliding optical laser beams of the cross-sectional area $\lesssim 0.01\,\mathrm{cm}^2$ and the laser pulse energy $\sim$ mJ. which are currently available in laboratories. Our study presents a valuable supplement to other theoretical and experimental frameworks to study and measure the nonlinear effects of photon-photon interaction in the quantum electrodynamics.

41. R. Mohammadi and S.-S. Xue, "CMB or laser photon circular polarization via interaction with neutrino beam or cosmic background ", Physics Letters B731 272–278, (2014).

    We study the phenomenon that laser photons acquire circular polarization by interacting with a Dirac or Majorana neutrino beam. It is shown that for the reason of neutrinos being left-handed and their gauge-couplings being parity-violated, linearly polarized photons acquire their circular polarization by interacting with neutrinos. Calculating the ratio of linear and circular polarizations of laser photons interacting with either Dirac or Majorana neutrino beam, we obtain this ratio for the Dirac neutrino case, which is about twice less than the ratio for the Majorana neutrino case. Based on this ratio, we discuss the possibility of using advanced laser facilities and the T2K neutrino experiment to measure the circular polarization of laser beams interacting with neutrino beams in ground laboratories. This could be an additional and useful way to gain some insight into the physics of neutrinos, for instance their Dirac or Majorana nature.

42. J. Khodagholizadeh, R. Mohammadi and S.-S. Xue, "Photon-neutrino scatter-

ing and the B-mode spectrum of CMB photons ", the Rapid communication section of Physics Review D 90, 091301(R) (2014).

On the basis of the quantum Boltzmann equation governing the time-evolution of the density matrix of polarized CMB photons in the primordial scalar perturbations of metric, we calculate the B-mode spectrum of polarized CMB photons contributed from the scattering of CMB photons and CNB neutrinos (Cosmic Neutrino Background). We show that such contribution to the B-mode spectrum is negligible for small ℓ, however is significantly large for $50 < \ell < 200$ by plotting our results together with the BICEP2 data. Our study and results imply that in order to theoretically better understand the origin of the observed B-mode spectrum of polarized CMB photons (r-parameter), it should be necessary to study the relevant and dominate processes in both tensor and scalar perturbations.

43. R. Mohammadi, J. Khodagholizadeh, M. Sadegh, and S.-S. Xue, "B-mode polarization of the CMB and the cosmic neutrino background ", PHYSICAL REVIEW D93, 125029 (2016).

    It is known that in contrast with the E-mode polarization the B-mode polarization of the cosmic microwave background cannot be generated by the Compton scattering in the case of the scalar mode of metric perturbation. However, it is possible to generate the B mode by the Compton scattering in the case of the tensor mode of metric perturbation. For this reason, the ratio of tensor to scalar modes of metric perturbation ($r \sim C_{Bl}/C_{El}$) is estimated by comparing the B-mode power spectrum with the E mode at least for small ℓ. We study the cosmic microwave background polarization, especially the B-mode due to the weak interaction of the cosmic neutrino background and cosmic microwave background, in addition to the Compton scattering in both cases of scalar and tensor metric perturbations. It is shown that the power spectrum C_{Bl} of the B-mode polarization receives some contributions from scalar and tensor modes, which have effects on the value of the r- parameter. We also show that the B-mode polarization power spectrum can be used as an indirect probe into the cosmic neutrino background. B-mode polarization receives some contributions from scalar and tensor modes, which have effects on the value of the r-parameter. We also show that the B-mode polarization power spectrum can be used as an indirect probe into the cosmic neutrino background. For the details of this part, see Physics Review D 93, 091301 (2016), R. Mohammadi, J. Khodagholizadeh, M. Sadegh, and S.-S. Xue.

44. R. Ruffini and S.-S. Xue, "Gravitational and electric energies in collapse of spherically thin capacitor ", Physics Letters A377 (2013) 2450.

We adopt a simplified model describing the collapse of a spherically thin capacitor to give an analytical description how gravitational energy is converted to both kinetic and electric energies in collapse. It is shown that (i) averaged kinetic and electric energies are the same order, about an half of gravitational energy of spherically thin capacitor in collapse; (ii) caused by radiating and rebuilding electric energy, gravitational collapse undergoes a sequence of "on and off" hopping steps in the microscopic Compton scale. Although such a collapse process is still continuous in terms of macroscopic scales, it is slowed down as kinetic energy is reduced and collapsing time is about an order of magnitude larger than that of collapse process eliminating electric processes.

45. Y.-B. Wu and S.-S. Xue, "Nonlinear Breit-Wheeler process in the collision of a photon with two plane waves ", Physics Review D 90, 013009 (2014).

    The nonlinear Breit-Wheeler process of electron-positron pair production off a probe photon colliding with a low-frequency and a high-frequency electromagnetic wave that propagate in the same direction is analyzed. We calculate the pair-production probability and the spectra of created pairs in the nonlinear Breit-Wheeler processes of pair production off a probe photon colliding with two plane waves or one of these two plane waves. The differences of these two cases are discussed. We evidently show, in the two-wave case, the possibility of Breit-Wheeler pair production with simultaneous photon emission into the low-frequency wave and the high multiphoton phenomena: (i) Breit-Wheeler pair production by absorption of the probe photon and a large number of photons from the low-frequency wave, in addition to the absorption of one photon from the high-frequency wave; (ii) Breit-Wheeler pair production by absorption of the probe photon and one photon from the high-frequency wave with simultaneous emission of a large number of photons into the low-frequency wave. The phenomenon of photon emission into the wave cannot happen in the one-wave case. Compared with the one-wave case, the contributions from high multiphoton processes are largely enhanced in the two-wave case. The results presented in this article show a possible way to access the observations of the phenomenon of photon emission into the wave and high multiphoton phenomenon in Breit-Wheeler pair production even with the laser-beam intensity of order 10^{18} W/cm^2.

46. E. Strobel and S.-S. Xue, "Semiclassical pair production rate for time-dependent electrical fields with more than one component: -WKB-approach and worldline instantons ", Nuclear Physics B886 (2014) 1153.

    We present an analytic calculation of the semiclassical electron-positron pair creation rate by time-dependent electrical fields. We use two methods, first

the imaginary time method in the WKB-approximation and second the world-line instanton approach. The analytic tools for both methods are generalized to time-dependent electric fields with more than one component.
For the WKB method an expansion of the momentum spectrum of produced pairs around the canonical momentum $\vec{P} = 0$ is presented which simplifies the computation of the pair creation rate. We argue that the world-line instanton method of Dunne et al. (2006) implicitly performs this expansion of the momentum spectrum around $\vec{P} = 0$. Accordingly the generalization to more than one component is shown to agree with the WKB result obtained via this expansion.
However the expansion is only a good approximation for the cases where the momentum spectrum is peaked around $\vec{P} = 0$. Thus the expanded WKB result and the world-line instanton method of Dunne et al. (2006) as well as the generalized method presented here are only applicable in these cases.
We study the two component case of a rotating electric field and find a new analytic closed form for the momentum spectrum using the generalized WKB method. The momentum spectrum for this field is not peaked around $\vec{P} = 0$.

47. H. Kleinert and S.-S. Xue, "Critical fermion density for restoring spontaneously broken symmetry ", Mod. Phys. Lett. A, Vol. 30, No. 24 (2015) 1550122.

    We show how the phenomenon of spontaneous symmetry breakdown is affected by the presence of a sea of fermions in the system. When its density exceeds a critical value, the broken symmetry can be restored. We calculate the critical value and discuss the consequences for three different physical systems: First, for the standard model of particle physics, where the spontaneous symmetry breakdown leads nonzero masses of intermediate gauge bosons and fermions. The symmetry restoration will greatly enhance various processes with dramatic consequences for the early universe. Second, for the Gell-Mann–Lèvy σ-model of nuclear physics, where the symmetry breakdown gives rise to the nucleon and meson masses. The symmetry restoration may have important consequences for formation or collapse of stellar cores. Third, for the superconductive phase of condensed-matter, where the BCS condensate at low-temperature may be destroyed by a too large electron density.

48. S.-S. Xue, "Particle spectra for matter and the candidates for dark matter, resonant and nonresonant phenomena of four-fermion operators in quantum Einstein-Cartan theory ", Physics Letters B744 88–94 (2015), B737 (2014) 172, B727, 308, B721, 347 (2013), and Physical Review D 93, 073001 (2016).

    In the fermion content and gauge symmetry of the standard model (SM), we study the four-fermion operators in the torsion-free quantum Einstein-Cartan

theory. The collider signatures of irrelevant operators are suppressed by the high-energy cutoff (torsion-field mass) Λ, and cannot be experimentally accessible at TeV scales. Whereas the dynamics of relevant operators accounts for (i) the SM symmetry-breaking in the domain of infrared-stable fixed point with the energy scale $v \approx 239.5$ GeV and (ii) composite Dirac particles restoring the SM symmetry in the domain of ultraviolet-stable fixed point with the energy scale $\mathcal{E} \gtrsim 5$ TeV. To search for the resonant phenomena of composite Dirac particles with peculiar kinematic distributions in final states, we discuss possible high-energy processes: multi-jets and dilepton Drell-Yan process in LHC $p\,p$ collisions, the resonant cross-section in $e^- e^+$ collisions annihilating to hadrons and deep inelastic lepton-hadron $e^-\,p$ scatterings. To search for the nonresonant phenomena due to the form-factor of Higgs boson, we calculate the variation of Higgs-boson production and decay rate with the CM energy in LHC. We also present the discussions on four-fermion operators in the lepton sector and the mass-squared differences for neutrino oscillations in short baseline experiments, as well as its resulted particle spectra for matter and the candidates for dark matter.

49. S.-S. Xue, "How universe evolves with cosmological and gravitational constants in the field theory of Einstein-Cartan gravity ", Nuclear Physics B897 326–345 (2015).

    With a basic varying space-time cutoff $\tilde{\ell}$, we study a regularized and quantized Einstein-Cartan gravitational field theory and its domains of ultraviolet-unstable fixed point $g_{\rm ir} \gtrsim 0$ and ultraviolet-stable fixed point $g_{\rm uv} \approx 4/3$ of the gravitational gauge coupling $g = (4/3)G/G_{\rm Newton}$. Because the fundamental operators of quantum gravitational field theory are dimension-2 area operators, the cosmological constant is inversely proportional to the squared correlation length $\Lambda \propto \xi^{-2}$. The correlation length ξ characterizes an infrared size of a causally correlate patch of the universe. The cosmological constant Λ and the gravitational constant G are related by a generalized Bianchi identity. As the basic space-time cutoff $\tilde{\ell}$ decreases and approaches to the Planck length $\ell_{\rm pl}$, the universe undergoes inflation in the domain of the ultraviolet-unstable fixed point $g_{\rm ir}$, then evolves to the low-redshift universe in the domain of ultraviolet-stable fixed point $g_{\rm uv}$. We give the quantitative description of the low-redshift universe in the scaling-invariant domain of the ultraviolet-stable fixed point $g_{\rm uv}$, and its deviation from the ΛCDM can be examined by low-redshift $(z \lesssim 1)$ cosmological observations, such as supernova Type Ia.

50. E. Strobel and S.-S. Xue, "Semiclassical pair production rate for rotating electric fields ", Physics Review D 91, 045016 (2015).

We semiclassically investigate Schwinger pair production for pulsed rotating electric fields depending on time. To do so we solve the Dirac equation for two-component fields in a WKB-like approximation. The result shows that for two-component fields the spin distribution of produced pairs is generally not 1:1. As a result the pair creation rates of spinor and scalar quantum electro dynamics (QED) are different even for one pair of turning points. For rotating electric fields the pair creation rate is dominated by particles with a specific spin depending on the sense of rotation for a certain range of pulse lengths and frequencies. We present an analytical solution for the momentum spectrum of the constant rotating field. We find interference effects not only in the momentum spectrum but also in the total particle number of rotating electric fields.

51. L. Hendrik, R. Ruffini, and S.-S. Xue, "Collective electronic pulsation of compressed atoms in Thomas-Fermi model ", Nuclear Physics A 941, 1–15 (2015).

    Based on the Thomas-Fermi solution for compressed electron gas around a giant nucleus, we study electric pulsations of electron number-density, pressure and electric fields, which could be caused by an external perturbations acting on the nucleus or the electrons themselves. We numerically obtain the eigen-frequencies and eigen-functions for stationary pulsation modes that fulfill the boundary-value problem established by electron-number and energy-momentum conservation, equation of state, and Maxwell's equations, as well as physical boundary conditions, and assume the nucleons in β-equilibrium at nuclear density. We particularly study the configuration of ultra-relativistic electrons with a large fraction contained within the nucleus. Such configurations can be realized for a giant nucleus or high external compression on the electrons. The lowest modes turn out to be heavily influenced by the relativistic plasma frequency induced by the positive charge background in the nucleus. Our results can be applied to heavy nuclei in the neutron star crust, as well as to the whole core of a neutron star. We discuss the possibility to apply our results to dynamic nuclei using the spectral method.

52. J. Rueda, R. Ruffini, Y.-B. Wu and S.-S. Xue, "Surface tension for heavy atoms ", submitted to Physics Review C.

    Based on the relativistic mean field theory and the Thomas-Fermi approximation, we study the surface properties of giant-nucleus compressed atoms; a giant-nucleus compressed atom has a giant nuclear core (giant nucleus) and degenerate electrons some of which have penetrated into the giant nucleus. Taking into account the strong, weak, and electromagnetic interactions, we numerically study the structure of giant-nucleus compressed atoms and calculate

the nuclear surface tension and Coulomb energy. We analyze the influence of the electron component and the background matter on the nuclear surface tension and Coulomb energy of giant-nucleus compressed atoms. We also compare and contrast these results in the case of giant-nucleus compressed atoms with phenomenological results in nuclear physics and the results of the core-crust interface of neutron stars with global charge neutrality. Based on the numerical results we study the instability against Bohr-Wheeler surface deformations in the case of giant-nucleus compressed atoms. The results in this article provide the evidence of strong effects of the electromagnetic interaction and electrons on the structure of giant-nucleus compressed atoms.

53. R. Ruffini, G. Vereshchagin and S.-S. Xue, "Cosmic absorption of ultra high energy particles ", Astrophysics and Space Science, Volume 361, article id.82, 2016 11 pp.

    This paper summarizes the limits on propagation of ultra high energy particles in the Universe, set up by their interactions with cosmic background of photons and neutrinos. By taking into account cosmic evolution of these backgrounds and considering appropriate interactions we derive the mean free path for ultra high energy photons, protons and neutrinos. For photons the relevant processes are the Breit-Wheeler process as well as the double pair production process. For protons the relevant reactions are the photopion production and the Bethe-Heitler process. We discuss the interplay between the energy loss length and mean free path for the Bethe-Heitler process. Neutrino opacity is determined by its scattering off the cosmic background neutrino. We compute for the first time the high energy neutrino horizon as a function of its energy.

54. Hendrik Ludwig, Remo Ruffini, "Gamow's Calculation of the Neutron Star's Critical Mass Revised ", Journal of the Korean Physical Society, September 2014, Volume 65, Issue 6, pp 892–896.

    It has at times been indicated that Landau introduced neutron stars in his classic paper of 1932. This is clearly impossible because the discovery of the neutron by Chadwick was submitted more than one month after Landau's work. Therefore, and according to his calculations, what Landau really did was to study white dwarfs, and the critical mass he obtained clearly matched the value derived by Stoner and later by Chandrasekhar. The birth of the concept of a neutron star is still today unclear. Clearly, in 1934, the work of Baade and Zwicky pointed to neutron stars as originating from supernovae. Oppenheimer in 1939 is also well known to have introduced general relativity (GR) in the study of neutron stars. The aim of this note is to point out that the crucial

idea for treating the neutron star has been advanced in Newtonian theory by Gamow. However, this pioneering work was plagued by mistakes. The critical mass he should have obtained was $6.9M_{\odot}$, not the one he declared, namely, $1.5M_{\odot}$. Probably, he was taken to this result by the work of Landau on white dwarfs. We revise Gamow's calculation of the critical mass regarding calculational and conceptual aspects and discuss whether it is justified to consider it the first neutron-star critical mass. We compare Gamow's approach to other early and modern approaches to the problem.

55. C. Stahl, and E. Strobel, "Semiclassical fermion pair creation in de Sitter spacetime", The proceeding of the 2nd Cesare Lattes Meeting, 2015, AIP Conf. Proc. 1693, 050005 (2015).

    We present a method to semiclassically compute the pair creation rate of bosons and fermions in de Sitter spacetime. The results in the bosonic case agree with the ones in the literature. We find that for the constant electric field the fermionic and bosonic pair creation rate are the same. This analogy of bosons and fermions in the semiclassical limit is known from several flat spacetime examples.

56. C. Stahl, E. Strobel, and S.-S. Xue, "Fermionic current and Schwinger effect in de Sitter spacetime ", Phys. Rev. D 93, 025004 – Published 6 January 2016.

    We study the fermionic Schwinger effect in two-dimensional de Sitter spacetime. To do so, we first present a method to semiclassically compute the number of pairs created per momentum mode for general time dependent fields. In addition, the constant electric field is studied in depth. In this case, solutions for the Dirac equation can be found and the number of pairs can be computed using the standard Bogoliubov method. This result is shown to agree with the semiclassical one in the appropriate limit. The solutions are also used to compute the expectation value of the induced current. Comparing these results to similar studies for bosons, we find that while the results agree in the semiclassical limit, they do not generally agree. In particular, there is no occurrence of a strong current for small electric fields.

57. E. Bavarsad ,C. Stahl, and S.-S. Xue, "Scalar current of created pairs by Schwinger mechanism in de Sitter spacetime ", Phys. Rev. D 94, 104011 (2016)

    We consider a charged scalar field in a D dimensional de Sitter spacetime and investigate pair creation by Schwinger mechanism in a constant electric field background. Using a semiclassical approximation the current of the created pairs has been estimated. We find that, the semiclassical current of the created pairs in the strong electric field limit responds as $E^{\frac{D}{2}}$. Going further but restricting to $D = 3$ dimensional de Sitter spacetime, the quantum expectation

value of the spacelike component of the induced current has been computed in the in-vacuum state by applying an adiabatic subtraction scheme. We find that, in the strong electric field limit, the current responds as $E^{\frac{3}{2}}$. In the weak electric field limit the current has a linear response in E and an inverse dependence on the mass of the scalar field. In the case of a massless scalar field, the current varies with E^{-1} which leads to a phenomenon of infrared hyperconductivity. A new relation between infrared hyperconductivity, tachyons and conformality is discussed and a scheme to avoid an infrared hyperconductivity regime is proposed. In D dimension, we eventually presented some first estimates of the backreaction of the Schwinger pairs to the gravitational field, we find a decrease of the Hubble constant due to the pair creation.

58. C. Stahl and S.-S. Xue, "Schwinger effect and backreaction in de Sitter spacetime ", Physics Letters B, Volume 760, p. 288-292. 2016.

    We consider the particle-antiparticle pairs produced by both a strong electric field and de Sitter curvature. We investigate in 1 + 1 D the backreaction of the pairs on the electromagnetic field. To do so we describe the canonical quantization of an electromagnetic field in de Sitter space and add in the Einstein-Maxwell equation the fermionic current induced by the pairs. After solving this equation, we find that the electric field gets either damped or unaffected depending on the value of the pair mass and the gauge coupling. No enhancement of the electromagnetic field to support a magnetogenesis scenario is found. The physical picture is that the Schwinger pairs locally created screen the production and amplification of the electromagnetic field. However, if one considers light bosons created by the Schwinger mechanism, we report a solution to the Einstein-Maxwell equation with an enhancement of the electromagnetic field. This solution could be a new path to primordial magnetogenesis.

59. S. Batebi, S. Tizchang, R. Mohammadi, R. Ruffini, S.-S. Xue, "The generation of circular polarization of GRB ", the MG XIV proceedings, World scientific, Singapore, 2017.

    A certain degree of linear polarization has been measured in several GRB afterglows. Astonishingly, circular polarization has been recently measured in GRB121024A for the first time. In this paper by considering Gamma Ray Burst interactions to cosmic microwave background photons through Euler-Heisenberg effective Lagrangian, GRB circular polarization is discussed.

60. R. Ruffini and C. Stahl, "Cosmological fractal matter with an upper cutoff ", the conference proceedings of the 15th Italian and Korean meeting, Pescara Italy July, 2016, World scientific, Singapore. The proceeding is published together with the MG XIV proceedings, 2017.

We report here a work on a simple inhomogeneous cosmological model within the Lemaître-Tolman-Bondi (LTB) metric. The mass-scale function of the LTB model is taken to be $M(r) \propto r^d$ and would correspond to a fractal distribution for $0 < d < 3$. The luminosity distance for this model is computed and then compared to supernovae data. Unlike LTB models which have in the most general case two free functions, our model has only two free parameters as the flat standard model of cosmology. The best fit obtained is a matter distribution with an exponent of $d = 3.44$. Finally by adding an upper cutoff on the scale $r = 2300$ Mpc, we find a better fit than the simple fractal model with an exponent $d = 3.36$.

61. C. Stahl, Eckhard Strobel and S.-S. Xue, "Pair creation in the early universe ", the MG XIV proceedings, World scientific, Singapore, 2017.

    In the very early universe, a generalized Schwinger effect can create pairs from both electrical and gravitational fields. The expectation value of fermionic current induced by these newly created pairs has been recently computed in de Sitter spacetime. I will discuss different limiting cases of this result and some of its possible physical interpretations.

62. S. Tizchang, S. Batebi, R. Mohammadi, R. Ruffini, G. Vereshchagin, S.-S. Xue, "On the interaction of high energy photons with the cosmic microwave background ", the MG XIV proceedings, World scientific, Singapore, 2017.

    We study the high energy photon interaction with cosmic microwave background (CMB) and calculate the optical depth due to Euler-Heisenberg photon-photon scattering at cosmological redshift. According to our results the photon-photon scattering is predominant with respect to the Breit-Wheeler pair production at energies below 1 GeV. However, it is relevant for sources of high energy photons at high redshift $z > 100$. We also discuss implications of our results for two astrophysical observations of gamma-ray bursts and blazars.

63. S. Batebi, R. Mohammadi, R. Ruffini, S. Tizchang, and S.-S. Xue, "Generation of circular polarization of gamma ray bursts ", Phys. Rev. D 94, 065033 – Published 22 September 2016.

    The generation of the circular polarization of gamma ray burst (GRB) photons is discussed in this paper via their interactions with astroparticles in the presence or absence of background fields such as magnetic fields and noncommutative space-time geometry. Solving the quantum Boltzmann equation for GRB photons as a photon ensemble, we discuss the generation of circular polarization (as Faraday conversion phase shift $\Delta\phi_{FC}$) of GRBs in the following cases: (i) intermediate interactions, i.e., the Compton scattering of GRBs in the galaxy

cluster magnetic field and in the presence of noncommutative space-time geometry, as well as the scattering of GRBs in the cosmic neutrino background (CNB) and cosmic microwave background (CMB); (ii) interactions with particles and fields in shockwaves, i.e., the Compton scattering of GRBs with accelerated charged particles in the presence of magnetic fields. We found that (i) after shockwave crossing, the greatest contribution of $\Delta\phi_{FC}$ for energetic GRBs (of the order of GeV and larger) comes from GRB-CMB interactions, but for low-energy GRBs the contributions of the Compton scattering of GRBs in the galaxy cluster magnetic field dominate; (ii) in shockwave crossing, the magnetic field has significant effects on converting a GRB's linear polarization to a circular one, and this effect can be used to better understand the magnetic profile in shockwaves. The main aim of this work is to study and measure the circular polarization of GRBs for a better understanding of the physics and mechanism of the generation of GRBs and their interactions before reaching us.

64. S.-S. Xue, "An effective strong-coupling theory in UV-domain ", JHEP 05, 146 (2017).

    We briefly review the effective field theory of massive composite particles, their gauge couplings and characteristic energy scale in the UV-domain of UV-stable fixed point of strong four-fermion coupling, then mainly focus the discussions on the decay channels of composite particles into the final states of the SM gauge bosons, leptons and quarks. We calculate the rates of composite bosons decaying into two gauge bosons and give the ratios of decay rates of different channels depending on gauge couplings only. It is shown that a composite fermion decays into an elementary fermion and a composite boson, the latter being an intermediate state decays into two gauge bosons, leading to a peculiar kinematics of final states of a quark (or a lepton) and two gauge bosons. These provide experimental implications of such an effective theory of composite particles beyond the SM. We also present some speculative discussions on the channels of composite fermions decaying into two boson-tagged jets with quark jets, or to four-quark jets. Moreover, at the same energy scale of composite particles produced in high-energy experiments, composite particles are also produced by high-energy sterile neutrino (dark matter) collisions, their decays lead to excesses of cosmic ray particles in space and signals of SM particles in underground laboratories.

65. S. Shakeri, S. Z. Kalantari, and S.-S. Xue, "Polarization of a probe laser beam due to nonlinear QED effects ", Physical Review A 95, 012108 (2017).

    Nonlinear QED interactions induce different polarization properties on a given

probe beam. We consider the polarization effects caused by the photon-photon interaction in laser experiments, when a laser beam propagates through a constant magnetic field or collides with another laser beam. We solve the quantum Boltzmann equation within the framework of the Euler-Heisenberg Lagrangian for both time-dependent and constant background field to explore the time evolution of the Stokes parameters Q, U, and V describing polarization. Assuming an initially linearly polarized probe laser beam, we also calculate the induced ellipticity and rotation of the polarization plane.

66. S. Shakeri, M. Haghighat, and S.-S. Xue, "Nonlinear QED effects in X-ray emission of pulsars ", JCAP 10, 014 (2017).

    In the presence of strong magnetic fields near pulsars, the QED vacuum becomes a birefringent medium due to nonlinear QED interactions. Here, we explore the impact of the effective photon-photon interaction on the polarization evolution of photons propagating through the magnetized QED vacuum of a pulsar. We solve the quantum Boltzmann equation within the framework of the Euler-Heisenberg Lagrangian to find the evolution of the Stokes parameters. We find that linearly polarized X-ray photons propagating outward in the magnetosphere of a rotating neutron star can acquire high values for the circular polarization parameter. Meanwhile, it is shown that the polarization characteristics of photons besides photon energy depend strongly on parameters of the pulsars such as magnetic field strength, inclination angle and rotational period. Our results are clear predictions of QED vacuum polarization effects in the near vicinity of magnetic stars which can be tested with the upcoming X-ray polarimetric observations.

67. R. Moradi, C. Stahl, J. Firouzjaee, S.-S. Xue, "Charged cosmological black hole ", Phys. Rev. D 96, 104007 (2017).

    The cosmological black holes are black holes living not in an asymptotically flat universe but in an expanding spacetime. They have a rich dynamics in particular for their mass and horizon. In this article we perform a natural step in investigating this new type of black hole: we consider the possibility of a *charged* cosmological black hole. We derive the general equations of motion governing its dynamics and report a new analytic solution for the special case of the charged Lemaître-Tolman-Bondi equations of motion that describe a charged cosmological black hole. We then study various relevant quantities for the characterization of the black hole such as the C-function, the effect of the charge on the black hole flux and the nature of the singularity. We also perform numerical investigations to strengthen our results. Finally we challenge a model of gamma ray burst within our framework.

68. C. Cherubini, S. Filippi, A. Loppini, R. Ruffini, R. Moradi, Y. Wang, and S.-S. Xue, "On Perfect Relativistic magnetohydrodynamics around black holes in horizon penetrating coordinates ", Physical Review D, Volume 97, Issue 6, 064038, 2018

    Plasma accreting processes on black holes represent a central problem for Relativistic Astrophysics. In this context, here we specifically revisit the classical Ruffini-Wilson work developed for analytically modelling via analytical solutions for geodesic equations the accretion of perfect magnetized plasma on a rotating Kerr black hole. Introducing the horizon penetrating coordinates found by Doran twenty five years later, we revisit the entire approach studying Maxwell invariants, electric and magnetic fields, volumetric charge density and electromagnetic total energy. We finally discuss the physical implications of this analysis.

69. E. Bavarsad, S. P. Kim, C. Stahl, S.-S. Xue, "Effect of a magnetic field on Schwinger mechanism in de Sitter spacetime ", Physical Review D, Volume 97, 025017, 2018.

    We investigate the effect of a constant magnetic field background on the scalar QED pair production in a four-dimensional de Sitter spacetime. We have obtained the pair production rate which agrees with the known Schwinger result in the limit of Minkowski spacetime and with the Hawking radiation in de Sitter spacetime (dS) in the zero electric field limit. Our results describe how the cosmic magnetic field affects the pair production rate in cosmological setups. In addition, using the zeta function regularization scheme we have calculated the induced current and examined the effect of a magnetic field on the vacuum expectation value of the current operator. We find that, in the case of a strong electromagnetic background the current responds as $E \cdot B$, while in the infrared regime, it responds as B/E, which leads to a phenomenon of infrared hyperconductivity. These results of the induced current have important applications for the cosmic magnetic field evolution.

70. Takahiro Hayashinaka, She-Sheng Xue, "Physical renormalization condition for de Sitter QED ", Phys. Rev. D 97, 105010 (2018).

    We considered a new renormalization condition for the vacuum expectation values of the scalar and spinor currents induced by a homogeneous and constant electric field background in de Sitter spacetime. Following a semiclassical argument, the condition named maximal subtraction imposes the exponential suppression on the massive charged particle limit of the renormalized currents. The maximal subtraction changes the behaviors of the induced currents previously obtained by the conventional minimal subtraction scheme. The

maximal subtraction is favored for a couple of physically decent predictions including the identical asymptotic behavior of the scalar and spinor currents, the removal of the infrared (IR) hyperconductivity from the scalar current, and the finite current for the massless fermion.

71. Hagen Kleinert, She-Sheng Xue, "Composite fermions and their pair states in a strongly-coupled Fermi liquid ", Nuclear Physics B. Volume 936, November 2018, Pages 352-363.

    Our goal is to understand the phenomena arising in optical lattice fermions at low temperature in an external magnetic field. Varying the field, the attraction between any two fermions can be made arbitrarily strong, where composite bosons form via so-called Feshbach resonances. By setting up strong-coupling equations for fermions, we find that in spatial dimension they couple to bosons which dress up fermions and lead to new massive composite fermions. At low enough temperature, we obtain the critical temperature at which composite bosons undergo the Bose–Einstein condensate (BEC), leading to BEC-dressing massive fermions. These form tightly bound pair states which are new bosonic quasi-particles producing a BEC-type condensate. A quantum critical point is found and the formation of condensates of complex quasi-particles is speculated over.

72. Remo, Ruffini, Wang Yu, et.al., "Early X-Ray Flares in GRBs ", 2018ApJ...852...53R

    The discovery of GRBs by the Vela satellites was presented at the AAAS meeting in February 1974 in San Francisco (Gursky and Ruffini 1975ASSL...48.....G). The Vela satellites were operating in gamma-rays in the 150-750keV energy range and only marginally in X-rays. Since 1991, the BATSE detectors on the Compton Gamma-Ray Observatory (CGRO) have been leading to the classification of GRBs on the basis of their spectral hardness and of their observed T90 duration in the 50-300keV energy band. The BeppoSAX satellite, operating since 1996, joined the expertise of the X-ray and gamma-ray communities. Its gamma-ray burst monitor (GRBM) operating in the 40-700keV energy band determined the trigger of the GRB, and two wide-field cameras operating in the 2-30keV X-ray energy band allowed the localization of the source within an arcminute resolution. The Swift Burst Alert Telescope (BAT), operating in the 15-150keV energy band, can detect GRB prompt emissions and accurately determine their position in the sky within 3 arcmin. Within 90s, Swift can re-point the narrow-field X-ray telescope (XRT), operating in the 0.3-10keV energy range, and relay the burst position to the ground. Thanks to the Swift satellite, the number of detected GRBs increased rapidly to 480 sources with known redshifts. We have used Swift-XRT data in differentiating two

distinct subclasses of long GRBs: X-ray flares (XRFs) with Eiso¡ 1052erg and binary-driven hypernovae (BdHNe) with Eiso¿ 1052erg (see Section 3). Finally, the Fermi satellite, launched in 2008, detects ultrahigh energy photons from 20MeV to 300GeV with the Large Area Telescope (LAT) and detects photons from 8keV to 30MeV with the Gamma-ray Burst Monitor (GBM).

73. Remo, Ruffini, Rahim Moradi, et.al., "On the role of the Kerr-Newman black hole in the GeV emission of long gamma-ray bursts, ", Submitted to ApJ

    X-ray Flashes (XRFs), binary-driven hypernovae (BdHNe) are long GRB subclasses with progenitor a CO_{core}, undergoing a supernova (SN) explosion and hypercritically accreting in a tight binary system onto a companion neutron star (NS) or black hole (BH). In XRFs the NS does not reach by accretion the critical mass and no BH is formed. In BdHNe I, with shorter binary periods, the NS gravitationally collapses and leads to a new born BH. In BdHNe II the accretion on an already formed BH leads to a more massive BH. We assume that the GeV emission observed by *Fermi*-LAT originates from the rotational energy of the BH. Consequently, we verify that, as expected, in XRFs no GeV emission is observed. In 16 BdHNe I and 5 BdHNe II, within the boresight angle of LAT, the integrated GeV emission allows to estimate the initial mass and spin of the BH. In the remaining 27 sources in the plane of the binary system no GeV emission occurs, hampered by the presence of the HN ejecta. From the ratio, 21/48, we infer a new asymmetric morphology for the BdHNe reminiscent of the one observed in active galactic nuclei (AGN): the GeV emission occurs within a cone of half-opening angle $\approx 60^\circ$ from the normal to the orbital plane of the binary progenitor. The transparency condition requires a Lorentz factor $\Gamma \sim 1500$ on the source of GeV emission. The GeV luminosity in the rest-frame of the source follows a universal power-law with index of -1.20 ± 0.04, allowing to estimate the spin-down rate of the BH

74. E. Bavarsad, S. P. Kim, C. Stahl, S.-S. Xue, "Effect of Schwinger pair production on the evolution of the Hubble constant in de Sitter spacetime, ", https://arxiv.org/abs/1909.09319, will appear soon in the proceeding of MG15 and regular scientific journal.

    Recently we consider a massive charged scalar field in a uniform electric field background in a de Sitter spacetime (dS). We compute the in-vacuum expectation value of the trace of the energy-momentum tensor for the created Schwinger pairs, and using adiabatic subtraction scheme the trace is regularized. The effect of the Schwinger pair creation on the evolution of the Hubble constant is investigated. We find that the production of the semiclassical pairs leads to a decay of the Hubble constant. Whereas, the production of a light scalar field in the weak electric field regime leads to a superacceleration phenomenon.

75. S. P. Kim, "Astrophysics in Strong Electromagnetic Fields and Laboratory Astrophysics, ", https://arxiv.org/abs/1905.13439, the review article will appear soon in the proceeding of MG15 and regular scientific journal IMPD.

    Recent observations of gravitational waves from binary mergers of black holes or neu- tron stars and the rapid development of ultrahigh intensity laser pulses lead strong field physics to a frontier of new physics in the 21st century. Strong gravity phenomena are most precisely described by general relativity, and lasers that are described by another most precisely tested quantum electrodynamics (QED) can be focused into a tiny area in a short period through the chirped pulse amplification (CPA) and generate extremely high intensity electromagnetic (EM) fields beyond the conventional methods. It is physically interesting to study QED phenomena in curved spacetimes, in which both strong gravitational and electromagnetic fields play important roles. There are many sources for strong gravitational and electromagnetic fields in the sky or universe, such highly magnetized neutron stars, magnetized black holes, and the early universe. We review quantum field theoretical frameworks for QED both in the Minkowski spacetime and curved spacetimes, in particular, charged black holes and the early universe, and discuss QED physics in strong EM fields, such as the vacuum polarization and Schwinger pair production and their implications to astrophysics and cosmology.

76. Clement Stahl, "Schwinger effect impacting primordial magnetogenesis, ", Nucl. Phys. B12, 017, 2018, https://arxiv.org/abs/1806.06692.

    We explore the enhancement of an electromagnetic field in an inflationary background with an anti-conductive plasma of scalar particles. The scalar particles are created by Schwinger effect in curved spacetime and backreact to the electromagnetic field. The possibility of a negative conductivity was recently put forward in the context of the renormalization of the Schwinger induced current in de Sitter spacetime. While a negative conductivity enhances the produced magnetic field, we find that it is too weak to seed the observed intergalactic magnetic field today. This results on pair creation in inflationary scenario is however important for primordial scenarios of magnetogenesis as the presence of a conductivity alters the spectral index of the magnetic field. This also shows on a specific example that backreaction can increase the electromagnetic field and not only suppress it. For details see Clement Stahl, Nucl. Phys. B12, 017, 2018, https://arxiv.org/abs/1806.06692

77. E. Bavarsad, S. P. Kim, C. Stahl, S.-S. Xue, "QED effective action in de Sitter space, ", will appear soon in arXiv and regular scientific journal.

    Particles creation under the in uence of both an electromagnetic field and a de

Sitter (dS) spacetime is an interesting topic to probe quantum electrodynamics (QED) and quantum gravitational effects. By applying the gamma-function regularization to the in-out formulation, we find the exact one-loop effective action in the proper-time integral representation for a charged scalar field in a uniform electric field and a parallel magnetic field in a dS space, which reduces to Weisskofp-Schwinger scalar QED action in the limit of Minkowski spacetime and the one-loop action in the pure dS space. We find the consistency of the effective action with the vacuum persistence amplitude and the Schwinger effect of Phys. Rev. D 97, 025017. The effective action is analyzed for the pure dS space and QED actions in the pure electric field in dS space and in both electric and magnetic fields. The effective action in the pure dS space consists of a series of the scalar curvature starting with the quadratic order. We explore the effect of curvature on the QED vacuum polarization and find consistency of the effective action with the perturbative expansion from the worldline formalism.

78. Roberto Leonardi, Orlando Panella, Francesco Romeo, Alfredo Gurrola, Hao Sun, She-Sheng Xue "Phenomenology at the LHC of composite particles from strongly interacting Standard Model fermions via four-fermion operators of NJL type ", The European Physical Journal C volume 80, Article number: 309 (2020), https://arxiv.org/abs/1810.11420

A new physics scenario shows that four-fermion operators of Nambu-Jona-Lasinio (NJL) type have a strong-coupling UV fixed point, where composite fermions F (bosons Π) form as bound states of three (two) SM elementary fermions and they couple to their constituents via effective contact interactions at the composite scale $\Lambda \approx \mathcal{O}$(TeV). We present, for the first time for this scenario, a phenomenological study to investigate such composite particles at the LHC. Using these contact interactions, we compute the production cross sections and decay widths of composite fermions in the context of the relevant experiments at the LHC with pp collisions at $\sqrt{s} = 13$ TeV and $\sqrt{s} = 14$ TeV. In particular, we systematically examine all the different composite particles, corresponding to different flavours of F, and the signatures with which they can manifest, considering comprehensively the model parameters. We found that there is a vast spectrum of composite particles F that could be discovered and have not yet been explored at the LHC. In order to constraint the model parameters for one specific composite particle F, we consider the resonant channel $pp \to e^+F \to e^+e^-qq'$, whose cross section has been recently limited by the CMS Collaboration, we recast this result and find that the composite fermion mass m_F below 4.25 TeV is excluded for $\Lambda/m_F = 1$. We further highlight the region of parameter space where this specific composite particle F can appear

using 3 ab^{-1}, expected by the High-Luminosity LHC, computing 3 and 5 σ contour plots of its statistical significance.

79. S. Tizchang, R. Mohammadi and S.-S. Xue "Lorentz violation effects via a laser beam interacting with a high-energy charged lepton beam, ", Eur. Phys. J. C (2019) 79: 224 https://arxiv.org/abs/1811.00486.

    Lorentz violation effects via a laser beam interacting with a high-energy charged lepton beam. The conversion of linear polarization of a laser beam to circular one through its forward scattering by a TeV order charged lepton beam in the presence of Lorentz violation correction is explored. We calculate the ratio of circular polarization to linear one (Faraday Conversion phase) of the laser beam interacting with either electron or the muon beam in the framework of the quantum Boltzmann equation. Regarding the experimentally available sensitivity to the Faraday conversion, we show that the scattering of a linearly polarized laser beam with energy 0.1 eV and an electron/muon beam with available flux places an upper bound on the combination of lepton sector Lorentz violation coefficients c components (cTT+1.4 c(TZ)+0.25(cXX+cYY+2 cZZ)). The obtained bound on the combination for the electron beam is at the 10^{15} level and for the muon beam at the 3.910^{13} level. It should be mentioned that the laser and charged lepton beams considered here to reach the experimentally measurable Faraday Conversion phase are currently available or will be accessible in the near future. This study provides a valuable supplementary to other theoretical and experimental frameworks for measuring and constraining Lorentz violation coefficients.

80. M. Haghighat, S. Mahmoudi, R.Mohammadi, S. Tizchang and S.S. Xue "Circular polarization of cosmic photons due to their interactions with Sterile neutrino dark matter ", Phys. Rev. D 101, 123016 (2020) https://arxiv.org/abs/1909.03883.

    In this paper, we explore the possibility of the polarization conversion of a wide energy range of cosmic photons to the circular polarization through their interaction with Sterile neutrino as a dark matter candidate. By considering the Sterile neutrino in the seesaw mechanism framework and right-handed current model, we estimate the Faraday conversion $\Delta\phi_{\rm FC}$ of gamma ray burst (GRB) photons interacting with the Sterile neutrinos at both the prompt and afterglow emission levels. We show that for active-Sterile neutrino with mixing angle $\theta^2 \lesssim 10^{-2}$ motivated by models with a hidden sector coupled to the sterile neutrino, the Faraday conversion can be estimated as $\Delta\phi_{\rm FC} \lesssim 10^{-2} - 10^{-17}$ rad. We also examine the V-mode power spectrum C_{Vl} of the cosmic microwave background (CMB) at the last scattering surface. We show that the circular polarization power spectrum at the leading order is proportional to

the linear polarization power spectrum C_{pl} and the mixing angle where for $\theta^2 \lesssim 10^{-2}$ leads to $C_{Vl} \lesssim 0.01$ Nano-Kelvin squared.

81. Mehdi Abdi (IUT), Roohollah Mohammadi (INMOST and SoA-IPM), She-Sheng Xue (ICRANet), Moslem Zarei (IUT) "Distinguishing Dirac from Majorana neutrinos in a microwave cavity ", https://arxiv.org/abs/1909.01536.

    We propose a novel scheme for distinguishing between the Dirac and Majorana nature of neutrinos via interaction of a neutrino beam with microwave photons inside a cavity. We study the effective photon-photon polarization exchange induced by the photon-neutrino scattering. The quantum field theoretical studies of such effective picture are presented for both Dirac and Majorana neutrinos. Our phenomenological analyses show that the difference between Dirac and Majorana neutrinos can manifest itself in scattering rate of the photons. To enhance the effect a cavity scheme is employed. An experimental setup based on microwave cavities is then designed and simulated by finite element method to measure the scattering rate. Our results suggest that an experiment based on the current state-of-the-art technology will be able to probe the difference in about one year. However, it can be done in a few days by enhancing the neutrino beam flux or implementing with the near future equipments. Therefore, our work provides the possibility for solving the long lasting puzzle of Dirac or Majorana nature of neutrinos.

82. She-Sheng Xue "Cosmological Λ driven inflation and produced particles ", https://arxiv.org/abs/1910.03938

    Suppose that the early Universe starts with a quantum spacetime originated cosmological Λ-term at the Planck scale $M_{\rm pl}$. The cosmological energy density $\rho_{_\Lambda}$ drives inflation and simultaneously reduces its value to create the matter-energy density $\rho_{_M}$ via the continuous pair productions of massive fermions and antifermions. The decreasing $\rho_{_\Lambda}$ and increasing $\rho_{_M}$, in turn, slows down the inflation to its end when the pair production rate Γ_M is larger than the Hubble rate H of inflation. Such back-reaction evolutions of the density $\rho_{_\Lambda}$ and Hubble rate H are uniquely determined by two independent equations from the Einstein equation and energy conservation law, in addition, the $\rho_{_M}$ and its equation of state as functions of H are determined by continuous massive pair productions. For very massive and dense pairs $m \gg H$, $\rho_{_M} \propto m^2H^2$ and $\rho_{_\Lambda} \propto M_{\rm pl}^2H^2 > \rho_{_M}$. As a result, inflation naturally appears and theoretical results agree to Planck 2018 observations. The CMB large-scale anomaly can be possibly explained and the dark-matter acoustic wave is speculated. Suppose that the reheating efficiently converts the cosmological energy density $\rho_{_\Lambda}$ to the matter-energy density $\rho_{_M} \gg \rho_{_\Lambda}$ accounting for the most relevant Universe

mass, and some massive pairs decay to relativistic particles of energy density $\rho_{_R}$ starting the hot Big Bang. Since then, the energy density $\rho_{_R}$ produced at the reheating predominately governs the decreasing Hubble rate $H^2 \propto \rho_{_R}$, and massive pair productions are small and unimportant. However, the aforementioned back reaction $\rho_{_M} \leftrightarrow H \leftrightarrow \rho_{_\Lambda}$ is weak but continues in standard cosmological evolution. As a consequence, the cosmological energy density $\rho_{_\Lambda}$ closely tracks down the energy density $\rho_{_R}$ from the reheating end up to the radiation-matter equilibrium, then it varies very slowly, $\rho_{_\Lambda} \propto$ constant, due to the transition from radiation dominate to matter dominate epoch. Therefore the cosmic coincidence problem can be possibly avoided. The relation between $\rho_{_\Lambda}$ and radiation and matter-energy densities is obtained and can be examined at large redshifts.

83. She-Sheng Xue "Cosmological constant, matter, cosmic inflation and coincidence ", Modern Physics Letters A, (2020) 2050123 https://arxiv.org/abs/2004.10859

    We present a possible understanding to the issues of cosmological constant, inflation, matter and coincidence problems based only on the Einstein equation and Hawking particle production. The inflation appears and results agree to observations. The CMB large-scale anomaly can be explained and the dark-matter acoustic wave is speculated. The entropy and reheating are discussed. The cosmological term $\Omega_{_\Lambda}$ tracks down the matter $\Omega_{_M}$ until the radiation-matter equilibrium, then slowly varies, thus the cosmic coincidence problem can be avoided. The relation between $\Omega_{_\Lambda}$ and $\Omega_{_M}$ is shown and can be examined at large redshifts.

84. She-Sheng Xue "Cosmological Λ converts to reheating energy and cold dark matter ", https://arxiv.org/abs/2006.15622

    Suppose that the early Universe starts with a quantum spacetime originated cosmological Λ-term at the Planck scale $M_{\rm Pl}$. The cosmological energy density $\rho_{_\Lambda}$ drives inflation and simultaneously reduces its value to create the pair-energy density $\rho_{_M}$ via the continuous pair productions of massive fermions and antifermions. The decreasing $\rho_{_\Lambda}$ and increasing $\rho_{_M}$, in turn, slows down the inflation to its end when the pair production rate Γ_M is larger than the Hubble rate H of inflation. A large number of massive pairs is produced and reheating epoch starts. In addition to Einstein equation and energy-conservation law, we introduce the Boltzmann-type rate equation describing the number of pairs produced from (annihilating to) the spacetime, and reheating equation describing massive unstable pairs decay to relativistic particles and thermodynamic laws. This forms a close set of four independent differential equations uniquely determining H, $\rho_{_\Lambda}$, $\rho_{_M}$ and radiation-energy density $\rho_{_R}$, given

the initial conditions at inflation end. Numerical solutions demonstrate three episodes of preheating, massive pairs dominate and genuine reheating. Results show that ρ_Λ can efficiently convert to ρ_M by producing massive pairs, whose decay accounts for reheating ρ_R, temperature and entropy of the Big-Bang Universe. The stable massive pairs instead account for cold dark matter. Using CMB and baryon number-to-entropy ratio measurements, we constrain effective mass of pairs, Yukawa coupling and degeneracies of relativistic particles. As a result, the obtained inflation e-folding number, reheating scale, temperature and entropy are in terms of the tensor-to-scalar ratio in the theoretically predicated range $0.042 \lesssim r \lesssim 0.048$, consistently with current observations.

85. She-Sheng Xue "Horizon crossing causes baryogenesis, magnetogenesis and dark-matter acoustic wave ", https://arxiv.org/abs/2007.03464

    Sapcetime $\mathcal{S}$ produces massive particle-antiparticle pairs $\bar{F}F$ that in turn annihilate to spacetime. Such back and forth gravitational process $\mathcal{S} \Leftrightarrow \bar{F}F$ is described by Boltzmann-type cosmic rate equation of pair-number conservation. This cosmic rate equation, Einstein equation, and the reheating equation of pairs decay to relativistic particles completely determine the horizon H, cosmological energy density, massive pair and radiation energy densities in reheating epoch. Moreover, oscillating $\mathcal{S} \Leftrightarrow \bar{F}F$ process leads to the acoustic perturbations of massive particle-antiparticle symmetric and asymmetric densities. We derive wave equations for these perturbations and find frequencies of lowest lying modes. Comparing their wavelengths with horizon variation, we show their subhorion crossing at preheating, and superhorizon crossing at reheating. The superhorizon crossing of particle-antiparticle asymmetric perturbations accounts for the baryogenesis of net baryon numbers, whose electric currents lead to magnetogenesis. The baryon number-to-entropy ratio, upper and lower limits of primeval magnetic fields are computed in accordance with observations. Given a pivot comoving wavelength, it is shown that these perturbations, as dark-matter acoustic waves, originate in pre-inflation and return back to the horizon after the recombination, possibly leaving imprints on the matter power spectrum at large length scales. Due to the Jeans instability, tiny pair-density acoustic perturbations in superhorizon can be amplified to the order of unity. Thus their amplitudes at reentry horizon become nonlinear and maintain approximately constant physical sizes, and have physical influences on the formation of large scale structure and galaxies.

86. Soroush Shakeri, David J. E. Marsh, She-Sheng Xue "Light by Light Scattering as a Probe for Axion Dark Matter ", https://arxiv.org/abs/2002.06123 .

The main goal of this paper is to probe axion or axion-like particles in light-by-light forward scattering process. We consider the polarization effects caused by on-shell axions in the photon-photon scattering process. We show that the circular polarization signal generated in light-by-light scattering in the current/future laser experiments can shed more light on different aspects of these mysterious particles. Our results show a large enhancement in the conversion rate between circular and linear polarizations at the domain close to the resonance point of inter-mediating axions. This signal enhancement can be used in order to discriminate between the ALP contribution to photon-photon scattering and one originates from the virtual electron-positron pairs in the pure QED framework.

87. Damien Bégué, Clément Stahl and She-Sheng Xue "A model of interacting dark fluids tested with supernovae and Baryon Acoustic Oscillations data, ", Nuclear Physics, Section B, Volume 940, p. 312-320, (2019), https://arxiv.org/abs/1702.03185

    We compare supernovae and Baryon Acoustic Oscillations data to the predictions of a cosmological model of interacting dark matter and dark energy. This theoretical model can be derived from the effective field theory of Einstein-Cartan gravity with two scaling exponents δ_G and δ_Λ, related to the interaction between dark matter and dark energy. We perform a χ^2 fit to the data to compare and contrast it with the standard ΛCDM model. We then explore the range of parameter of the model which gives a better χ^2 than the standard cosmological model. All those results lead to tight constraints on the scaling exponents of the model. Our conclusion is that this class of models, provides a decent alternative to the ΛCDM model.

88. Soroush Shakeri, Fazlollah Hajkarim, She-Sheng Xue "Shedding New Light on Sterile Neutrinos from XENON1T Experiment ", JHEP12 (2020) 194, https://arxiv.org/abs/2008.0

    The XENON1T collaboration recently reported the excess of events from recoil electrons, possibly giving an insight into new area beyond the Standard Model (SM) of particle physics. We try to explain this excess by considering effective interactions between the sterile neutrinos and the SM particles. In this paper, we present an effective model based on one-particle-irreducible interaction vertices at low energies that are induced from the SM gauge symmetric four-fermion operators at high energies. The effective interaction strength is constrained by the SM precision measurements, astrophysical and cosmological observations. We introduce a novel effective electromagnetic interaction between sterile neutrinos and SM neutrinos, which can successfully explain the XENON1T event rate through inelastic scattering of the sterile neutrino dark matter from Xenon electrons. We find that sterile neutrinos with masses

around 90 keV and specific effective coupling can fit well with the XENON1T data where the best fit points preserving DM constraints and possibly describe the anomalies in other experiments.

89. Cheng-Jun Xia, She-Sheng Xue, Ren-Xin Xu, Shan-Gui Zhou "Supercritically charged objects and electron-positron pair creation ", Phys. Rev. D 101, 103031 (2020), https://arxiv.org/abs/2001.03531

    We investigate the stability and e^+e^- pair creation of supercritically charged superheavy nuclei, udQM nuggets, strangelets, and strangeon nuggets based on the Thomas-Fermi approximation. The model parameters are fixed by reproducing masses and charge properties of these supercritically charged objects reported in earlier publications. It is found that udQM nuggets, strangelets, and strangeon nuggets may be more stable than ^{56}Fe at the baryon number $A \gtrsim 315$, 5×10^4, and 1.2×10^8, respectively. For those stable against neutron emission, the most massive superheavy element has a baryon number $\sim$965, while udQM nuggets, strangelets, and strangeon nuggets need to have baryon numbers larger than 39, 433, and 2.7×10^5. The e^+e^- pair creation will inevitably start for superheavy nuclei with charge numbers $Z \geq 177$, for udQM nuggets with $Z \geq 163$, for strangelets with $Z \geq 192$, and for strangeon nuggets with $Z \geq 212$. A universal relation $Q/R_e = (m_e - \bar{\mu}_e)/\alpha$ is obtained at a given electron chemical potential $\bar{\mu}_e$, where Q is the total charge and R_e the radius of electron cloud. The maximum number of Q without causing e^+e^- pair creation is then fixed by taking $\bar{\mu}_e = -m_e$. For supercritically charged objects with $\bar{\mu}_e < -m_e$, the decay rate for e^+e^- pair production is estimated based on the Jeffreys-Wentzel-Kramers-Brillouin (JWKB) approximation. It is found that most positrons are emitted at $t \lesssim 10^{-15}$ s, while a long lasting positron emission can be observed for large objects with $R \gtrsim 1000$ fm. The emission of positrons and electron-positron annihilation from supercritically charged objects may be partially responsible for the short γ-ray burst during the merger of binary compact stars, the 511 keV continuum emission, as well as the narrow faint emission lines in X-ray spectra from galaxies and galaxy clusters.

90. She-Sheng Xue "Gravo-thermal catastrophe in gravitational collapse and energy progenitor of Gamma-Ray Bursts ", JCAP07 (2021) 044, https://arxiv.org/abs/2104.03021

    We study the homologous collapse of stellar nuclear core, the virial theorem for hadron collisional relaxations, and photon productions from hadron collisions. We thus show the gravo-thermal dynamical process that transforms gravitational energy to photon energy. The process is energetically and entropically favourable. The total baryon number conservation, Euler equation for energy-momentum conservation and Poisson's equation for gravitational

potential are adopted to describe homologous core collapses. The virial theorem determines the hadron collision energy gain from gravitational potential. The hadronic photon production rate determines the photon energy density. The time scales of macroscopic and microscopic processes are studied to verify approximations. As a result, we show the formation of opaque photon-pair spheres, whose total energy, size, temperature and number density, accounting for the main energetic features of Gamma-Ray Burst progenitors. We obtain the intrinsic correlations of these quantities. They depend only on the averaged thermal index of the stellar core. We discuss the possibility to confront them with observational data.

91. She-Sheng Xue "Spontaneous Peccei-Quinn symmetry breaking renders sterile neutrino, axion and χboson to be candidates for dark matter particles ", Nuclear Physics B Volume 980, July 2022, 115817, https://arxiv.org/abs/2012.04648

    We study the Peccei-Quinn (PQ) symmetry of sterile right-handed neutrino sector and the gauge symmetries of the Standard Model (SM). Due to four-fermion interactions, spontaneous breaking of these symmetries at the electroweak scale generates top-quark Dirac mass and sterile-neutrino Majorana mass. The top quark channels yields massive Higgs, $W^{\pm}$ and Z^0 bosons. The sterile neutrino channel yields the heaviest sterile neutrino Majorana mass, sterile Nambu-Goldstone axion (or majoron) and massive scalar χboson ($m_\chi \sim 10^2$ GeV). Their tiny couplings to SM particles are effectively induced by four-fermion operators. We show that such sterile axion is the PQ solution to the strong CP problem. The lightest sterile neutrino ($m_N^e \sim 10^2$ keV), sterile QCD axion ($m_a < 10^{-6}$ eV, $g_{a\gamma} < 10^{-13}\text{GeV}^{-1}$) and χboson can be dark matter particle candidates, for their tiny couplings and long lifetimes inferred from the Xenon1T experiment. The axion and χboson couplings to SM particles are below the values reached by current laboratory experiments and astrophysical observations for directly or indirectly detecting dark matter particles.

92. S. Campion, J. A.Rueda, S. S. Xue, R. Ruffini "Magnetic field screening process in a Kerr Black Hole ", https://arxiv.org/abs/2002.11681, Physics Letters B Volume 820, 10 September 2021, 136562. This work has been already presented at the 30th Texas Symposium Meeting on Relativistic Astrophysics held in "Portsmouth" in December 2019 and at the SIF National Congress held in "L'Aquila" in September 2019

    It has been shown that a rotating BH immersed in a test background magnetic field, of initial strength B0 and aligned parallel to the BH rotation axis, generates an induced electric field, that is proportional to the magnetic field. In this system, an huge number of pairs can be emitted by vacuum polarization

process and start to be accelerated to high energies, mean this electric field, emitting synchrotron photons. In this paper we study the screening effect of magnetic and electric field due to the magnetic pair production process (hereafter MPP) $\gamma + B \rightarrow e^+ + e^-$ made by the created pairs. The principal results of this study are that: these combined processes of synchrotron emission by accelerated electrons and MPP can decrease magnetic field of several order of magnitude on a small time scale; exist a lower limit for the magnetic field after that it cannot be screened anymore.

93. S. Campion, J. A.Rueda, S. S. Xue, R. Ruffini "On the magnetic field screening in strong crossed electromagnetic field ", This work has been already presented at Sixteenth Marcel Grossmann Meeting - MG16 Virtual Meeting - July 5-10, 2021

    We study the screening of a strong magnetic field operated by an initial huge number of $e^{\pm}$ pairs (we do not discuss here their production mechanism). The background fields configuration is of crossed fields, $\left(\vec{B} = B\,\hat{z},\ \vec{E} = E\,\hat{y}\right)$, with $E/B < 1$. In this system the following series of processes occur: 1) the electric field accelerates the pairs, which radiate high-energy synchrotron photons; 2) these synchrotron photons interact with the background magnetic field via the magnetic pair production process (MPP hereafter), i.e. $\gamma + B \rightarrow e^+ + e^-$, producing additional pairs; 3) the dynamic of all the pairs around the magnetic field lines generates a current that induces a magnetic field oriented in the opposite direction to the background one and then shielding it. We get that, for instance, for an initial number of pairs $N_{\pm,0} = 10^{10}$, an initial magnetic field of 10^{12} G can be reduced of a few percent. The whole screening process described by the steps above, occurs in the short timescales $10^{-21} \leq t \leq 10^{-15}$ s, i.e. the time necessary before the particles acceleration timescale equals the synchrotron cooling timescale. Further developments (as the study of this mechanism in different geometries of the $\vec{E}$ and $\vec{B}$ fields, quantum effects in overcritical fields, other mechanisms for the production, distribution and multiplicity of the $e^{\pm}$ pairs) are necessary in order to apply this model to specific and extreme astrophysical systems (as Black Hole or Neutron Star).

94. S. Tizchang, R. Mohammadi, S. S. Xue "The impact of the Lorentz symmetry violation on the CMB polarization ", This work has been already presented at Sixteenth Marcel Grossmann Meeting - MG16 Virtual Meeting - July 5-10, 2021

    In the standard cosmological scenario, no circular polarization is predicted for Cosmic Microwave Background (CMB) radiation. However, in the frame of moving particle, Lorentz symmetry can violate and lead to circular polarization for CMB radiation. We estimate the circular polarization power spectrum

in CMB radiation due to Compton scattering in presence of the Lorentz symmetry violation. We show that the V-mode power spectrum can be obtained in terms of linear polarization power spectrum at the last scattering surface.

95. Mian Zhu, Amara Ilyas, Yunlong Zheng, Yi-Fu Cai, Emmanuel N. Saridakis "Scalar and Tensor Perturbations in DHOST Bounce Cosmology ", JCAP11 (2021) 045, https://arxiv.org/abs/2108.01339

    We investigate the bounce realization in the framework of DHOST cosmology, focusing on the relation with observables. We perform a detailed analysis of the scalar and tensor perturbations during the Ekpyrotic contraction phase, the bounce phase, and the fast-roll expansion phase, calculating the power spectra, the spectral indices, and the tensor to-scalar ratio. Furthermore, we study the initial conditions, incorporating perturbations generated by Ekpyrotic vacuum fluctuations, by matter vacuum fluctuations, and by thermal fluctuations. The scale invariance of the scalar power spectrum can be acquired by introducing a matter contraction phase before the Ekpyrotic phase or invoking a thermal gas as the source. The DHOST bounce scenario with cosmological perturbations generated by thermal fluctuations proves to be the most efficient one, and the corresponding predictions are in perfect agreement with observational bounds. Especially the tensor-to-scalar ratio is many orders of magnitude within the allowed region since it is suppressed by the Hubble parameter at the beginning of the bounce phase.

96. Mian Zhu, Yunlong Zheng "Improved DHOST Genesis ", JHEP11(2021)163, http://128.84.4.34/abs/2109.05277v2

    We improve the DHOST Genesis proposed in [1], such that the near scale invariant scalar power spectrum can be generated from the model itself, without invoking extra mechanism like a string gas. Besides, the superluminality problem of scalar perturbation plagued in [1] can be rescued by choosing proper DHOST action.

97. Mian Zhu, Yunlong Zheng "Improved DHOST Genesis ", JHEP11(2021)163, http://128.84.4.34/abs/2109.05277v2

    We improve the DHOST Genesis proposed in [1], such that the near scale invariant scalar power spectrum can be generated from the model itself, without invoking extra mechanism like a string gas. Besides, the superluminality problem of scalar perturbation plagued in [1] can be rescued by choosing proper DHOST action.

98. She-Sheng Xue "Massive particle pair production and oscillation in Friedman Universe: its consequence on inflation ", https://arxiv.org/abs/2112.09661

We study the Friedman equation for the time-varying cosmological term and Hubble function H, and quantised field equation for massive modes $M \gg H$. Classical slow components $\mathcal{O}(H^{-1})$ and quantum fast components $\mathcal{O}(M^{-1})$ are coupled. Numerically solving these equations, we show the production of particle-antiparticle pairs and the oscillation of pair density and pressure. Their quantum-time averages effectively modify the classical equation. We present resultant impacts and consequences on inflation. The obtained relation of spectral index and tensor-to-scalar ratio agrees with recent observations.

99. Li-Yang Gao, Ze-Wei Zhao, She-Sheng Xue, Xin Zhang "Relieving the H_0 tension with a new interacting dark energy model ", JCAP 07 (2021) 005, https://arxiv.org/abs/2101.10

We investigate an extended cosmological model motivated by the asymptotic safety of gravitational field theory, in which the matter and radiation densities and the cosmological constant receive a correction parametrized by the parameters δ_G and δ_Λ, leading to that both the evolutions of the matter and radiation densities and the cosmological constant slightly deviate from the standard forms. Here we explain this model as a scenario of vacuum energy interacting with matter and radiation. We consider two cases of the model: (i) $\tilde{\Lambda}$CDM with one additional free parameter δ_G with δ_G and δ_Λ related by a low-redshift limit relation and (ii) e$\tilde{\Lambda}$CDM with two additional free parameters δ_G and δ_Λ independent of each other. We use two data combinations, CMB+BAO+SN (CBS) and CMB+BAO+SN+H_0 (CBSH), to constrain the models. We find that, in the case of using the CBS data, neither $\tilde{\Lambda}$CDM nor e$\tilde{\Lambda}$CDM can effectively alleviate the H_0 tension. However, it is found that using the CBSH data the H_0 tension can be greatly relieved by the models. In particular, in the case of e$\tilde{\Lambda}$CDM, the H_0 tension can be resolved to 0.71σ. We conclude that as an interacting dark energy model, $\tilde{\Lambda}$CDM is much better than $\Lambda(t)$CDM in the sense of both relieving the H_0 tension and fitting to the current observational data.

100. She-Sheng Xue "Massive particle pair production and oscillation in Friedman Universe: dark energy and matter interaction ", https://arxiv.org/abs/2203.11918

The classical Friedman equations of time-varying Hubble function H, dark-energy and matter densities couple to quantised field equations for massive modes $M \gg H$. Numerically solving these equations, we show the particle-antiparticle pairs production and oscillation in microscopic time scale $\mathcal{O}(M^{-1})$. A massive pair plasma state is formed in macroscopic time scale $\mathcal{O}(H^{-1})$. Its density and pressure introduce the interaction of matter and dark energy densities in the Friedman equations. Focusing on epochs after reheating, we show that the negative dark energy tracks down the radiation energy in the radiation epoch. Such tracking dynamics end and dark energy become positive in

the matter epoch. The matter converts to dark energy, and their present values are comparable, explaining the cosmic coincidence. As a result, a class of effective interacting dark energy models is advocated to confront cosmological observations.

101. She-Sheng Xue "W boson mass tension caused by its right-handed gauge coupling at high energies? ", Nuclear Physics B Volume 985, December 2022, 115992 https://arxiv.org/abs/2205.14957

The CDF collaboration's recent high-precision measurement of the Wmass is in 7.0 σ disagreement with the Standard Model expectation. This tension will be relieved if the W boson has a non-trivial right-handed gauge coupling at high energies. At TeV scales, the SM gauge symmetric four-fermion interactions induce a right-handed gauge coupling, and SM fermions compose massive composite particles. We investigate the top-quark mass produced by spontaneous symmetry breaking and compute the W and Z boson propagators and decays. The right-handed coupling corrections to their masses and widths are consistent with experimental measurements. We discuss how SM gauge bosons and composite particles can restore parity-preserving gauge symmetries at TeV scales.

102. She-Sheng Xue "Higgs boson origin from a gauge symmetric theory of massive composite particles and massless $W^{\pm}$ and Z^0 bosons at the TeV scale ", https://arxiv.org/abs/2210.04825

The ultraviolet completion is the Standard Model (SM) gauge-symmetric four-fermion couplings at the high-energy cutoff. Composite particles appear in the gauge symmetric phase in contrast with SM particles in the spontaneous symmetry-breaking phase. The critical point between the two phases is a weak first-order transition. It relates to an ultraviolet fixed point for an SM gauge symmetric theory of composite particles in the strong coupling regime. The low-energy SM realizes at an infrared fixed point in the weak coupling regime. Composite bosons dissolve into SM particles at the phase transition, and in the top-quark channel, they become a composite Higgs boson and three Goldstone bosons. Extrapolation of SM renormalization-group solutions to high energies implies that the gauge-symmetric theory of composite particles has a characteristic scale of about 5.1 TeV. We discuss the phenomenological implications of massive composite bosons coupling to massless $W^{\pm}$ and Z^0 gauge bosons in the gauge symmetric phase.

103. Liang Li, She-Sheng Xue, Zhi-Gao Dai "Relativistic Effects and GRB Polarization in Power-Law Evolution ", https://arxiv.org/abs/2208.03583

Despite decades of polarization observations and high-significance polarized γ-ray, X-ray, optical, and radio emissions in gamma-ray bursts (GRBs) have been accumulating in dozens of cases, people have yet to find a consistent scenario for understanding the globally observed timing properties of GRB polarization to date. Here, we report that the observed properties of GRB polarization exhibit a four-segment timing evolution at the cosmological distance: (I) an initial hump early on (within the first few seconds); (II) a later on power-law decay (from $\sim 10^1$ to $\sim 10^4$ s), which takes the form of $\pi_{\rm obs} \propto t^{-0.50\pm0.02}$; (III) afterwards a late-time rebrightening hump (from $\sim 10^4$ to $\sim 10^5$ s); and (IV) finally a flatting power-law decay (from $\sim 10^5$ to $\sim 10^7$ s), with the the form of $\pi_{\rm obs} \propto t^{-0.21\pm0.08}$. These findings may present a challenge to the mainstream of polarization models that assume the polarization time evolution change in different emission regions. We show that these results can be explained by relativistic and geometric effects of a highly relativistic and magnetized jet generated by central engine, and "magnetic patches" distributed as a globally random but locally coherent form. The long-term timing evolution of observed GRB polarization follows a scaling law $\pi_{\rm obs} \propto 1/S_{\rm obs}$, dominantly determined by how "magnetic patches" are randomly distributed in observed emission region $S_{\rm obs}$ on the jet plane of $1/\Gamma$ cone. It predicts the polarization hump and tail form in accordance with the luminosity jet break phenomenon. Our analysis suggests that there is a single dominant mechanism (relativistic and geometric effects) that may account for the global observational properties of GRB polarization, and other emission mechanisms and effects may play a role in spatially local and temporally short effects on GRB polarization.

104. Li-Yang Gao, She-Sheng Xue, Xin Zhang "Dark energy and matter interacting scenario relieves H_0 and S_8 tensions ", https://arxiv.org/abs/

Given the course of history, significant advancements in cosmology can be attributed to the production of fresh observational data. Nevertheless, it is getting harder and harder to increase the data's precision due to the limitations of observational methods. Additionally, H_0 tension and S_8 tension have emerged as new issues due to the data's accuracy. There is a 4.85σ tension in the ΛCDM model between $H_0 = (67.36 \pm 0.54)$ km s^{-1} Mpc^{-1} provided by *Planck* 2018 from the CMB of the early universe and $H_0 = (73.04 \pm 1.04)$ km s^{-1} Mpc^{-1} provided by Riess et al. from direct observations of the late universe. Additionally, the $S_8 = 0.832 \pm 0.013$ value reported by *Planck* is likewise in a 3.08σ tension with the $S_8 = 0.766^{+0.020}_{-0.014}$ value reported by the combination of the KiDS/Viking and SDSS data based on the late universe. In this work, we examine the $\tilde{\Lambda}$CDM model inspired by the Weinberg asymptotic safety and Parker particle production of gravitational field theory. Using the CBS data only, we

find that the model relieves both H_0 tension to 1.28σ and S_8 tension to 2.67σ. The CBS+H_0 data set constrains the H_0 tension to 0.53σ. The CBS+$H_0 + S_8$ data set constrains the S_8 tension to 2.09σ. And we explain the rationality of the model in terms of both the correlation and the evolution of the density parameter. This demonstrates the $\tilde{\Lambda}$CDM model's consistency with the available evidence and offers some new perspectives on how cosmology works.

6. Invited talks in international conferences

1. Yamada conference "On the dyadosphere of black holes" in Kyoto Japan, April 1998 .
2. International workshop on Gamma Ray Bursts, Rome (1998) .
3. 19th Texas Symposium, Dec. 1998
4. "Exploring the Universe", a Festschrift in honour of Riccardo Giacconi, (2000).
5. Fluctuating Paths and Fields - Dedicated to Hagen Kleinert on the Occasion of His 60th Birthday, Berlin 2001.
6. The ESO workshop on "Black Holes in Binaries and Galactic Nuclei", in honour of Prof. R. Giacconi, (2000) .
7. Marcel Grossmann Meetings IX (Rome) (2000), X (Brazil) (2003) and XI Berlin (2006).
8. International conference in the quantum aspect of beam physics in Hiroshima Japan (2003)
9. "Frontiers in Astroparticle Physics and Cosmology", 6th RESCEU International Symposium, Tokyo 2003.
10. International Conference "Analysis, manifolds and geometric structures in physics", in Honour of Y. Choquet-Bruhat, Isola d'Elba June 24th-26th, 2004 .
11. Brazilian School of Cosmology and Gravitation X (2002), XI (2004) and XII (2006) (Portobello, Brazile).
12. Relativistic Astrophysics and Cosmology - Einstein's Legacy meeting, November 7-11, 2005,
13. 35th COSPAR scientific assembly (Paris, 2004) and 36th COSPAR scientific assembly (Beijing , 2006).

14. 9th International Conference Path Integrals - New Trends and Perspectives, DRESDEN, Germany 23 - 28 September 2007
15. APS April meeting, April 12-15 2008, Saint Louis (USA).
16. V Italian-Sino Workshop, May 28- June 1 2008, Taipei (Taiwan).
17. III Stueckelberg Workshop, July 8-18 2008, Pescara (Italy).
18. XIII Brazilian School of Cosmology and Gravitation, July 20-August 2 2008, Rio de Janeiro (Brazil).
19. Path Integrals - New Trends and Perspectives, September 23 - 28 2007, Dresden (Germany)
20. APS April meeting, April 14-17 2007, Jacksonville (USA).
21. The first Sobral Meeting, May 26-29, 2009 Fortaleza (Ceara) Brazile
22. Zeldovich Meeting, April 20-23, 2009 Minsk - (BELARUS).
23. XI Marcel Grossmann Meeting on General Relativity, July 23-29 2006, Berlin (Germany).
24. The first Galileo - Xu Guangqi Meeting October 26-30, 2009 - Shanghai - (CHINA).
25. 11th Italian-Korean Meeting November 2-4, 2009 - Seoul - (KOREA).
26. Christchurch Meeting December 16-18, 2009 - Christchurch - (New Zealand).
27. Annual Meeting of the Korean Physical Society October 19-22, 2010 - Seoul - (KOREA).
28. The second Galileo - Xu Guangqi Meeting July 12-18, 2010 - Ventimiglia and Nice - (Italy and France).
29. 12th Italian-Korean Meeting July 4-8, 2011, Pescara, Italy .
30. The third Galileo - Xu Guangqi Meeting October 12-16, 2011 Beijing (China).
31. The first LeCosPA Symposium: Towards Ultimate Understanding of the Universe, Feb 6-9, 2012, Taipei Taiwan.
32. The meeting for Italian-Korean cooperation, Nov 5-6, 2012, Seoul, South Korea.
33. The 13th MG meeting, July 1-7, 2012, Stockholm, Sweden.

34. The Scientific meeting of ICRANet, June, 2013, Pescara, Italy.
35. The meeting for 9th Italian-Korean meeting, July 12-18, 2013, Seoul, South Korea.
36. The first Scientific ICRANet Meeting in Armenia, 30 June - 4 July 2014 – Yerevan (Armenia)
37. IZEST-ELI-NP Meeting (Extreme Light's New Horizons Introducting Zepto and Zettawatt Science Societal Applications), Sept. 17-19, 2014, Paris, France.
38. 14th Italian-Korean Symposium on Relativistic Astrophysics, July 20-24, 2015 ICRANet, Pescara Italy.
39. International Conference on Gravitation and Cosmology the fourth Galileo-Xu Guangqi meeting, May 4-8, 2015, Kavli Institute for Theoretical Physics China at the Chinese Academy of Sciences (KITPC) Beijing - China.
40. Fourteenth Marcel Grossmann Meeting - MG14 University of Rome "La Sapienza" - Rome, July 12-18, 2015 The Chair of the parallel session"SF1 - Strong (EM) Fields Physics and Astrophysics" and "SF2 - Ground experiments and astrophysical observations in Strong Field Physics".
41. The Fifth Galileo - Xu Guangqi Meeting June, 2016, Chengdu (China).
42. The parallel session "SF2 - Ground experiments and astrophysical observations in Strong Field Physics", in The Fifteenth Marcel Grossmann Meeting - MG15, University of Rome "La Sapienza" - Rome, July 1-7, 2018
43. Yau Mathematical Sciences Center, Tsinghua University, Beijing China, Dec. 7-15, 2018
44. The first Hangzhou International Meeing on Gravitational Waves Oct, 2016, Hangzhou (China).
45. 16th Italian-Korean Symposium on Relativistic Astrophysics, Pescara, Italy, June 1-5, 2019
46. Open Universe International doctoral School "The discovery of Black Holes", Nice, France, June 11 - 14, 2019
47. Compose-IT: Unitarity for composite models and beyond in1the HL-LHC era, Perugia, Italy, 27-28 January 2020.
48. The 6th China LHC Physics Workshop (CLHCP2020), Beijing, China, November 7, 2020.

49. The Fourth Zeldovich meeting, an international conference in honor of Ya. B. Zeldovich held in Minsk, Belarus on September 7–11, 2020.

50. Sixteenth Marcel Grossmann Meeting - MG16 Virtual Meeting - July 5-10, 2021.

51. The 17th Italian-Korean Symposium for Relativistic Astrophysics - IK17 Virtual Meeting - August 02 (Mon), 2021 August 06 (Fri), 2021.

52. ICRANet-ISFAHAN Astronomy Meeting - Virtual Meeting - 3-5 November 2021 .

7. APPENDICES

A. Dyadosphere (electron-positron-photon plasma) formation in gravitational collapse.

The e^+e^- pairs generated by the vacuum polarization process around the core are entangled in the electromagnetic field Ruffini et al. (2003a), and thermalize in an electron–positron–photon plasma on a time scale $\sim 10^4\tau_C$ Ruffini et al. (2003b) (see Fig. 3.1). As soon as the thermalization has occurred, the hydrodynamic expansion of this electrically neutral plasma starts Ruffini et al. (1999, 2000). While the temporal evolution of the $e^+e^-\gamma$ plasma takes place, the gravitationally collapsing core moves inwards, giving rise to a further amplified supercritical field, which in turn generates a larger amount of e^+e^- pairs leading to a yet higher temperature in the newly formed $e^+e^-\gamma$ plasma. We report progress in this theoretically challenging process which is marked by distinctive and precise quantum and general relativistic effects. As presented in Ref. Ruffini et al. (2003a): we follow the dynamical phase of the formation of Dyadosphere and of the asymptotic approach to the horizon by examining the time varying process at the surface of the gravitationally collapsing core.

It is worthy to remark that the time–scale of hydrodynamic evolution ($t \sim 0.1s$) is, in any case, much larger than both the time scale needed for "all pairs to be created" ($\sim 10^3\tau_C$), and the thermalization time–scale ($\sim 10^4\tau_C$, see Fig. 3.1) and therefore it is consistent to consider pair production, plus thermalization, and hydrodynamic expansion as separate regimes of the system. We assume the initial condition that the Dyadosphere starts to be formed at the instant of gravitational collapse $t_{ds} = t_0(r_{ds}) = 0$, and $r_{ds} = R_c$ the radius of massive nuclear core. Having formulated the core collapse in General Relativity in Eq. (3.8.2), we discretize the gravitational collapse of a spherically symmetric core by considering a set of events ($N-$events) along the world line of a point of fixed angular position on the collapsing core surface. Between each of these events we consider a spherical shell of plasma of constant coordinate thickness Δr so that:

1. Δr is assumed to be a constant which is small with respect to the core radius;
2. Δr is assumed to be large with respect to the mean free path of the particles so that the statistical description of the $e^+e^-\gamma$ plasma can be used;
3. There is no overlap among the slabs and their union describes the entirety of the process.

We check that the final results are independent of the special value of the chosen Δr and N.

In each slab the processes of e^+e^--pair production, oscillation with electric field and thermalization with photons are considered. While the average of the electric field $\mathcal{E}$ over one oscillation is 0, the average of $\mathcal{E}^2$ is of the order of $\mathcal{E}_c^2$, therefore the energy density in the pairs and photons, as a function of r_0, is given by

$$\epsilon_0(r_0) = \frac{1}{8\pi}\left[\mathcal{E}^2(r_0) - \mathcal{E}_c^2\right] = \frac{\mathcal{E}_c^2}{8\pi}\left[\left(\frac{r_{ds}}{r_0}\right)^4 - 1\right]. \tag{A.0.1}$$

For the number densities of e^+e^- pairs and photons at thermal equilibrium we have $n_{e^+e^-} \simeq n_\gamma$; correspondingly the equilibrium temperature T_0, which is clearly a function of r_0 and is different for each slab, is such that Ruffini et al. (1999, 2000)

$$\epsilon(T_0) \equiv \epsilon_\gamma(T_0) + \epsilon_{e^+}(T_0) + \epsilon_{e^-}(T_0) = \epsilon_0, \tag{A.0.2}$$

with ϵ and n given by Fermi (Bose) integrals (with zero chemical potential):

$$\epsilon_{e^+e^-}(T_0) = \frac{2}{\pi^2\hbar^3}\int_{m_e}^{\infty}\frac{\left(E^2-m_e^2\right)^{1/2}}{\exp(E/kT_0)+1}E^2dE, \quad \epsilon_\gamma(T_0) = \frac{\pi^2}{15\hbar^3}(T_0)^4, \tag{A.0.3}$$

$$n_{e^+e^-}(T_0) = \frac{1}{\pi^2\hbar^3}\int_{m_e}^{\infty}\frac{\left(E^2-m_e^2\right)^{1/2}}{\exp(E/kT_0)+1}EdE, \quad n_\gamma(T_0) = \frac{2\zeta(3)}{\hbar^3}(T_0)^3. \tag{A.0.4}$$

From the conditions set by Eqs. (A.0.2), (A.0.3), (A.0.4), we can now turn to the dynamical evolution of the $e^+e^-\gamma$ plasma in each slab. We use the covariant conservation of energy momentum and the rate equation for the number of pairs in the Reissner–Nordström geometry external to the core:

$$\nabla_a T^{ab} = 0, \tag{A.0.5}$$

$$\nabla_a\left(n_{e^+e^-}u^a\right) = \overline{\sigma v}\left[n_{e^+e^-}^2(T) - n_{e^+e^-}^2\right], \tag{A.0.6}$$

where $T^{ab} = (\epsilon + p)u^a u^b + pg^{ab}$ is the energy–momentum tensor of the plasma with proper energy density ϵ and proper pressure p, u^a is the fluid 4−velocity, $n_{e^+e^-}$ is the number of pairs, $n_{e^+e^-}(T)$ is the equilibrium number of pairs and $\overline{\sigma v}$ is the mean of

the product of the e^+e^- annihilation cross-section and the thermal velocity of pairs. In each slab the plasma remains at thermal equilibrium in the initial phase of the expansion and the right hand side of the rate Eq. (A.0.6) is effectively 0.

If we denote by ξ^a the static Killing vector field normalized at unity at spacial infinity and by $\{\Sigma_t\}_t$ the family of space-like hypersurfaces orthogonal to ξ^a (t being the Killing time) in the Reissner–Nordström geometry, from Eqs. (A.0.6), the following integral conservation laws can be derived

$$\int_{\Sigma_t} \xi_a T^{ab} d\Sigma_b = E, \quad \int_{\Sigma_t} n_{e^+e^-} u^b d\Sigma_b = N_{e^+e^-}, \tag{A.0.7}$$

where $d\Sigma_b = \alpha^{-2}\xi_b r^2 \sin\theta dr d\theta d\phi$ is the vector surface element, E the total energy and $N_{e^+e^-}$ the total number of pairs which remain constant in each slab. We then have

$$\left[(\epsilon + p)\gamma^2 - p\right] r^2 = \mathfrak{E}, \quad n_{e^+e^-}\gamma\alpha^{-1}r^2 = \mathfrak{N}_{e^+e^-}, \tag{A.0.8}$$

where $\mathfrak{E}$ and $\mathfrak{N}_{e^+e^-}$ are constants and

$$\gamma \equiv \alpha^{-1}u^a\xi_a = \left[1 - \alpha^{-4}\left(\frac{dr}{dt}\right)^2\right]^{-1/2} \tag{A.0.9}$$

is the Lorentz γ factor of the slab as measured by static observers. We can rewrite Eqs. (A.0.7) for each slab as

$$\left(\frac{dr}{dt}\right)^2 = \alpha^4 f_{r_0}, \tag{A.0.10}$$

$$\left(\frac{r}{r_0}\right)^2 = \left(\frac{\epsilon+p}{\epsilon_0}\right)\left(\frac{n_{e^+e^-0}}{n_{e^+e^-}}\right)^2\left(\frac{\alpha}{\alpha_0}\right)^2 - \frac{p}{\epsilon_0}\left(\frac{r}{r_0}\right)^4, \tag{A.0.11}$$

$$f_{r_0} = 1 - \left(\frac{n_{e^+e^-}}{n_{e^+e^-0}}\right)^2\left(\frac{\alpha_0}{\alpha}\right)^2\left(\frac{r}{r_0}\right)^4 \tag{A.0.12}$$

where pedex $_0$ refers to quantities evaluated at selected initial times $t_0 > 0$, having assumed $r(t_0) = r_0$, $dr/dt|_{t=t_0} = 0$, $T(t_0) = T_0$.

Eq. (A.0.10) is only meaningful when $f_{r_0}(r) \geq 0$. From the structural analysis of such equation it is clearly identifiable a critical radius r_0 such that:

- for any slab initially located at $r_0 > \bar{R}$ we have $f_{r_0}(r) \geq 0$ for any value of $r \geq r_0$ and $f_{r_0}(r) < 0$ for $r \lesssim r_0$; therefore a slab initially located at a radial coordinate $r_0 > \bar{R}$ moves outwards,

- for any slab initially located at $r_0 < \bar{R}$ we have $f_{r_0}(r) \geq 0$ for any value of $r_+ < r \leq r_0$ and $f_{r_0}(r) < 0$ for $r \gtrsim r_0$; therefore a slab initially located at a radial coordinate $r_0 < \bar{R}$ moves inwards and is trapped by the gravitational

field of the collapsing core.

We define the surface $r = \bar{R}$, the *Dyadosphere trapping surface* (DTS). The radius $\bar{R}$ of DTS is generally evaluated by the condition $\left.\frac{df_{\bar{R}}}{dr}\right|_{r=\bar{R}} = 0$. $\bar{R}$ is so close to the horizon value r_+ that the initial temperature T_0 satisfies $kT_0 \gg m_e c^2$ and we can obtain for $\bar{R}$ an analytical expression. Namely the ultra relativistic approximation of all Fermi integrals, Eqs. (A.0.3) and (A.0.4), is justified and we have $n_{e^+e^-}(T) \propto T^3$ and therefore $f_{r_0} \simeq 1 - (T/T_0)^6 (\alpha_0/\alpha)^2 (r/r_0)^4$ ($r \leq \bar{R}$). The defining equation of $\bar{R}$, together with (A.0.12), then gives

$$\bar{R} = 2M \left[1 + \left(1 - 3Q^2/4M^2\right)^{1/2}\right] > r_+. \tag{A.0.13}$$

In the case of an EMBH with $M = 20M_\odot$, $Q = 0.1M$, we compute:

- the fraction of energy trapped in DTS:

$$\bar{E} = \int_{r_+<r<\bar{R}} \alpha\epsilon_0 d\Sigma \simeq 0.53 \int_{r_+<r<r_{\rm ds}} \alpha\epsilon_0 d\Sigma; \tag{A.0.14}$$

- the world–lines of slabs of plasma for selected r_0 in the interval $(\bar{R}, r_{\rm ds})$ (see left figure in Fig. A.1);
- the world–lines of slabs of plasma for selected r_0 in the interval $(r_+, \bar{R})$ (see Fig. A.2).

At time $\bar{t} \equiv t_0(\bar{R})$ when the DTS is formed, the plasma extends over a region of space which is almost one order of magnitude larger than the Dyadosphere and which we define as the *effective Dyadosphere*. The values of the Lorentz γ factor, the temperature and e^+e^- number density in the effective Dyadosphere are given in the right figure in Fig. A.1.

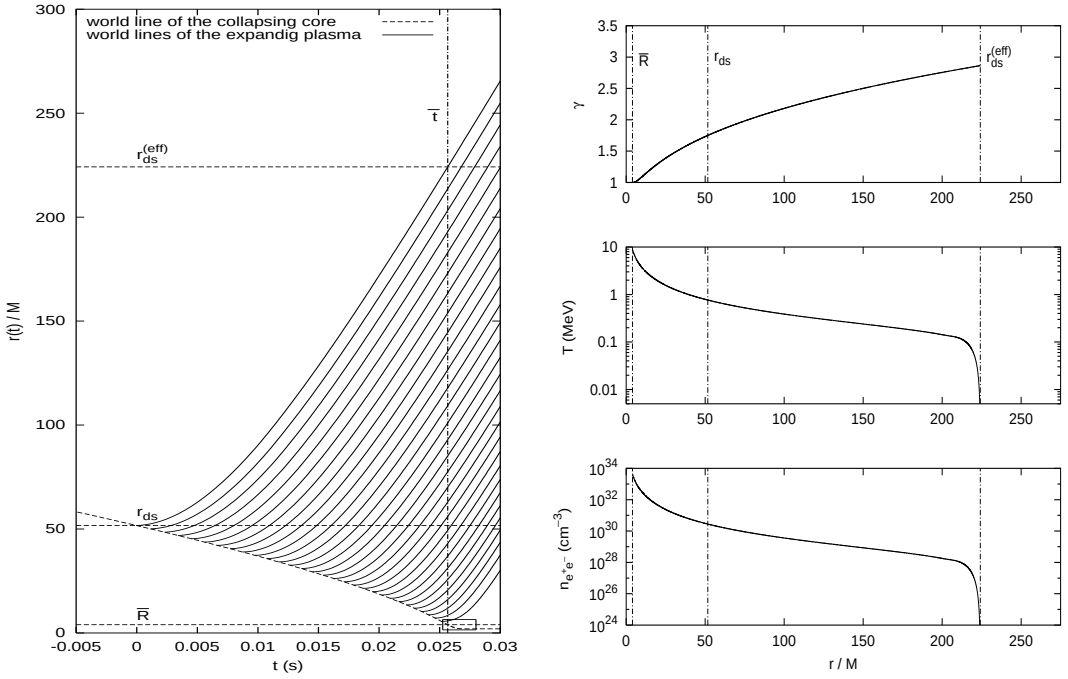

Figure A.1.: In left figure: World line of the collapsing charged core (dashed line) as derived from Eq. (3.8.2); world lines of slabs of plasma for selected radii r_0 in the interval $(\bar{R}, r_{\rm ds})$. At time $\bar{t}$ the expanding plasma extends over a region which is almost one order of magnitude larger than the Dyadosphere. The small rectangle in the right bottom is enlarged in Fig. A.2. The right figure: Physical parameters in the effective Dyadosphere: Lorentz γ factor, proper temperature and proper e^+e^- number density as functions at time $\bar{t}$.

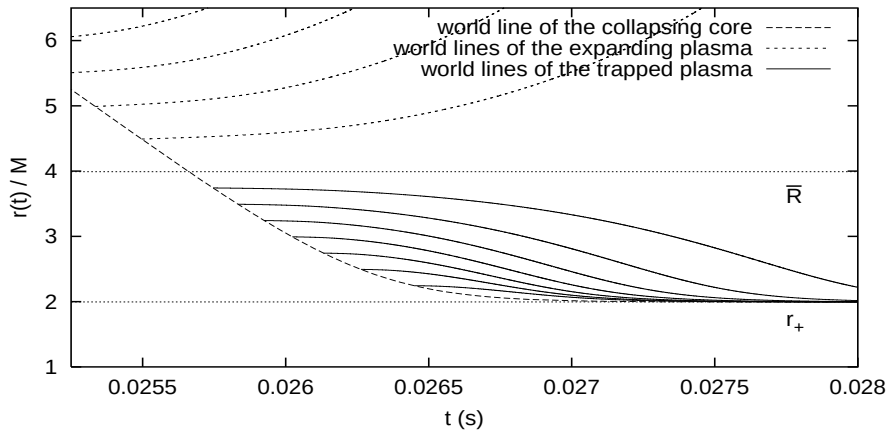

Figure A.2.: Enlargement of the small rectangle in the right bottom of left figure in Fig. A.1. World–lines of slabs of plasma for selected radii r_0 in the interval $(r_+, \bar{R})$.

B. Electron-positron pair oscillation in spatially inhomogeneous electric fields and radiation

Introduction. As reviewed in the recent report Ruffini et al. (2010), since the pioneer works by Sauter Sauter (1931), Heisenberg and Euler Heisenberg and Euler (1936) in 1930's, then by Schwinger Schwinger (1951) in 1950's, it has been well known that positron-electron pairs are produced from the vacuum in external electric fields. In a constant electric field E_0 in dependent of space and time, the pair-creation rate per unit volume is given by Heisenberg and Euler (1936),

$$S \equiv \frac{dN}{dVdt} = \frac{m_e^4}{4\pi^3}\left(\frac{E_0}{E_c}\right)^2 \exp\left(-\pi\frac{E_c}{E_0}\right), \tag{B.0.1}$$

where the critical field $E_c \equiv m_e^2 c^3/(e\hbar)$, the Plank's constant $\hbar$, the speed of light c, the electron mass m_e, the absolute value of electron charge e and the fine structure constant $\alpha = e^2/\hbar c$ (in this article we use the natural units $\hbar = c = 1$, unless otherwise specified). The pair-production rate (B.0.1) is significantly large for strong electric fields $E \gtrsim E_c \simeq 1.3 \cdot 10^{16}$V/cm. The critical field will probably be reached by recent advanced laser technologies in laboratory experiments Ringwald (2001); Tajima and Mourou (2002); Gordienko et al. (2005), X-ray free electron laser (XFEL) facilities[1], optical high-intensity laser facilities such as Vulcan or ELI[2], and SLAC E144 using nonlinear Compton scattering Burke et al. (1997). On the other hand, strong over-critical electric fields ($E \geq 10E_c$) can be created in astrophysical environments, for instance, quark stars Usov (1998); Usov et al. (2005) and neutron stars Ruffini et al. (2007a)-Popov et al. (2009).

The back-reaction and screening effects of electron and positron pairs on external electric fields lead to the phenomenon of plasma oscillations: electrons and positrons

[1] http://www.xfel.eu

[2] http://www.extreme-light-infrastructure.eu

moving back and forth coherently with alternating electric fields. This means that external electric fields are not eliminated within the Compton time $\hbar/m_e c^2$ of pair-production process, rather oscillate collectively with the motion of pairs in a much longer timescale.

In a constant electric field E_0 (B.0.1), the phenomenon of plasma oscillations is studied in the two frameworks Ruffini et al. (2010): (1) the semi-classical QED with quantized Dirac field and classical electric field Kluger et al. (1991, 1992); Cooper and Mottola (1989); (2) the kinetic description using the Boltzmann-Vlasov and Maxwell equations Biro et al. (1984); Gatoff et al. (1987); Cooper et al. (1993); Ruffini et al. (2003b, 2007b). In the second framework, the Boltzmann-Vlasov equation is used to obtain the equations for the continuity and energy-momentum conservations Gatoff et al. (1987).

Ref. Ruffini et al. (2007b) shows the evidence of plasma oscillation in under-critical field ($E < E_c$) and the relation between the kinetic energy and numbers of oscillating pairs in a given electric field strength E_0. Taking into account the creation and annihilation process $e^+ + e^- \Leftrightarrow \gamma + \gamma$, it is shown Ruffini et al. (2003b) that the plasma oscillation in an overcritical field is led to a plasma of photons, electrons and positions with the equipartition of their number- and energy-densities. The phenomenon of plasma oscillations is studied in connection with pair creation in heavy ions collisions Biro et al. (1984)-Cooper et al. (1993), the laser field Ringwald (2001)-Hebenstreit et al. (2008), and gravitational collapse Ruffini et al. (2003a). It is worthwhile to emphasize that the plasma oscillation occurs not only at overcritical field-strengths $E_0 \gtrsim E_c$ (see for instance Refs. Kluger et al. (1991, 1992); Ruffini et al. (2003b)), but also undercritical field-strengths $E_0 \lesssim E_c$ (see Ref. Ruffini et al. (2007b)), and plasma oscillation frequency is related to field-strength E_0, while the number of oscillating pairs depends on the pair-production rate (B.0.1). More details can be found in the recent review article Ruffini et al. (2010).

The realistic ultra-strong electric fields are not only vary with space and time, but also confined in a finite region. In this letter, studying the plasma oscillations in spatially inhomogeneous electric field, we present the evidence of electric fields propagation, leading to electromagnetic radiation with a peculiar narrow spectrum in the keV-region, which should be distinctive and experimentally observable.

In the kinetic description for the plasma fluids of positrons ($+$) or electrons ($-$), whose single-particle spectrum $p^0_\pm = (\mathbf{p}^2_\pm + m_e^2)^{1/2}$, we define the number-densities

$n_\pm(t,\mathbf{x})$ and "averaged" velocities $\mathbf{v}_\pm(t,\mathbf{x})$ of the fluids:

$$n_\pm(t,\mathbf{x}) \equiv \int \frac{d^3\mathbf{p}_\pm}{(2\pi)^3} f_\pm(t,\mathbf{p}_\pm,\mathbf{x}), \tag{B.0.2}$$

$$\mathbf{v}_\pm(t,\mathbf{x}) \equiv \frac{1}{n_\pm}\int \frac{d^3\mathbf{p}_\pm}{(2\pi)^3}\left(\frac{\mathbf{p}_\pm}{p^0_\pm}\right) f_\pm(t,\mathbf{p}_\pm,\mathbf{x}), \tag{B.0.3}$$

where $f_\pm(t,\mathbf{p}_\pm,\mathbf{x})$ is the distribution function in the phase space. The four-velocities of the electron and positron fluids $U^\mu_\pm = \gamma_\pm(1,\mathbf{v}_\pm)$, the Lorentz factor $\gamma_\pm = (1 - |\mathbf{v}_\pm|^2)^{-1/2}$, and the comoving number-densities $\bar{n}_\pm = n_\pm(\gamma_\pm)^{-1}$, where we choose the laboratory frame where pairs are created at rest. The collision-less plasma fluid of electrons and positrons coupling to electromagnetic fields is governed by the continuity, energy-momentum conservation and Maxwell equations:

$$\frac{\partial\left(\bar{n}_\pm U^\mu_\pm\right)}{\partial x^\mu} = S, \tag{B.0.4}$$

$$\frac{\partial T^{\mu\nu}_\pm}{\partial x^\nu} = -F^\mu_\sigma(J^\sigma_\pm + J^\sigma_{\pm\mathrm{pola}}), \tag{B.0.5}$$

$$\frac{\partial F^{\mu\nu}}{\partial x^\nu} = -4\pi(J^\mu_{\mathrm{cond}} + J^\mu_{\mathrm{pola}} + J^\mu_{\mathrm{ext}}), \tag{B.0.6}$$

where is the pair-production rate, $J^\mu_\pm = \pm e\bar{n}_\pm U^\mu_\pm$ electric currents and the energy-momentum tensors Weinberg (1972)

$$T^{\mu\nu}_\pm = \bar{p}_\pm g^{\mu\nu} + (\bar{p}_\pm + \bar{\epsilon}_\pm)U^\mu_\pm U^\nu_\pm, \tag{B.0.7}$$

and the pressure $\bar{p}_\pm$ and comoving energy-density $\bar{\epsilon}_\pm$ is related by the equation of state, in general $0 \le \bar{p}_\pm \le \bar{\epsilon}_\pm/3$. In the laboratory frame, the fluid energy-density $\epsilon_\pm \equiv T^{00}$ and momentum-density $p^i_\pm \equiv T^{i0}$ are given by

$$\epsilon_\pm = (\bar{\epsilon}_\pm + \bar{p}_\pm\mathbf{v}^2_\pm)\gamma^2_\pm, \quad \mathbf{p}_\pm = (\bar{\epsilon}_\pm + \bar{p}_\pm)\gamma^2_\pm\mathbf{v}_\pm. \tag{B.0.8}$$

In Eqs. (B.0.5,B.0.6) F^μ_σ is the tensor of electromagnetic fields $(\mathbf{E},\mathbf{B})$, the conducting four-current density

$$J^\mu_{\mathrm{cond}} \equiv e(\bar{n}_+U^\mu_+ - \bar{n}_-U^\mu_-), \quad \partial_\mu J^\mu_{\mathrm{cond}} = 0, \tag{B.0.9}$$

and polarized four-current density $J^\mu_{\mathrm{pola}} = \sum_\pm J^\mu_{\pm\mathrm{pola}}$ and $J^\mu_{\pm\mathrm{pola}} = \left(\rho^\pm_{\mathrm{pola}}, \mathbf{J}^\pm_{\mathrm{pola}}\right)$ Gatoff

et al. (1987); Kajantie and Matsui (1985)

$$F^{\nu}_{\mu} J^{\mu}_{\pm\text{pola}} = \Sigma^{\nu}_{\pm}, \quad \Sigma^{\nu}_{\pm} \equiv \int \frac{d^3\mathbf{p}_{\pm}}{(2\pi)^3 p^0_{\pm}} p^{\nu}_{\pm} \mathcal{S}, \tag{B.0.10}$$

and $S = \int d^3\mathbf{p}_{\pm}/[(2\pi)^3 p^0_{\pm}]\mathcal{S}$. Using "averaged" velocities (B.0.3) of the fluids, we approximately have

$$\mathbf{J}^{\pm}_{\text{pola}} \simeq \frac{m_e \gamma_{\pm} S}{|\mathbf{E}|}\hat{\mathbf{E}}, \quad \rho^{\pm}_{\text{pola}} \simeq \pm \frac{m_e \gamma_{\pm} |\mathbf{v}_{\pm}| S}{|\mathbf{E}|}, \tag{B.0.11}$$

where the magnetic field $\mathbf{B} = 0$. In Eq. (B.0.6), $J^{\mu}_{\text{ext}} = (\rho_{\text{ext}}, \mathbf{J}_{\text{ext}})$ is an external electric current.

Basic equations of motion. For simplicity to start with, we consider the electric field $\mathbf{E}_{\text{ext}}$ created by a capacitor made of two parallel plates, one carries an external charge $+Q$ and another $-Q$. The sizes of two parallel plats are L_x and L_y, which are much larger than their separation ℓ in the $\hat{\mathbf{z}}$-direction, i.e., $L_x \gg \ell$ and $L_y \gg \ell$. For $|z| \sim \mathcal{O}(\ell)$, the system has an approximate translation symmetry in the (x, y) plane. As results the electric field $\mathbf{E}_{\text{ext}}(x, y, z) \approx E_{\text{ext}}(z)\hat{\mathbf{z}}$ and $\mathbf{B}_{\text{ext}}(x, y, z) \approx 0$, is approximately homogeneous in the (x, y) plane and confined within the capacitor. In addition, $\partial \mathbf{E}_{\text{ext}}/\partial t \approx 0$, namely, this electric field is assumed to be continuously supplied by an external source $(+Q, -Q)$ or slowly varying. In order to do calculations we model this electric field as the one-dimensional Sauter electric field in the $\hat{\mathbf{z}}$-direction

$$E_{\text{ext}}(z) = E_0/\cosh^2(z/\ell), \quad \sigma \equiv eE_0\ell/m_e c^2 = (\ell/\lambda_C)(E_0/E_c), \tag{B.0.12}$$

where the λ_C is Compton wavelength, the external electric charge is given by $\partial E_{\text{ext}}(z)/\partial z = 4\pi\rho_{\text{ext}}$ and the external electric current vanishes $J_{\text{ext}} = 0$ for the field being static $\partial E_{\text{ext}}/\partial t = 0$. In the electric field configuration (B.0.12) and $\mathbf{B} \approx 0$, the "averaged" velocities $v_{\pm}$ of electrons and positrons fluids are in the $\hat{\mathbf{z}}$-direction,

$$U^{\mu}_{\pm} = \gamma_{\pm}\left(1, 0, 0, \pm v_{\pm}\right), \tag{B.0.13}$$

and the total fluid current- and charge-densities (B.0.6) $J^{\mu} = (\rho, \mathbf{J})$ are

$$J_z = en_+ v_+ + en_- v_- + \frac{m_e(\gamma_+ + \gamma_-)S}{E}, \tag{B.0.14}$$

$$\rho = e\left(n_+ - n_-\right) + \frac{m_e(\gamma_+ v_+ - \gamma_- v_-)S}{E}. \tag{B.0.15}$$

The system can be approximately treated as a $1+1$ dimensional system in terms of

space-time variables (z,t), and Eqs. (B.0.4-B.0.6) become for zero pressure [3],

$$\frac{\partial n_\pm}{\partial t} \pm \frac{\partial n_\pm v_\pm}{\partial z} = S, \tag{B.0.16}$$

$$\frac{\partial \epsilon_\pm}{\partial t} \pm \frac{\partial p_\pm}{\partial z} = e n_\pm v_\pm E + m_e \gamma_\pm S, \tag{B.0.17}$$

$$\frac{\partial p_\pm}{\partial t} \pm \frac{\partial p_\pm v_\pm}{\partial z} = e n_\pm E + m_e \gamma_\pm v_\pm S, \tag{B.0.18}$$

$$\frac{\partial E}{\partial t} = -4\pi J_z, \tag{B.0.19}$$

$$\frac{\partial E}{\partial z} = 4\pi(\rho + \rho_{\rm ext}). \tag{B.0.20}$$

The total electric field $E(z,t)$ in Eqs. (B.0.14-B.0.20) is the superposition of two components:

$$E(z,t) = E_{\rm ext}(z) + E_{\rm ind}(z,t), \tag{B.0.21}$$

where the space- and time-dependent $E_{\rm ind}(z,t)$ is the electric field created by electron and positron pairs. We call $J_z(z,t)$ (B.0.14), $\rho(z,t)$ (B.0.15) and $E_{\rm ind}(z,t)$ pair-induced electric current, charge and field.

As for the pair-production rate S in Eqs. (B.0.16-B.0.19), instead of the pair-production rate (B.0.1) for a constant field E_0, we adopt the following z-dependent formula for the pair-production rate in the Sauter field (B.0.12), obtained by using the WKB-method to calculate the probability of quantum-mechanical tunneling Kleinert et al. (2008),

$$S(z) = \frac{m_e^4}{4\pi^3}\frac{E_0 E(z)}{E_c^2 \tilde{G}[0,\mathcal{E}]} e^{-\pi G[0,\mathcal{E}]E_c/E_0}, \tag{B.0.22}$$

where $G(0,\mathcal{E})$ and $\tilde{G}(0,\mathcal{E})$ are functions of the energy-level crossings $\mathcal{E}(z)$ and we approximately adopt $E(z) \approx E_0/G(0,\mathcal{E}) \approx E_0/\tilde{G}(0,\mathcal{E})$ in Eq. (B.0.22) in order to

[3] For an electric field $E \sim E_c$, the number-density of electron-positron pairs is small and the pressure of pairs can be neglected. While for an over electric field $E \gg E_c$, the number-density of pairs is large and the collisions and annihilation of pairs into photons are important, leading to the energy equipartition of electron, positrons and photons. In this case, the pressure, effective temperature and equation of state have to be considered.For an electric field $E \sim E_c$, the number-density of electron-positron pairs is small and the pressure of pairs can be neglected. While for an over electric field $E \gg E_c$, the number-density of pairs is large and the collisions and annihilation of pairs into photons are important, leading to the energy equipartition of electron, positrons and photons. In this case, the pressure, effective temperature and equation of state have to be considered.

do feasible numerical calculations. As shown by the Fig. 2 in Ref. Kleinert et al. (2008), the deviation of the pair-production rate (B.0.22) due to this approximation is small. The formula (B.0.22) is derived for the static Sauter field (B.0.12). However, analogously to the discussions for the plasma oscillations in spatially homogeneous fields Cooper et al. (1993)-Ruffini et al. (2007b), it can be approximately used for a time-varying electric field $E(z,t)$ (B.0.21), provided the time-dependent component $E_{\rm ind}(z,t)$, created by electron-positron pair-oscillations, varies much slowly compared with the rate of electron-positron pair-productions $\mathcal{O}(m_e c^2/\hbar)$. This can be justified by the inverse adiabaticity parameter Greiner et al. (1985)-Popov (1973a),

$$\eta = \frac{m_e}{\omega}\frac{E_0}{E_c} \gg 1, \tag{B.0.23}$$

where ω is the frequency of pair-oscillations.

Eqs. (B.0.16,B.0.17,B.0.18) describe the motion of electron-positron plasma coupling to the electric field E and source S of pair-productions. The Maxwell equations (B.0.19,B.0.20) describe the motion of the electric field (B.0.21) coupled to the current- and charge-densities (B.0.15), leading to the wave equation of the propagating electric field $E_{\rm ind}(z,t)$ Jackson (1998),

$$\frac{\partial^2 E_{\rm ind}}{\partial t^2} - \frac{1}{c^2}\frac{\partial^2 E_{\rm ind}}{\partial z^2} = 4\pi\left(\frac{\partial \rho}{\partial z} + \frac{1}{c^2}\frac{\partial J_z}{\partial t}\right), \tag{B.0.24}$$

where we use $\partial E_{\rm ext}/\partial z = 4\pi\rho_{\rm ext}$ and $\partial E_{\rm ext}/\partial t = 0$. This wave equation shows the propagating electric field $E_{\rm ind}(z,t)$ in the region $\mathcal{R}$ where the non-vanishing current J_z and charge ρ are, and both the propagation and polarization of the electric field are in the $\hat{\mathbf{z}}$-direction. This implies a wave transportation of electromagnetic energies inside the region $\mathcal{R}$. Since the current- and charge-densities (ρ, J_z) are functions of the field $E(t,z)$ (B.0.21), the wave equation is highly nonlinear, the dispersion relation of the field is very complex and the velocity of field-propagation is not the speed of light.

Numerical integrations. Given the parameters $E_0 = E_c$ and $\ell = 10^5\lambda_C$ of the Sauter field (B.0.12) as an initial electric field $E_{\rm ext}$, we numerically integrate Eqs.(B.0.16-B.0.19) in the spatial region $\mathcal{R}$: $-\ell/2 \le z \le \ell/2$ and time interval $\mathcal{T}$: $0 \le t \le 3500\tau_C$, where τ_C is the Compton time. The value $\mathcal{T} \le 3500\tau_C$ is chosen so that the adiabatic condition (B.0.23) is satisfied, and the spatial range $\mathcal{R}$ is determined by the capacity of computer for numerical calculations. The electric field strength E_0 is chosen around the critical value E_c, so that the semiclassical pair-production rate (B.0.22) can be approximately used. Actually, E_0, ℓ and $\mathcal{T}$ are attributed to the characteristics of external ultra-strong electric fields $E_{\rm ext}$ established by either experimental setups or astrophysical conditions.

In Figs. B.1 and B.2, we respectively plot the time- and space-evolution of the total electric fields $E(z,t)$ (B.0.21) as functions of t and z at three different spatial points and times. As discussed in Figure captions, numerical results show the properties of the electric field wave $E_{\rm ind}(z,t)$ propagating in the plasma of oscillating electron-positron pairs, as described by the wave equation (B.0.24). This electric field wave propagates along the directions in which external electric field-strength decreases. The wave propagation is rather complex, depending on the space and time variations of the net charge density $\rho(z,t)$ and current density $j_z(z,t)$, as shown in Figs. B.4-B.5. The net charge density ρ oscillates (see Figs. B.3 and B.4) proportionally to the field-gradient (B.0.20) and at the center $z=0$ the charge density and field-gradient are zero independent of time evolution (see Fig. B.4). However, the total charge of pairs $Q=\int_{\mathcal{R}} d^3x\rho$ must be zero at any time, as required by the neutrality. The electric current $j_z(z,t)$ alternating in space and time follows the space and time evolution of the electric field $E(z,t)$ see Eq. (B.0.19), as shown in Figs. B.5 and B.6.

We recall the discussions of the plasma oscillations in the case of spatially homogeneous electric field E_0 without boundary Ruffini et al. (2003b, 2007b). Due to the spatial homogeneity of electric fields and pair-production rate S (B.0.1), the number-densities $n_\pm(t,\mathbf{x})=n(t)$ (B.0.2), "averaged" velocities $|\mathbf{v}_\pm(t,\mathbf{x})|=v(t)$ (B.0.3) and energy-momenta $\epsilon_\pm(t,\mathbf{x})=\epsilon(t), |\mathbf{p}_\pm(t,\mathbf{x})|=p(t)$ (B.0.8) are spatially homogeneous so that the charge density (B.0.15) $\rho\equiv 0$ identically vanishes and current (B.0.14) $J_z=J_z(t)$. All spatial derivative terms in Eqs. (B.0.16-B.0.18) and Eq. (B.0.24) vanish and Eq. (B.0.20) becomes irrelevant. As results, the plasma oscillations described is the oscillations of electric fields and currents with respect time at each spatial point, and the electric field has no any spatial correlation and does not propagate.

In contrary to the plasma oscillation in homogeneous fields, the presence of such field-propagation in inhomogeneous fields is due to: (i) non-vanishing field-gradient $\partial_z E$ (B.0.20) and net charge-density ρ (B.0.15), as shown in Figs. B.3 and B.4, give the spatial correlations of the fields at neighboring points; (ii) the stronger field-strength, the larger field-oscillation frequency is, as shown in Fig. B.1; (iii) at the center $z=0$ the field-strength is largest and the field-oscillation is most rapid, and the field-oscillations at points $|z|>0$ are slower and in retard phases, as shown in Fig. B.2. The point (i) is essential, the charge density ρ oscillates (see Figs. B.3 and B.4) proportionally to the field-gradient Eq. (B.0.20) and at the center $z=0$ the charge density and field-gradient are zero independent of time evolution (see Fig. B.4). Such field-propagation is reminiscent of the drift motion of particles driven by a field-gradient ("ponderomotive") force, which is a cycle-averaged force on a charged particle in a spatially inhomogeneous oscillating electromagnetic field Boot and R.-S.-Harvie (1957); Kibble (1966); Hopf et al. (1976).

Radiation fields. As numerically shown in Fig. B.1-B.6, the propagation of the electric field wave $E_{\rm ind}(z,t)$ inside the region $\mathcal{R}$ is rather complex, due to th high non-

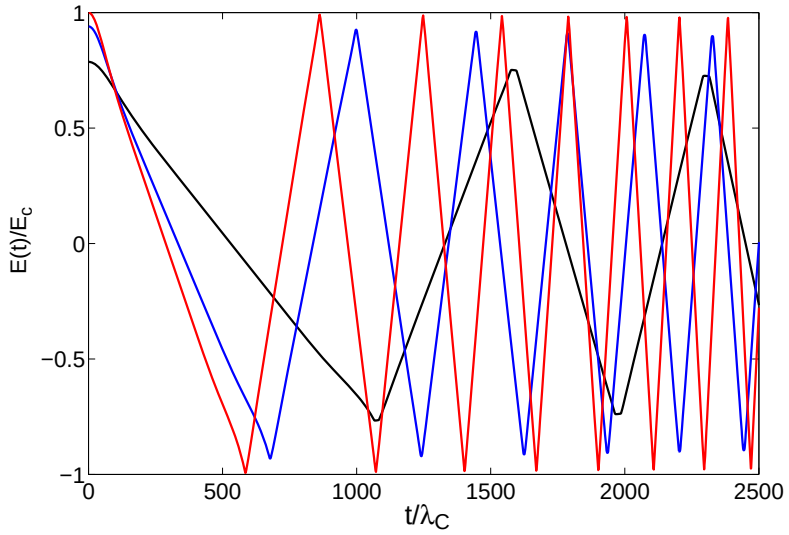

Figure B.1.: Electric fields $E(z,t)$ are plotted as functions of t at three different points: $z=0$ (red), $z=\ell/4$ (blue) and $z=\ell/2$ (black). Analogously to the plasma oscillation in homogeneous fields, the stronger initial field-strength, the larger field-oscillation frequency is, i.e., $\omega(z=0)>\omega(z=\ell/4)>\omega(z=\ell/2)$, where $\omega(z)$ is the field oscillating frequency at the spatial point z.

linearity of wave equation (B.0.24). Nevertheless, the electromagnetic radiation fields $\mathbf{E}_{\rm rad}$ and $\mathbf{B}_{\rm rad}$ far away from the region $\mathcal{R}$ are completely determined and could be experimentally observable. At the space-time point $(t,\mathbf{x})$ of an observer, the electromagnetic radiation fields $\mathbf{E}_{\rm rad}(z,t)$ and $\mathbf{B}_{\rm rad}(z,t)$, emitted by the variations of electric charge density $\rho(\mathbf{x}',t')$ and current-density $\mathbf{J}(\mathbf{x}',t')$ in the region $\mathcal{R}$ $(\mathbf{x}'\in\mathcal{R})$ and time t' $(t'\in\mathcal{T})$, are given by Jackson (1998)

$$\mathbf{E}_{\rm rad}(t,\mathbf{x}) = -\int_{\mathcal{R}} d^3\mathbf{x}'\Big\{\frac{\hat{\mathbf{R}}}{R^2}\left[\rho(t',\mathbf{x}')\right]_{\rm ret}+\frac{\hat{\mathbf{R}}}{cR}\left[\frac{\partial\rho(t',\mathbf{x}')}{\partial t'}\right]_{\rm ret} + \frac{1}{c^2R}\left[\frac{\partial\mathbf{J}(t',\mathbf{x}')}{\partial t'}\right]_{\rm ret}\Big\}, \tag{B.0.25}$$

$$\mathbf{B}_{\rm rad}(t,\mathbf{x}) = \int_{\mathcal{R}} d^3\mathbf{x}'\left\{\left[\mathbf{J}(t',\mathbf{x}')\right]_{\rm ret}\times\frac{\hat{\mathbf{R}}}{cR^2}+\left[\frac{\partial\mathbf{J}(t',\mathbf{x}')}{\partial t'}\right]_{\rm ret}\times\frac{\hat{\mathbf{R}}}{c^2R}\right\}. \tag{B.0.26}$$

where the subscript "ret" indicates $t'=t-R/c$, $R=|\mathbf{x}-\mathbf{x}'|$. In the radiation zone

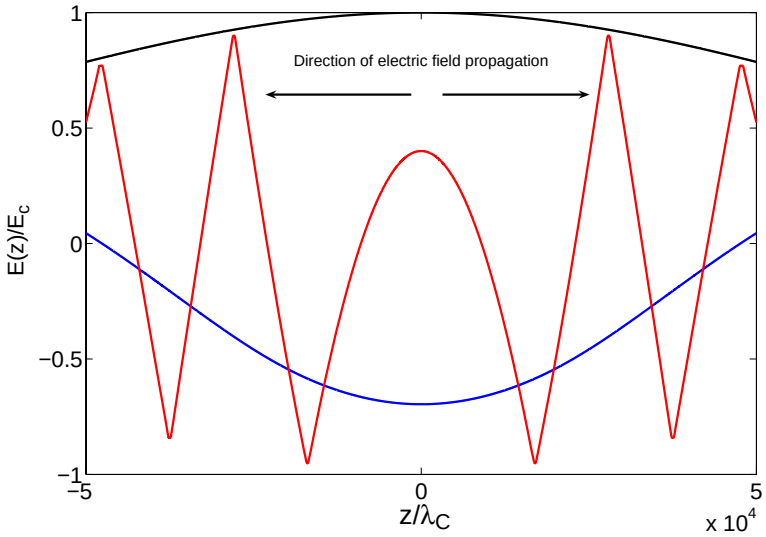

Figure B.2.: Electric fields $E(z,t)$ are plotted as functions of z at three different times in the Compton unit: $t = 1$(black), $t = 500$ (blue) and $t = 1500$ (red). As shown in Fig. B.1, the electric field $E(z,t)$ oscillation at the center ($z = 0$) is most rapid, and gets slower and slower at spatial points ($|z| > 0$) further away from the center. This implies the electric field wave propagating in the space, and the directions of propagations are indicated.

$|\mathbf{x}| \gg |\mathbf{x}'|$ and $R \approx |\mathbf{x}|$, where is far away from the plasma oscillation region $\mathcal{R}$, the radiation fields (B.0.25,B.0.26) approximately are

$$\mathbf{E}_{\rm rad}(t,\mathbf{x}) \approx -\frac{1}{c^2|\mathbf{x}|}\int d^3\mathbf{x}' \left[\frac{\partial \mathbf{J}(t',\mathbf{x}')}{\partial t'}\right]_{\rm ret}, \tag{B.0.27}$$

$$\mathbf{B}_{\rm rad}(t,\mathbf{x}) \approx \hat{\mathbf{R}} \times \mathbf{E}_{\rm rad}(t,\mathbf{x}), \tag{B.0.28}$$

where we use the charge conservation (B.0.9) and total neutrality condition of pairs $\int_{\mathcal{R}} d^3\mathbf{x}'\rho(t',\mathbf{x}') = 0$. The first terms in Eqs. (B.0.25,B.0.26) are the Coulomb-type fields

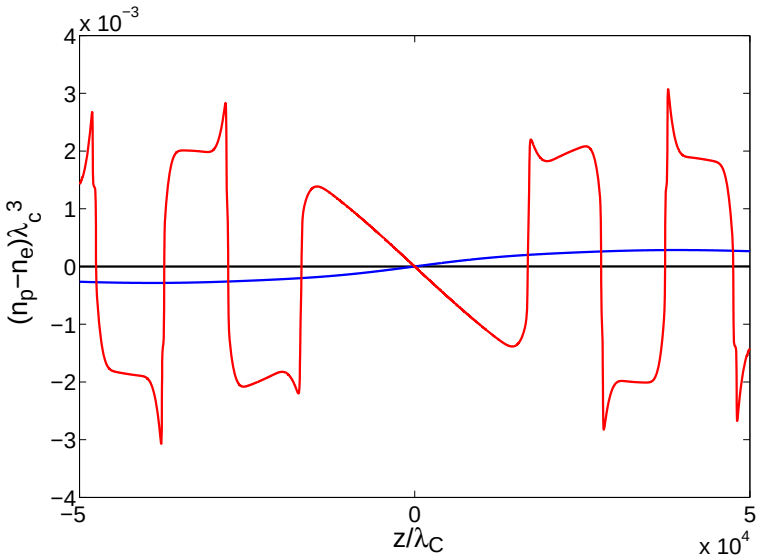

Figure B.3.: The net charge density $\rho(z,t)$ [see Eq. (B.0.15)] as a function of z at three different times: $t = 1$ (black, nearly zero), $t = 500$ (blue) and $t = 1500$ (red). It is shown that the net charged density value $|\rho(z,t)|$ is zero at the center where the initial electric field gradient vanishes [see Eq. (B.0.20)], whereas it increases as the initial electric field gradient increases for $|z| > 0$.

decaying away as $\mathcal{O}(1/|\mathbf{x}|^2)$. The Fourier transforms of Eqs. (B.0.27) and (B.0.28) are

$$\tilde{\mathbf{E}}_{\rm rad}(\omega,\mathbf{x}) \approx -\frac{e^{-ik|\mathbf{x}|}}{c^2|\mathbf{x}|}\tilde{\mathbf{D}}(\omega), \quad \tilde{\mathbf{B}}_{\rm rad}(\omega,\mathbf{x}) \approx \hat{\mathbf{R}} \times \tilde{\mathbf{E}}_{\rm rad}(\omega,\mathbf{x}) \tag{B.0.29}$$

$$\tilde{\mathbf{D}}(\omega) \equiv \int_{\mathcal{R}} d^3\mathbf{x}' \int_{\mathcal{T}} dt' e^{i\omega t'} \left[\frac{\partial \mathbf{J}(t',\mathbf{x}')}{\partial t'}\right], \tag{B.0.30}$$

where the wave number $k = \omega/c$ and the numerical integration (B.0.30) is carried out overall the space-time evolution of the electric current $\mathbf{J}(\mathbf{x}',t')$ (see Figs. B.6 and B.5). For definiteness we thinks of the oscillation currents occurring for some finite interval of time $\mathcal{T}$ or at least falling off for remote past and future times, so that the total energy radiated is finite, thus the energy radiated per unit solid angle per frequency interval is given by Jackson (1998)

$$\frac{d^2 I}{d\omega d\Omega} = 2|\tilde{\mathbf{D}}(\omega)|^2. \tag{B.0.31}$$

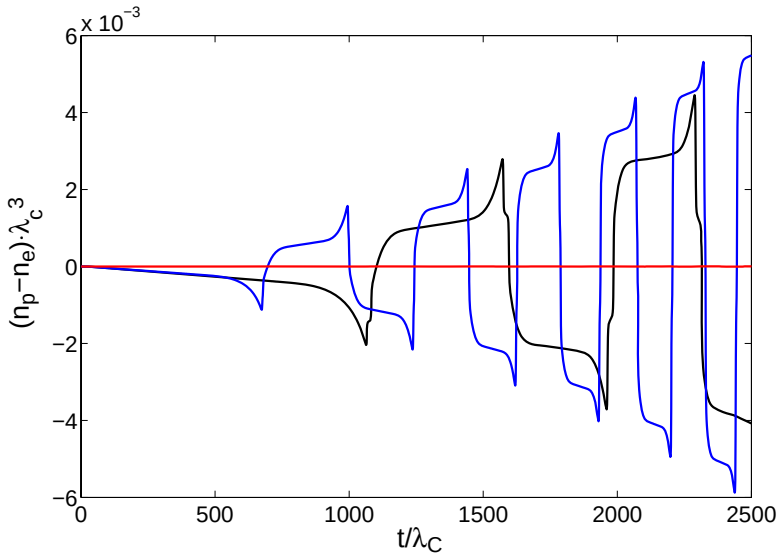

Figure B.4.: The net electric charge density $\rho(z,t)$ [see Eq. (B.0.15)] as a function of t at three different points: $z=0$ (red, nearly zero) , $z=\ell/4$ (blue) and $z=\ell/2$ (black). It is shown that the net electric charge density $\rho(z,t)$ (except the center $z=0$) increases as time.

The squared amplitude $|\tilde{\mathbf{D}}(\omega)|^2$ as a function of ω gives the spectrum of the radiation (see Fig. B.7), which is very narrow as expected with a peak locating at $\omega_{\rm peak}\approx 0.08m_e = 4$keV for $E_0=E_c$, consistently with the plasma oscillation frequency (see Fig. B.1). The energy-spectrum and its peak are shifted to high-energies as the initial electric field-strength increases, and the relation between the spectrum peak location and the electric field-strength is shown in Fig. B.8. In addition, the energy-spectrum and its peak are also shifted to high-energies as the temporary duration $\mathcal{T}$ of plasma oscillations increases (see Fig. B.1). In calculations, the temporary duration $\mathcal{T}=3500\tau_C$ is chosen, not only to satisfy the adiabaticity condition Eq. (B.0.23) [4], but also to be in the time duration when the oscillatory behavior is distinctive (see Figs. B.1,B.4,B.6), since the oscillations of pair-induced currents damp and pairs annihilate into photons Ruffini et al. (2003b). The radiation intensity (B.0.31) depends on the strength, spatial dimension and temporal duration of

[4]We check the two cases $E_0=E_c$ and $E_0=10E_c$, and find for the first oscillation $\eta=865$ and $\eta=487$ respectively. As can be seen for the Fig. B.1 the frequencies ω of pair-oscillations increase with time which means the parameter η becoming smaller. Eventually it may reach unity so the formula (B.0.22) becomes inapplicable.

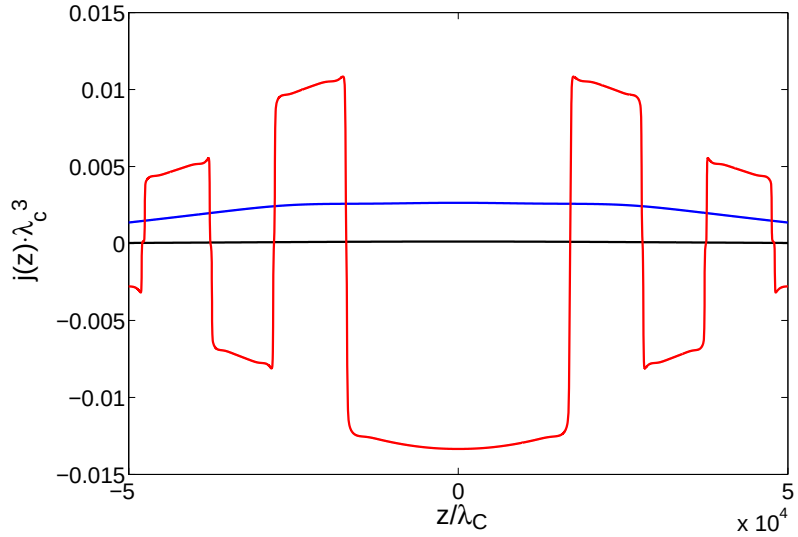

Figure B.5.: Electric current densities $j_z(z,t)$ [see Eq. (B.0.14)] as functions of z at three different times: $t = 1$ (black), $t = 500$ (blue) and $t = 1500$ (red). Following Eq. (B.0.19), the electric current alternates following the alternating electric field (see Fig. B.1), the plateaus indicate the current saturation for $v \sim c$ and its spatial distribution is determined by the initial electric field $E_{\text{ext}}(z)$.

strong external electric fields, created by either experimental setups or astrophysical conditions.

Conclusions and remarks. We show the space and time evolutions of pair-induced electric charges, currents and fields in strong external electric fields bounded within a spatial region. These results imply the wave propagation of the pair-induced electric field and wave-transportation of the electromagnetic energy in the strong field region. Analogously to the electromagnetic radiation emitted from an alternating electric current, the space and time variations of pair-induced electric currents and charges emit an electromagnetic radiation. We show that this radiation has a the peculiar energy-spectrum (see Fig. B.7) that is clearly distinguishable from the energy-spectra of the bremsstrahlung radiation, electron-positron annihilation and other possible background events. This possibly provides a distinctive way to detect the radiative signatures for the production and oscillation of electron-positron pairs in ultra-strong electric fields that can be realized in either ground laboratories

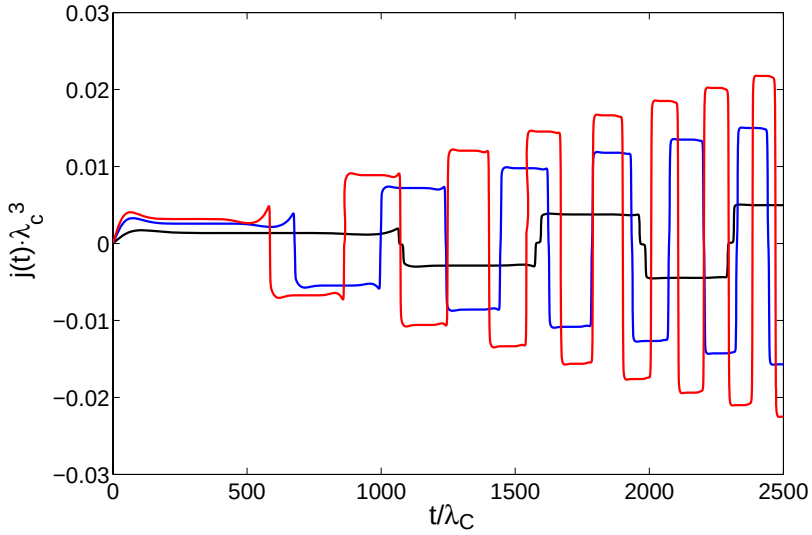

Figure B.6.: Electric current densities $j_z(z,t)$ [see Eq. (B.0.14)] as functions of t at three different points: $z = \ell/2$ (black), $z = \ell/4$ (blue) and $z = 0$ (red). The plateaus (see also Fig. B.6) for the current saturation values increases as time, mainly due to the number-densities $n_\pm$ of electron-positron pairs increase with time. In addition, they are maximal at the center $z = 0$ where the initial electric field is maximal, and decrease as the initial electric field $E_{\text{ext}}(z)$ decreasing for $|z| > 0$.

or astrophysical environments.

As mentioned in introduction, the critical electric field E_c will be reached soon in ground laboratories and sensible methods to detect signatures of pair-productions become important. Recently, the momentum signatures of pair-production is found Hebenstreit et al. (2009) in a time-varying electric field $E(t)$ with sub-cycle structure. On the other hand, space-based telescopes the Swift-BAT NASA (2004), NuSTAR caltech (2010) and Astro-H japan (2010) focusing high-energy X-ray missions, will also give possibilities of detecting X-ray radiation signature, discussed in this paper, from compact stars with electromagnetic structure.

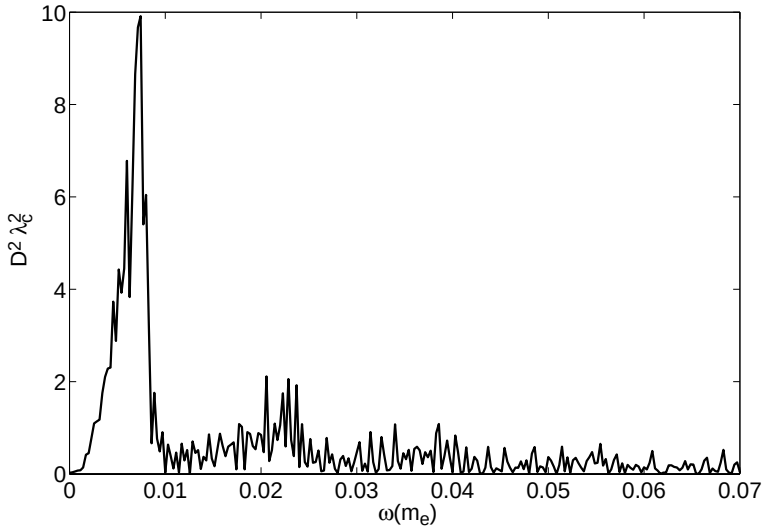

Figure B.7.: In the Compton unit, normalizing $\tilde{D}(\omega)$ [see Eq. (B.0.30)] by the volume $\mathcal{V} \equiv \int d^3\mathbf{x}'$ of the radiation source $\mathbf{J}(t', \mathbf{x}')$, we plot $|\tilde{D}(\omega)|^2$ [see Eq. (B.0.31)] representing the narrow energy-spectrum of the radiation field $\mathbf{E}_{\text{rad}}$ and peak locates at the frequency $\omega_{\text{peak}} \approx 0.08 m_e$.

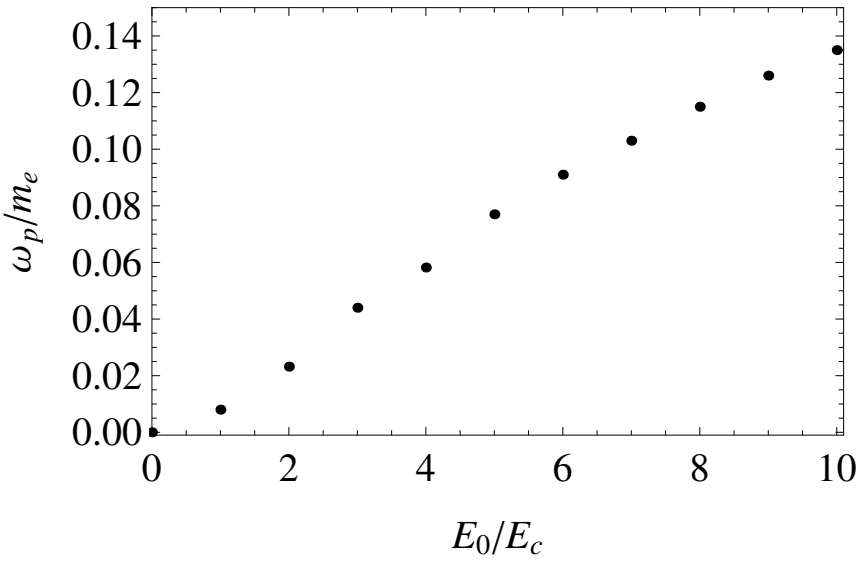

Figure B.8.: The peak frequency ω_{peak} of the radiation approximately varies from 4keV to 70 keV as the initial electric field strength E_0 varies from E_c to $10E_c$. The values for very large field-strengths $E_0/E_c > 1$ possibly receive corrections, since the semiclassical pair-production rate (B.0.22) is approximately adopted and the pressure term (see footnote on page 657) is not properly taken into account.

C. Electron and positron pair production in gravitational collapse

C.1. Introduction.

In the gravitational collapse or pulsation of neutral stellar cores at densities comparable to the nuclear density, complex dynamical processes are expected to take place. These involve both macroscopic processes such as gravitational and hydrodynamical processes, as well as microscopic processes due to the strong and electroweak interactions. The time and length scales of macroscopic processes are much larger than those of the microscopic processes. Despite the existence of only a few exact solutions of Einstein's equations for simplified cases, macroscopic processes can be studied rather well by numerical algorithms. In both analytical solutions and numerical simulations it is rather difficult to simultaneously analyze both macroscopic and microscopic processes characterized by such different time and length scales. In these approaches, microscopic processes are approximately treated as local and instantaneous processes that are effectively represented by a model-dependent parametrized equation of state (EOS). We call this *approximate locality*.

Applying *approximate locality* to electric processes, as required by the charge conservation, one is led to *local neutrality* : positive and negative charge densities are exactly equal over all space and time. As a consequence, all electric fields and processes are eliminated. An internal electric field (charge separation) *must* be developed Olson and Bailyn (1975, 1976); Rotondo et al. (2011a,b) in a totally neutral system of proton and electron fluids in a gravitational field. If the electric field (process) is weak (slow) enough, *approximate locality* is applicable. However, this should be seriously questioned when the electric field (process) is strong (rapid). For example, neutral stellar cores reach the nuclear density where positive charged baryons interact via the strong interaction while electrons do not, in addition to their widely different masses. As a result, their pressure, number, and energy density are described by different EOS, and a strong electric field (charge separation) on the baryon core surface is realized Usov (1998); Popov et al. (2009) in an electrostatic equilibrium state.

Furthermore, either gravitationally collapsing or pulsating of the baryon core leads to the dynamical evolution of electrons. As a consequence, the strong electric field dynamically evolves in space and time, and some electromagnetic processes can result if their reaction rates are rapid enough, for example, the electron-positron pair-production process of Sauter-Heisenberg-Euler-Schwinger (see the review Ruffini et al. (2010)) for electric fields $E \gtrsim E_c \equiv m_e^2 c^3/(e\hbar)$. If this indeed occurs, gravitational and pulsating energies of neutral stellar cores are converted into the observable energy of electron-positron pairs via the space and time evolution of electric fields. In this chapter, we present our studies of this possibility (the natural units $\hbar = c = 1$ are adopted, unless otherwise specified).

C.2. Basic equations for dynamical evolution.

We attempt to study possible electric processes in the dynamical perturbations of neutral stellar cores. These dynamical perturbations can be caused by either the gravitational collapse or pulsation of neutral stellar cores. The basic equations are the Einstein-Maxwell equations and those governing the particle number and energy-momentum conservation

$$\begin{aligned}(\bar{n}_{e,B}U^{\nu}_{e,B})_{;\nu} &= 0,\\ G_{\mu\nu} &= -8\pi G(T_{\mu\nu} + T^{\rm em}_{\mu\nu}),\\ (T^{\nu}{}_{\mu})_{;\nu} &= -F_{\mu\nu}J^{\nu},\\ F^{\mu\nu}{}_{;\nu} &= 4\pi J^{\mu},\end{aligned} \tag{C.2.1}$$

in which the Einstein tensor $G_{\mu\nu}$, the electromagnetic field $F^{\mu\nu}$ (satisfying $F_{[\alpha\beta,\gamma]} = 0$) and its energy-momentum tensor $T^{\rm em}_{\mu\nu}$ appear; $U^{\nu}_{e,B}$ and $\bar{n}_{e,B}$ are, respectively, the four velocities and proper number-densities of the electrons and baryons. The electric current density is

$$J^{\mu} = e\bar{n}_p U^{\mu}_B - e\bar{n}_e U^{\mu}_e, \tag{C.2.2}$$

where $\bar{n}_p$ is the proper number-density of the positively charged baryons. The energy-momentum tensor $T^{\mu\nu} = T^{\mu\nu}_e + T^{\mu\nu}_B$ is taken to be that of two simple perfect fluids representing the electrons and the baryons, each of the form

$$T^{\mu\nu}_{e,B} = \bar{p}_{e,B}g^{\mu\nu} + (\bar{p}_{e,B} + \bar{\rho}_{e,B})U^{\mu}_{e,B}U^{\nu}_{e,B}, \tag{C.2.3}$$

where $\bar{\rho}_{e,B}(r,t)$ and $\bar{p}_{e,B}(r,t)$ are the respective proper energy densities and pressures.

In this chapter, baryons indicate hadrons, or their constituents (quarks) that carry

baryon numbers. Electrons indicate all negatively charged leptons. Baryon fluid and electron fluid are separately described for the reason that in addition to baryons being much more massive than electrons, the EOS of baryons $\bar{p}_B = \bar{p}_B(\bar{\rho}_B)$ is very different from the electron one $\bar{p}_e = \bar{p}_e(\bar{\rho}_e)$ due to the strong interaction. Therefore, in the dynamical perturbations of neutral stellar cores, one should not expect that the space-time evolution of number density, energy density, four velocity, and pressure of baryon fluid be identical to the space-time evolution of counterparts of electron fluid. The difference of space-time evolutions of two fluids results in the electric current (C.2.2) and field $F^{\mu\nu}$, possibly leading to some electric processes. In a simplified model for the dynamical perturbations of neutral stellar cores, we approximately study possible electric processes by assuming that the equilibrium configurations of neutral stellar cores are initial configurations.

C.3. Equilibrium configurations.

In Refs. Olson and Bailyn (1975, 1976); Rotondo et al. (2011a,b), the equilibrium configurations of neutral stellar cores, whose densities are smaller than nuclear density $n_{\rm nucl}$, are studied on the basis of hydrostatic dynamics of baryon and electron fluids in the presence of long-ranged gravitational and Coulomb forces. In these equilibrium configurations, very weak electric fields $E \ll E_c$ are present, resulted from the balance between attractive gravitational force and repulsive Coulomb force. This electric field is too weak to make important electric processes, for example, electron-positron pair productions. We are interested in the case where strong electric fields are present. This leads us to consider strong electric fields in the surface layer of baryon cores of compact stars (quark or neutron stars) at or over the nuclear density. In this case, we assume that baryons form a rigid core of radius R_c and density

$$\frac{\bar{n}_{B,p}(r)}{\bar{n}_{B,p}} = \left[\exp\frac{r-R_c}{\zeta}+1\right]^{-1}, \bar{n}_{B,p} \approx \frac{N_{B,p}}{(4\pi R_c^3/3)}, \tag{C.3.1}$$

where $\bar{n}_p/\bar{n}_B \approx N_p/N_B < 1$, $N_B(N_p)$ is the number of total (charged) baryons and $\bar{n}_{B,p} \gtrsim n_{\rm nucl} \approx 1.4\times 10^{38}{\rm cm}^{-3}$. The baryon core has a sharp boundary ($r \sim R_c$) of the width $\zeta \sim m_\pi^{-1}$ due to the strong interaction. The line element is Bekenstein (1971); Mashhoon and Partovi (1979)

$$\begin{aligned} ds^2 &= -g_{tt}dt^2 + g_{rr}dr^2 + r^2d\theta^2 + r^2\sin^2\theta d\phi^2\,, \\ g_{rr}^{-1}(r) &= 1 - 2GM(r)/r + GQ^2(r)/r^2\,, \end{aligned} \tag{C.3.2}$$

where mass $M(r)$, charge $Q(r)$ and radial electric field $E(r) = Q(r)/r^2$.

Electrons form a complete degenerate fluid and their density $n_e^{\rm eq}(r)$ obeys the fol-

lowing Poisson equation and equilibrium condition Popov et al. (2009); Rueda et al. (2011):

$$\begin{aligned}
&\frac{d^2V_{\rm eq}}{dr^2}+\left[\frac{2}{r}-\frac{1}{2}\frac{d}{dr}\ln(g_{tt}g_{rr})\right]\frac{dV_{\rm eq}}{dr}\\
&\quad=-4\pi e g_{rr}(\bar{n}_p U_p^t-n_e^{\rm eq}U_e^t),\\
&E_e^F=g_{tt}^{1/2}\sqrt{|P_e^F|^2+m_e^2}-m_e-eV_{\rm eq}=\text{const.},
\end{aligned}\tag{C.3.3}$$

where $U_p^t=U_e^t=(1,0,0,0)$, E_e^F, and $P_e^F=(3\pi^2 n_e^{\rm eq})^{1/3}$ are the Fermi energy and momentum, $V_{\rm eq}(r)$ and $E_{\rm eq}=-(g_{rr})^{-1/2}\partial V_{\rm eq}(r)/\partial r$ are the static electric potential and field. In the ultrarelativistic case $|P_e^F|\gg m_e$, we numerically integrate Eq. (C.3.3) with boundary conditions:

$$\begin{aligned}
&n_e^{\rm eq}(r)|_{r\ll R_c}=n_B\\
&n_e^{\rm eq}(r)|_{r\gg R_c}=\frac{dn_e^{\rm eq}(r)}{dr}\Big|_{r\gg R_c}=\frac{dn_e^{\rm eq}(r)}{dr}\Big|_{r\ll R_c}=0.
\end{aligned}\tag{C.3.4}$$

As a result, we obtain on the baryon core boundary $r\approx R_c$, the nontrivial charge-separation $(n_p-n_e^{\rm eq})/n_B$ and overcritical electric field $E_{\rm eq}/E_c>0$ in a thin layer of a few electron Compton length λ_e [the curves ($t=0$) in Fig. C.1]. This is due to the sharpness boundary ($\zeta\sim m_\pi^{-1}$) of the baryon core (C.3.1) at the nuclear density, as discussed for compact stars Usov (1998); Popov et al. (2009). Note that all electronic energy-levels Kleinert et al. (2008)

$$\mathcal{E}_{\rm occupied}=e\int g_{rr}^{1/2}drE_{\rm eq}(r)\tag{C.3.5}$$

are fully occupied and pair-production is not permitted due to Pauli blocking, although electric fields in the surface layer are over critical. We want to understand the space and time evolution of the electric field in this thin layer and its consequence in the dynamical perturbations of baryon cores, which can be caused by either the gravitational collapse or pulsation of baryon cores.

C.4. Modeling dynamical perturbations of baryon cores.

It is rather difficult to solve the dynamical system (C.2.1-C.2.3) with the EOS $\bar{p}_B=\bar{p}_B(\bar{\rho}_B)$ and $\bar{p}_e=\bar{p}_e(\bar{\rho}_e)$ for the gravitational collapse or pulsation of baryon core and electron fluid, and to examine possible electromagnetic processes. The main diffi-

culty comes from the fact that the time and length scales of gravitational and electromagnetic processes differ by many orders of magnitude. In order to gain some physical insight into the problem, we are bound to split the problem into three parts: (i) first, we adopt a simplified model to describe the dynamical perturbations of baryon cores; (ii) second, we examine how electron fluid responds to this dynamical perturbation of baryon cores; (iii) third, we check whether the resulted strong electric fields can lead to very rapid electromagnetic processes, for example, electron-positron pair production.

As for the first part, we adopt the following simplified model. Suppose that at the time $t = 0$ the baryon core is in the equilibrium configuration (C.3.1) with the radius R_c and starts dynamical perturbations with an inward velocity $\dot{R}_c(t)$ or pulsation frequency $\omega_{\rm pulsa} \simeq \dot{R}_c/R_c$. The rate of dynamical perturbations of baryon cores is defined as $\tau_{\rm coll}^{-1} = \dot{R}_c/R_c \lesssim c/R_c$. We further assume that in these dynamical perturbations, baryon cores are rigid, based on the argument that as the baryon core density $\bar{n}_{B,p}$ (C.3.1) increases, the EOS of baryons $\bar{p}_B = \bar{p}_B(\bar{\rho}_B)$ due to the strong interaction is such that the baryon core profile (C.3.1) and boundary width $\zeta \sim m_\pi^{-1}$ are maintained in the nuclear relaxation rate $\tau_{\rm stro}^{-1} \sim m_\pi$, which is much larger than $\tau_{\rm coll}^{-1}$. Thus, due to these properties of strong interaction, the dynamical perturbation of the baryon core induces an inward charged baryon current-density

$$J_B^r(R_c) = e\bar{n}_p(R_c)U_B^r(R_c), \tag{C.4.1}$$

on the sharp boundary of baryon core density (C.3.1) at R_c, where the baryon density $\bar{n}_{B,p}(R_c) = 0.5\bar{n}_{B,p}$ and the four-velocity $U_B^r(R_c) \neq 0$. We have not yet been able, from the first principle of strong interaction theory, to derive this boundary property (C.4.1) of baryon cores undergoing dynamical perturbations, which essentially are assumptions in the present chapter, and the boundary density $\bar{n}_{B,p}(R_c)$ and the boundary four-velocity $U_B^r(R_c)$ are two parameters depending on dynamical perturbations. This is in the same situation that so far one has not yet been able, from the first principle of strong interaction theory, to derive the sharp boundary profile (C.3.1) of baryon core densities of static compact stars Usov (1998); Popov et al. (2009). However, we have to point out that the boundary properties (C.3.1) and (C.4.1) of the baryon core undergoing dynamical perturbations are rather technical assumptions for the following numerical calculations of dynamical evolution of electron fluid and electric processes in the Compton time and length scales. These assumptions could be abandoned if we were able to simultaneously make numerical integration of differential equations for both dynamical perturbations of baryon cores at macroscopic length scale and strong and electric processes at microscopic length scale.

C.5. Dynamical evolution of electron fluid

In this section, we attempt to examine how the electron fluid around the boundary layer of the baryon core responds to the dynamical perturbations of the baryon core described by the boundary properties (C.3.1) and (C.4.1). Given these boundary properties at different values of baryon core radii R_c, we describe electrons and electric fields around the boundary layer of baryon core by Maxwell's equations, the electron number and energy-momentum conservation laws (C.2.1) in the external metric field (C.3.2). In addition, we assume that the electron fluid is completely degenerate, and its EOS is given by

$$\begin{aligned}\bar{\rho}_e(t,r) &= 2\int_0^{P_e^F} p^0 d^3\mathbf{p}/(2\pi)^3,\\ \bar{p}_e(t,r) &= \frac{1}{3}\frac{2}{(2\pi)^3}\int_0^{P_e^F}\frac{\mathbf{p}^2}{p^0}d^3\mathbf{p}\,,\end{aligned} \tag{C.5.1}$$

where the single-particle spectrum is $p^0 = (\mathbf{p}^2 + m_e^2)^{1/2}$ and the Fermi momentum is $P_e^F = (3\pi^2\bar{n}_e)^{1/3}$. In the present chapter, for the sake of simplicity, we set the temperature of electron fluid to be zero and neglect all temperature effects, which may be important and will be studied in future.

The electron fluid has four velocity $U_e^\mu = (U^t, U^r)_e$, radial velocity $v_e \equiv (U^r/U^t)_e$, $U_e^t = g_{tt}^{-1/2}\gamma_e$ and Lorentz factor $\gamma_e \equiv (1 + U_r U^r)_e^{1/2} = [1 + (g_{rr}/g_{tt})v_e^2]^{-1/2}$. In the rest frame at a given radius r it has the number density $n_e = \bar{n}_e\gamma_e$, energy density $\epsilon_e = (\bar{\rho}_e + \bar{p}_e v_e^2)\gamma_e^2$, momentum density $P_e = (\bar{\rho}_e + \bar{p}_e)\gamma_e^2 v_e$, and $v_e = P_e/(\epsilon_e + \bar{p}_e)$. In the rest frame, the number and energy-momentum conservation laws for the electron fluid, and Maxwell's equations are given by

$$\left(n_e g_{tt}^{-1/2}\right)_{,t} + \left(n_e v_e g_{tt}^{-1/2}\right)_{,r} = 0, \tag{C.5.2}$$

$$\begin{aligned}&(\epsilon_e)_{,t} + (P_e)_{,r} + \frac{1}{2g_{tt}}\left[\frac{\partial g_{rr}}{\partial t}P_e v_e - \frac{\partial g_{tt}}{\partial t}(\epsilon_e + \bar{p}_e)\right]\\ &\quad = -e n_e v_e E g_{tt}^{-1/2},\end{aligned} \tag{C.5.3}$$

$$\begin{aligned}&\left(P_e\frac{g_{rr}}{g_{tt}}\right)_{,t} + \left(\bar{p}_e + P_e v_e\frac{g_{rr}}{g_{tt}}\right)_{,r}\\ &\quad + \frac{\epsilon_e + \bar{p}_e}{2g_{tt}}\left(\frac{\partial g_{tt}}{\partial r} - \frac{\partial g_{rr}}{\partial r}v_e^2\right) = -e n_e E g_{tt}^{-1/2},\end{aligned} \tag{C.5.4}$$

$$(E)_{,t} = -4\pi e(n_p v_p - n_e v_e)g_{tt}^{-1/2}, \tag{C.5.5}$$

where $(\cdots)_{,x} \equiv (-g)^{-1/2}\partial(-g)^{1/2}(\cdots)/\partial x$, and in the line (C.5.5), the boundary

velocity v_p of the baryon core comes from the baryon current-density (C.4.1). We have the boundary four-velocity U_B^r of the baryon core,

$$v_p = v_B \equiv (U^r/U^t)_B, \quad U_B^t = g_{tt}^{-1/2}\gamma_B, \tag{C.5.6}$$

and the Lorentz factor

$$\gamma_B \equiv (1 + U_r U^r)_B^{1/2} = [1 + (g_{rr}/g_{tt})v_p^2]^{-1/2}, \tag{C.5.7}$$

at the baryon core boundary R_c.

In the static case for $v_p = v_e = 0$, Eqs. (C.5.1-C.5.5) are equivalent to Eq. (C.3.3). Provided an initial equilibrium configuration (C.3.3) and proper boundary conditions, we numerically integrate these five equations (C.5.1-C.5.5) to obtain five variables $n_e(t,r), \epsilon_e(t,r), P_e(t,r), \bar{p}(t,r)$ and $E(t,r)$ describing the electric processes around the baryon core boundary.

C.6. Oscillations of electron fluid and electric field.

We consider the baryon core of mass $M = 10M_\odot$ and radius $R_c \sim 10^7$cm at the nuclear density $n_{\rm nucl}$, and select its boundary velocity $v_p = 0.2c$ to represent possible dynamical perturbations of baryon cores. In the proper frame of a rest observer at the core radius R_c, where $g_{tt}(R_c) \approx g_{rr}^{-1}(R_c)$, we chose the surface layer boundaries $\xi_- \approx -\lambda_e, \xi_+ \approx 3.5\lambda_e$, at which $E_{\rm eq}(\xi_\pm) \approx 0$ and proper thickness $\ell = \xi_+ - \xi_-$, and numerically integrate Eqs. (C.5.1-C.5.5) for the electron fluid. Numerical results are presented in Figs. C.1 and C.2, showing that total electric field

$$E(t,r) = E_{\rm eq}(r) + \tilde{E}(t,r), \tag{C.6.1}$$

where electron number density, energy density, and pressure oscillate around their equilibrium configurations Han et al. (2010). This is due to the fact that electrons do not possess the strong interaction and their mass is much smaller than the baryon one, as a result, the current density of electron fluid in the boundary layer does not exactly follow the baryon core current density (C.4.1). Instead, triggered by the baryon core current (C.4.1), total electric fields $E(t,r)$ deviate from $E_{\rm eq}(r)$ and increase, which breaks the equilibrium condition (C.3.3), namely, the balance between pressure and electric force acting on electrons, $dP_e^F/dr + eE_{\rm eq} = 0$. Accelerated by increasing electric fields, electrons outside the core start to move inwards following the collapsing baryon core. This leads to the increase of the electron pressure (C.5.1) and the decrease of the electric fields. On the contrary, increasing electron pressure pushes electrons backwards, and bounces them back. Overcritical electric

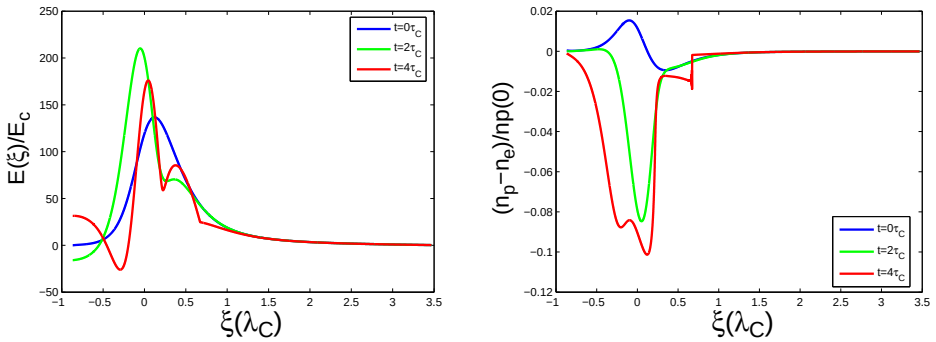

Figure C.1.: The space and time evolution of the electric field (left) and charge-separation (right) around the boundary layer of the baryon core, $M = 10M_\odot$, $R_c \approx 10^7$cm, and $v_p = 0.2c$. The coordinate is $\tilde{\xi} \equiv r - R_c$.

fields work against the pressure of ultrarelativistic electrons. As a consequence, oscillations with frequency $\omega = \tau_{\rm osci}^{-1} \sim 1.5 m_e$ around the equilibrium configuration take place in a thin layer of a few Compton lengths around the boundary of baryon core. These are the main results presented in this chapter. We would like to point out that these results should not depend on the boundary properties (C.3.1) and (C.4.1) that we assume for the dynamical perturbations of baryon cores. The reason is that both electron and proton fluids in baryon cores are at or over nuclear density, and their Fermi momenta are the order of the pion mass m_π; therefore, electric fields must be at or over critical value $E_c = m_e^2/e$ to do work against motion of charge separation between positively charged baryon and electron fluids, and the frequency of oscillation because of the backreaction should also be the order of m_e. It is worthwhile that these results are further checked by full numerical calculations without assuming the boundary properties (C.3.1) and (C.4.1) of baryon cores, which undergo the dynamical perturbations caused by the gravitational collapse or pulsation.

Suppose that the dynamical perturbation of the baryon core is caused by either the gravitational collapse or pulsation of the baryon core, that gains the gravitational energy. Then, in this oscillating process, energy transforms from the dynamical perturbation of the baryon core to the electron fluid via an oscillating electric field. This can been seen from the energy conservation (C.2.1) along a flow line of the electron fluid for $v_e \neq v_p$

$$U_e^\mu (T^\nu{}_\mu)_{;\nu} = e\bar{n}_p F_{\mu\nu} U_e^\mu U_B^\nu = e\bar{n}_p \gamma_e \gamma_B (v_p - v_e) g_{rr} E, \tag{C.6.2}$$

although we have not yet explicitly proved it. The energy density of the oscillating

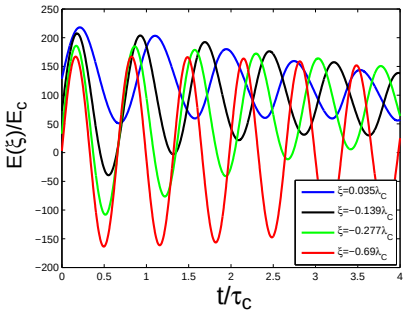

Figure C.2.: Time evolution of electric fields at different radial positions around the boundary layer of the baryon core, $M = 10M_\odot$, $R_c \approx 10^7$cm and $v_p = 0.2c$. The coordinate is $\xi \equiv r - R_c$.

electric field is

$$\epsilon_{\rm osci} \equiv [E^2(t,r) - E^2_{\rm eq}(r)]/(8\pi). \tag{C.6.3}$$

The energy densities of the oscillating electric field and electron fluid are converted from one to another in the oscillating process with frequencies $\omega \sim \tau^{-1}_{\rm osci} \sim 1.5m_e$ around the equilibrium configuration. However, the oscillating electron fluid has to relax to the new equilibrium configuration determined by Eqs. (C.3.3) and (C.3.4) with a smaller baryon core radius $R'_c < R_c$. As a result, the oscillating electric field must damp out and its lifetime $\tau_{\rm relax}$ is actually a relaxation time to the new equilibrium configuration. As shown in Fig. C.2 the relaxation rate $\tau^{-1}_{\rm relax} \sim 0.05m_e$. We notice very different time scales of strong interacting processes, electric interacting processes and dynamical perturbations of baryon cores: $\tau^{-1}_{\rm stro} \gg \tau^{-1}_{\rm osci} \gg \tau^{-1}_{\rm relax} \gg \tau^{-1}_{\rm coll}$.

Moreover, when $E(r,t) > E_{\rm eq}(r)$ (see Fig. C.1), the unoccupied electronic energy-level can be obtained by Kleinert et al. (2008)

$$\begin{aligned}\mathcal{E}_{\rm unocuppied} &= e\int g_{rr}^{1/2} dr E(t,r) - \mathcal{E}_{\rm ocuppied} \\ &= e\int g_{rr}^{1/2} dr \tilde{E}(t,r),\end{aligned} \tag{C.6.4}$$

see Eq. (C.3.5). This leads to pair production in strong electric fields and converts electric energy into the energy of electron-positron pairs, provided the pair-production rate $\tau^{-1}_{\rm pair}$ is faster than the oscillating frequency $\omega = \tau^{-1}_{\rm osci}$. Otherwise, the energy of oscillating electric fields would completely be converted into the electrostatic Coulomb energy of the new equilibrium configuration of electron fluid, which cannot be not

radiative.

C.7. Electron-positron pair production

We turn to the pair-production rate in spatially inhomogeneous and temporally oscillating electric fields $E(t,r)$. Although the oscillating frequency ω is rather large, the pair-production rate $\tau_{\rm pair}^{-1}$ can be even larger due to the very strong electric fields $E(t,r)$. The pair-production rate can be approximately calculated by the formula for static fields. The validity of this approximation is justified (see Ruffini et al. (2010); Brezin and Itzykson (1970)) by the adiabaticity parameter $\eta^{-1} = (\omega/m_e)(E_c/E_{\rm max}) \ll 1$, where $E_{\rm max}$ is the maximal value of the electric field on the baryon core surface $r \simeq R_c$. Therefore we adopt Eqs. (38) and (39) and (64)-(66) in Ref. Kleinert et al. (2008) for the Sauter electric field to estimate the density of the pair-production rate in the proper frame at the core radius R_c

$$\mathcal{R}_{\rm pair} \approx \frac{e^2 E\tilde{E}}{4\pi^3\,\bar{G}_0(\sigma)} e^{-\pi(E_c/E)G_0(\sigma)} \sim \frac{e^2 E\tilde{E}}{4\pi^3}, \tag{C.7.1}$$

where $\tilde{E}$ (instead of E) in the prefactor accounts for the unoccupied electric energy levels, $G_0(\sigma) \to 0$ and $\bar{G}_0(\sigma) \to 1$ for $\sigma = (\ell/\lambda_e)(E/E_c) \gg 1$. The electron-positron pairs screen the oscillating field $\tilde{E}$ so that the number of pairs can be estimated by $\mathcal{N}_{\rm pair} \approx 4\pi R_c^2(\tilde{E}/e)$. The pair-production rate is $\tau_{\rm pair}^{-1} \approx \mathcal{R}_{\rm pair}(4\pi R_c^2\ell)/\mathcal{N}_{\rm pair} \sim \alpha m_e(\ell/\lambda_e)(E/E_c) \simeq 6.6 m_e > \tau_{\rm osci}^{-1}$. The number density of pairs is estimated by $n_{\rm pair} \approx \mathcal{N}_{\rm pair}/(4\pi R_c^2\ell)$. Assuming the energy density $\epsilon_{\rm osci}$ of oscillating fields is totally converted into the pair energy density, we have the pair mean energy $\bar{\epsilon}_{\rm pair} \equiv \epsilon_{\rm osci}/n_{\rm pair}$. Using the parameters $v_p \approx 0.2c$, $R_c \approx 10^7$cm, and $M = 10M_\odot$, we obtain $\epsilon_{\rm osci} \approx 4.3\times10^{28}\,{\rm ergs/cm^3}$, $n_{\rm pair} \approx 1.1\times10^{33}/{\rm cm^3}$, and $\bar{\epsilon}_{\rm pair} \approx 24.5$MeV. These estimates are preliminary without considering the efficiency of pair-productions, possible suppression due to strong magnetic fields, and possible enhancement due to finite temperature effect.

C.8. Gravitational collapse and Dyadosphere

Up to now, we have not discussed how the dynamical perturbations of baryon cores can be caused by either the gravitational collapse or pulsation of baryon cores. Actually, we have not been able to completely integrate the dynamical equations discussed in Sec. C.2 for the reasons discussed in Secs. C.1 and C.4. Nevertheless, we attempt to use the results of electric field oscillation and pair production obtained

in Secs. C.5, C.6 and C.7 to gain some physical insight into what and how electric processes could possibly occur in the gravitational collapse of baryon cores. For this purpose and in order to do some quantitative calculations, we first model the gravitational collapse of baryon cores by the following assumptions:

1. the gravitationally collapsing process is made of the sequence of events (in time) occurring at different radii R_c of the baryon core;

2. at each event the baryon core maintains its density profile and sharp boundary as described by Eqs. (C.3.1) and (C.4.1).

The first assumption is based on the arguments that (i) in the electric processes discussed in Sec. C.6, the charge-mass ratio Q/M of the baryon core can possibly be approaching to 1, then the collapse process of the baryon core is slowing down and its kinetic energy is vanishing because the attractive gravitational energy gained is mostly converted into the repulsive Coulomb energy of the baryon core; (ii) then this Coulomb energy can be possibly converted into the radiative energy of electron-positron pairs as discussed in Sec. C.7, and the baryon core restarts acceleration by gaining gravitational energy. We have already discussed the second assumption in Secs. C.4 and C.6. Here we want to emphasize that (i) the sharp boundary properties (C.3.1) and (C.4.1) in the second assumption are technically used in order to numerically calculate the dynamics of electron fluid in the thin shell around the baryon boundary (Secs. C.5, C.6 and C.7); (ii) in the gravitational collapse or pulsation of neutral stellar cores at or over nuclear density, these sharp boundary properties (C.3.1) and (C.4.1) should be abandoned in a more realistic model of simultaneously integrating dynamical equations of electron and baryon fluids over the entire stellar core at macroscopic scales. This turns out to be much more complicated and we will focus on this study in the future.

On the basis of these assumptions, the boundary velocity $v_p(R_c)$ (C.5.6) and boundary radius R_c [or boundary density $\bar{n}_{B,p}(R_c)$ (C.3.1)] of the baryon core at or over the nuclear density are no longer independent parameters, instead they should be related by the gravitational collapse equation of the baryon core. We adopt a simplified model for the gravitational collapse of the baryon core by approximately using the collapsing equation for a thin shell Israel (1966); De la Cruz and Israel (1967); Bekenstein (1971); Cherubini et al. (2002); Ruffini and Vitagliano (2002)

$$\left(\frac{\Omega}{F}\right)^2\left(\frac{dR_c}{dt}\right)^2=\left[1+\frac{GM}{2R_c}(1-\xi_Q^2)\right]^2-1, \tag{C.8.1}$$

where at different radii R_c of the baryon core, we define the charge-mass ratio

$$\xi_Q\equiv Q^{\rm eq}/(G^{1/2}M)<1;\quad Q^{\rm eq}=R_c^2E_{\rm eq}, \tag{C.8.2}$$

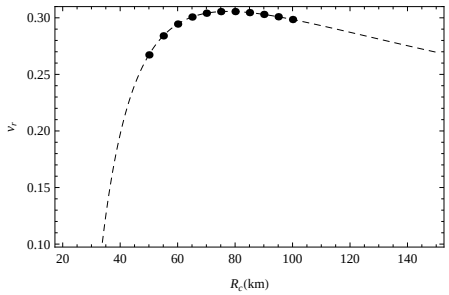

Figure C.3.: The estimate of the core collapsing velocity $v_p \equiv \dot{R}_c = dR_c/dt$ at different collapsing radii R_c for the baryon core of mass $M = 10\,M_\odot$.

and

$$\Omega \equiv 1 - (M/2R_c)(1 + \xi_Q^2)$$
$$F \equiv 1 - (2M/R_c) + (Q^{\rm eq}/R_c)^2. \tag{C.8.3}$$

The collapsing Eq. (C.8.1) for the collapsing velocity $\dot{R}_c$ is based on the condition that at each collapsing radius R_c, the shell starts to collapse from rest. As a result, using these Eqs. (C.8.1-C.8.3) we describe the sequence of events in the gravitationally collapsing process in terms of the collapsing velocities $v_p = \dot{R}_c = dR_c/dt$ defined by (C.5.6) and (C.5.7) at different collapsing radii R_c of the baryon core, as shown in Fig. C.3. Thus, at each event the induced inward charged baryon current-density (C.4.1) is given by

$$J_B^r = e\bar{n}_p U_B^r \approx e\bar{n}_p(\dot{R}_c\Omega/F), \tag{C.8.4}$$

as a function of the collapsing radius R_c. The strength of this charged baryon current density (C.8.4) depends also on the ratio of the charged baryon number and total baryon number (N_p/N_B), which varies in the gravitational collapsing process because of the β processes Mohammadi et al. (2012). In this chapter, the β processes are not considered and the charged baryon (proton) number N_p is constant; we select two values $N_p/N_B \approx 1/38$ or $N_p/N_B \approx 1/380$ for the charged baryon current density Eq. (C.8.4). The collapsing process rate is $\tau_{\rm coll}^{-1} = \dot{R}_c/R_c \lesssim c/R_c$. If the dynamical perturbation of the baryon core is caused by the gravitational core pulsation, the pulsation frequency can be expressed as $\omega_{\rm pulsa} \simeq \dot{R}_c/R_c = \tau_{\rm coll}$.

In the sequence of the gravitationally collapsing process, at each event characterized by $[R_c, v_p(R_c)]$, we first solve Eqs. (C.3.3) and (C.3.4) of the equilibrium configuration to obtain the number density ($n_e^{\rm eq}$) and electric field ($E_{\rm eq}$) as the initial con-

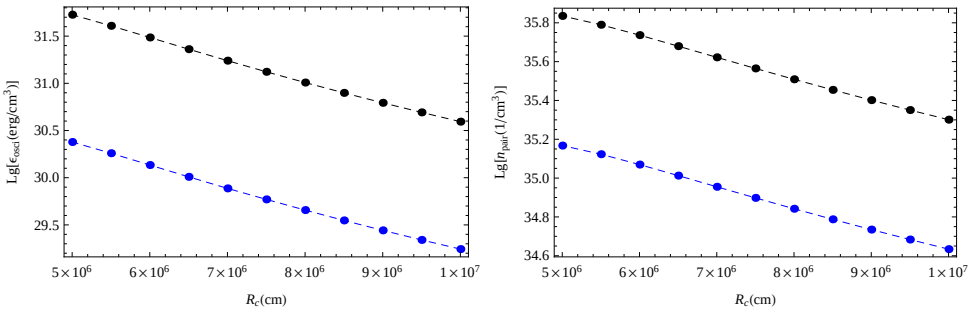

Figure C.4.: The energy (left) and number (right) densities of electron-positron pairs at selected values of collapsing radii R_c for $M = 10M_\odot$ and $N_p/N_B \approx 1/38\,(\text{upper}); 1/380\,(\text{lower})$. We select $R_c^{\max} \sim 10^7$cm so that $\bar{n}_B \sim n_{\text{nucl}}$.

figuration of the electron fluid and electric field. Then, with this initial configuration we numerically solve the dynamical equations (C.5.1-C.5.5) to obtain the dynamical evolution of electron fluid and electric field within the thin shell (a few Compton lengths) around the baryon core boundary, described by Eqs. (C.3.1) and (C.8.4). As a result, based on the analysis presented in Sec. C.7 we calculate the energy and number densities of the electron-positron pairs produced at each event in the sequence of the gravitationally collapsing process. These results are plotted in Figs. C.4. Limited by numerical methods, we cannot do calculations for smaller radii.

In addition, at each event in the sequence of the gravitationally collapsing process, using the Gauss law, $Q = R_c^2 E$, we calculate the charge-mass ratio Q/M averaged over oscillations of electric fields, $Q/M < 1$ as shown in Fig. C.5. The averaged charge-mass ratio Q/M is not very small, rather about 0.4 (see Fig. C.5), implying the possible validity of the first assumption we made that the gravitational collapsing process is approximately made of a sequence of events. In principle, at $Q/M = 1$ the gravitational collapsing process should stop, whereas the gravitational collapsing process is continuous for $Q/M = 0$ without considering electric interactions.

It is clear that the ratio N_p/N_B becomes larger, the charged baryon current density (C.4.1) or (C.8.4) becomes larger, and all effects of electrical processes we discussed in Secs. C.5, C.6 and C.7 become larger. As shown in Figs. C.4, for the ratio $N_p/N_B \approx 1/38$, the energy density of electron-positron pairs is about 10^{31} ergs/cm^3, and the number density of electron-positron pairs is about $10^{35.6}$ /cm^3. The mean energy of electron-positron pairs is $\bar{\epsilon}_{\text{pair}} \equiv \epsilon_{\text{osci}}/n_{\text{pair}} \sim$ 10–50 MeV. While, for the ratio $N_p/N_B \approx 1/380$, the energy density of electron-positron pairs is about 10^{30} ergs/cm^3, the number density of electron-positron pairs is about $10^{34.6}$ /cm^3,

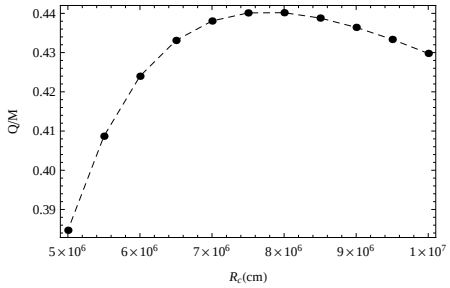

Figure C.5.: The charge-mass ratio Q/M averaged over oscillations of electric fields is plotted at different collapsing radii R_c for the baryon core of mass $M = 10\,M_\odot$.

and the mean energy of electron-positron pairs $\bar{\epsilon}_{\rm pair} \equiv \epsilon_{\rm osci}/n_{\rm pair} \sim$ 10–50 MeV does not change very much.

It this chapter, it is an assumption that the gravitationally collapsing process is represented by the sequence of events: the baryon core starts to collapse from rest by gaining gravitational energy, the increasing Coulomb energy results in decreasing kinetic energy and slowing down the collapse process, the electric processes discussed in Secs. C.5, C.6 and C.7 convert the Coulomb energy into the radiative energy of electron-positron pairs, and as a result the baryon core restarts to accelerate the collapse process by further gaining gravitational energy. This indicates that in the gravitationally collapsing process, the gravitational energy must be partly converted into the radiative energy of electron-positron pairs. However, we have not been able so far to calculate all processes with very different time and length scales from one event to another in the sequence, so that it is impossible to quantitatively obtain the rate of the conversion of the gravitational energy to the energy of electron-positron pairs. Nevertheless, by summing over all events in the sequence of the gravitationally collapsing process, we approximately estimate the total number and energy of electron-positron pairs produced in the range $R_c \sim 5 \times 10^5 - 10^7$cm: 10^{56}–10^{57} and 10^{52}–10^{53} erg for the ratio $N_p/N_B \approx 1/38$; 10^{55}–10^{56} and 10^{51}–10^{52} erg for the ratio $N_p/N_B \approx 1/380$. These electron-positron pairs undergo the plasma oscillation in strong electric fields and annihilate to photons to form a neutral plasma of photons and electron-positron pairs Ruffini et al. (2003b,a). This is reminiscent of the vacuum polarization of a charged black hole Damour and Ruffini (1975); Cherubini et al. (2009) and a sphere of electron-positron pairs and photons, called a Dyadosphere that is supposed to be dynamically created during gravitational collapse in Refs. Ruffini and Xue (2008a); Preparata et al. (1998, 2003).

C.9. Summary and remarks.

In the simplified model for the baryon cores of neutral compact stars, we show possible electric processes for the production of electron-positron pairs within the thin shell (a few Compton lengths) around the boundary of baryon cores that undergo gravitationally collapsing or pulsating processes, depending on the balance between attractive gravitational energy and repulsive electric and internal energies (see the numerical results in Ref. Ghezzi (2005); Ghezzi and Letelier (2007)). This indicates a possible mechanism that the gravitational energy is converted into the energy of electron-positron pairs in either baryon core collapse or pulsation.

In theory, this is a well-defined problem based on the Einstein-Maxwell equations, particle-number and energy-momentum conservation (C.2.1)-(C.2.3), and equations of states, as well as the Sauter-Heisenberg-Euler-Schwinger mechanism. However, in practice, it is a rather complicated problem that one has to deal with various interacting processes with very different time and length scales. The approach we adopt in this chapter is the adiabatic approximation: the interacting processes with very small rates are considered to be adiabatic processes in comparison with the interacting processes with very large rates. Therefore, we try to split the problem of rapid microscopic processes from the problem of slow macroscopic processes, and focus on studying rapid microscopic processes in the background of adiabatic (slowly varying) macroscopic processes. The adiabatic approximation we adopted here is self-consistently and quantitatively justified by process rates

$$\tau_{\rm strong}^{-1} \gg \tau_{\rm pair}^{-1} > \tau_{\rm osci}^{-1} \gg \tau_{\rm relax}^{-1} \gg \tau_{\rm coll}^{-1}, \tag{C.9.1}$$

studied in this chapter. In addition to the adiabatic approximation, we have not considered in this over simplified model the hydrodynamical evolution of baryon cores, the back-reaction of oscillations and pair-production on the collapsing or pulsating processes, and the dynamical evolution of the electron-positron pairs and photons. Needless to say, these results should be further checked by numerical algorithms integrating the full Einstein-Maxwell equations and proper EOS of particles in gravitational collapse. Nevertheless, the possible consequences of these electromagnetic processes discussed in this chapter are definitely interesting and could be possibly relevant and important for understanding energetic sources of supernovae and gamma-ray bursts.

D. Gravitational and electric energies in gravitational collapse

D.1. Introduction

In the gravitational collapse of neutral stellar cores at densities comparable to the nuclear density, both macroscopic processes of gravitational and hydrodynamical interactions and microscopic processes of the strong and electroweak interactions occur. In theoretical principle, these can be well described by the Einstein-Maxwell equations and the equations for the number and energy-momentum conservations of particles, duly taking into account their interactions. In practical calculations of analytical or numerical approach, however, it is rather difficult to simultaneously analyze both macroscopic and microscopic processes for the reason that the time and length scales of macroscopic processes are much larger than those of the microscopic processes. The approximation normally adopted is that microscopic processes are treated as local and instantaneous processes which are effectively represented by a model-dependent parameterized equation of state (EOS). We call this *approximate locality*.

Applying the *approximate locality* to electric processes, as required by the charge conservation, one is led to *local neutrality*: positive and negative charge densities are exactly equal overall space and time. As a consequence, all electric processes are completely eliminated in the assumption of the *approximate locality*. On the other hand, it is well known that an internal electric field (charge-separation) *must* be developed Olson and Bailyn (1975, 1976); Rotondo et al. (2011a,b) in a totally neutral system of proton and electron fluids in the presence of gravitational fields. If the electric field (process) is weak (slow) enough, the *approximate locality* is applicable. However, this should be seriously questioned when the electric field (process) is strong (rapid) in the case that neutral stellar cores reach the nuclear density where positive charged baryons interact via strong interactions that do not associate to negative charged electrons, in addition to widely different gravitational masses of baryons and electrons. In fact, strong electric fields are created on the baryon core surface in

an electrostatic equilibrium state Usov (1998); Popov et al. (2009). Furthermore, it is shown in Ref. Han et al. (2012), either pulsating or gravitationally collapsing of the baryon core results in the dynamical evolution of electrons, as a consequence, the strong electric field dynamically evolves in space and time, and leads to the electron-positron pair-production process of Sauter-Heisenberg-Euler-Schwinger (see the review Ruffini et al. (2010)) for overcritical electric fields $E \gtrsim E_c \equiv m_e^2 c^3/(e\hbar)$. When this occurs in gravitational collapses of neutral stellar cores, some part of the gravitational energy of neutral stellar cores converts to the observable energy of electron-positron pairs, as a result the kinetic and internal energies of neutral stellar cores are reduced.

As mentioned above, the difficulties of dealing with such a problem come from very different space-time scales of macroscopic and microscopic processes. We are forced to properly split the problem into three parts: (i) microscopic processes of electrodynamics; (ii) macroscopic processes of gravitational collapses; (iii) the back-reaction of microscopic processes on macroscopic processes. In Ref. Han et al. (2012), we study the first part of the problem: microscopic processes of electrodynamics for strong electric field oscillations and pair-productions, which form a radiative electric energy, in a postulated space-time world line of gravitational collapse. However, the back-reaction of such radiative electric energy on collapse is not considered. In this chapter, we start to quantitatively understand the second and third parts of the problem in a simplified model how gravitational, electric and kinetic energies of neutral stellar cores transfer from one to another in gravitational collapses, to see the possibility of converting the gravitational energy to the electromagnetic energy by the "breaking process" of reducing kinetic energy Ruffini and Vitagliano (2003). The Planck units $G = \hbar = c = 1$ are adopted, unless otherwise specified.

D.2. Einstein-Maxwell Equations and conservation laws of two fluids

The gravitational collapse of neutral stellar cores is generally described by the Einstein-Maxwell equations and those governing the particle number and energy-momentum conservations

$$\begin{aligned} G_{\mu\nu} &= -8\pi G(T_{\mu\nu} + T^{\rm em}_{\mu\nu}), \quad F^{\mu\nu}{}_{;\nu} = 4\pi J^\mu, \\ (T^\nu{}_\mu)_{;\nu} &= -F_{\mu\nu}J^\nu, \qquad\qquad (\bar{n}_{e,B}U^\nu_{e,B})_{;\nu} = 0, \end{aligned} \tag{D.2.1}$$

in which appear the Einstein tensor $G_{\mu\nu}$, the electromagnetic field $F^{\mu\nu}$ (satisfying $F_{[\alpha\beta,\gamma]} = 0$) and its energy-momentum tensor

$$T^{\rm em}_{\mu\nu} = \frac{1}{4\pi}\left(F_\mu{}^\rho F_{\rho\nu} - \frac{1}{4} g_{\mu\nu} F^{\rho\sigma} F_{\rho\sigma}\right); \tag{D.2.2}$$

$U^\nu_{e,B}$ and $\bar{n}_{e,B}$ are respectively the four-velocities and proper number-densities of electrons and baryons,

$$J^\mu = e\bar{n}_p U^\mu_B - e\bar{n}_e U^\mu_e \tag{D.2.3}$$

is the electric current density, and $\bar{n}_p < \bar{n}_B$ the proper number-density of the positively charged baryons. The energy-momentum tensor $T^{\mu\nu} = T^{\mu\nu}_e + T^{\mu\nu}_B$ is taken to be that of two simple perfect fluids representing electrons and the baryons, each of the form

$$T^{\mu\nu}_B = \bar{p}_B g^{\mu\nu} + (\bar{p}_B + \bar{\rho}_B) U^\mu_B U^\nu_B, \tag{D.2.4}$$

$$T^{\mu\nu}_e = \bar{p}_e g^{\mu\nu} + (\bar{p}_e + \bar{\rho}_e) U^\mu_e U^\nu_e, \tag{D.2.5}$$

where $\bar{\rho}_{e,B}$ and $\bar{p}_{e,B}$ are the respective proper energy densities and pressures. In this scenario, electrons and baryons are respectively described by two perfect fluids at or over the nuclear density, and they couple each other via the electromagnetic interaction.

Baryon fluid and electron fluid must be separately described for the reasons that in addition to the different kinematics of baryons and electrons, the most important differences between their dynamics are: (i) baryons are much more massive than electrons in terms of the long-range gravitational force and baryon cores undergo relativistically collapsing processes; (ii) at or over the nuclear density $\bar{n}_{\rm nucl}$, the electron pressure is much larger that baryon one, and baryons interact each other via the short-range strong force that does not act on electrons. Electron and baryon fluids interact via the long-range electromagnetic force, when two fluids are at or over the nuclear density, this interaction between two fluids becomes rather strong, as will be specified below. Note that we ignore the short-range weak interactions for the β-process in this chapter. The long-range gravitational and electromagnetic forces are explicitly present in Eqs. (D.2.1-D.2.3). Instead, the short-range strong interaction is taken into account by pressure and energy density in the proper frame (see

Ref. Weinberg (1972)),

$$\bar{p}_{_B} = \frac{1}{3}\sum_{i=1}^{3} T^{ii} = \frac{1}{3}\sum_{_B} \delta^3(\mathbf{x}-\mathbf{x}_{_B})\frac{\mathbf{p}_{_B}^2}{E_{_B}}, \tag{D.2.6}$$

$$\bar{\rho}_{_B} = T^{tt} = \sum_{_B} \delta^3(\mathbf{x}-\mathbf{x}_{_B})E_{_B} \tag{D.2.7}$$

where $E_{_B} = E_{_B}(\mathbf{p}_{_B})$ is the energy spectrum of baryons, duly taking into account their short-range strong interactions (nuclear potential) at a given density $\bar{n}_{_B} \gtrsim \bar{n}_{\rm nucl}$. Electrons' pressure and energy density are analogously given by Eqs. (D.2.6) and (D.2.7) by replacing the subscript $B \to e$, however, the spectrum $E_e = E_e(\mathbf{p}_e)$ is different from baryon one, due to the fact that electrons are blind with the short-range strong interactions. As a result, the baryon and electron EOS $\bar{p}_B = \bar{p}_B(\bar{\rho}_B)$ and $\bar{p}_e = \bar{p}_e(\bar{\rho}_e)$ are different, moreover, the space-time gradients $\nabla\bar{p}_{_{e,B}}$ and $\partial\bar{p}_{_{e,B}}/\partial t$ are different.

We turn now to discuss how the short-range strong interaction effect on the baryon fluid velocity $v^i_{_B} = (U^i/U^t)_{_B}$. In the Newtonian limit, Eqs. (D.2.1-D.2.4) lead to the Euler equation (see Ref. Weinberg (1972))

$$\frac{\partial \mathbf{v}_{_B}}{\partial t} + (\mathbf{v}_{_B}\cdot\nabla)\mathbf{v}_{_B} = -\frac{1-\mathbf{v}_{_B}^2}{\bar{\rho}_{_B}+\bar{p}_{_B}}\left[\nabla\bar{p}_{_B} + \mathbf{v}_{_B}\frac{\partial\bar{p}_{_B}}{\partial t}\right] \tag{D.2.8}$$
$$+\text{terms of long–range forces.}$$

The first term in the right-handed side of Eq. (D.2.8) indicates the force due to the space-time gradients of baryon fluid pressure. This implies that the space-time gradients of baryon fluid velocity $\mathbf{v}_{_B}(\mathbf{x},t)$ should have the rates of short-range strong interactions, which are proportional to the inverses of π, σ, ρ and ω meson masses ($\sim m^{-1}_{\pi,\sigma,\rho,\omega,\cdots}$), depending on values of the baryon density $\bar{n}_{_B}(\mathbf{x},t)$. These nuclear reaction rates must be larger than the rate ($\gtrsim m_e^{-1}$) of electromagnetic interactions. In other words, the baryon fluid and electron fluid have the different values of the incompressibility so that they have different rates (frequencies) of reactions in space and time. However, this still remains as an argument, because we has not so far been able to quantitatively calculate the space-time gradients of baryon fluid pressure by Eqs. (D.2.6) and (D.2.7), then to obtain the space-time gradients of baryon fluid velocity by Euler equation (D.2.8) together with the Einstein-Maxwell field equations.

In the following, we attempt to address our attention to the issue how the gravitational energy gained by the baryon fluid in collapses is transfered to the electromagnetic energy and how kinetic and internal energies are reduced as a consequence of total energy conservation. The energy conservation (D.2.1) along a flow line of the

electron fluid yields

$$U_e^\mu (T^\nu{}_\mu)_{;\nu} = e\bar{n}_p F_{\mu\nu} U_e^\mu U_B^\nu = e\bar{n}_p \gamma_e \gamma_B (v_B - v_e) g_{rr} E, \tag{D.2.9}$$

where e and E are electric charge and field, the fluid velocity $v_{(e,B)} \equiv v^r_{(e,B)} = (U^r/U^t)_{(e,B)}$ and Lorentz factor $\gamma_{(e,B)} \equiv (1 + U_r U^r)^{1/2}_{(e,B)}$ in the spherical geometry

$$ds^2 = -g_{tt}dt^2 + g_{rr}dr^2 + r^2 d\theta^2 + r^2 \sin^2\theta d\phi^2 \, . \tag{D.2.10}$$

Eq. (D.2.9) indicates that the dynamical evolutions of the baryon fluid caused by the gravitational or strong interactions can transfer the energy that the baryon fluid gains to the electron fluid via an electric field, provided $v_e \not\equiv v_B$. As explained in the introductory section, for the reason that the differential equations governing macroscopic processes (e.g. gravitational collapse) and the differential equations governing microscopic processes (e.g. electrodynamic pair-production, nuclear reaction) have very different space-time scales at least of the order of 10^{17}, it is very difficult to simultaneously integrate these differential equations and quantitatively show the energy transformation as indicated by Eq. (D.2.9) in the realistic case of gravitational collapses. In order to overcome these difficulties and make steps toward the understanding of the issue, on the basis of some assumptions and approximations, we decouple the differential equations governing macroscopic processes from the differential equations governing microscopic processes as follows.

1. The first, we study the static case of compact stars at/over the nuclear density, e.g., baryons and electrons of neutral compact stars are in their equilibrium states. The local equilibrium profile of baryons must be determined by the strong interaction, whereas the local equilibrium profile of electrons must be determined instead by the electromagnetic interaction. In the Thomas-Fermi model, an overcritical "equilibrium" electric fields are found Usov (1998); Popov et al. (2009) on the surface of baryon cores. These results provide the initial configurations for the dynamical space-time evolution of baryon core and electron fluid in the gravitational collapse or pulsation.

2. Because of the dynamics of gravitational collapse or pulsation, the baryon core deviates from its equilibrium state. We postulate that due to the nuclear rigidity of baryon cores, an inward velocity v_B and charged current J_B (Eqs. (9) in Han et al. (2012)) of baryon cores are introduced at the rate of the nuclear reaction scales, rather than the rate of the gravitational collapse, as already indicated in Eqs. (D.2.6,D.2.7,D.2.8).We asked the question how the electron fluid responses to this external baryon current J_B. In Ref. Han et al. (2012), by solving the microscopic kinetic transport equations (particle number and

energy-momentum conservations) of the electron fluid as well as the Maxwell equation, we obtained the space-time evolution (non-equilibrium) of the electron fluid and overcritical electric fields in the Compton scale, and estimated the rate of pair-productions. These results are essentially due to the postulation that the inward baryon current J_B is introduced at the rate of the strong interaction scale, rather than the gravitational one. The rate of gravitational collapses is too slow to trigger these electrodynamic processes at the Compton scale. In addition, it should be pointed out that in these calculations we did not solve the differential equations for the electron fluid and the Maxwell equation together with the differential equation for the gravitational collapse. The baryon velocity v_B is treated as a parameter and its values are given by a simple collapsing equation of thin shell at different radii of gravitational collapse (Figure 3 in Ref. Han et al. (2012)). In summary, two important assumptions were made: (i) the baryon core is treated as a giant nucleus and the deviation from its equilibrium state, represented by the baryon electric current $J_B \sim v_B$, is introduced at the rate of the strong introduction; (ii) the values of v_B are given by a simple collapsing model without considering dynamics of the gravitational collapses.

3. On the contrary, instead of solving the differential equations for microscopic electrical processes in a given dynamics of gravitational collapse, in this chapter we focus on solving differential equations for macroscopic gravitational collapse processes in a given dynamics of electric processes studied in Ref. Han et al. (2012), represented by an ansatz function. Our purpose is to see the back-reaction of microscopic electrical processes on macroscopic gravitational collapse processes. In order to gain some insight into this issue, we study the gravitational collapse of a spherically thin capacitor, which might present a thin layer of collapsing stellar cores. Although this spherically thin capacitor is totally neutral, it carries electric and gravitational energies. Using such a simplified model, we try to find an analytical description and make a step in understanding the issue how the gravitational energy is converted to electric, kinetic and internal energies in a neutral stellar core collapse.

This has been so far our approach to the electromagnetic processes in the gravitational collapse of neutral compact stars at/over nuclear density. This approach is clearly far from being complete. In order to quantitatively show that the production, oscillation and annihilation of electron-positron pairs with overcritical electric fields indeed dynamically take place, one must solve altogether the Maxwell equation and the quantum Boltzmann-Vlasov transport equations not only for the electrons fluid Ruffini et al. (2003b), but also for the baryon fluid with the strong interaction. We have not yet been able to model the strong interaction for doing these

quantitative calculations. On the basis of the rates of various microscopic processes and interactions, we argue the possibility of the production, oscillation and annihilation of electron-positron pairs and dynamical evolution of overcritical electric fields (Eq. (26) in Ref. Han et al. (2012)). We clarify that in our model these electric processes are triggered by the rapid action rate of the baryon core due to the strong interaction, rather than the gravitational interaction. However, the question is to understand how to quantitatively describe and calculate the dynamics of strongly interacting baryon core in gravitational collapse, and how the baryon charged current J_B is introduced at the rate of strong interactions. This will be the subject for our future work.

D.3. A thin shell of spherical capacitor

The thin shell of spherical capacitor is composed by a layer of positively charged baryons and a layer of negatively charged electrons. The baryon layer is defined as a mathematically thin layer, while the electron layer is understood as a physically thin layer with a thickness "d" specified below. The total numbers of charged baryons and electrons are exactly equal so that the thin shell of spherical capacitor is totally neutral but carries non-vanishing the electric energy stored inside two spherical layers. The number-densities of two spherical layers are at least order of the nuclear density, as a consequence the radial separation "d" between two spherical layers must be a few orders of the Compton length λ_C. The reasons are the following: electric fields between two layers $E \approx e\bar{n}_{\rm nucl}d$ are overcritical and electric force acting on ultra-relativistic electrons balances their Fermi momenta $eEd \approx P_e^F \approx \bar{n}_{\rm nucl}^{1/3}$. Let the baryon layer locate at the Schwarzschild-like radial coordinate r_0 and electron layer distributes from r_0 to $r_0 + d$. The spherical capacitor can be physically considered as an infinitely thin shell for $d/r_0 \to 0$. The spherical capacitor is henceforth denoted by "the thin shell" in short.

As the baryon layer is mathematically thin, in Eq. (D.2.4) the baryon pressure $\bar{p}_B = 0$ and mass density $\bar{\rho}_B(x) = \bar{\rho}_B\delta^{(4)}(x, x_0)$, where $\bar{\rho}_B$ is the constant surface density in the proper frame of the baryon layer and the 4-dimensional Dirac distribution is defined as

$$\int \delta^{(4)}(x, x_0)\sqrt{-g}d^4x = 1,$$

where $g = \det\|g_{\mu\nu}\|$. Then we have ($d\Omega = \sin\theta d\theta d\phi$)

$$\int \bar{\rho}_B\delta^{(4)}(x, x_0)\, r^2 dr d\Omega d\tau = M_0, \tag{D.3.1}$$

where M_0 is the rest mass of the baryon layer, and τ is the proper time along the

world surface $S : x_0 = x_0(\tau, \theta, \phi)$ of the baryon layer. S divides the space-time into two complementary static space-times: an internal one $\mathcal{M}_-$ and an external one $\mathcal{M}_+$. Their time-like Killing vectors are denoted by ξ^μ_- and ξ^μ_+. $\mathcal{M}_+$ is foliated by the family $\{\Sigma^+_t : t_+ = t\}$ of space-like hypersurfaces of constant t_+.

On the other hand, introducing the orthonormal tetrad

$$\boldsymbol{\omega}^{(0)}_\pm = (g^\pm_{tt})^{1/2} dt, \quad \boldsymbol{\omega}^{(1)}_\pm = (g^\pm_{rr})^{-1/2} dr, \quad \boldsymbol{\omega}^{(2)} = r d\theta, \quad \boldsymbol{\omega}^{(3)} = r \sin\theta d\phi, \quad \text{(D.3.2)}$$

we describe the electric field $\boldsymbol{E} = E\boldsymbol{\omega}^{(1)}$ and electromagnetic tensor $(T^{\rm em})_t{}^t = E^2/(8\pi)$ and $(T^{\rm em})_i{}^i = -E^2/(8\pi)$ inside the thin shell ($r_0 \le r \le r_0 + d$). The electric energy of the thin shell, measured by an observer at rest at infinity, is obtained by evaluating the Killing integral

$$\int_{\Sigma^+_t} \xi^\mu_+ T^{\rm em}_{\mu\nu} d\Sigma^\nu_+ = 4\pi \int_r^\infty r^2 dr\, (T^{\rm em})_t{}^t \equiv \frac{Q^2_{\rm eff}(r)}{2r}, \quad \text{(D.3.3)}$$

where $d\Sigma^\nu_+$ is the surface element vector of the space-like hypersurfaces Σ^+_t in $\mathcal{M}_+$. In Eq. (D.3.3), we introduce the quantity $Q^2_{\rm eff}(r) \neq 0$ for $r_0 \le r \le r_0 + d$ to characterize the electric energy stored inside the thin shell. $Q^2_{\rm eff}(r) = 0$ for $r > r_0 + d$ and $r < r_0$. The total electric energy inside the thin shell is given by

$$\mathcal{E}_{\rm em}(r_0) = \frac{Q^2_{\rm eff}(r_0)}{2r_0}, \quad \text{(D.3.4)}$$

where the quantity $Q^2_{\rm eff}(r_0)$ parametrizes the total electric energy stored inside the thin shell that locates at radius $r_0(t_0)$ and time t_0. $Q_{\rm eff}(r)$ does not represent an electric charge carried by the thin shell. We express the repulsive electric energy (D.3.3) or (D.3.4) in the same form of the Coulomb energy of a spherical charged layer for the reason that it is useful to study the collapse equation of the thin shell in next section.

The energy-momentum tensor (D.2.5) of the electron layer has a physical distribution over the size "d" of the thin shell. Analogously to Eq. (D.3.3), we define the total energy of the electron layer as

$$\mathcal{E}_{\rm electron}(r_0) \equiv \int_{\Sigma^+_t} \xi^\mu_+ (T_e)_{\mu\nu} d\Sigma^\nu_+ = 4\pi \int_{r_0}^\infty r^2 dr\, (T_e)_t{}^t, \quad \text{(D.3.5)}$$

where $(T_e)^{tt} = (\bar{\rho}_e + \bar{p}_e \langle \mathbf{v}_e^2 \rangle)/(1 - \langle \mathbf{v}_e^2 \rangle)$ and $\mathbf{v}_e$ is the electron fluid velocity. In Ref. Han et al. (2012), it is shown that the electron fluid velocity $\mathbf{v}_e$ is ultra-relativistically oscillating back and forth collectively with oscillating electric fields inside the thin shell, $\langle \mathbf{v}_e^2 \rangle$ indicates the averaged value over rapid oscillations in the Compton scale.

In Eq. (D.3.5), the rest mass of the electron layer is negligible, compared with its internal energy for ultra-relativistically oscillating electrons. Moreover, at or over the nuclear density, electron Fermi momenta $P_e^F \sim m_\pi$ in the proper frame of the electron fluid is rather smaller than the baryon mass m_B. Therefore, compared with the rest mass of baryon layer M_0, we neglect the internal energy of electron layer $\mathcal{E}_{\text{electron}}(r_0)$ of Eq. (D.3.5) in this chapter.

Here, we disregard the detailed space-time oscillations of electric field and electron fluid in the Compton length scale, leading to the energy radiation in the form of electron-positron pairs. Instead, we attempt to properly model the quantity $Q^2_{\text{eff}}(r_0)$ to represent these microscopic processes of building the electric energy (D.3.4) and radiating it away from the thin shell, so as to study the back-reaction of these microscopic processes on the macroscopic process of gravitational collapse of the thin shell.

D.4. Collapse of spherically thin capacitor

A lot of attention has been focused on the exact solution of thin charged shell in gravitational collapse Israel (1966); De la Cruz and Israel (1967); Bekenstein (1971); Cherubini et al. (2002); Ruffini and Vitagliano (2002). Following the line presented in Refs. Cherubini et al. (2002) and Ruffini and Vitagliano (2002) for finding an exact solution of thin charged shell in gravitational collapse, we try to approximately solve the Einstein equations (D.2.1,D.2.2) for the gravitational collapse of the spherically thin capacitor (the thin shell). We have $g^-_{tt} = (g^-_{rr})^{-1} \equiv f_-$ and $g^+_{tt} \approx (g^+_{rr})^{-1} \equiv f_+$, where the sign "$\approx$" indicates for the range $r_0 \geq r \geq r_0 + d$, where we neglect the charge and mass-energy distributions of the electron layer. From the G_{tt} Einstein equation, we get

$$ds^2 = \begin{cases} -f_+ dt_+^2 + f_+^{-1} dr^2 + r^2(d\theta^2 + \sin^2\theta d\phi^2) & \text{in } \mathcal{M}_+ \\ -f_- dt_-^2 + f_-^{-1} dr^2 + r^2(d\theta^2 + \sin^2\theta d\phi^2) & \text{in } \mathcal{M}_- \end{cases}, \tag{D.4.1}$$

where

$$f_+ = 1 - \tfrac{2M}{r} + \tfrac{Q^2_{\text{eff}}(r)}{r^2}, \quad \text{and} \quad f_- = 1; \tag{D.4.2}$$

t_- and t_+ are the Schwarzschild-like time coordinates in $\mathcal{M}_-$ and $\mathcal{M}_+$ respectively. M is the total mass-energy of the thin shell, measured by an observer at rest at infinity. Indicating by $t_{0\pm}$ the Schwarzschild-like time coordinate of the thin shell, from the G_{tr} Einstein equation we have

$$\tfrac{M_0}{2}\left[f_+(r_0)\tfrac{dt_{0+}}{d\tau} + f_-(r_0)\tfrac{dt_{0-}}{d\tau}\right] = M - \tfrac{Q^2_{\text{eff}}}{2r_0}, \tag{D.4.3}$$

where we introduce the notation $Q^2_{\rm eff} \equiv Q^2_{\rm eff}(r_0)$. The remaining Einstein equations are identically satisfied. From (D.4.3) we have that the inequality

$$M - \frac{Q^2_{\rm eff}}{2r_0} > 0, \tag{D.4.4}$$

holds since the left-handed side of Eq. (D.4.3) is clearly positive. We define the four-velocity U^μ of the thin shell as the four-velocity U^μ_B of the baryon layer, for the reasons discussed in the paragraphs where Eqs. (D.2.6-D.2.8) are. From (D.4.3) and the normalization condition of the four-velocity of the thin shell $U_\mu U^\mu = -1$,

$$\left[-f_\pm\left(r_0\right)\frac{dt_{0\pm}}{d\tau} + f_\pm\left(r_0\right)\frac{dt_{0\pm}}{d\tau}\right] = -1, \tag{D.4.5}$$

we find

$$\left(\frac{dr_0}{d\tau}\right)^2 = \frac{1}{M_0^2}\left(M \pm \frac{M_0^2}{2r_0} - \frac{Q^2_{\rm eff}}{2r_0}\right)^2 - f_\mp\left(r_0\right), \tag{D.4.6}$$

$$\frac{dt_{0\pm}}{d\tau} = \frac{1}{M_0 f_\pm(r_0)}\left(M \mp \frac{M_0^2}{2r_0} - \frac{Q^2_{\rm eff}}{2r_0}\right), \tag{D.4.7}$$

in the space-times $\mathcal{M}_\pm$. Eqs. (D.4.1-D.4.7) completely describe a 3-parameter (M, $Q^2_{\rm eff}$, M_0) family of solutions of the Einstein equations. As we will see, for the description of the collapse we can choose either $\mathcal{M}_-$ or $\mathcal{M}_+$. The two descriptions are equivalent and relevant for the physical interpretation of the solutions.

For astrophysical applications, see for example Ref. Ruffini et al. (2003a), we attempt to approximately solve the equation of motion of the thin shell and obtain the trajectory $r_0 = r_0\left(t_{0+}\right)$ as a function of the time coordinate t_{0+} relative to the space-time region $\mathcal{M}_+$. In the following we drop the $+$ index from t_{0+}. From (D.4.6) and (D.4.7) we have the equation of motion of the thin shell

$$\begin{aligned}\frac{dr_0}{dt_0} &= \frac{dr_0}{d\tau}\frac{d\tau}{dt_0} = \pm\frac{F}{\Omega}\sqrt{\Omega^2 - F},\\ \frac{dr_0}{d\tau} &= \pm\sqrt{\Omega^2 - F}\end{aligned} \tag{D.4.8}$$

where $F \equiv f_+\left(r_0\right)$ of Eq. (D.4.2),

$$\Omega \equiv \Gamma - \frac{M_0^2 + Q^2_{\rm eff}}{2M_0 r_0}, \quad \Gamma \equiv \frac{M}{M_0}. \tag{D.4.9}$$

Since we are interested in an imploding thin shell, only the minus sign case in (D.4.8) will be studied. We can give the following physical interpretation of Γ. For $M \geq M_0$, Γ coincides with the Lorentz factor of the imploding thin shell at infinity; from (D.4.8)

it satisfies

$$\Gamma = \frac{1}{\sqrt{1-\left(\frac{dr_0}{dt_0}\right)^2_{r_0=\infty}}} \geq 1. \tag{D.4.10}$$

We rewrite equation of motion (D.4.8) as

$$\left(\frac{dr_0}{d\tau}\right)^2 = \left[\Gamma + \frac{M_0}{2r_0}(1-\xi^2)\right]^2 - 1,$$

or

$$\left(\frac{\Omega}{F}\right)^2 \left(\frac{dr_0}{dt_0}\right)^2 = \left[\Gamma + \frac{M_0}{2r_0}(1-\xi^2)\right]^2 - 1, \tag{D.4.11}$$

where $\Omega \equiv \Gamma - (M_0/2r_0)(1+\xi^2)$ and we define an effective "charge-mass-ratio"

$$\xi \equiv \frac{Q_{\rm eff}}{M_0}. \tag{D.4.12}$$

Actually ξ^2 represents the ratio of electric energy and gravitational energy of the thin shell. For the case $\Gamma = 1$ ($M = M_0$), i.e., the thin shell collapses at rest from infinity. Eq. (D.4.4) requires $M_0 \geq Q^2_{\rm eff}/2r_0$ to start gravitational collapse and Eq. (D.4.11) requires $\xi < 1$ to continue gravitational collapse. When $\xi = 1$, gravitational collapse stops and kinetic energy of the thin shell vanishes as will be seen below. The trajectory of the thin shell is given by the solution:

$$\int dt_0 = -\int \frac{\Omega}{F\sqrt{\Omega^2 - F}} dr_0. \tag{D.4.13}$$

to the equation of motion (D.4.8).

To understand the total energy conservation of the thin shell in gravitational collapse, we use the solution (D.4.6) in the flat space-time $\mathcal{M}_-$,

$$\left(M_0 \frac{dr_0}{d\tau}\right)^2 = \left(M + \frac{M_0^2}{2r_0} - \frac{Q^2_{\rm eff}}{2r_0}\right)^2 - M_0^2, \tag{D.4.14}$$

we can interpret $-\frac{M_0^2}{2r_0}$ as the gravitational attractive energy of the thin shell and $\frac{Q^2_{\rm eff}}{2r_0}$ is its repulsive electric energy. Introducing the total four-momentum of the shell $P^\mu = M_0 U^\mu$ and its radial component $P \equiv M_0 U^r = M_0 \frac{dr_0}{d\tau}$, the kinetic energy of the thin shell as measured by static observers in $\mathcal{M}_-$ is expressed as Ruffini and Vitagliano (2002)

$$T(r_0) \equiv -P_\mu \xi^\mu_- - M_0 = \sqrt{P^2 + M_0^2} - M_0. \tag{D.4.15}$$

Then from Eqs. (D.4.14,D.4.15) we have

$$\begin{aligned} M(r_0) &= -\frac{M_0^2}{2r_0} + \frac{Q_{\rm eff}^2}{2r_0} + \sqrt{P^2 + M_0^2} \\ &= M_0 + T(r_0) - \frac{M_0^2}{2r_0} + \frac{Q_{\rm eff}^2}{2r_0}, \end{aligned} \tag{D.4.16}$$

where we choose the positive root solution due to the constraint (D.4.4). Eq. (D.4.16) is the total energy-conservation of the thin shell, whose rest mass M_0, kinetic energy $T(r_0)$, gravitational energy $-\frac{M_0^2}{2r_0}$, and electric energy $\frac{Q_{\rm eff}^2}{2r_0}$ depends on the radial coordinate $r_0(t_0)$ in gravitational collapse.

In the following discussion, we consider the shell is at rest at infinity and starts to gravitational collapse, $T(r_0) = 0$, $-\frac{M_0^2}{2r_0} = 0$ and $\frac{Q_{\rm eff}^2}{2r_0} = 0$ at $r_0 \to \infty$. The initial energy of the thin shell $M(r_0 \to \infty) = M_0$, i.e., $\Gamma = 1$. The total shell energy $M(r_0) = M_0$ is conserved in the entire collapsing process.

D.5. Collapse of the thin shell with varying electric energy

In Ref. Han et al. (2012), assuming that in gravitational collapses, the baryon layer induces an inward current-density

$$J_B^r(r_0) = e\bar{n}_p U_B^r \approx e\bar{n}_p(\dot{r}_0\Omega/F), \quad \dot{r}_0 = dr_0/dt_0, \tag{D.5.1}$$

at the rate of strong interaction scales, we show that triggered by this baryon current (D.5.1), the current-density $J_e^r = e\bar{n}_e U_e^r$ of the electron layer oscillates collectively with overcritical electric fields E at frequency $\omega_{\rm osci} = \tau_{\rm osci}^{-1} \simeq 1.5\, m_e$, leading to the production of electron-positron pairs at rate $\tau_{\rm pair}^{-1} \simeq 6.6\, m_e$. Selecting values $J_B^r(r_0)$ and $\dot{r}_0$ of Eq. (D.5.1) at different collapsing radii, we calculated Han et al. (2012) the averaged energy and number densities of electron-positron pairs produced, as well as the averaged electric energy (Coulomb energy) of oscillating overcritical electric fields. In addition, our results presented in Refs. Ruffini et al. (2003b,a) show that these electron-positron pairs annihilate to photons and the ultra-dense plasma of electron-positron pairs and photons is formed with the equipartition of energy and number of electron-positron pairs and photons, beside this plasma undergoes the hydrodynamical expansion and the photon radiation occurs. This indicates that the electric energy is established by the electron-positron oscillations collectively with overcritical electric fields, then dissipated by electron-positron annihilations to photons radiating away. Clearly, these results and discussions are based on the postula-

tion that the baryon current of Eq. (D.5.1) introduced by the strong interaction in a gravitational collapse process triggers all electric processes, provided that the reaction rates of processes satisfy the inequality of Eq. (26) in Ref. Han et al. (2012). In the light of the total energy conservation in gravitational collapses and Eq. (D.2.9), we further postulate that the electric energy of these electric processes is converted from the gravitational energy, as a consequence, the gravitational energy gained by the collapsing baryon core is transfered to the photon radiation energy. In future work, we are bound to show this energy conversion by solving the equations of gravitational collapses altogether with the equations of electric processes and nuclear processes. In the present chapter, we attempt to study the back-reaction effect of this energy conversion on the gravitational collapse.

In the simplified model of collapsing thin shell, we represent $\frac{Q_{\rm eff}^2}{2r_0}$ the electric energy established by electron-positron pair production and oscillation with overcritical electric fields, then dissipated by electron-positron annihilations to photons radiating away at the collapsing radius r_0. The time variation rate of this electric energy $\frac{Q_{\rm eff}^2}{2r_0}$ is characterized by the frequency $\omega_{\rm osci} \simeq 1.5m_e$ Han et al. (2012). On the other hand, from collapse equation (D.4.11) for $\Gamma = 1$, it is shown that the collapsing velocity (dr_0/dt_0) varies between zero and its maximal value as the "charge-mass-ratio" ξ varies from 1 and 0, corresponding to the microscopic processes of the electric energy $\frac{Q_{\rm eff}^2}{2r_0}$ built up and completely radiating away. In order to see the back-reaction of this radiative electric energy on the gravitational collapse of the thin shell, we model the electric energy $\frac{Q_{\rm eff}^2}{2r_0}$ by an ansatz function for varying "charge-mass-ratio" ξ in the collapse equation (D.4.11)

$$\xi = \xi^{\rm max}|\sin(\omega_{\rm osci} r_0)| + \xi^{\rm min}, \quad r_0 = r_0(t_0). \tag{D.5.2}$$

As indicated by the results of Ref. Han et al. (2012) for $M_0 = 20M_\odot$, we adopt values $\omega_{\rm osci} \simeq 1.5m_e$, $\xi^{\rm max} = 0.6$ and $\xi^{\rm min} = 0.1$ for illustrating the back-reaction effect. This postulates that at the collapsing radius $r_0(t_0)$ of the baryon layer, the microscopic processes of the electric energy $\frac{Q_{\rm eff}^2}{2r_0}$ built up and radiating away are in the rate of the Compton scale $\omega_{\rm osci} \simeq 1.5m_e$ and effectively described by a simple function of Eq. (D.5.2), and $\xi^{\rm min} \neq 0$ representing the part of the electric energy that does not radiate away from the shin shell. Whereas the case ($\xi \equiv 0$) represents the collapse of a neutral thin shell without carrying any electric energy.

We express r_0 and t_0 in units of GM_0 and GM_0/c, then $\omega r_0 = 1.5(m_e GM_0)r_0$, $\lambda_C/GM_0 = 1.05 \times 10^{-16}$, $20GM_\odot/c^2 \simeq 10^{-4}$ second and $M_0 = 20GM_\odot/c \simeq 3 \times 10^6$ cm. Plotting the velocity $\dot{r}_0 = dr_0/dt_0$ of Eq. (D.4.11) in Fig. D.1, we find that in collapse process, the thin shell velocity is oscillating between zero and the envelop curve, which represents the collapsing velocity of the thin shell carrying the electric

energy described by $\xi^{\min} \neq 0.1$. This result shows a sequence of "on and off" collapsing steps: the thin shell at rest starts to move inwards due to the gravitational attraction of the baryon layer, and stops due to the repulsion of the electric energy $\frac{Q^2_{\rm eff}}{2r_0}$ built up to $\xi = 1$, then restarts to move inwards again due to the electric energy $\frac{Q^2_{\rm eff}}{2r_0}$ partially radiating away in the form of electron-positron pairs and photons. The frequency of this "on and off" hopping sequence is about $\omega_{\rm osci} \sim m_e$, the Compton scale. The collapse process is still continuous in terms of macroscopic scale. However, as will be seen soon, the time scale and kinetic energy of collapses are changed.

The averaged collapsing velocity of the thin shell of Eq. (D.5.2) is smaller than the collapsing velocity (envelop curve) for the case $\xi = 0$. As a result, the time duration of collapse process becomes longer. Assuming that the thin shell is at rest at the radius $R_0 = 30M_0$ and starts to collapse, we plot in Fig. D.2 the time coordinate t_0 of Eq. (D.4.13) as a function of the radial coordinate r_0 of the collapsing thin shell, in comparison with that of the case $\xi = 0$. The blue line for the case $\xi = 0$ shows that the collapsing shell takes time $\sim 10^2\, GM_0/c^2$ to approach the horizon, whereas the red line for the case ξ of Eq. (D.5.2) shows that the collapsing thin shell takes time $\sim 10^3\, GM_0/c^2$ to approach the horizon. The collapsing time for the case ξ of Eq. (D.5.2) is about 10 times longer than the collapsing time for the case $\xi = 0$. This result is not sensitive to the value of the frequency $\omega_{\rm osci}$ in the Compton scale and the detailed form of an oscillating function (D.5.2) of the frequency $\omega_{\rm osci}$.

It should be pointed out that in this simplified toy model of thin shell collapsing, to evidently illustrate the back-reaction effect that slows down the collapsing process in comparison with the free fall collapsing process in the same plot (see Fig. D.2), we select the initial radius $R_0 = 30M_0$ at which the thin shell starts to collapse. As discussed, the baryon core must be at (over) the nuclear density and the mean distance between baryons is about one Fermi (smaller than one Fermi), where the strong interaction plays an important role. This is the one of necessary conditions for the electric processes of production and oscillation of electron-positron pairs together with "non-equilibrium" overcritical electric fields to occur. Under this consideration, the initial radius R_0 of the baryon core starting to collapse should be smaller than $30M_0$. However, in this simplified toy model of thin shell collapsing, the surface density of the baryon thin shell is over the nuclear density at the initial radius $R_0 = 30M_0$. Nevertheless, the necessary condition of baryon cores being at/over the nuclear density should be duly taken into account, when we study the back-reaction in a more realistic model describing the gravitational collapse of neutral stellar cores.

Using the velocity $\dot{r}_0 = dr_0/dt_0$ of Eqs. (D.4.8) and (D.4.11), we plot in Fig. D.3 the kinetic energy $T(r_0)$ of Eq. (D.4.15) and the gravitational energy $M_0^2/2r_0$ of the collapsing thin shell as a function of collapsing radius r_0. Following the total energy

conservation of Eq. (D.4.16) and $M(r_0) = M_0$,

$$T(r_0) - \frac{M_0^2}{2r_0} + \frac{Q_{\rm eff}^2}{2r_0} = 0, \tag{D.5.3}$$

the electric energy $\frac{Q_{\rm eff}^2}{2r_0}$ is given by the difference between gravitational energy and kinetic energy, as shown in Fig. D.3. In the collapse process, the kinetic energy $T(r_0)$ and electric energy $\frac{Q_{\rm eff}^2}{2r_0}$ are rapidly oscillating, following the ansatz function (D.5.2) with the frequency $\omega_{\rm osci}$ of microscopic processes. Averaging over these rapid oscillations, we obtain the averaged values of the kinetic energy and electric energy, which are approximately equal to an half of gravitational energy:

$$\langle T(r_0)\rangle \approx \langle \frac{Q_{\rm eff}^2}{2r_0}\rangle \approx \frac{1}{2}\frac{M_0^2}{2r_0}. \tag{D.5.4}$$

This implies that the averaged electric energy radiating away from the thin shell is about an half of the gravitational energy gained by the collapsing thin shell in the collapsing process. When the black hole horizon is reached, using Eq. (D.4.16), the irreducible mass of black hole is introduced Ruffini and Vitagliano (2002)

$$M = M_{\rm ir} + \frac{Q_{\rm eff}^2}{2r_+}, \quad \text{and} \quad M_{\rm ir} = M_0 - \frac{M_0^2}{2r_+} + T(r_+), \tag{D.5.5}$$

where $\frac{Q_{\rm eff}^2}{2r_+}$ is the total electric energy of the thin shell approaching the horizon r_+. Suppose that the electric energy $\frac{Q_{\rm eff}^2}{2r_+}$ completely radiates away, a black hole is formed with the horizon $r_0 \to r_+ = 2M_0$ for $F \equiv f_+(r_0) \to 0$. In this case, the total electric energy radiating away from the thin shell is about an half of gravitational energy of the thin shell

$$\langle \frac{Q_{\rm eff}^2}{2r_+}\rangle \approx \frac{1}{2}\left(\frac{M_0^2}{2r_+}\right) = \frac{1}{8}M_0, \tag{D.5.6}$$

and the irreducible mass of the formed black hole is about

$$M_{\rm ir} = M_0 - \frac{M_0^2}{2r_+} + \langle T(r_+)\rangle \approx \frac{7}{8}M_0, \tag{D.5.7}$$

$$M_0 = M_{\rm ir} + \langle \frac{Q_{\rm eff}^2}{2r_+}\rangle, \tag{D.5.8}$$

which implies about $1/8$ of the gravitational energy extracted in gravitational collapses.

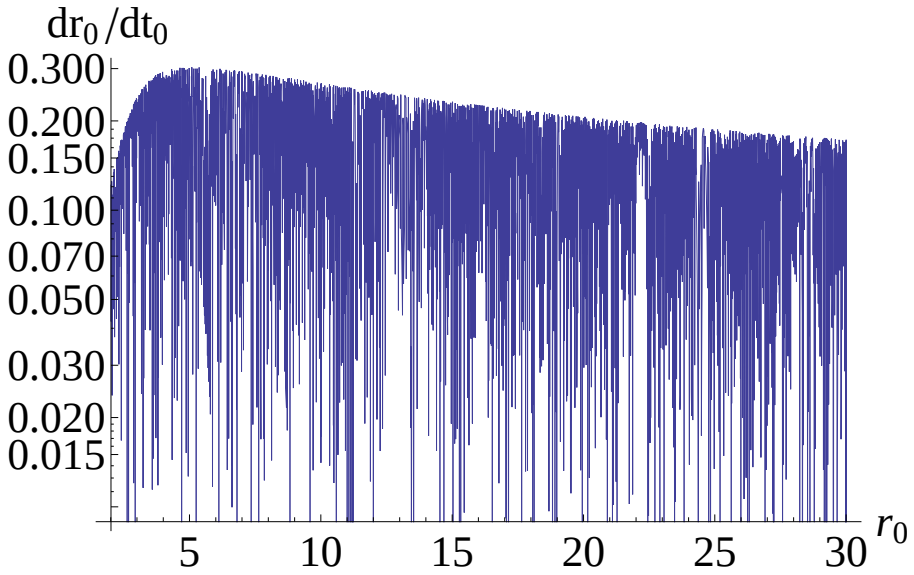

Figure D.1.: In unit of the speed of light c, the collapse velocity (dr_0/dt_0) is plotted (fast oscillating lines in blue) as a function of radius r_0 of the collapsing thin shell. The thin shell is at rest at the radius $R_0 = 30\,GM_0$ and starts to collapse. The thin shell mass $M_0 = 20M_\odot$.

D.6. Summary and remarks

In this chapter, on the basis of a simple model for describing the gravitational collapse of a spherically thin capacitor, we analytically study how the gravitational energy gained in collapse converts to the kinetic energy and electric energy, the latter can be radiated away. Using an ansatz function for the effective "charge-mass-ratio" (D.4.12) to model the microscopic processes that create this electric energy and radiate it away in the Compton scale, we study how the back-reaction of such radiative electric energy on the macroscopic process of gravitational collapse. We find that the rebuilding and radiating of repulsive electric energy cause the collapse process undergoing a sequence of "on and off" hopping steps in the microscopic Compton scale. Although such a collapse process is still continuous in the macroscopic scales, it is slowed down as the kinetic energy is reduced and collapsing time is about an order of magnitude larger than that of collapse process eliminating electric processes. The averaged kinetic and electric energies are the same order, about an half of gravitational energy in collapse.

These results are obtained from an over simplified model for both macroscopic

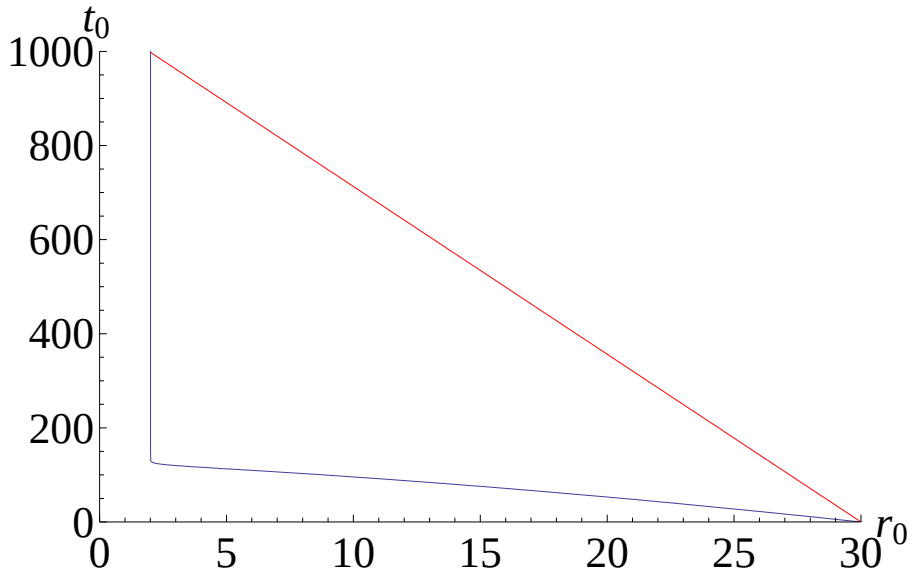

Figure D.2.: In thin shell collapsing process, the time coordinate t_0 is plotted as a function of radial coordinate r_0 of the thin shell. t_0 and r_0 are in unit of GM_0. The red line is for ξ of Eq. (D.5.2) and the blue for $\xi = 0$. The shell is at rest at the radius $R_0 = 30\,GM_0$ and starts to collapse. The thin shell mass $M_0 = 20M_\odot$.

and microscopic processes. Nevertheless they indicate that apart from an electromagnetic energy radiation, the microscopic processes of electrodynamics have significant back-reaction and effects on gravitational collapsing processes in macroscopic scales. It is thus essential to take into account, rather than ignore, electric processes in more realistic models for studying gravitational collapse of neutral stellar core at/over the nuclear density, even though calculations are very complicate.

To end this chapter, we would like to mention the relevance of these results to our previous studies of energetic budget and time duration of Gamma-Ray Bursts (GRBs) as a signal of the final stage of gravitational collapse of massive stellar cores. The total electromagnetic energy extractable from a charged black hole Damour and Ruffini (1975); Ruffini and Xue (2008a); Preparata et al. (1998, 2003) (from the collapse of a neutral stellar core Han et al. (2012)) is a fraction of its mass, which reasonably accounts for the energetic budget of GRBs. In addition, the time duration T_{90} of electromagnetic radiation is about 10^{-2} second obtained Ruffini et al. (1999, 2000) by solving hydrodynamical equations with an initial configuration of electro-positron

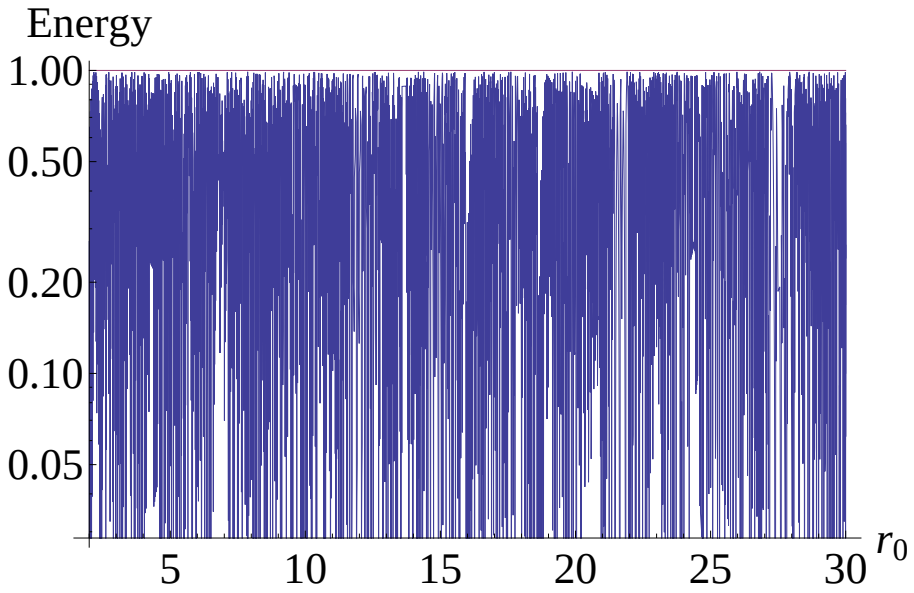

Figure D.3.: In unit of the gravitational energy $M_0^2/(2r_0)$, the gravitational energy (constant red line at 1) and kinetic energy (fast oscillating lines in blue) and electric energy (fast oscillating lines in white) of the thin shell are plotted as a function of collapsing radius r_0.

pairs and photons sphere (dyadosphere) around a charged black hole. This time duration scale is elongated to be an order of magnitude larger $\sim 10^{-1}$ second Ruffini et al. (2003a); Fraschetti et al. (2006); Ruffini et al. (2005) by considering both the dynamical formation and hydrodynamical evolution of dyadosphere in a collapsing charged core. The results of this chapter imply that due to the back-reaction of the dynamical formation and hydrodynamical evolution of dyadosphere on collapsing neutral stellar cores at or over the nuclear density, the slowing down of gravitational collapsing processes should elongate this time duration scale by another factor of 10, i.e., $T_{90} \sim 1$ second that reasonably accounts for the time duration of short GRBs.

E. Einstein-Euler-Heisenberg theory and charged black holes

E.1. Introduction

For several decades the nonlinear electromagnetic generalization of the Reissner-Nordström solution of the Einstein-Maxwell equations has attracted a great deal of attention. The most popular example is the gravitating Born-Infeld (BI) theory Born and Infeld (1934). The static charged black holes in gravitating nonlinear electrodynamics were studied in the 1930s Hoffmann (1935); Hoffmann and Infeld (1937). The discovery that the string theory, as well as the D-brane physics, leads to Abelian and non-Abelian BI-like Lagrangians in its low-energy limit (see, e.g., Refs. Fradkin and Tseytlin (1985); Abouelsaood et al. (1987); Tseytlin (1997)), has renewed the interest in these kinds of nonlinear actions. Asymptotically flat, static, spherically symmetric black hole solutions for the Einstein-Born-Infeld theory were obtained in the literature Garcia et al. (1984); Demianski (1986).

Generalization of the exact solutions of spherically symmetric Born-Infeld black holes with a cosmological constant in arbitrary dimensions has been considered Fernando and Krug (2003); Dey (2004); Cai et al. (2004), as well as in other gravitational backgrounds Wiltshire (1998); Aiello et al. (2004). Many other models of nonlinear electrodynamics leading to static and spherically symmetric structures have been considered in the last decades, such as the theory with a nonlinear Lagrangian of a general function of the gauge invariants ($F^{\mu\nu}F_{\mu\nu}$ and $F_{\mu\nu}\tilde{F}^{\mu\nu}$) Diaz-Alonso and Rubiera-Garcia (2010b,a, 2011a,b) or a logarithmic function of the Maxwell invariant ($F^{\mu\nu}F_{\mu\nu}$) Soleng (1995), and the theory with a generalized nonlinear Lagrangian De Oliveira (1994) which can lead to the BI Lagrangian and the weak-field limit of the Euler-Heisenberg effective Lagrangian Heisenberg and Euler (1936). The static and spherically symmetric black hole, whose gravity coupled to the nonlinear electrodynamics of the weak-field limit of the Euler-Heisenberg effective Lagrangian as a low-energy limit of the Born-Infeld theory, was studied in Ref. Yajima and Tamaki (2001). Some attempts in the obtention of regular (singularity-free) static and spherically symmetric black hole solutions in gravitating nonlinear electrodynamics have been made Ayón-Beato and García (1998, 1999); Cirilo Lombardo (2009); Burinskii

and Hildebrandt (2002); Dymnikova (2004), and the unusual properties of these solutions have been discussed in Refs. Novello et al. (2000); Bronnikov (2001). Generalization of spherically symmetric black holes in higher dimension in the theory with a nonlinear Lagrangian of a function of power of the Maxwell invariant has been considered in the literature Hassaïne and C. Martínez (2007, 2008); González et al. (2009); Mazharimousavi et al. (2010). Finally, we mention that rotating black branes Dehghani and Rastegar Sedehi (2006); Dehghani et al. (2007) and rotating black strings Hendi (2010) in the Einstein-Born-Infeld theory have been also considered.

The effective Lagrangian of nonlinear electromagnetic fields has been formulated for the first time by Heisenberg and Euler using the Dirac electron-positron theory Heisenberg and Euler (1936). Schwinger reformulated this nonperturbative one-loop effective Lagrangian within the quantum electrodynamics (QED) framework Schwinger (1951). This effective Lagrangian characterizes the phenomenon of vacuum polarization. Its imaginary part describes the probability of the vacuum decay via the electron-positron pair production. If electric fields are stronger than the critical value $E_c = m^2c^3/e\hbar$, the energy of the vacuum can be lowered by spontaneously creating electron-positron pairs Heisenberg and Euler (1936); Schwinger (1951); Sauter (1931). For many decades, both theorists and experimentalists have been interested in the aspects of the electron-positron pair production from the QED vacuum and the vacuum polarization by an external electromagnetic field (see, e.g., Refs. Ruffini et al. (2010); ELI).

As a fundamental theory, QED gives an elegant description of the electromagnetic interaction; moreover, it has been experimentally verified. Therefore, it is important to study the QED effects in black hole physics. As a result of one-loop nonperturbative QED, the Euler-Heisenberg effective Lagrangian deserves to attract more attention in the topic of generalized black hole solutions mentioned above. In this chapter, we adopt the contribution from the Euler-Heisenberg effective Lagrangian to formulate the Einstein-Euler-Heisenberg theory, and study the solutions of electrically and magnetically charged black holes in spherical geometry. We calculate and discuss the QED corrections to the black hole horizon area, entropy, total energy, and the maximally extractable energy.

The chapter is organized as follows. In Sec. E.2, we first recall the Euler-Heisenberg effective Lagrangian. We formulate the Einstein-Euler-Heisenberg theory in Sec. E.3. The study of electrically charged black holes in the weak electric field case is presented in Sec. E.4. The study of magnetically charged black holes in both weak and strong magnetic field cases is presented in Sec. E.5. Then we present the study of black holes with both electric and magnetic charges in the Einstein-Euler-Heisenberg theory in Sec. E.6. A summary is given in Sec. E.7. The use of units with $\hbar = c = 1$ is throughout the chapter.

E.2. The Euler-Heisenberg effective Lagrangian

The QED one-loop effective Lagrangian was obtained by Heisenberg and Euler Heisenberg and Euler (1936) for constant electromagnetic fields,

$$\Delta\mathcal{L}_{\text{eff}} = \frac{1}{2(2\pi)^2}\int_0^\infty \frac{ds}{s^3}\Big[e^2\varepsilon\beta s^2\coth(e\varepsilon s)\cot(e\beta s) \\ -1-\frac{e^2}{3}(\varepsilon^2-\beta^2)s^2\Big]e^{-is(m_e^2-i\eta)}, \tag{E.2.1}$$

as a function of two invariants: the scalar S and the pseudoscalar P,

$$S \equiv -\frac{1}{4}F_{\mu\nu}F^{\mu\nu} = \frac{1}{2}(\mathbf{E}^2-\mathbf{B}^2) \equiv \varepsilon^2-\beta^2, \\ P \equiv -\frac{1}{4}F_{\mu\nu}\tilde{F}^{\mu\nu} = \mathbf{E}\cdot\mathbf{B} \equiv \varepsilon\beta, \tag{E.2.2}$$

where the field strength is $F^{\mu\nu}$, $\tilde{F}^{\mu\nu} \equiv \epsilon^{\mu\nu\lambda\kappa}F_{\lambda\kappa}/2$, and

$$\varepsilon = \sqrt{(S^2+P^2)^{1/2}+S}, \tag{E.2.3}$$

$$\beta = \sqrt{(S^2+P^2)^{1/2}-S}. \tag{E.2.4}$$

The effective Lagrangian reads

$$\mathcal{L}_{\text{eff}} = \mathcal{L}_M + \Delta\mathcal{L}_{\text{eff}}, \tag{E.2.5}$$

where $\mathcal{L}_M = S$ is the Maxwell Lagrangian. Its imaginary part is related to the decay rate of the vacuum per unit volume Heisenberg and Euler (1936); Schwinger (1951),

$$\frac{\Gamma}{V} = \frac{\alpha\varepsilon^2}{\pi^2}\sum_{n=1}\frac{1}{n^2}\frac{n\pi\beta/\varepsilon}{\tanh n\pi\beta/\varepsilon}\exp\left(-\frac{n\pi E_c}{\varepsilon}\right) \tag{E.2.6}$$

for fermionic fields, and

$$\frac{\Gamma}{V} = \frac{\alpha\varepsilon^2}{2\pi^2}\sum_{n=1}\frac{(-1)^n}{n^2}\frac{n\pi\beta/\varepsilon}{\sinh n\pi\beta/\varepsilon}\exp\left(-\frac{n\pi E_c}{\varepsilon}\right) \tag{E.2.7}$$

for bosonic fields; here, $E_c = \frac{m_e^2 c^3}{e\hbar}$ is the critical field. Using the expressions Gradshteyn and Ryzhik (1994)

$$e\varepsilon s \coth(e\varepsilon s) = \sum_{n=-\infty}^{\infty} \frac{s^2}{(s^2+\tau_n^2)}, \quad \tau_n \equiv n\pi/e\varepsilon, \tag{E.2.8}$$

$$e\beta s \cot(e\beta s) = \sum_{m=-\infty}^{\infty} \frac{s^2}{(s^2-\tau_m^2)}, \quad \tau_m \equiv m\pi/e\beta, \tag{E.2.9}$$

one obtains the real part of the Euler-Heisenberg effective Lagrangian (E.2.1) (see Refs. Ruffini et al. (2010); Ruffini and Xue (2006); Mielniczuk (1982); Valluri et al. (1993); Cho and Pak (2001); Kleinert et al. (2013)),

$$(\Delta\mathcal{L}_{\rm eff}^{\cos})_{\mathcal{P}} = \frac{1}{2(2\pi)^2} \sum_{n,m=-\infty}^{\infty} \frac{1}{\tau_m^2+\tau_n^2} \Big[\bar{\delta}_{m0} J(i\tau_m m_e^2) - \bar{\delta}_{n0} J(\tau_n m_e^2)\Big] \tag{E.2.10}$$

$$= -\frac{1}{(2\pi)^2} \left[\sum_{n=1}^{\infty} \frac{e\beta}{\tau_n} \coth(e\beta\tau_n) J(\tau_n m_e^2) - \sum_{m=1}^{\infty} \frac{e\epsilon}{\tau_m} \coth(e\epsilon\tau_m) J(i\tau_m m_e^2)\right] \tag{E.2.11}$$

The symbol $\bar{\delta}_{ij} \equiv 1 - \delta_{ij}$ denotes the complimentary Kronecker δ, which vanishes for $i = j$, and

$$J(z) \equiv \mathcal{P}\int_0^{\infty} ds \frac{se^{-s}}{s^2-z^2} = -\frac{1}{2}\Big[e^{-z}\mathrm{Ei}(z) + e^{z}\mathrm{Ei}(-z)\Big]. \tag{E.2.12}$$

Here, $\mathcal{P}$ indicates the principle value integral, and $\mathrm{Ei}(z)$ is the exponential-integral function,

$$\mathrm{Ei}(z) \equiv \mathcal{P}\int_{-\infty}^{z} dt \frac{e^t}{t} = \log(-z) + \sum_{k=1}^{\infty} \frac{z^k}{kk!}. \tag{E.2.13}$$

Using the series and asymptotic representation of the exponential-integral function $\mathrm{Ei}(z)$ for large z corresponding to weak electromagnetic fields ($\varepsilon/E_c \ll 1, \beta/E_c \ll 1$),

$$J(z) = -\frac{1}{z^2} - \frac{6}{z^4} - \frac{120}{z^6} - \frac{5040}{z^8} - \frac{362880}{z^{10}} + \cdots, \tag{E.2.14}$$

the weak-field expansion of Eq. (E.2.10) is

$$(\Delta\mathcal{L}_{\rm eff})_{\mathcal{P}} = \frac{2\alpha^2}{45m_e^4}\left\{4S^2+7P^2\right\} + \frac{64\pi\alpha^3}{315m_e^8}\left\{16S^3+26SP^2\right\} + \cdots, \tag{E.2.15}$$

which is expressed in terms of a powers series of weak electromagnetic fields up to $O(\alpha^3)$, the first term was obtained by Heisenberg and Euler in their original article Heisenberg and Euler (1936).

On the other hand, using the series and asymptotic representation of the exponential-

integral function $\mathrm{Ei}(z)$ for small $z \ll 1$ Gradshteyn and Ryzhik (1994) corresponding to strong electromagnetic fields ($\varepsilon/E_c \gg 1$, $\beta/E_c \gg 1$),

$$J(z) = -\frac{1}{2}\Big[e^z \ln(z) + e^{-z}\ln(-z)\Big] - \frac{1}{2}\gamma\Big[e^z + e^{-z}\Big] + \mathcal{O}(z), \tag{E.2.16}$$

the leading terms in the strong-field expansion of Eqs. (E.2.10) and (E.2.11) are given by (see Refs. Ruffini et al. (2010); Ruffini and Xue (2006); Kleinert et al. (2013); Kleinert (2011))

$$(\Delta\mathcal{L}^{\cos}_{\text{eff}})_{\mathcal{P}} = \frac{1}{2(2\pi)^2}\sum_{n,m=-\infty}^{\infty}\frac{1}{\tau_m^2+\tau_n^2}\Big[\bar{\delta}_{n0}\ln(\tau_n m_e^2) - \bar{\delta}_{m0}\ln(\tau_m m_e^2)\Big] + \cdots \tag{E.2.17}$$

$$= \frac{1}{2(2\pi)^2}\left[\sum_{n=1}^{\infty}\frac{e\beta}{\tau_n}\coth(e\beta\tau_n)\ln(\tau_n m_e^2) - \sum_{m=1}^{\infty}\frac{e\epsilon}{\tau_m}\coth(e\epsilon\tau_m)\ln(\tau_m m_e^2)\right] + \cdots \tag{E.2.18}$$

In the case of vanishing magnetic field $\mathbf{B} = 0$ and a strong electric field $E \gg E_c$ using $\lim_{z\to\infty} J(iz) = 0$ and $\lim_{z\to 0} z\coth(az) = 1/a$, Eq. (E.2.18) becomes (see Refs. Ruffini et al. (2010); Ruffini and Xue (2006); Kleinert et al. (2013))

$$(\Delta\mathcal{L}^{\cos}_{\text{eff}})_{\mathcal{P}} = \frac{e^2E^2}{4\pi^4}\sum_{n=1}^{\infty}\frac{1}{n^2}\left[\ln\left(\frac{n\pi E_c}{E}\right)+\gamma\right] + \cdots \tag{E.2.19}$$

$$= \frac{e^2E^2}{24\pi^2}\left[\ln\left(\frac{\pi E_c}{E}\right)+\gamma\right] - \frac{e^2E^2}{4\pi^4}\zeta'(2) + \cdots, \tag{E.2.20}$$

with the Euler-Mascheroni constant $\gamma = 0.577216$, the Riemann zeta function $\zeta(k) = \sum_n 1/n^k$, and

$$\zeta'(2) = \frac{\pi^2}{6}\left[\gamma + \ln(2\pi) - 12\ln A\right] \simeq -0.937548, \tag{E.2.21}$$

with $A = 1.28243$ being the Glaisher constant. Similarly, in the case of vanishing electric field $\mathbf{E} = 0$ and a strong magnetic field $B \gg E_c$, Eq. (E.2.18) becomes (see Refs. Ruffini et al. (2010); Ruffini and Xue (2006); Kleinert et al. (2013))

$$(\Delta\mathcal{L}^{\cos}_{\text{eff}})_{\mathcal{P}} = -\frac{e^2B^2}{4\pi^4}\sum_{m=1}^{\infty}\frac{1}{n^2}\left[\ln\left(\frac{n\pi E_c}{B}\right)+\gamma\right] + \cdots \tag{E.2.22}$$

$$= -\frac{e^2B^2}{24\pi^2}\left[\ln\left(\frac{\pi E_c}{B}\right)+\gamma\right] + \frac{e^2B^2}{4\pi^4}\zeta'(2) + \cdots. \tag{E.2.23}$$

The ($n = 1$) term in Eq. (E.2.22) is the one obtained by Weisskopf Weisskopf (1936).

E.3. The Einstein-Euler-Heisenberg theory

Since the real part of the Euler-Heisenberg effective Lagrangian $(\Delta\mathcal{L}_{\rm eff}^{\rm cos})_{\mathcal{P}}$ of Eq. (E.2.10) is expressed in terms of Lorentz invariants (ε, β) or (S, P), the Euler-Heisenberg effective action in the curve space-time described by metric $g_{\mu\nu}$ can be written as

$$\mathcal{S}_{\rm EH} = \int d^4x\sqrt{-g}\mathcal{L}_{\rm EH}, \quad \mathcal{L}_{\rm EH} = [S + (\Delta\mathcal{L}_{\rm eff}^{\rm cos})_{\mathcal{P}}]\,. \tag{E.3.1}$$

The Einstein and Euler-Heisenberg action is then given by

$$\mathcal{S}_{\rm EEH} = -\frac{1}{16\pi G}\int d^4x\sqrt{-g}R + \mathcal{S}_{\rm EH}, \tag{E.3.2}$$

where R is the Ricci scalar.

The Einstein field equations are

$$G^{\mu\nu} \equiv R^{\mu\nu} - \frac{1}{2}g^{\mu\nu}R = 8\pi G T^{\mu\nu}, \tag{E.3.3}$$

where the energy-momentum tensor is

$$T^{\mu\nu} = \frac{2}{\sqrt{-g}}\frac{\delta\mathcal{S}_{\rm EH}}{\delta g_{\mu\nu}}. \tag{E.3.4}$$

The electromagnetic field equations and Bianchi identities are given by

$$\mathcal{D}_\mu P^{\nu\mu} = j^\nu, \quad \mathcal{D}_\mu \tilde{F}^{\mu\nu} = 0, \tag{E.3.5}$$

and the displacement fields $P^{\nu\mu}$, $D^i = P^{0i}$, and $H^i = -\epsilon^{ijk}P_{jk}$ are defined as

$$P^{\mu\nu} = \frac{\delta\mathcal{L}_{\rm EH}}{\delta F_{\mu\nu}}, \quad D^i = \frac{\delta\mathcal{L}_{\rm EH}}{\delta E_i}, \quad H^i = -\frac{\delta\mathcal{L}_{\rm EH}}{\delta B_i}. \tag{E.3.6}$$

Here, electromagnetic fields are treated as smooth varying fields over all space generated by external charge currents j^μ at infinity.

Using functional derivatives, we obtain

$$\begin{aligned} T^{\mu\nu} &= -g^{\mu\nu}\left[S + (\Delta\mathcal{L}_{\rm eff}^{\rm cos})_{\mathcal{P}}\right] + 2\left[\frac{\delta S}{\delta g_{\mu\nu}}\frac{\delta\mathcal{L}_{\rm EH}}{\delta S} + \frac{\delta P}{\delta g_{\mu\nu}}\frac{\delta\mathcal{L}_{\rm EH}}{\delta P}\right], \\ &= -g^{\mu\nu}\left[S + (\Delta\mathcal{L}_{\rm eff}^{\rm cos})_{\mathcal{P}}\right] + 2\left[(1+\mathcal{A}_S)\frac{\delta S}{\delta g_{\mu\nu}} + \mathcal{A}_P\frac{\delta P}{\delta g_{\mu\nu}}\right], \end{aligned} \tag{E.3.7}$$

where two invariants are defined as

$$\mathcal{A}_S \equiv \frac{\delta(\Delta\mathcal{L}_{\rm eff}^{\rm cos})_{\mathcal{P}}}{\delta S}; \quad \mathcal{A}_P \equiv \frac{\delta(\Delta\mathcal{L}_{\rm eff}^{\rm cos})_{\mathcal{P}}}{\delta P}. \tag{E.3.8}$$

It is straightforward to obtain

$$\frac{\delta S}{\delta g_{\mu\nu}} = \frac{1}{2}F^{\mu}{}_{\lambda}F^{\lambda\nu}, \quad \frac{\delta P}{\delta g_{\mu\nu}} = F^{\mu}{}_{\lambda}\tilde{F}^{\lambda\nu} = g^{\mu\nu}P, \tag{E.3.9}$$

and as a result, we rewrite Eq. (E.3.7) as

$$\begin{aligned} T^{\mu\nu} &= T_M^{\mu\nu} + g^{\mu\nu}\left[\mathcal{A}_P P - (\Delta\mathcal{L}_{\rm eff}^{\rm cos})_{\mathcal{P}}\right] + \mathcal{A}_S F^{\mu}{}_{\lambda}F^{\lambda\nu}, \\ &= T_M^{\mu\nu}(1+\mathcal{A}_S) + g^{\mu\nu}\left[\mathcal{A}_S S + \mathcal{A}_P P - (\Delta\mathcal{L}_{\rm eff}^{\rm cos})_{\mathcal{P}}\right], \end{aligned} \tag{E.3.10}$$

where $T_M^{\mu\nu} = -g^{\mu\nu}S + F^{\mu}{}_{\lambda}F^{\lambda\nu}$ is the energy-momentum tensor of the electromagnetic fields of the linear Maxwell theory. Equation (E.3.10) is in fact a general result, independent of the explicit form of nonlinear Lagrangian $(\Delta\mathcal{L}_{\rm eff}^{\rm cos})_{\mathcal{P}}$. Equations (E.3.1)-(E.3.10) in principle give a complete set of equations for Einstein and Euler-Heisenberg effective theory, together with total charge (Q), angular-momentum (L), and energy (M) conservations. In this chapter, adopting the Euler-Heisenberg effective Lagrangian (E.2.10), we explicitly calculate invariants $\mathcal{A}_S$ and $\mathcal{A}_P$ of Eq. (E.3.8) as well as the energy-momentum $T^{\mu\nu}$ of Eq. (E.3.10) in the following cases.

It is necessary to point out that in present chapter, we do not consider the couplings between photons and gravitons that are also induced by QED vacuum polarization effects at the level of one-fermion loop. Drummond and Hathrell obtained the photon effective action from the lowest term of one-loop vacuum polarization on a general curved background manifold; i.e., a graviton couples to two on-mass-shell photons through a fermionic loop Drummond and Hathrell (1980),

$$\begin{aligned} \mathcal{S}_{\rm DH} = -\frac{\alpha}{720\pi m_e^2}\int d^4x\sqrt{-g}\,\big(&5RF_{\mu\nu}F^{\mu\nu} - 26R_{\mu\nu}F^{\mu\sigma}F_{\sigma}^{\nu} \\ &+2R_{\mu\nu\sigma\tau}F^{\mu\nu}F^{\sigma\tau} + 24\mathcal{D}_{\mu}F^{\mu\nu}\mathcal{D}_{\sigma}F_{\nu}^{\sigma}\big). \end{aligned} \tag{E.3.11}$$

Further studies of one-loop effective action (E.3.11) were made based on the approach of the heat-kernel or "inverse mass" expansion Gilkey (1975); Bastianelli et al. (2000), the approach of the so-called "derivative expansion" Barvinsky and Vilkovisky (1985, 1990a,b); Gusev (2009), and the consideration of the one-loop one particle irreducible of one graviton interacting with any number of photons Bastianelli et al. (2009). This effective action (E.3.11) was used to study the modified photon dispersion relation by a generic gravitational background Drummond and Hathrell (1980) and the possible consequences Latorre et al. (1995); Dittrich and Gies (1998);

Shore (1996); Hollowood and Shore (2007, 2008b,a).

At the level of one-loop quantum corrections of the QED theory in the presence of gravitational field, the effective Lagrangian (E.3.11) should be considered as an addition to the Euler and Heisenberg effective Lagrangian (E.2.15) in the weak-field limit. In this chapter, we try to quantitatively study the QED corrections in spherically symmetric black holes with mass M and charge Q. In this case, the corrections from the Euler and Heisenberg effective Lagrangian (E.2.15) must be much larger than the one from the effective Lagrangian (E.3.11). Studying the discussion and result of Ref. Drummond and Hathrell (1980) for spherical symmetric black holes, we approximately estimate the ratio of Eqs. (E.2.15) and (E.3.11) around the horizon of black holes with mass M and charge Q. As a result, this ratio is $\sim 10^{-2}\left(\frac{Q}{M\sqrt{G}}\right)^2 \frac{\alpha}{Gm_e^2} \gg 1$. It is not surprising that the electromagnetic coupling $e \sim 1/\sqrt{137}$ is much larger than the effective gravitational counterpart $Gm_e^2 \sim 10^{-45}$. Besides, it is expected that calculations involving both the Euler-Heisenberg effective Lagrangian (E.2.15) and Eq. (E.3.11) are much more complex and tedious. Nevertheless, it is interesting to investigate the effect of the photon-graviton amplitudes on black hole physics. In this chapter, for the sake of simplicity, we first consider only the Einstein-Euler-Heisenberg action (E.3.2) as a leading contribution in order to gain some physical insight into the QED corrections in black hole physics.

E.3.1. $\mathbf{B} = 0, \mathbf{E} \neq 0$ or $\mathbf{E} = 0, \mathbf{B} \neq 0$

We consider the case of $\mathbf{B} = 0$ and $\mathbf{E} \neq 0$, namely, $\beta = P = 0$, $\varepsilon = E = |\mathbf{E}|$, and $S = E^2/2$. $\mathcal{A}_P = 0$ and the effective Lagrangian Eq. (E.2.10) becomes

$$(\Delta\mathcal{L}_{\text{eff}}^{\cos})_{\mathcal{P}} = -\frac{e^2E^2}{4\pi^4}\sum_{n=1}^{\infty}\frac{1}{n^2}J(n\pi E_c/E). \tag{E.3.12}$$

Using

$$\mathcal{P}\int_0^\infty ds\frac{e^{-s}}{(s^2-z^2)} = -\frac{1}{2z}\Big[e^{-z}\text{Ei}(z) - e^{z}\text{Ei}(-z)\Big], \tag{E.3.13}$$

we calculate

$$\frac{dJ(z)}{dz^2} = \mathcal{P}\int_0^\infty ds\frac{se^{-s}}{(s^2-z^2)^2} = \frac{1}{2z^2} - \mathcal{P}\int_0^\infty ds\frac{e^{-s}}{(s^2-z^2)} \tag{E.3.14}$$

and obtain

$$\mathcal{A}_S = -\frac{e^2}{2\pi^4}\sum_{n=1}^{\infty}\frac{1}{n^2}J(n\pi E_c/E) \\ -\frac{e^2}{4\pi^2}\zeta(2)+\frac{e^2}{4\pi}\frac{E_c}{E}\sum_{n=1}^{\infty}\frac{1}{n}\tilde{J}(n\pi E_c/E), \tag{E.3.15}$$

where

$$\tilde{J}(z) = e^{-z}\mathrm{Ei}(z) - e^{z}\mathrm{Ei}(-z). \tag{E.3.16}$$

Substituting these quantities into Eq. (E.3.10), we obtain the expression of the energy-momentum tensor $T^{\mu\nu}(\varepsilon)$. In the case of $\mathbf{E} = 0$ and $\mathbf{B} \neq 0$, the energy-momentum tensor $T^{\mu\nu}(\beta)$ can be straightforwardly obtained from $T^{\mu\nu}(\varepsilon)$ by the discrete duality transformation $\varepsilon \to i\beta$, i.e., $|\mathbf{E}| \to i|\mathbf{B}|$. In principle, using the complete Euler-Heisenberg effective Lagrangian $(\Delta\mathcal{L}^{\cos}_{\mathrm{eff}})_{\mathcal{P}}$ (E.2.10) for arbitrary electromagnetic fields $\mathbf{E}$ and $\mathbf{B}$, one can obtain the energy-momentum tensor $T^{\mu\nu}(\varepsilon,\beta)$ of Eq. (E.3.10). For the reason of practical calculations, we consider the cases of weak and strong fields.

E.3.2. Weak- and strong-field cases

In the weak-field case, using Eq. (E.2.15) and calculating Eqs. (E.3.7)-(E.3.10), we obtain

$$\mathcal{A}_S = \frac{2\alpha^2}{45m_e^4}(8S)+\frac{64\pi\alpha^3}{315m_e^8}(48S^2+26P^2)+\cdots, \\ \mathcal{A}_P = \frac{2\alpha^2}{45m_e^4}(14P)+\frac{64\pi\alpha^3}{315m_e^8}(52SP)+\cdots, \tag{E.3.17}$$

and

$$T^{\mu\nu} = T^{\mu\nu}_M\left[1+8\left(\frac{2\alpha^2}{45m_e^4}\right)S\right]+g^{\mu\nu}\left(\frac{2\alpha^2}{45m_e^4}\right)\left[4S^2+7P^2\right]+\cdots, \tag{E.3.18}$$

up to the leading order.

In strong-field case $\varepsilon/E_c \gg 1$ and $\beta/E_c \gg 1$ using Eq. (E.2.17) and calculating Eqs. (E.3.7)-(E.3.10), we obtain

$$\mathcal{A}_S = \frac{1}{2(2\pi)^2}\frac{2}{\varepsilon^2+\beta^2}\sum_{n,m=-\infty}^{\infty}\frac{1}{(\tau_m^2+\tau_n^2)^2}\Big\{\bar{\delta}_{n0}\Big[(\tau_n^2-\tau_m^2)\ln(\tau_n m_e^2)-\frac{1}{2}(\tau_m^2+\tau_n^2)\Big] \\ -\bar{\delta}_{m0}\Big[(\tau_n^2-\tau_m^2)\ln(\tau_m m_e^2)+\frac{1}{2}(\tau_m^2+\tau_n^2)\Big]\Big\}+\cdots \tag{E.3.19}$$

and

$$\mathcal{A}_P = \frac{1}{2(2\pi)^2}\frac{2\varepsilon\beta}{\varepsilon^2+\beta^2}\sum_{n,m=-\infty}^{\infty}\frac{1}{(\tau_m^2+\tau_n^2)^2}\Big\{\bar{\delta}_{n0}\Big[\left(\frac{\tau_n^2}{\varepsilon^2}+\frac{\tau_m^2}{\beta^2}\right)\ln(\tau_n m_e^2)-\frac{1}{2}\frac{(\tau_m^2+\tau_n^2)}{\varepsilon^2}\Big]$$
$$-\bar{\delta}_{m0}\Big[\left(\frac{\tau_n^2}{\varepsilon^2}+\frac{\tau_m^2}{\beta^2}\right)\ln(\tau_m m_e^2)-\frac{1}{2}\frac{(\tau_m^2+\tau_n^2)}{\beta^2}\Big]\Big\}+\cdots. \tag{E.3.20}$$

From Eq. (E.2.20) for $\mathbf{B}=0$ and a strong electric field, we obtain

$$\mathcal{A}_S = \frac{e^2}{24\pi^2}\left[2\ln\left(\frac{\pi E_c}{E}\right)+2\gamma-1\right]-\frac{e^2}{2\pi^4}\zeta'(2)+\cdots, \tag{E.3.21}$$

and the energy-momentum tensor $T^{\mu\nu}$ of Eq. (E.3.10),

$$T^{\mu\nu} = T_M^{\mu\nu}\left\{1+\frac{e^2}{24\pi^2}\left[2\ln\left(\frac{\pi E_c}{E}\right)+2\gamma-1\right]-\frac{e^2}{2\pi^4}\zeta'(2)\right\}-g^{\mu\nu}\frac{e^2E^2}{48\pi^2}+\cdots. \tag{E.3.22}$$

Analogously, from Eq. (E.2.23) for $\mathbf{E}=0$ and a strong magnetic field, we obtain

$$\mathcal{A}_S = \frac{e^2}{24\pi^2}\left[2\ln\left(\frac{\pi E_c}{B}\right)+2\gamma-1\right]-\frac{e^2}{2\pi^4}\zeta'(2)+\cdots, \tag{E.3.23}$$

and the energy-momentum tensor

$$T^{\mu\nu} = T_M^{\mu\nu}\left\{1+\frac{e^2}{24\pi^2}\left[2\ln\left(\frac{\pi E_c}{B}\right)+2\gamma-1\right]-\frac{e^2}{2\pi^4}\zeta'(2)\right\}+g^{\mu\nu}\frac{e^2B^2}{48\pi^2}+\cdots. \tag{E.3.24}$$

In the following sections, using the energy-momentum tensors $T^{\mu\nu}$ of Eqs. (E.3.18), (E.3.22), and (E.3.24), we try to study the solutions of the Einstein-Euler-Heisenberg theory for nonrotating (spherically symmetric), electrically or magnetically charged black holes.

E.4. Electrically charged black holes

In this section, we study a nonrotating (spherically symmetric) electrically charged black hole. In this spherical symmetry case, the gauge potential is

$$A_\mu(x) = [A_0(r), 0, 0, 0], \tag{E.4.1}$$

corresponding to the electric field $E(r) = -A_0'(r) = -\partial A_0(r)/\partial r$ in the radial direction, and the metric field is assumed to be

$$ds^2 = f(r)dt^2 - f(r)^{-1}dr^2 - r^2 d\Omega; \quad f(r) \equiv 1 - 2Gm(r)/r. \tag{E.4.2}$$

The metric function $f(r)$ and the electric field $E(r)$ fulfill the Einstein equations (E.3.3) and electromagnetic field equations (E.3.5) and their asymptotically flat solutions at $r \gg 1$,

$$A_0(r) \to -\frac{Q}{4\pi r}, \quad E(r) \to \frac{Q}{4\pi r^2}, \quad \frac{Gm(r)}{r} \to \frac{GM}{r} \tag{E.4.3}$$

satisfy the Gauss law, where Q and M are the black hole electric charge and mass seen at infinity.

In order to find the solution near to the horizon of the black hole by taking into account the QED effects, we approximately adopt the Euler-Heisenberg effective Lagrangian for constant fields that leads to the energy-momentum tensor (E.3.18) or (E.3.22) for $\mathbf{B} = 0$. This approximation is based on the assumption that the macroscopic electric field $E(r)$ is approximated as a constant field E over the microscopic scale of the electron Compton lengths. When the electric field of charged black holes are overcritical, electron-positron pair productions take place and the electric field is screened down to its critical value E_c (see Refs. Damour and Ruffini (1975); Preparata et al. (1998, 2003); Ruffini et al. (2008)). In this chapter, we study the QED effects on electrically charged black holes with spherical symmetry, whose electric field is much smaller than the critical field E_c. In this weak electric field case using Eq. (E.3.18) we obtain the energy-momentum tensor

$$T^{\mu\nu} = T_M^{\mu\nu}\left(1 + \frac{2\alpha E^2}{45\pi E_c^2}\right) + g^{\mu\nu}\frac{\alpha E^4}{90\pi E_c^2} + \cdots. \tag{E.4.4}$$

As a result, the (0-0) component of Einstein equations is

$$\frac{2m'(r)}{r^2} = 4\pi\left[E^2(r) + \frac{\alpha}{15\pi}E^4(r)/E_c^2\right], \tag{E.4.5}$$

which relates to the energy conservation. Analogously, using Eqs. (E.3.5) and (E.3.6) and the metric of Eq. (E.4.2), we obtain the field equation up to the leading order,

$$\frac{2\alpha}{45\pi}E^3(r)/E_c^2 + E(r) = \frac{Q}{4\pi r^2}, \tag{E.4.6}$$

which is the zero component of $\mathcal{D}_\mu P^{\nu\mu} = j^\nu$ of Eq. (E.3.5) in the spherical symmetry case. This equation relates to the total charge conservation.

A similar case was studied in Ref. Yajima and Tamaki (2001), in which, however, the effective Lagrangian [the first term in Eq. (E.2.15)] was considered as a low-energy limit of the Born-Infeld theory; the coefficients of the S^2 and P^2 terms in Eq. (E.2.15) are treated as free parameters, so as to either numerically or analytically study the properties of spherically symmetric black hole solutions in the Einstein-Euler-Heisenberg system. In the following, in order to analytically study the QED effects on the black hole solution, we use the Euler-Heisenberg effective Lagrangian (E.2.15) and find the black hole solution by a series expansion in powers of α. Introducing $\overline{E}(r) \equiv E(r)/E_c$, up to the first order of α, the solution to Eq. (E.4.6) is approximately given by

$$\overline{E}(r) = E_Q \left(1 - \frac{2\alpha}{45\pi} E_Q^2 + \cdots\right), \tag{E.4.7}$$

where $E_Q \equiv E_Q(r) \equiv Q/(4\pi r^2 E_c)$. We find that the electric field $E(r)$ is smaller than $Q/4\pi r^2$, due to the charge screening effect of the vacuum polarization. Substituting this solution (E.4.7) into the Einstein equation (E.4.5), we obtain the integration

$$m(r) = M - \int_r^\infty 4\pi r^2 dr \frac{1}{2}\left[E^2(r) + \frac{\alpha}{15\pi} E^4(r)/E_c^2\right]. \tag{E.4.8}$$

This equation clearly shows that the energy-mass function $m(r)$ of Eq. (E.4.2) is the total gravitational mass M (attractive) "screened down" by the electromagnetic energy (repulsive). In the Maxwell theory $(\Delta\mathcal{L}_{\rm eff}^{\cos})_{\mathcal{P}} = 0$ and $E(r) = Q/(4\pi r^2)$, we obtain the Reissner-Nordström solution $m(r) = M - Q^2/8\pi r$. In the Euler-Heisenberg system, it is not proper to make the integration in Eq. (E.4.8), since the integrand comes from the Euler-Heisenberg effective Lagrangian, which is valid only for constant fields. In order to gain some physical insight into the energy-mass function (E.4.8), we integrate Eq. (E.4.8) to the leading order of α,

$$m(r) \approx M - \frac{Q^2}{8\pi r}\left[1 - \frac{\alpha}{225\pi}\frac{1}{(4\pi)^2}\frac{Q^2}{r^4}\frac{1}{E_c^2}\right] = M - \frac{Q^2}{8\pi r}\left[1 - \frac{\alpha}{225\pi}E_Q^2\right], \tag{E.4.9}$$

which shows the QED correction to the Reissner-Nordström solution. Due to the QED vacuum polarization effect, the black hole charge Q is screened

$$Q \to Q\left[1 - \frac{\alpha}{225\pi}E_Q^2\right]^{1/2}. \tag{E.4.10}$$

As a consequence, the electrostatic energy of Eq. (E.4.9) is smaller than $Q^2/(8\pi r)$ in the Reissner-Nordström solution.

Moreover, we study the QED correction to the black hole horizon. For this pur-

pose, we define the horizon radius $r_{_H}$ at which the function $f(r)$ of Eq. (E.4.2) vanishes, i.e., $f(r_{_H}) = 0$, leading to

$$\frac{Gm(r_H)}{r_{_H}} = \frac{1}{2}. \tag{E.4.11}$$

Using the energy-mass function $m(r)$ of Eq. (E.4.9), we obtain

$$\frac{GM}{r_{_H}} - \frac{GQ^2}{8\pi r_{_H}^2}\left[1 - \frac{\alpha}{225\pi}E_{Qh}^2\right] = \frac{1}{2}, \tag{E.4.12}$$

where $E_{Qh} \equiv E_Q(r_{_H})$. Up to the leading order of α, we obtain

$$r_{_{H+}} = GM + \sqrt{G^2M^2 - \frac{GQ^2}{4\pi}\left[1 - \frac{\alpha}{225\pi}E_{Q+}^2\right]}, \tag{E.4.13}$$

$$r_{_{H-}} = GM - \sqrt{G^2M^2 - \frac{GQ^2}{4\pi}\left[1 - \frac{\alpha}{225\pi}E_{Q-}^2\right]}, \tag{E.4.14}$$

where $E_{Q+} \equiv E_Q(r_{_{H+}})$ and $E_{Q-} \equiv E_Q(r_{_{H-}})$. Equation (E.4.13) shows that the black hole horizon radius $r_{_{H+}}$ becomes larger than the Reissner-Nordström one r_+ given by Eq. (E.4.13) for setting $\alpha = 0$. The black hole horizon area $4\pi r_{_{H+}}^2$ becomes larger than the Reissner-Nordström one $4\pi r_+^2$ given by Eq. (E.4.13) for setting $\alpha = 0$. This is again due to the black hole charge Q screened by the QED vacuum polarization (E.4.10).

In the Reissner-Nordström solution, the extreme black hole solution is given by $r_+ = r_-$ or $4\pi GM^2 = Q^2$. In our case, this is given by $r_{_{H+}} = r_{_{H-}} = r_{_H}$ yielding

$$G^2M^2 - \frac{GQ^2}{4\pi}\left[1 - \frac{\alpha}{225\pi}E_{Qh}^2\right] = 0. \tag{E.4.15}$$

From Eqs. (E.4.13) and (E.4.14), we obtain

$$\begin{aligned} 4\pi r_{_H}^2 &= 4\pi G^2M^2 = GQ^2\left[1 - \frac{\alpha}{225\pi}E_{Qh}^2\right] \\ &= GQ^2\left[1 - \frac{\alpha}{225\pi}\frac{1}{G^2Q^2E_c^2}\right], \end{aligned} \tag{E.4.16}$$

$$r_{_{H_\pm}} \approx Q\left[1 - \frac{\alpha}{225\pi}E_{Qh}^2\right]^{1/2} = Q\left[1 - \frac{\alpha}{225\pi}\frac{1}{(E_cQ)^2}\right]^{1/2}. \tag{E.4.17}$$

In Eq. (E.4.17) we adopt $G/4\pi = 1$. Due to the QED correction, the condition of extremely electrically charged black holes with spherical symmetry changes from

$M = Q/4\pi$ to

$$M = \frac{Q}{4\pi}\left[1 - \frac{\alpha}{225\pi}\frac{1}{(E_c Q)^2}\right]^{1/2}. \tag{E.4.18}$$

This implies that for a given M, the black holes are allowed to carry more charge Q than the Reissner-Nordström case. These results show that when the black hole mass M is fixed, the horizon area and radius of the extremely electrically charged black hole are the same as the extreme Reissner-Nordström one. However, when the black hole charge Q is fixed, the black hole horizon area and radius are smaller than those of the extreme Reissner-Nordström black hole. The reason is that the charge screening effect decreases the electrostatic energy; hence, this leads to a smaller mass M for the extreme black hole.

Now we turn to the maximal energy extractable from a black hole. As pointed out in Ref. Christodoulou and Ruffini (1971), the surface area S_a of the black hole horizon is related to the irreducible mass M_{ir} of the black hole

$$S_a = 16\pi G^2 M_{ir}^2 = 4\pi r_{_{H+}}^2, \tag{E.4.19}$$

where $r_{_{H+}}$ is given by Eq. (E.4.13). The surface area of the black hole horizon cannot be decreased by classical processes Christodoulou and Ruffini (1971); Christodoulou (1970); Hawking (1971). Any transformation of the black hole which leaves fixed the irreducible mass is called reversible Christodoulou and Ruffini (1971); Christodoulou (1970). Any transformation of the black hole which increases its irreducible mass, for instance, the capture of a particle with nonzero radial momentum at the horizon, is called irreversible. In irreversible transformations there is always some kinetic energy that is irretrievably lost behind the horizon. Note that transformations which arbitrarily close to reversible ones are the most efficient transformations for extracting energy from a black hole Christodoulou and Ruffini (1971); Christodoulou (1970). Following the same argument presented in Ref. Christodoulou and Ruffini (1971), and including the leading-order QED correction (E.4.9), we obtain the Christodoulou-Ruffini mass formula

$$M = M_{ir} + \frac{Q^2}{16\pi G M_{ir}}\left[1 - \frac{\alpha}{225\pi}E_{Q+}^2\right], \tag{E.4.20}$$

where the electrostatic energy of the black hole is reduced for the reason that the black hole charge is screened down by the QED vacuum polarization effect (E.4.10).

The properties of the surface area S_a of the black hole horizon and irreducible mass M_{ir} can also been understood from the concepts of information theory Bekenstein (1973). The black hole entropy S_{en} is introduced as the measure of information about

a black hole interior which is inaccessible to an exterior observer and is proportional to the surface area S_a of the black hole horizon Bekenstein (1973)

$$S_{en} = S_a/4 = \pi r_{H+}^2. \tag{E.4.21}$$

The physical content of the concept of the black hole entropy derives from the generalized second law of thermodynamics: when common entropy in the black hole exterior plus the black hole entropy never decreases Bekenstein (1973). In the Einstein-Euler-Heisenberg theory, the black hole irreducible mass of Eq. (E.4.19) and entropy of Eq. (E.4.21) with the QED correction are determined by the horizon radius r_{H+} of Eq. (E.4.13) for charged black holes and Eq. (E.4.16) for extreme black holes.

Now we consider the physical interpretation of the electromagnetic term in Eq. (E.4.20). This term represents the maximal energy extractable from a black hole, which can be obtained by evaluating the conserved Killing integral Ruffini et al. (2010); Ruffini and Vitagliano (2002)

$$\int_{\Sigma_t^+} \xi_+^\mu T_{\mu\nu} d\Sigma^\nu = 4\pi \int_{r_{H+}}^{\infty} r^2 T_0^0 dr, \tag{E.4.22}$$

where Σ_t^+ is the spacelike hypersurface in the space-time region that is outside the horizon $r > r_{H+}$ described by the equation $t =$ constant, with $d\Sigma^\nu$ as its surface element vector. ξ_+^μ is the static Killing vector field. This electromagnetic term in Eq. (E.4.20) is the total energy of the electromagnetic field and includes its own gravitational binding energy. Using the energy-momentum tensor of Eq. (E.4.4) and weak-field solution (E.4.7), we obtain the maximal energy extractable from an electrically charged black hole

$$\varepsilon_{ex} = \frac{Q^2}{8\pi r_{H+}} \left[1 - \frac{\alpha}{225\pi} E_{Q+}^2\right]. \tag{E.4.23}$$

This shows that the black hole maximal extractable energy decreases in comparison with the Reissner-Nordström case ($Q^2/8\pi r_+$). This can be explained by the following: (i) the charge screening effect decreases the electrostatic energy; (ii) the black hole horizon radius r_{H+} of Eq. (E.4.13) increases, leading to the decrease of the maximally extractable energy, because the most efficient transformations that extract energy from a black hole occur near the horizon. For the extremely electrically charged black hole, the maximally extractable energy is the same as that in the Reissner-Nordström case, when the black hole mass M is fixed; however, it becomes smaller than the Reissner-Nordström one when the black hole electric charge Q is fixed.

E.5. Magnetically charged black holes

Now we turn to study the Einstein-Euler-Heisenberg theory (E.3.18) and (E.3.24) in the presence of the magnetic field **B**. As shown by Eq. (E.2.6), the magnetic field **B** does not contribute to the pair-production rate so that the process of the electron-positron pair production does not occur for a strong magnetic field **B**. For this reason, we consider black holes with strong magnetic fields. The conventional black hole with electric and magnetic fields is the rotating charged black hole of the Kerr-Newman black hole Newman et al. (1965). However, the solution to a rotating charged black hole in the Einstein-Euler-Heisenberg theory is rather complicated, and we do not consider it in this work. For the sake of simplicity, we study the nonrotating magnetically charged black hole with spherical symmetry in order to investigate the QED corrections in the presence of the magnetic field **B** in the Einstein-Euler-Heisenberg theory.

For a nonrotating magnetically charged black hole with magnetic charge Q_m, the tensor $F_{\mu\nu}$ compatible with spherical symmetry can involve only a radial magnetic field $F_{23} = -F_{32}$. In the Einstein-Maxwell theory, the field equations (E.3.5) give (see, e.g., Refs. Hawking and Ross (1995); Gibbons and Rasheed (1995))

$$F_{23} = \frac{Q_m \sin\theta}{4\pi}, \tag{E.5.1}$$

and the gauge potential will be (see, e.g., Refs. Hawking and Ross (1995))

$$A_\mu(x) = [0, 0, 0, Q_m(1 - \cos\theta)/4\pi]. \tag{E.5.2}$$

The metric is similar to the one of nonrotating electrically charged black holes,

$$ds^2 = f(r)dt^2 - f(r)^{-1}dr^2 - r^2 d\Omega, \quad f(r) \equiv 1 - 2Gm(r)/r, \tag{E.5.3}$$

where $m(r)$ is the mass-energy function. In the Einstein-Maxwell theory, the metric function $f(r)$ of magnetically charged black holes with spherical symmetry is given by (see, e.g., Refs. Hawking and Ross (1995))

$$f(r) = 1 - \frac{2GM}{r} + \frac{GQ_m^2}{4\pi r^2}, \tag{E.5.4}$$

where M is the black hole mass seen at infinity.

E.5.1. Weak magnetic field case

Using Eq. (E.3.18), we obtain the energy-momentum tensor for the weak magnetic field B case,

$$T^{\mu\nu} = T^{\mu\nu}_M \left(1 - \frac{2\alpha B^2}{45\pi E_c^2}\right) + g^{\mu\nu}\frac{\alpha B^4}{90\pi E_c^2} + \cdots . \tag{E.5.5}$$

Similar to the analysis of electrically charged black holes with spherical symmetry, we obtain the (0-0) component of Einstein equations,

$$\frac{2m'(r)}{r^2} = 4\pi\left[B^2(r) - \frac{\alpha}{45\pi}B^4(r)/E_c^2\right]. \tag{E.5.6}$$

For the magnetically charged black hole with spherical symmetry, only a radial magnetic field is present. The field equations (E.3.5) give $B(r) = Q_m/(4\pi r^2)$ (see, e.g., Refs. Yajima and Tamaki (2001); Bronnikov (2001)). Substituting $B(r)$ into the Einstein equation (E.5.6), we obtain the mass-energy function

$$m(r) = M - \int_r^\infty 4\pi r^2 dr \frac{1}{2}\left[B^2(r) - \frac{\alpha}{45\pi}B^4(r)/E_c^2\right]. \tag{E.5.7}$$

Neglecting the QED correction of the Euler-Heisenberg effective Lagrangian, Eq. (E.5.7) gives $m(r) = M - Q_m^2/8\pi r$, which is the solution of the magnetically charged Reissner-Nordström black hole in the Einstein-Maxwell theory. Making the integration in Eq. (E.5.7), one obtains Yajima and Tamaki (2001)

$$m(r) = M - \frac{Q_m^2}{8\pi r}\left[1 - \frac{\alpha}{225\pi}\frac{1}{(4\pi)^2}\frac{Q_m^2}{r^4}\frac{1}{E_c^2}\right] = M - \frac{Q_m^2}{8\pi r}\left[1 - \frac{\alpha}{225\pi}B_{\rm Q}^2\right], \tag{E.5.8}$$

where $B_Q \equiv B_Q(r) \equiv Q_m/(4\pi r^2 E_c)$. As shown in Eq. (E.5.8), taking into account the QED vacuum polarization effect, the total magnetostatic energy is smaller than $Q_m^2/8\pi r$ in the magnetically charged Reissner-Nordström case. This can be understood as follows. In the magnetic field **B** of the black holes, the vacuum polarization effect results in a positive magnetic polarization **M**. Then the magnetic **H** field defined $\mathbf{B} = \mathbf{H} + \mathbf{M}$ is smaller than the magnetic field **B**. The magnetostatic energy density $\varepsilon_{EM} \propto \mathbf{B}\cdot\mathbf{H}$ decreases. This shows that in weak magnetic fields, the vacuum polarization effect exhibits the paramagnetic property.

Compared to the result of the electrically charged black hole in the first order of α, Eqs. (E.4.9) and (E.5.8) have the same expression. One can obtain Eq. (E.5.8) by simply replacing E_Q in Eq. (E.4.9) by B_Q, namely, replacing Q by Q_m because of the duality symmetry (see, e.g., Ref. Hawking and Ross (1995)). Similar to the analysis of electric charged black holes, we obtain the horizon radii r_{H_+} and r_{H_-} of

the magnetically charged black hole, up to the leading order of α,

$$r_{H+} = GM + \sqrt{G^2M^2 - \frac{GQ_m^2}{4\pi}\left[1 - \frac{\alpha}{225\pi}B_{Q+}^2\right]}, \tag{E.5.9}$$

$$r_{H-} = GM - \sqrt{G^2M^2 - \frac{GQ_m^2}{4\pi}\left[1 - \frac{\alpha}{225\pi}B_{Q-}^2\right]}, \tag{E.5.10}$$

where $B_{Q+} \equiv B_Q(r_{H+})$ and $B_{Q-} \equiv B_Q(r_{H-})$. The result (E.5.9) shows that the black hole horizon radius r_{H+} increases in comparison with the magnetically charged Reissner-Nordström one r_+. This is again due to the paramagnetic effect of the vacuum polarization that decreases the magnetostatic energy of the black hole.

Now we turn to the extreme black hole ($r_{H+} = r_{H-} = r_H$). Similarly, we have

$$G^2M^2 - \frac{GQ_m^2}{4\pi}\left[1 - \frac{\alpha}{225\pi}B_{Qh}^2\right] = 0, \tag{E.5.11}$$

where $B_{Qh} \equiv B_Q(r_H)$, and we obtain the black hole horizon area and radius

$$4\pi r_H^2 = 4\pi G^2M^2 = GQ_m^2\left[1 - \frac{\alpha}{225\pi}B_{Qh}^2\right] = GQ_m^2\left[1 - \frac{\alpha}{225\pi}\frac{1}{G^2Q_m^2E_c^2}\right], \tag{E.5.12}$$

$$r_H \approx Q_m\left[1 - \frac{\alpha}{225\pi}B_{Qh}^2\right]^{1/2} = Q_m\left[1 - \frac{\alpha}{225\pi}\frac{1}{(E_cQ_m)^2}\right]^{1/2}. \tag{E.5.13}$$

In the second line, we adopt $G/4\pi = 1$. The QED correction changes the condition of extremely magnetically charged black holes with spherical symmetry from $M = Q_m/4\pi$ to

$$M = \frac{Q_m}{4\pi}\left[1 - \frac{\alpha}{225\pi}\frac{1}{(E_cQ_m)^2}\right]^{1/2}. \tag{E.5.14}$$

The properties of the horizon area and radius of the extremely magnetically charged black hole are the same as their counterparts in the extremely electrically charged black hole, given by the duality transformation $Q \leftrightarrow Q_m$.

Following the same argument presented in Ref. Christodoulou and Ruffini (1971), we obtain the Christodoulou-Ruffini mass formula

$$M = M_{ir} + \frac{Q_m^2}{16\pi GM_{ir}}\left[1 - \frac{\alpha}{225\pi}B_{Q+}^2\right] \tag{E.5.15}$$

for magnetically charged black holes with spherical symmetry in the Einstein-Euler-Heisenberg theory. One is able to obtain the irreducible mass M_{ir} by substituting Eq. (E.5.9) into Eq. (E.4.19), and the black hole entropy S_{en} by substituting Eq. (E.5.9)

into Eq. (E.4.21). The irreducible mass M_{ir} and the black hole entropy S_{en} in terms of black hole horizon radius r_{H+} Eq. (E.5.9) have the same paramagnetic property in the presence of the QED vacuum polarization effect, as already discussed.

As shown in Eq. (E.5.15), the maximal energy extractable from a magnetically charged black hole is

$$\varepsilon_{ex} = \frac{Q_m^2}{8\pi r_{H+}} \left[1 - \frac{\alpha}{225\pi} B_{Q+}^2\right], \tag{E.5.16}$$

where r_{H+} is given by Eq. (E.5.9). The result shows that the maximal energy extractable from a magnetically charged black hole is smaller than $\frac{Q_m^2}{8\pi r_+}$ of the magnetically charged Reissner-Nordström black hole. The reasons are the following: (i) the vacuum polarization effect decreases the magnetostatic energy; (ii) the black hole horizon radius r_{H+} of Eq. (E.5.9) increases, therefore the maximally extractable energy decreases. The maximal energy extractable from an extremely magnetically charged black hole is the same as that from an extremely magnetically charged Reissner-Nordström black hole when the black hole mass M is fixed, while it decreases when the black hole magnetic charge Q_m is fixed, as we have already discussed at the end of Sec. E.4 for the case of the extremely electrically charged black hole.

E.5.2. Strong magnetic field case

In this section, we study the magnetically charged black holes with a strong magnetic field $B(r)$. From Eq. (E.3.24), we obtain the energy-momentum tensor of the magnetically charged black hole with spherical symmetry in the strong magnetic field case. Analogous to the weak magnetic field case of magnetically charged black holes with spherical symmetry, we obtain the (0-0) component of Einstein equations

$$\frac{2m'(r)}{4\pi r^2} = 4\pi \left\{ B^2(r) + \frac{e^2B^2}{12\pi^2} \left[\ln\left(\frac{\pi E_c}{B}\right) + \gamma - \frac{6}{\pi^2}\zeta'(2)\right]\right\}, \tag{E.5.17}$$

and the field equations (E.3.5) give $B(r) = Q_m/(4\pi r^2)$. Substituting this magnetic field $B(r)$ into the Einstein equation (E.5.17), we obtain

$$m(r) \approx M - \int_r^\infty 4\pi r^2 dr \frac{1}{2}\left\{ B^2 + \frac{e^2B^2}{12\pi^2} \left[\ln\left(\frac{\pi E_c}{B}\right) + \gamma - \frac{6}{\pi^2}\zeta'(2)\right]\right\} \tag{E.5.18}$$

$$\approx M - \frac{Q_m^2}{8\pi r}\left\{1 + \frac{\alpha}{3\pi}\left[\ln\left(\frac{\pi}{B_Q}\right) + \gamma + 2 - \frac{6}{\pi^2}\zeta'(2)\right]\right\}. \tag{E.5.19}$$

This result is valid for $B \gg E_c$, for which the value of $\ln(\pi/B_Q) + \gamma + 2 - \frac{6}{\pi^2}\zeta'(2)$ is negative. As a result, Eq. (E.5.19) shows that the total magnetostatic energy in

the presence of the vacuum polarization is smaller than $Q_m^2/8\pi r$ of the magnetically charged Reissner-Nordström black hole. Similar to the weak-field case, this is again due to the paramagnetic effect of the vacuum polarization that decreases the magnetostatic energy of black holes. In the strong magnetic field case, the QED vacuum polarization effect is much larger than the result (E.5.8) in the weak-field case, where the QED correction term in Eq. (E.5.8) is small for the smallness of $\alpha/(225\pi)$ and B_Q^2. This result (E.5.19) shows a significant QED effect of the vacuum polarization on the energy of magnetically charged black holes in the strong magnetic field case.

Now we turn to the study of the black hole horizon radius and area in the strong magnetic field case. Using the condition $f(r_{_H}) = 0$, we obtain the horizon radii $r_{_{H+}}$ and $r_{_{H-}}$ up to the leading order of α,

$$r_{_{H+}} = GM + \sqrt{G^2M^2 - \frac{GQ_m^2}{4\pi}\left[1 + \frac{\alpha}{3\pi}\mathcal{K}_{NR+}\right]}, \tag{E.5.20}$$

$$r_{_{H-}} = GM - \sqrt{G^2M^2 - \frac{GQ_m^2}{4\pi}\left[1 + \frac{\alpha}{3\pi}\mathcal{K}_{NR-}\right]}, \tag{E.5.21}$$

where

$$\mathcal{K}_{NR+} = \ln\left(\frac{\pi}{B_{Q+}}\right) + \gamma + 2 - \frac{6}{\pi^2}\zeta'(2), \tag{E.5.22}$$

$$\mathcal{K}_{NR-} = \ln\left(\frac{\pi}{B_{Q-}}\right) + \gamma + 2 - \frac{6}{\pi^2}\zeta'(2). \tag{E.5.23}$$

Equation (E.5.20) shows that the horizon radius $r_{_{H+}}$ increases in comparison with the magnetically charged Reissner-Nordström one r_+. This is again due to the paramagnetic effect of the vacuum polarization that decreases the magnetostatic contribution to the total energy of black holes.

For the case of the extreme black hole ($r_{_{H+}} = r_{_{H-}} = r_{_H}$), we have

$$G^2M^2 - \frac{GQ_m^2}{4\pi}\left[1 + \frac{\alpha}{3\pi}\mathcal{K}_{NR}\right] = 0, \tag{E.5.24}$$

where

$$\mathcal{K}_{NR} = \ln\left(\frac{\pi}{B_{Qh}}\right) + \gamma + 2 - \frac{6}{\pi^2}\zeta'(2). \tag{E.5.25}$$

As a result, we obtain

$$4\pi r_{_H}^2 = 4\pi G^2M^2 = GQ_m^2\left[1 + \frac{\alpha}{3\pi}\mathcal{K}_{NR}\right], \tag{E.5.26}$$

$$r_{_H} \approx Q_m\left[1 + \frac{\alpha}{3\pi}\mathcal{K}_{NR}\right]^{1/2}. \tag{E.5.27}$$

Similar to the weak magnetic field case, the QED correction changes the condition of extremely magnetically charged black holes with spherical symmetry from $M = Q_m/4\pi$ to

$$M = \frac{Q_m}{4\pi}\left[1+\frac{\alpha}{3\pi}\mathcal{K}_{NR}\right]^{1/2}. \tag{E.5.28}$$

These results show that the horizon area and radius of the extreme black hole are the same as their counterparts of the extremely magnetically charged Reissner-Nordström black hole, when the black hole mass M is fixed. Whereas, the black hole magnetic charge Q_m is fixed, Eqs. (E.5.26) and (E.5.27) show that the black hole horizon area and radius become smaller than their counterparts of extremely magnetically charged Reissner-Nordström black holes. We have discussed this behavior in Eqs. (E.4.15)-(E.4.18) for the case of extremely electrically charged black holes.

Analogously, we obtain the Christodoulou-Ruffini mass formula in the strong-field case of magnetically charged black holes,

$$M = M_{ir} + \frac{Q^2}{16\pi G M_{ir}}\left[1+\frac{\alpha}{3\pi}\mathcal{K}_{NR+}\right]. \tag{E.5.29}$$

It is straightforward to obtain irreducible mass M_{ir} by substituting Eq. (E.5.20) into Eq. (E.4.19), and the black hole entropy S_{en} by substituting Eq. (E.5.20) into Eq. (E.4.21). Analogous to the case of the electrically charged black hole, the black hole irreducible mass M_{ir} and entropy S_{en} in the strong magnetic field case depend on the black hole horizon radius $r_{_{H+}}$ of Eqs. (E.5.20) and (E.5.26). Equation (E.5.29) indicates that the maximal energy extractable from a magnetically charged black hole is

$$\varepsilon_{ex} = \frac{Q_m^2}{8\pi r_{_{H+}}}\left[1+\frac{\alpha}{3\pi}\mathcal{K}_{NR+}\right]. \tag{E.5.30}$$

The properties of the maximally extractable energy in the strong magnetic field case are similar to those of the magnetically charged black hole in the weak magnetic field case. However, the QED correction of the vacuum polarization effect to the energy of the magnetically charged black hole in the strong magnetic field case is much more significant in comparison with that in the weak magnetic field case.

E.6. Black holes with electric and magnetic charges

If the spherically symmetric (nonrotating) black hole is both electrically and magnetically charged, electric and magnetic fields do not vanish. As shown in Eq. (E.2.11), both invariants S and P contribute to the Euler-Heisenberg effective Lagrangian. The metric takes the same form as the metric of Eq. (E.4.2) for electrically charged black holes with spherical symmetry. In this case, the tensor $F_{\mu\nu}$ compatible with spherical symmetry can involve only a radial electric field $F_{01} = -F_{10}$ and a radial magnetic field $F_{23} = -F_{32}$, and the gauge potential is (see, e.g., Ref. Hawking and Ross (1995))

$$A_\mu(x) = [A(r), 0, 0, Q_m(1-\cos\theta)/4\pi]. \tag{E.6.1}$$

In the Einstein-Maxwell theory, $A(r) = -Q/(4\pi r)$, and the metric function $f(r)$ of Eq. (E.4.2) is given by (see, e.g., Ref. Hawking and Ross (1995))

$$f(r) = 1 - \frac{2GM}{r} + \frac{GQ^2}{4\pi r^2} + \frac{GQ_m^2}{4\pi r^2}. \tag{E.6.2}$$

In the Einstein-Euler-Heisenberg theory, we study the spherically symmetric black hole with electric and magnetic charges in the weak-field case. Using Eq. (E.3.18), we derive the energy-momentum tensor with a radial electric field E and a radial magnetic field B,

$$T^{\mu\nu} = T_M^{\mu\nu}\left[1 + \frac{2\alpha}{45\pi E_c^2}(E^2 - B^2)\right] + g^{\mu\nu}\frac{\alpha}{90\pi E_c^2}\left[(E^2-B^2)^2 + 7(E\cdot B)^2\right] + \cdots . \tag{E.6.3}$$

Analogous to the analysis of electrically/magnetically charged black holes with spherical symmetry, we obtain the (0-0) component of Einstein equations,

$$\frac{2m'(r)}{r^2} = 4\pi\left[E^2(r) + B^2(r) + \frac{\alpha}{15\pi}E^4(r)/E_c^2 - \frac{\alpha}{45\pi}B^4(r)/E_c^2 + \frac{\alpha}{9\pi E_c^2}E^2(r)B^2(r)\right]. \tag{E.6.4}$$

In addition, we obtain the field equations from Eq. (E.3.5) (see also Ref. Yajima and Tamaki (2001)),

$$E(r) + \frac{2\alpha}{45\pi}E^3(r)/E_c^2 + \frac{\alpha B^2}{9\pi E_c^2}E(r) = \frac{Q}{4\pi r^2}, \tag{E.6.5}$$

$$B(r) = \frac{Q_m}{4\pi r^2}. \tag{E.6.6}$$

Note that the mixing terms of the electric and magnetic fields in Eqs. (E.6.4) and

(E.6.5) come from the contribution of the invariant P. Introducing $\overline{E}(r) \equiv E(r)/E_c$, we have

$$\overline{E}(r) = E_Q - \frac{2\alpha}{45\pi}E_Q^3 - \frac{\alpha}{9\pi}B_Q^2 E_Q + \cdots, \tag{E.6.7}$$

up to the first order of α. We substitute the solutions of (E.6.6) and (E.6.7) into the Einstein equation (E.6.4) and obtain the mass-energy function

$$m(r) = M - \int_r^\infty 4\pi r^2 dr \frac{1}{2}E_c^2 \left[E_Q^2 + B_Q^2 - \frac{\alpha}{45\pi}E_Q^4 - \frac{\alpha}{45\pi}B_Q^4 - \frac{\alpha}{9\pi}B_Q^2 E_Q^2\right]. \tag{E.6.8}$$

Disregarding the QED correction of the Euler-Heisenberg effective Lagrangian, Eq. (E.6.8) gives the solution $m(r) = M - Q^2/8\pi r - Q_m^2/8\pi r$ for the Reissner-Nordström black hole with electric and magnetic charges. Performing the integration in Eq. (E.6.8), we approximately obtain

$$m(r) = M - \frac{Q^2}{8\pi r}\left[1 - \frac{\alpha}{225\pi}E_Q^2\right] - \frac{Q_m^2}{8\pi r}\left[1 - \frac{\alpha}{225\pi}B_Q^2\right] + \frac{\alpha}{45\pi}\frac{Q_m^2}{8\pi r}E_Q^2. \tag{E.6.9}$$

In the limit $Q \gg Q_m$, Eq. (E.6.9) becomes Eq. (E.4.9) of the electrically charged black hole. On the contrary, in the limit $Q_m \gg Q$, Eq. (E.6.9) becomes Eq. (E.5.8) of the magnetically charged black hole. In order to study the effect of the P term in the Euler-Heisenberg effective Lagrangian, we consider the case with large P and small S, i.e., $Q_m \approx Q$. In this situation, Eq. (E.6.9) becomes

$$m(r) = M - \frac{Q^2}{8\pi r}\left[2 - \frac{7\alpha}{225\pi}E_Q^2\right], \tag{E.6.10}$$

for $Q_m = Q$, i.e., $S = 0$ and large P. Comparing to the cases of electrically/magnetically charged black holes, the QED correction to the black hole energy becomes larger, which results from the combination effects of the vacuum polarization on electric and magnetic charges of black holes in the Einstein-Euler-Heisenberg theory.

In the same way that has been discussed in previous sections, up to the leading order of α, we obtain the horizon radii r_{H+} and r_{H-} from Eq. (E.6.10),

$$r_{H+} = GM + \sqrt{G^2M^2 - \frac{GQ^2}{4\pi}\left[2 - \frac{7\alpha}{225\pi}E_{Q+}^2\right]}, \tag{E.6.11}$$

$$r_{H-} = GM - \sqrt{G^2M^2 - \frac{GQ^2}{4\pi}\left[2 - \frac{7\alpha}{225\pi}E_{Q-}^2\right]}, \tag{E.6.12}$$

and the Christodoulou-Ruffini mass formula

$$M = M_{ir} + \frac{Q^2}{16\pi G M_{ir}} \left[2 - \frac{7\alpha}{225\pi} E_{Q+}^2 \right], \tag{E.6.13}$$

as well as the maximal energy extractable from a black hole

$$\varepsilon_{ex} = \frac{Q^2}{8\pi r_{_{H+}}} \left[2 - \frac{7\alpha}{225\pi} E_{Q+}^2 \right]. \tag{E.6.14}$$

Analogously, we obtain the irreducible mass M_{ir} by substituting Eq. (E.6.11) into Eq. (E.4.19), and the black hole entropy S_{en} by substituting Eq. (E.6.11) into Eq. (E.4.21). The irreducible mass M_{ir}, the black hole entropy S_{en}, and the maximal energy extractable from a black hole receive the same QED correction, but a factor of $7/2$ larger, as compared with their counterparts in the case of either electrically or magnetically charged black holes in the weak-field case.

E.7. Summary

In this chapter, in addition to the Maxwell Lagrangian, we consider the contribution from the QED Euler-Heisenberg effective Lagrangian to formulate the Einstein-Euler-Heisenberg theory. On the basis of this theory, we study the horizon radius, area, total energy, entropy, and irreducible mass as well as the maximally extractable energy of spherically symmetric (nonrotating) black holes with electric and magnetic charges. Our calculations are made up to the leading order of the QED corrections in the limits of strong and weak fields. Our results show that the QED correction of the vacuum polarization results in the increase of the black hole horizon area, entropy and irreducible mass, as well as the decrease of the black hole total energy and maximally extractable energy. The reason is that the QED vacuum polarization gives rise to the screening effect on the black hole electric charge and the paramagnetic effect on the black hole magnetic charge. The condition of the extremely charged black hole $M = Q/4\pi$ or $M = Q_m/4\pi$ is modified [see Eqs. (E.4.18), (E.5.14), and (E.5.28)], which results from the screening and paramagnetic effects.

To end this chapter, we would like to mention that in the Einstein-Euler-Heisenberg theory, it is worthwhile to study Kerr-Newman black holes, whose electric field $\mathbf{E}$ and magnetic field $\mathbf{B}$ are determined by the black hole mass M, charge Q, and angular momentum a Newman et al. (1965). In addition, it will be interesting to study the QED corrections in black hole physics by taking into account the one-loop photon-graviton amplitudes of the effective Lagrangian (E.3.11) Drummond and Hathrell (1980) and its generalizations Gilkey (1975); Bastianelli et al. (2000); Barvinsky and

Vilkovisky (1985); Gusev (2009); Bastianelli et al. (2009). We leave these studies for future work.

Bibliography

Eli (????).

ABOUELSAOOD, A., CALLAN, C.G., NAPPI, C.R. AND YOST, S.A.
Open strings in background gauge fields.
Nucl. Phys. B, **280**, pp. 599–624 (1987).

AHARONIAN, F., AKHPERJANIAN, A.G., BAZER-BACHI, A.R., BEILICKE, M., BENBOW, W., BERGE, D., BERNLÖHR, K., BOISSON, C., BOLZ, O., BORREL, V. ET AL.
A low level of extragalactic background light as revealed by γ-rays from blazars.
Nature , **440**, pp. 1018–1021 (2006).

AHARONIAN, F.A.
Very High Energy Cosmic Gamma Radiation (World Scientific, 2003).

AHARONIAN, F.A., AKHPERJANIAN, A.G., BARRIO, J.A., BERNLÖHR, K., BOJAHR, H., CALLE, I., CONTRERAS, J.L., CORTINA, J., DENNINGHOFF, S., FONSECA, V. ET AL.
The Energy Spectrum of TEV Gamma Rays from the Crab Nebula as Measured by the HEGRA System of Imaging Air Cerenkov Telescopes.
ApJ , **539**, pp. 317–324 (2000).
doi:10.1086/309225.

AIELLO, M., FERRARO, R. AND GIRIBET, G.
Exact solutions of lovelock-born-infeld black holes.
Phys. Rev. D, **70**, p. 104014 (2004).

AKSENOV, A.G., RUFFINI, R. AND VERESHCHAGIN, G.V.
Thermalization of Nonequilibrium Electron-Positron-Photon Plasmas.
Phys. Rev. Lett. , **99(12)**, pp. 125003–+ (2007).

AKSENOV, A.G., RUFFINI, R. AND VERESHCHAGIN, G.V.
Thermalization of Electron-Positron-Photon Plasmas with an application to GRB.
In *American Institute of Physics Conference Series*, volume 966 of *American Institute of Physics Conference Series*, pp. 191–196 (2008).

AYÓN-BEATO, E. AND GARCÍA, A.
Regular black hole in general relativity coupled to nonlinear electrodynamics.
Phys. Rev. Lett., **80**, pp. 5056–5059 (1998).

AYÓN-BEATO, E. AND GARCÍA, A.
New regular black hole solution from nonlinear electrodynamics.
Phys. Lett. B, **464**, pp. 25–29 (1999).

BARVINSKY, A.O. AND VILKOVISKY, G.A.
The generalized schwinger-dewitt technique in gauge theories and quantum gravity.
Phys. Rep., **119**, pp. 1–74 (1985).

BARVINSKY, A.O. AND VILKOVISKY, G.A.
Covariant perturbation theory (ii). second order in the curvature. general algorithms.
Nucl. Phys. B, **333**, pp. 471–511 (1990a).

BARVINSKY, A.O. AND VILKOVISKY, G.A.
Covariant perturbation theory (iii). spectral representations of the third-order form factors.
Nucl. Phys. B, **333**, pp. 512–524 (1990b).

BASTIANELLI, F., DÁVILA, J.M. AND SCHUBERT, C.
Gravitational corrections to the euler-heisenberg lagrangian.
J. High Energy Phys., **03**, p. 086 (2009).

BASTIANELLI, F., FROLOV, S. AND TSEYTLIN, A.A.
Conformal anomaly of (2,0) tensor multiplet in six dimensions and ads/cft correspondence.
J. High Energy Phys., **02**, p. 013 (2000).

BATALIN, I.A. AND FRADKIN, E.S.
Quantum electrodynamics in external fields. I.
Theoretical and Mathematical Physics, **5**, pp. 1080–1100 (1970a).

BATALIN, I.A. AND FRADKIN, E.S.
Quantum electrodynamics in external fields. I.
Theor. Math. Phys., **5**, pp. 1080–1100 (1970b).

BEKENSTEIN, J.D.
Hydrostatic equilibrium and gravitational collapse of relativistic charged fluid balls.
Phys. Rev. D, **4**, pp. 2185–2190 (1971).

BEKENSTEIN, J.D.
Black holes and entropy.
Phys. Rev. D, **7**, pp. 2333–2346 (1973).

BELL, A.R. AND KIRK, J.G.
Possibility of prolific pair production with high-power lasers.
Phys. Rev. Lett., **101(20)**, p. 200403 (2008).

BENEDETTI, A., HAN, W.B., RUFFINI, R. AND VERESHCHAGIN, G.V.
On the frequency of oscillations in the pair plasma generated by a strong electric field.
Physics Letters B, **698**, pp. 75–79 (2011).
doi:10.1016/j.physletb.2011.02.050.

BERNARDINI, C.
AdA:The First Electron-Positron Collider.
Physics in Perspective, **6**, pp. 156–183 (2004).

BIRO, T.S., NIELSEN, H.B. AND KNOLL, J.
Colour rope model for extreme relativistic heavy ion collisions.
Nucl. Phys. B, **245**, pp. 449–468 (1984).

BLINNE, A. AND GIES, H.
Pair production in rotating electric fields.
arXiv preprint arXiv:1311.1678 (2013).

BONOMETTO, S. AND REES, M.J.
On possible observable effects of electron pair-production in QSOs.
MNRAS , **152**, pp. 21–+ (1971).

BOOT, H.A.H. AND R.-S.-HARVIE, R.B.
Charged Particles in a Non-uniform Radio-frequency Field.
Nature , **180**, pp. 1187–+ (1957).
doi:10.1038/1801187a0.

BORN, M.
Modified Field Equations with a Finite Radius of the Electron.
Nature , **132**, pp. 282–+ (1933).

BORN, M.
On the Quantum Theory of the Electromagnetic Field.
Royal Society of London Proceedings Series A, **143**, pp. 410–437 (1934).

BORN, M. AND INFELD, L.
Foundations of the New Field Theory.
Royal Society of London Proceedings Series A, **144**, pp. 425–451 (1934).

BORN, M. AND INFELD, L.
Foundations of the new field theory.
Proc. R. Soc. A, **144**, pp. 425–451 (1934).

BREIT, G. AND WHEELER, J.A.
Collision of Two Light Quanta.
Physical Review, **46**, pp. 1087–1091 (1934).

BREZIN, E. AND ITZYKSON, C.
Pair Production in Vacuum by an Alternating Field.
Phys. Rev. D, **2**, pp. 1191–1199 (1970).

BREZIN, E. AND ITZYKSON, C.
Pair production in vacuum by an alternating field.
Phys. Rev. D, **2**, pp. 1191–1199 (1970).

BRONNIKOV, K.A.
Regular magnetic black holes and monopoles from nonlinear electrodynamics.
Phys. Rev. D, **63**, p. 044005 (2001).

BULA, C., MCDONALD, K.T., PREBYS, E.J., BAMBER, C., BOEGE, S., KOTSEROGLOU, T., MELISSINOS, A.C., MEYERHOFER, D.D., RAGG, W., BURKE, D.L. ET AL.
Observation of Nonlinear Effects in Compton Scattering.
Physical Review Letters, **76**, pp. 3116–3119 (1996).

BULANOV, S.S., MUR, V.D., NAROZHNY, N.B., NEES, J. AND POPOV, V.S.
Multiple colliding electromagnetic pulses: A way to lower the threshold of e^{+} e^{-} pair production from vacuum.
Phys. Rev. Lett., **104(22)**, p. 220404 (2010).

BULANOV, S.V., ESIRKEPOV, T. AND TAJIMA, T.
Light Intensification towards the Schwinger Limit.
Phys. Rev. Lett. , **91(8)**, pp. 085001–+ (2003).

BURINSKII, A. AND HILDEBRANDT, S.R.
New type of regular black holes and particlelike solutions from nonlinear electrodynamics.
Phys. Rev. D, **65**, p. 104017 (2002).

BURKE, D.L., FIELD, R.C., HORTON-SMITH, G., SPENCER, J.E., WALZ, D., BERRIDGE, S.C., BUGG, W.M., SHMAKOV, K., WEIDEMANN, A.W., BULA, C. ET AL.
Positron Production in Multiphoton Light-by-Light Scattering.

Physical Review Letters, **79**, pp. 1626–1629 (1997).

CAI, R.G., PANG, D.W. AND WANG, A.
Born-infeld black holes in (a)ds spaces.
Phys. Rev. D, **70**, p. 124034 (2004).

CALTECH (2010).

CARTER, B.
Hamilton-jacobi and schrodinger separable solutions of einstein's equations.
Communications in Mathematical Physics, **10**, pp. 280–310 (1968).

CAVALLO, G. AND REES, M.J.
A qualitative study of cosmic fireballs and gamma-ray bursts.
MNRAS , **183**, pp. 359–365 (1978).

CHERUBINI, C., GERALICO, A., J. A. RUEDA, H. AND RUFFINI, R.
$e^- - e^+$ pair creation by vacuum polarization around electromagnetic black holes.
Phys. Rev. D, **79(12)**, pp. 124002–+ (2009).

CHERUBINI, C., RUFFINI, R. AND VITAGLIANO, L.
On the electromagnetic field of a charged collapsing spherical shell in general relativity.
Physics Letters B, **545**, pp. 226–232 (2002).

CHO, Y.M. AND PAK, D.G.
A convergent series for the qed effective action.
Phys. Rev. Lett., **86(10)**, pp. 1947–1950 (2001).

CHRISTODOULOU, D.
Reversible and irreversible transformations in black-hole physics.
Phys. Rev. Lett., **25**, pp. 1596–1597 (1970).

CHRISTODOULOU, D. AND RUFFINI, R.
Reversible transformations of a charged black hole.
Phys. Rev. D, **4**, pp. 3552–3555 (1971).

CIRILO LOMBARDO, D.J.
Charge without charge, regular spherically symmetric solutions and the einstein-born-infeld theory.
Int. J. Theor. Phys., **48**, pp. 2267–2285 (2009).

COOPER, F., EISENBERG, J.M., KLUGER, Y., MOTTOLA, E. AND SVETITSKY, B.
Particle production in the central rapidity region.
Phys. Rev. D, **48**, pp. 190–208 (1993).

COOPER, F. AND MOTTOLA, E.
Quantum back reaction in scalar QED as an initial-value problem.
Phys. Rev. D, **40**, pp. 456–464 (1989).

COPPI, P.S. AND AHARONIAN, F.A.
Understanding the spectra of TeV blazars: implications for the cosmic infrared background.
Astroparticle Physics, **11**, pp. 35–39 (1999).

DAMOUR, T. AND RUFFINI, R.
Quantum electrodynamical effects in Kerr-Newman geometries.
Physical Review Letters, **35**, pp. 463–466 (1975).

DAMOUR, T. AND RUFFINI, R.
Quantum electrodynamical effects in kerr-newmann geometries.
Phys. Rev. Lett., **35**, pp. 463–466 (1975).

DE LA CRUZ, V. AND ISRAEL, W.
Gravitational bounce.
Nuovo Cimento A Serie, **51**, pp. 744–760 (1967).

DE OLIVEIRA, H.P.
Non-linear charged black holes.
Classical Quantum Gravity, **11**, p. 1469 (1994).

DEACON, D.A.G., ELIAS, L.R., MADEY, J.M.J., RAMIAN, G.J., SCHWETTMAN, H.A. AND SMITH, T.I.
First operation of a free-electron laser.
Physical Review Letters, **38**, pp. 892–894 (1977).

DEHGHANI, M.H., HENDI, S.H., SHEYKHI, A. AND RASTEGAR SEDEHI, H.
Thermodynamics of rotating black branes in einstein-born-infeld-dilaton gravity.
J. Cosmol. Astropart. Phys., **02**, p. 020 (2007).

DEHGHANI, M.H. AND RASTEGAR SEDEHI, H.R.
Thermodynamics of rotating black branes in (n+1)-dimensional einstein-born-infeld gravity.
Phys. Rev. D, **84**, p. 124018 (2006).

DEMIANSKI, M.
Static electromagnetic geon.
Found. Phys., **16**, pp. 187–190 (1986).

DEY, T.K.
Born-infeld black holes in the presence of a cosmological constant.
Phys. Lett. B, **595**, pp. 484–490 (2004).

DI PIAZZA, A., LÖTSTEDT, E., MILSTEIN, A.I. AND KEITEL, C.H.
Barrier control in tunneling e^{+}-e^{-} photoproduction.
Phys. Rev. Lett., **103(17)**, p. 170403 (2009).

DIAZ-ALONSO, J. AND RUBIERA-GARCIA, D.
Asymptotically anomalous black hole configurations in gravitating nonlinear electrodynamics.
Phys. Rev. D, **82**, p. 085024 (2010a).

DIAZ-ALONSO, J. AND RUBIERA-GARCIA, D.
Electrostatic spherically symmetric configurations in gravitating nonlinear electrodynamics.
Phys. Rev. D, **81**, p. 064021 (2010b).

DIAZ-ALONSO, J. AND RUBIERA-GARCIA, D.
Black holes from generalized gauge field theories.
J. Phys. Conf. Ser., **283**, p. 012014 (2011a).

DIAZ-ALONSO, J. AND RUBIERA-GARCIA, D.
Electrically charged black hole solutions in generalized gauge field theories.
J. Phys. Conf. Ser., **314**, p. 012065 (2011b).

DIRAC, P.A.M.
Annihilation of electrons and protons.
Proceedings of the Cambridge Philosophical Society, **26**, pp. 361–375 (1930).

DITTRICH, W. AND GIES, H.
Light propagation in nontrivial qed vacua.
Phys. Rev. D, **58**, p. 025004 (1998).

DRUMMOND, I.T. AND HATHRELL, S.J.
Qed vacuum polarization in a background gravitational field and its effect on the velocity of photons.
Phys. Rev. D, **22**, pp. 343–355 (1980).

DUMLU, C.K. AND DUNNE, G.V.
Stokes phenomenon and schwinger vacuum pair production in time-dependent laser pulses.
Phys. Rev. Lett., **104(25)**, p. 250402 (2010).

DUMLU, C.K. AND DUNNE, G.V.
Complex worldline instantons and quantum interference in vacuum pair production.
Phys. Rev. D, **84(12)**, p. 125023 (2011a).

DUMLU, C.K. AND DUNNE, G.V.
Interference effects in schwinger vacuum pair production for time-dependent laser pulses.
Phys. Rev. D, **83(6)**, p. 065028 (2011b).

DUNNE, G.V.
Heisenberg-euler effective lagrangians: basics and extensions.
From Fields to Strings: Circumnavigating Theoretical Physics, **1**, p. 445 (2005).

DUNNE, G.V. AND SCHUBERT, C.
Two-loop Euler-Heisenberg QED pair-production rate.
Nucl. Phys. B, **564**, pp. 591–604 (2000).

DUNNE, G.V. AND SCHUBERT, C.
Worldline instantons and pair production in inhomogenous fields.
Phys. Rev. D, **72(10)**, pp. 105004–+ (2005a).

DUNNE, G.V. AND SCHUBERT, C.
Worldline instantons and pair production in inhomogenous fields.
Phys. Rev. D, **72(10)**, pp. 105004–+ (2005b).

DUNNE, G.V. AND WANG, Q.
Multidimensional Worldline Instantons.
Phys. Rev., **D74**, p. 065015 (2006).
doi:10.1103/PhysRevD.74.065015.

DUNNE, G.V., WANG, Q., GIES, H. AND SCHUBERT, C.
Worldline instantons. II. The Fluctuation prefactor.
Phys. Rev., **D73**, p. 065028 (2006).
doi:10.1103/PhysRevD.73.065028.

DUNNE, G.V. AND WANG, Q.H.
Multidimensional worldline instantons.
Phys. Rev. D, **74(6)**, pp. 065015–+ (2006).

DUNNE, G.V., WANG, Q.H., GIES, H. AND SCHUBERT, C.
Worldline instantons and the fluctuation prefactor.
Phys. Rev. D, **73(6)**, pp. 065028–+ (2006).

DUNNE, G.V., GIES, H. AND SCHÜTZHOLD, R.
Catalysis of schwinger vacuum pair production.
Phys. Rev. D, **80(11)**, p. 111301 (2009).

DWEK, E. AND KRENNRICH, F.
Simultaneous Constraints on the Spectrum of the Extragalactic Background Light and the Intrinsic TeV Spectra of Markarian 421, Markarian 501, and H1426+428.
ApJ , **618**, pp. 657–674 (2005).

DYMNIKOVA, I.
Regular electrically charged vacuum structures with de sitter centre in nonlinear electrodynamics coupled to general relativity.
Classical Quantum Gravity, **21**, p. 4417 (2004).

DYSON, F.J.
The Radiation Theories of Tomonaga, Schwinger, and Feynman.
Physical Review, **75**, pp. 486–502 (1949a).

DYSON, F.J.
The S Matrix in Quantum Electrodynamics.
Physical Review, **75**, pp. 1736–1755 (1949b).

EHLERS, J.
Survey of general relativity theory.
In *Relativity, Astrophysics and Cosmology*, pp. 1–125 (1973).

EULER, H.
Über die Streuung von Licht an Licht nach der Diracschen Theorie.
Annalen der Physik, **418**, pp. 398–448 (1936).

FAZIO, G.G. AND STECKER, F.W.
Predicted High Energy Break in the Isotropic Gamma Ray Spectrum: a Test of Cosmological Origin.
Nature , **226**, pp. 135–+ (1970).

FERNANDO, S. AND KRUG, D.
Charged black hole solutions in einstein-born-infeld gravity with a cosmological constant.
Gen. Relativ. Gravit., **35**, pp. 129–137 (2003).

FEYNMAN, R.P.
Space-Time Approach to Non-Relativistic Quantum Mechanics.
Reviews of Modern Physics, **20**, pp. 367–387 (1948).

FEYNMAN, R.P.
Space-Time Approach to Quantum Electrodynamics.
Physical Review, **76**, pp. 769–789 (1949a).

FEYNMAN, R.P.
The Theory of Positrons.
Physical Review, **76**, pp. 749–759 (1949b).

FRADKIN, E.S. AND TSEYTLIN, A.A.
Non-linear electrodynamics from quantized strings.
Phys. Lett. B, **163**, pp. 123–130 (1985).

FRADKIN, E., GITMAN, D. AND M., S.S.
Quantum Electrodynamics: With Unstable Vacuum (Springer, 1991).

FRASCHETTI, F., RUFFINI, R., VITAGLIANO, L. AND XUE, S.S.
Theoretical predictions of spectral evolution of short GRBs.
Nuovo Cimento B Serie, **121**, pp. 1477–1478 (2006).

FRISHMAN, Y.
Nonperturbative calculation of $z_{-}\{3\}$ in massless electrodynamics.
Phys. Rev., **138(6B)**, p. 1450 (1965).

GAMOW, G.
Constitution of Atomic Nuclei And Radioactivity (Oxford University Press, 1931).

GARCIA, A., SALAZAR, H. AND PLEBANSKI, J.F.
Type-d solutions of the einstein and born-infeld nonlinear-electrodynamics equations.
Nuovo Cimento B, **84**, pp. 65–90 (1984).

GATOFF, G., KERMAN, A.K. AND MATSUI, T.
Flux-tube model for ultrarelativistic heavy-ion collisions: Electrohydrodynamics of a quark-gluon plasma.
Phys. Rev. D, **36**, pp. 114–129 (1987).

GELL-MANN, M. AND LOW, F.E.
Quantum electrodynamics at small distances.
Phys. Rev., **95(5)**, p. 1300 (1954).

GHEZZI, C.R.
Relativistic structure, stability, and gravitational collapse of charged neutron stars.
Phys. Rev. D, **72(10)**, 104017 (2005).
doi:10.1103/PhysRevD.72.104017.

GHEZZI, C.R. AND LETELIER, P.S.
Numeric simulation of relativistic stellar core collapse and the formation of Reissner-Nordström black holes.
Phys. Rev. D, **75(2)**, 024020 (2007).
doi:10.1103/PhysRevD.75.024020.

GIBBONS, G.W. AND RASHEED, D.A.
Electric-magnetic duality rotations in non-linear electrodynamics.
Nucl. Phys. B, **454**, pp. 185–206 (1995).

GILKEY, P.B.
The spectral geometry of a riemannian manifold.
J. Dif. Geom., **10**, pp. 601–618 (1975).

GONZÁLEZ, H.A., HASSAÏNE, M. AND MARTÍNEZ, C.
Thermodynamics of charged black holes with a nonlinear electrodynamics source.
Phys. Rev. D, **80**, p. 104008 (2009).

GORDIENKO, S., PUKHOV, A., SHOROKHOV, O. AND BAEVA, T.
Coherent Focusing of High Harmonics: A New Way Towards the Extreme Intensities.
Physical Review Letters, **94(10)**, pp. 103903–+ (2005).
doi:10.1103/PhysRevLett.94.103903.

GOULD, R.J. AND SCHRÉDER, G.P.
Opacity of the Universe to High-Energy Photons.
Physical Review, **155**, pp. 1408–1411 (1967).

GRADSHTEYN, I.S. AND RYZHIK, I.M.
Table of Integrals, Series and Products (Academic Press, New York, 1994).
5th ed.

GREINER, W., MULLER, B. AND RAFELSKI, J.
Quantum Electrodynamics of Strong Fields (Berlin, Springer, 1985).

GREINER, W. AND REINHARDT, J.
Supercritical fields in heavy ion physics - a status report.
In P. Chen (ed.), *Quantum Aspects of Beam Physics*, pp. 438–463 (World Scientific, 1999).
Proceedings of the 15th Advanced ICFA Beam Dynamics Workshop on Quantum Aspects of Beam Physics, Monterey, California, 4-9 Jan 1998.

GRIB, A.A., MAMAEV, S.G. AND MOSTEPANENKO, V.M.
Vacuum Quantum Effects in Strong External Fields (Atomizdat, 1980).

GUSEV, Y.V.
Heat kernel expansion in the covariant perturbation theory.
Nucl. Phys. B, **807**, pp. 566–590 (2009).

HAN, W., RUFFINI, R. AND XUE, S.
Electron-positron pair oscillation in spatially inhomogeneous electric fields and radiation.
Physics Letters B, **691**, pp. 99–104 (2010).
doi:10.1016/j.physletb.2010.06.021.

HAN, W.B., RUFFINI, R. AND XUE, S.S.
Electron and positron pair production of compact stars.
Phys. Rev. D, **86(8)**, 084004 (2012).
doi:10.1103/PhysRevD.86.084004.

HASSAÏNE, M. AND C. MARTÍNEZ, C.
Higher-dimensional black holes with a conformally invariant maxwell source.
Phys. Rev. D, **75**, p. 027502 (2007).

HASSAÏNE, M. AND C. MARTÍNEZ, C.
Higher-dimensional charged black hole solutions with a nonlinear electrodynamics source.
Classical Quantum Gravity, **25**, p. 195023 (2008).

HAUSER, M.G. AND DWEK, E.
The Cosmic Infrared Background: Measurements and Implications.
ARA&A , **39**, pp. 249–307 (2001).

HAWKING, S.
Gravitational radiation from colliding black holes.
Phys. Rev. Lett., **26**, pp. 1344–1346 (1971).

HAWKING, S.W. AND ROSS, S.F.
Duality between electric and magnetic black holes.
Phys. Rev. D, **52**, pp. 5865–5876 (1995).

HEBENSTREIT, F., ALKOFER, R., DUNNE, G.V. AND GIES, H.
Momentum Signatures for Schwinger Pair Production in Short Laser Pulses with a Subcycle Structure.
Physical Review Letters, **102(15)**, pp. 150404–+ (2009).

HEBENSTREIT, F., ALKOFER, R. AND GIES, H.
Pair production beyond the Schwinger formula in time-dependent electric fields.
Phys. Rev. D, **78(6)**, pp. 061701–+ (2008).
doi:10.1103/PhysRevD.78.061701.

HEINZL, T., ILDERTON, A. AND MARKLUND, M.
Finite size effects in stimulated laser pair production.
Phys. Lett. B, **692(4)**, pp. 250–256 (2010).

HEISENBERG, W. AND EULER, H.
Folgerungen aus der Diracschen Theorie des Positrons.
Zeitschrift fur Physik, **98**, pp. 714–732 (1936).

HEISENBERG, W. AND EULER, H.
Folgerungen aus der diracschen theorie des positrons (consequences of dirac theory of the positron).
Z. Phys., **98**, pp. 714–732 (1936).

HENDI, S.H.
Rotating black string with nonlinear source.
Phys. Rev. D, **82**, p. 064040 (2010).

HOFFMANN, B.
Gravitational and Electromagnetic Mass in the Born-Infeld Electrodynamics.
Physical Review, **47**, pp. 877–880 (1935).

HOFFMANN, B.
Gravitational and electromagnetic mass in the born-infeld electrodynamics.
Phys. Rev., **47**, pp. 877–880 (1935).

HOFFMANN, B. AND INFELD, L.
On the Choice of the Action Function in the New Field Theory.
Physical Review, **51**, pp. 765–773 (1937).

HOFFMANN, B. AND INFELD, L.
On the choice of the action function in the new field theory.
Phys. Rev., **51**, pp. 765–773 (1937).

HOLLOWOOD, T.J. AND SHORE, G.M.
Causality and micro-causality in curved spacetime.
Phys. Lett. B, **655**, pp. 67–74 (2007).

HOLLOWOOD, T.J. AND SHORE, G.M.
The causal structure of qed in curved spacetime: analyticity and the refractive index.
J. High Energy Phys., **12**, p. 091 (2008a).

HOLLOWOOD, T.J. AND SHORE, G.M.
The refractive index of curved spacetime: The fate of causality in qed.
Nucl. Phys. B, **795**, pp. 138–171 (2008b).

HOPF, F.A., MEYSTRE, P., SCULLY, M.O. AND LOUISELL, W.H.
Strong-signal theory of a free-electron laser.
Physical Review Letters, **37**, pp. 1342–1345 (1976).
doi:10.1103/PhysRevLett.37.1342.

ISRAEL, W.
Singular hypersurfaces and thin shells in general relativity.
Nuovo Cimento B Serie, **44**, pp. 1–14 (1966).

ITZYKSON, C. AND ZUBER, J.B.
Quantum Field Theory (Dover Publications, 2006).

JACKSON, J.D.
Classical Electrodynamics, 3rd Edition (Wiley-VCH, 1998).

JAPAN (2010).

JOHNSON, K., BAKER, M. AND WILLEY, R.
Self-energy of the electron.
Phys. Rev., **136(4B)**, pp. B1111–B1119 (1964).

JOHNSON, K., BAKER, M. AND WILLEY, R.S.
Quantum electrodynamics.
Phys. Rev. Lett., **11(11)**, pp. 518–520 (1963).

KAJANTIE, K. AND MATSUI, T.
Decay of strong color electric field and thermalization in ultra-relativistic nucleus-nucleus collisions.
Physics Letters B, **164**, pp. 373–378 (1985).
doi:10.1016/0370-2693(85)90343-0.

KHRIPLOVICH, I.B.
Charged-particle creation by charged black holes.
Nuovo Cimento B Serie, **115**, pp. 761–+ (2000).

KIBBLE, T.W.
Refraction of Electron Beams by Intense Electromagnetic Waves.
Physical Review Letters, **16**, pp. 1054–1056 (1966).
doi:10.1103/PhysRevLett.16.1054.

KIM, S.P. AND PAGE, D.N.
Schwinger pair production via instantons in strong electric fields.
Phys. Rev. D, **65(10)**, pp. 105002–+ (2002).

KIM, S.P. AND PAGE, D.N.
Schwinger pair production in electric and magnetic fields.
Phys. Rev. D, **73(6)**, pp. 065020–+ (2006).

KIM, S.P. AND PAGE, D.N.
Improved approximations for fermion pair production in inhomogeneous electric fields.
Phys. Rev. D, **75(4)**, pp. 045013–+ (2007).

KLEIN, O.
Die Reflexion von Elektronen an einem Potentialsprung nach der relativistischen Dynamik von Dirac.
Zeitschrift fur Physik, **53**, pp. 157–165 (1929).

KLEINERT, H.
Effective action and field equation for bec from weak to strong couplings (????).

KLEINERT, H.
Particles and quantum fields (2008).

KLEINERT, H.
Particles and quantum fields (2011).
Section 12.

KLEINERT, H.
Fractional quantum field theory, path integral, and stochastic differential equation for strongly interacting many-particle systems.
Europhys. Lett., **100**, p. 10001 (2012).
doi:10.1209/0295-5075/100/10001.

KLEINERT, H.
Quantum field theory of black-swan events (2012).
Lecture presented at the conference http://www.quantumhorizons.org/.

KLEINERT, H. AND FROHLINDE, V.S.
Critical Properties of ϕ^4-theories (World Scientific Publishing Company, Incorporated, 2001).

KLEINERT, H., RUFFINI, R. AND XUE, S.
Electron-positron pair production in space- or time-dependent electric fields.
Phys. Rev. D, **78(2)**, pp. 025011–+ (2008).
doi:10.1103/PhysRevD.78.025011.

KLEINERT, H., STROBEL, E. AND XUE, S.S.
Fractional effective action at strong electromagnetic fields.
Phys. Rev. D, **88**, p. 025049 (2013).

KLEINERT, H. AND XUE, S.S.
Vacuum pair-production in classical electric field and electromagnetic wave.
Annals of Physics, **333**, pp. 104–126 (2013).

KLEINERT, H., RUFFINI, R. AND XUE, S.S.
Electron-positron pair production in space- or time-dependent electric fields.
Physical Review D (Particles, Fields, Gravitation, and Cosmology), **78(2)**, 025011 (2008).

KLEMPERER, O.
The annihilation radiation of the positron.
Proceedings of the Cambridge Philosophical Society, **30**, pp. 347–354 (1934).

KLUGER, Y., EISENBERG, J.M., SVETITSKY, B., COOPER, F. AND MOTTOLA, E.
Pair production in a strong electric field.
Physical Review Letters, **67**, pp. 2427–2430 (1991).

KLUGER, Y., EISENBERG, J.M., SVETITSKY, B., COOPER, F. AND MOTTOLA, E.
Fermion pair production in a strong electric field.
Phys. Rev. D, **45**, pp. 4659–4671 (1992).

KNEISKE, T.M., BRETZ, T., MANNHEIM, K. AND HARTMANN, D.H.
Implications of cosmological gamma-ray absorption. II. Modification of gamma-ray spectra.
A&A , **413**, pp. 807–815 (2004).

KNEISKE, T.M., MANNHEIM, K. AND HARTMANN, D.H.
Implications of cosmological gamma-ray absorption. I. Evolution of the metagalactic radiation field.
A&A , **386**, pp. 1–11 (2002).

KOTSEROGLOU, T., BAMBER, C., BOEGE, S., MELISSINOS, A.C., MEYERHOFER, D.D., RAGG, W., BULA, C., MCDONALD, K.T., PREBYS, E.J., BERNSTEIN, D. ET AL.
Picosecond timing of terawatt laser pulses with the SLAC 46 GeV electron beam.
Nuclear Instruments and Methods in Physics Research A, **383**, pp. 309–317 (1996).

LANDAU, L.D. AND LIFSHITZ, E.M.

The classical theory of fields (Course of theoretical physics - Pergamon International Library of Science, Technology, Engineering and Social Studies, Oxford: Pergamon Press, 1975, 4th rev.engl.ed., 1975).

LATORRE, J.I., PASCUAL, P. AND TARRACH, R.
Speed of light in non-trivial vacua.
Nucl. Phys. B, **437**, pp. 60–82 (1995).

MACMINN, D. AND PRIMACK, J.R.
Probing the ERA of Galaxy Formation via TeV Gamma-Ray Absorption by the Near Infrared Extragalactic Background.
Space Science Reviews, **75**, pp. 413–422 (1996).

MARINOV, M.S. AND POPOV, V.S.
Electron-positron pair creation from vacuum induced by variable electric field.
Fortschritte der Physik, **25**, pp. 373–400 (1977).

MARIS, T.A.J., HERSCOVITZ, V.E. AND JACOB, G.
Quantum electrodynamics with zero bare fermion mass.
Phys. Rev. Lett., **12(11)**, pp. 313–315 (1964).

MARIS, T.A.J., HERSCOVITZ, V.E. AND JACOB, G.
The length scale in quantum electrodynamics without a bare mass.
Il Nuovo Cimento Series 10, **38(2)**, pp. 783–795 (1965).

MASHHOON, B. AND PARTOVI, M.H.
Gravitational collapse of a charged fluid sphere.
Phys. Rev. D, **20**, pp. 2455–2468 (1979).
doi:10.1103/PhysRevD.20.2455.

MAZHARIMOUSAVI, S.H., HALILSOY, M. AND GURTUG, O.
Theorem to generate einstein-nonlinear maxwell fields.
Classical Quantum Gravity, **27**, p. 205022 (2010).

MIELNICZUK, W.J.
The representation of the heisenberg-euler lagrangian by means of special functions.
J. Phys. A: Math. Gen., **15(9)**, p. 2905 (1982).
Note that there were some misprints regarding equation (**??**).

MOHAMMADI, R., RUFFINI, R. AND XUE, S.S.
Neutrinos decoupled from β-processes and supernova explosion.
ArXiv e-prints (2012).

MONIN, A. AND VOLOSHIN, M.B.
Photon-stimulated production of electron-positron pairs in an electric field.
Phys. Rev. D, **81(2)**, p. 025001 (2010a).

MONIN, A. AND VOLOSHIN, M.B.
Semiclassical calculation of photon-stimulated schwinger pair creation.
Phys. Rev. D, **81(8)**, p. 085014 (2010b).

NAROZHNYI, N.B. AND NIKISHOV, A.I.
The Simplist processes in the pair creating electric field.
Yad. Fiz., **11**, p. 1072 (1970).

NAROZHNYI, N. AND NIKISHOV, A.
On Gauge Invariance and Vacuum Polarization.
Sov. J. Nucl. Phys., **11**, pp. 596–+ (1970).

NAROZHNYĬ, N.B., NIKISHOV, A.I. AND RITUS, V.I.
Quantum processes in the field of circulary polarized electromagnetic wave.
Sov. Phys. JETP, **20**, p. 622 (1965).

NASA (2004).

NEWMAN, E.T., COUCH, E., CHINNAPARED, K., EXTON, A., PRAKASH, A. AND TORRENCE, R.
Metric of a rotating, charged mass.
J. Math. Phys., **6**, p. 918 (1965).

NIKISHOV, A.I.
Absorption of high-energy photons in the universe.
Zhurnal Eksperimental'noi i Teoreticheskoi Fiziki, **41**, pp. 549–550 (1961).

NIKISHOV, A.I.
Pair production by a constant electric field.
Sov. Phys. JETP, **30**, pp. 660–662 (1970).

NIKISHOV, A.I. AND RITUS, V.I.
Quantum processes in the field of a plane electromagnetic wave and in a constant field. i.
Sov. Phys. JETP, **19**, pp. 529–541 (1964a).

NIKISHOV, A.I. AND RITUS, V.I.
Quantum processes in the field of a plane electromagnetic wave and in a constant field. ii.
Sov. Phys. JETP, **19**, pp. 1191–1199 (1964b).

NIKISHOV, A.I. AND RITUS, V.I.
Nonlinear effects in compton scattering and pair production owing to absorption of several photons.
Sov. Phys. JETP, **20**, pp. 757–759 (1965).

NIKISHOV, A.I. AND RITUS, V.I.
Pair Production by a Photon and Photon Emission by an Electron in the Field of an Intense Electromagnetic Wave and in a Constant Field.
Soviet Journal of Experimental and Theoretical Physics, **25**, pp. 1135–+ (1967).

NIKISHOV, A.I. AND RITUS, V.I.
Quantum electrodynamics of phenmena in intensive field.
Proc. (Tr.) P. N. Lebedev Phys. Inst. Acad. Sci. USSR, **111** (1979).

NOVELLO, M., PEREZ BERGLIAFFA, S.E. AND SALIM, J.M.
Singularities in general relativity coupled to nonlinear electrodynamics.
Classical Quantum Gravity, **17**, p. 3821 (2000).

NUHN, H.D. AND PELLEGRINI, C.
Proceedings of the x-ray fel theory and simulation codes workshop (2000).

OLSON, E. AND BAILYN, M.
Internal structure of multicomponent static spherical gravitating fluids.
Phys. Rev. D, **12**, pp. 3030–3036 (1975).
doi:10.1103/PhysRevD.12.3030.

OLSON, E. AND BAILYN, M.
Charge effects in a static, spherically symmetric, gravitating fluid.
Phys. Rev. D, **13**, pp. 2204–2211 (1976).
doi:10.1103/PhysRevD.13.2204.

OPPENHEIMER, J.R. AND SNYDER, H.
On Continued Gravitational Contraction.
Physical Review, **56**, pp. 455–459 (1939).

POMERANCHUK, I.Y. AND SMORODINSKII, Y.
Energy levels of systems with z greater than 137.
Journal of Physics (USSR), **9**, pp. 97–100 (1945).

POPOV, V., ROTONDO, M., RUFFINI, R. AND XUE, S.S.
On the relativistic and electrodynamical stability of massive nuclear density cores.
ArXiv e-prints (2009).

POPOV, V.S.
Production of e^+e^- Pairs in an Alternating External Field.
ZhETF Pis ma Redaktsiiu, **13**, pp. 261–+ (1971).

POPOV, V.S.
Pair Production in a Variable and Homogeneous Electric Field as an Oscillator Problem.
Soviet Journal of Experimental and Theoretical Physics, **35**, pp. 659–+ (1972a).

POPOV, V.S.
Pair Production in a Variable External Field (Quasiclassical Approximation).
Soviet Journal of Experimental and Theoretical Physics, **34**, pp. 709–+ (1972b).

POPOV, V.S.
Pair Production in a Variable External Field (Quasiclassical Approximation).
J. Exp. Theor. Phys., **34**, p. 709 (1972c).

POPOV, V.S.
Resonant pair production in a strong electric field.
Soviet Journal of Experimental and Theoretical Physics Letters, **18**, pp. 255–+ (1973a).

POPOV, V.S.
Spontaneous positron production in collisions between heavy nuclei.
Zhurnal Eksperimental'noi i Teoreticheskoi Fiziki, **65**, pp. 35–53 (1973b).

POPOV, V.S.
Schwinger Mechanism of Electron-Positron Pair Production by the Field of Optical and X-ray Lasers in Vacuum.
Soviet Journal of Experimental and Theoretical Physics Letters, **74**, pp. 133–138 (2001a).

POPOV, V.S.
Schwinger Mechanism of Electron-Positron Pair Production by the Field of Optical and X-ray Lasers in Vacuum.
J. Exp. Theor. Phys. Lett., **74**, pp. 133–138 (2001b).

POPOV, V.
Sov. J. Nucl. Phys., **14**, p. 257 (1972d).

POPOV, V.
Resonant pair production in a strong electric field.
JETP Lett., **18**, p. 255 (1973).

PREPARATA, G., RUFFINI, R. AND XUE, S.
On the Dyadosphere of Black Holes.
J. of Korean Phys. Soc. , **42**, pp. S99–S105 (2003).

PREPARATA, G., RUFFINI, R. AND XUE, S.S.
The dyadosphere of black holes and gamma-ray bursts.
Astron. Astrophys., **338**, pp. L87–L90 (1998).

PREPARATA, G., RUFFINI, R. AND XUE, S.S.
The dyadosphere of black holes and gamma-ray bursts.
A&A , **338**, pp. L87–L90 (1998).

PREPARATA, G., RUFFINI, R. AND XUE, S.S.
On the dyadosphere of black holes.
J. Korean Phys. Soc., **42**, pp. 99–104 (2003).

REISS, H.R.
Absorption of Light by Light.
Journal of Mathematical Physics, **3**, pp. 59–67 (1962).

REISS, H.R.
Production of Electron Pairs from a Zero-Mass State.
Physical Review Letters, **26**, pp. 1072–1075 (1971).

RINGWALD, A.
Pair production from vacuum at the focus of an X-ray free electron laser.
Physics Letters B, **510**, pp. 107–116 (2001).

ROTONDO, M., RUEDA, J.A., RUFFINI, R. AND XUE, S.S.
Relativistic Thomas-Fermi treatment of compressed atoms and compressed nuclear matter cores of stellar dimensions.
Phys. Rev. C, **83(4)**, 045805 (2011a).
doi:10.1103/PhysRevC.83.045805.

ROTONDO, M., RUEDA, J.A., RUFFINI, R. AND XUE, S.S.
The self-consistent general relativistic solution for a system of degenerate neutrons, protons and electrons in β-equilibrium.
Physics Letters B, **701**, pp. 667–671 (2011b).
doi:10.1016/j.physletb.2011.06.041.

RUEDA, J.A., RUFFINI, R. AND XUE, S.S.
The Klein first integrals in an equilibrium system with electromagnetic, weak, strong and gravitational interactions.
Nuclear Physics A, **872**, pp. 286–295 (2011).
doi:10.1016/j.nuclphysa.2011.09.005.

RUFFINI, R., FRASCHETTI, F., VITAGLIANO, L. AND XUE, S.S.
Observational Signatures of AN Electromagnetic Overcritical Gravitational Collapse.
International Journal of Modern Physics D, **14**, pp. 131–141 (2005).

RUFFINI, R., ROTONDO, M. AND XUE, S.S.
Electrodynamics for Nuclear Matter in Bulk.
International Journal of Modern Physics D, **16**, pp. 1–9 (2007a).

RUFFINI, R., SALMONSON, J.D., WILSON, J.R. AND XUE, S.S.
On the pair electromagnetic pulse of a black hole with electromagnetic structure.
A&A , **350**, pp. 334–343 (1999).

RUFFINI, R., SALMONSON, J.D., WILSON, J.R. AND XUE, S.S.
On the pair-electromagnetic pulse from an electromagnetic black hole surrounded by a baryonic remnant.
A&A , **359**, pp. 855–864 (2000).

RUFFINI, R., VERESHCHAGIN, G. AND XUE, S.S.
Electron–positron pairs in physics and astrophysics: From heavy nuclei to black holes.
Phys. Rep., **487(1)**, pp. 1–140 (2010).

RUFFINI, R., VERESHCHAGIN, G. AND XUE, S.
Electron-positron pairs in physics and astrophysics: From heavy nuclei to black holes.
Phys. Rep. , **487**, pp. 1–140 (2010).
doi:10.1016/j.physrep.2009.10.004.

RUFFINI, R., VERESHCHAGIN, G.V. AND XUE, S.S.
Vacuum polarization and plasma oscillations.
Phys. Lett. A, **371**, pp. 399–405 (2007b).

RUFFINI, R., VERESHCHAGIN, G. AND XUE, S.S.
The breit-wheeler cutoff in high-energy γ-rays.
to be published (2008).

RUFFINI, R. AND VITAGLIANO, L.
Irreducible mass and energetics of an electromagnetic black hole.
Physics Letters B, **545**, pp. 233–237 (2002).

RUFFINI, R. AND VITAGLIANO, L.
Irreducible mass and energetics of an electromagnetic black hole.
Phys. Lett. B, **545**, pp. 233–237 (2002).

RUFFINI, R. AND VITAGLIANO, L.
Energy Extraction from Gravitational Collapse to Static Black Holes.
International Journal of Modern Physics D, **12**, pp. 121–127 (2003).

RUFFINI, R., VITAGLIANO, L. AND XUE, S.S.
On a separatrix in the gravitational collapse to an overcritical electromagnetic black hole.
Physics Letters B, **573**, pp. 33–38 (2003a).

RUFFINI, R., VITAGLIANO, L. AND XUE, S.S.
On plasma oscillations in strong electric fields.
Phys. Lett. B, **559**, pp. 12–19 (2003b).

RUFFINI, R. AND XUE, S.
Effective lagrangian of quantum electrodynamics.
J. of Korean Phys. Soc. , **49**, p. 715 (2006).

RUFFINI, R. AND XUE, S.S.
Effective Lagrangian of QED.
J. Korean Phys. Soc., **49**, pp. S715–S721 (2006).

RUFFINI, R. AND XUE, S.S.
Dyadosphere formed in gravitational collapse.
In *American Institute of Physics Conference Series*, volume 1059 of *American Institute of Physics Conference Series*, pp. 72–100 (2008a).

RUFFINI, R. AND XUE, S.S.
Effective Dyadosphere.
In Y.F. Huang, Z.G. Dai and B. Zhang (eds.), *American Institute of Physics Conference Series*, volume 1065 of *American Institute of Physics Conference Series*, pp. 289–293 (2008b).

SAUTER, F.
Über das Verhalten eines Elektrons im homogenen elektrischen Feld nach der relativistischen Theorie Diracs.
Zeitschrift fur Physik, **69**, pp. 742–764 (1931).

SAUTER, F.
Über das verhalten eines elektrons im homogenen elektrischen feld nach der relativistischen theorie diracs.
Z. Phys., **69(11-12)**, pp. 742–764 (1931).

SAUTER, F.
Zum "Kleinschen Paradoxon".

Zeitschrift fur Physik, **73**, pp. 547–+ (1931).

SCHUBERT, C.
Perturbative quantum field theory in the string-inspired formalism.
Phys. Rep. , **355**, pp. 73–234 (2001).

SCHUBERT, C.
Perturbative quantum field theory in the string-inspired formalism.
Phys. Rep., **355(2)**, pp. 73–234 (2001).

SCHÜTZHOLD, R., GIES, H. AND DUNNE, G.
Dynamically assisted schwinger mechanism.
Phys. Rev. Lett., **101(13)**, p. 130404 (2008).

SCHWINGER, J.
Quantum Electrodynamics. I. A Covariant Formulation.
Physical Review, **74**, pp. 1439–1461 (1948).

SCHWINGER, J.
Quantum Electrodynamics. II. Vacuum Polarization and Self-Energy.
Physical Review, **75**, pp. 651–679 (1949a).

SCHWINGER, J.
Quantum Electrodynamics. III. The Electromagnetic Properties of the Electron-Radiative Corrections to Scattering.
Physical Review, **76**, pp. 790–817 (1949b).

SCHWINGER, J.
On Gauge Invariance and Vacuum Polarization.
Physical Review, **82**, pp. 664–679 (1951).

SCHWINGER, J.
On gauge invariance and vacuum polarization.
Phys. Rev., **82(5)**, p. 664 (1951).

SCHWINGER, J.
The Theory of Quantized Fields. V.
Physical Review, **93**, pp. 615–628 (1954a).

SCHWINGER, J.
The Theory of Quantized Fields. VI.
Physical Review, **94**, pp. 1362–1384 (1954b).

SCHWINGER, J.
The theory of quantized fields. v.
Phys. Rev., **93(3)**, p. 615 (1954a).

SCHWINGER, J.
The theory of quantized fields. vi.
Phys. Rev., **94(5)**, p. 1362 (1954b).

SHORE, G.M.
faster than light photons in gravitational fields - causality, anomalies and horizons.
Nucl. Phys. B, **460**, pp. 379–394 (1996).

SOLENG, H.H.
Charged black points in general relativity coupled to the logarithmic u(1) gauge theory.
Phys. Rev. D, **52**, pp. 6178–6181 (1995).

STECKER, F.W., DE JAGER, O.C. AND SALAMON, M.H.
TeV gamma rays from 3C 279 - A possible probe of origin and intergalactic infrared radiation fields.
ApJ , **390**, pp. L49–L52 (1992).

STECKER, F.W., MALKAN, M.A. AND SCULLY, S.T.
Intergalactic Photon Spectra from the Far-IR to the UV Lyman Limit for 0 ¡ z ¡ 6 and the Optical Depth of the Universe to High-Energy Gamma Rays.
ApJ , **648**, pp. 774–783 (2006).

STECKER, F.W., PUGET, J.L. AND FAZIO, G.G.
The cosmic far-infrared background at high galactic latitudes.
ApJ , **214**, pp. L51–L55 (1977).

STUECKELBERG, E.C.G. AND PETERMANN, A.
La renormalisation des constantes dans la theorie de quanta (normalization of the constants in the theory of quanta).
Helvetica Physica Acta (Switzerland), **26**, p. 499 (1953).

SUSLOV, I.M.
Gell-Mann-Low function in QED.
JETP Lett., **74**, pp. 191–195 (2001).
doi:10.1134/1.1413543.

TAJIMA, T. AND MOUROU, G.
Zettawatt-exawatt lasers and their applications in ultrastrong-field physics.
Phys. Rev. ST Accelerators and Beams, **5(3)**, pp. 031301–+ (2002).

TOMONAGA, S.
On a Relativistically Invariant Formulation of the Quantum Theory of Wave Fields.
Progress of Theoretical Physics, **1**, pp. 27–42 (1946).

TREMAINE, A., WANG, X.J., BABZIEN, M., BEN-ZVI, I., CORNACCHIA, M., NUHN, H.D., MALONE, R., MUROKH, A., PELLEGRINI, C., REICHE, S. ET AL.
Experimental Characterization of Nonlinear Harmonic Radiation from a Visible Self-Amplified Spontaneous Emission Free-Electron Laser at Saturation.
Physical Review Letters, **88(20)**, pp. 204801–+ (2002).

TSEYTLIN, A.A.
On non-abelian generalisation of the born-infeld action in string theory.
Nucl. Phys. B, **501**, pp. 41–52 (1997).

USOV, V.V.
Bare Quark Matter Surfaces of Strange Stars and e^+e^- Emission.
Phys. Rev. Lett. , **80**, pp. 230–233 (1998).

USOV, V.V., HARKO, T. AND CHENG, K.S.
Structure of the Electrospheres of Bare Strange Stars.
ApJ , **620**, pp. 915–921 (2005).
doi:10.1086/427074.

VALLURI, S.R., LAMM, D.R. AND MIELNICZUK, W.J.
Applications of the representation of the heisenberg-euler lagrangian by means of special functions.
Can. J. Phys., **71(7-8)**, pp. 389–397 (1993).

VANYASHIN, V.S. AND TERENT'EV, M.V.
The Vacuum Polarization of a Charged Vector Field.
Soviet Journal of Experimental and Theoretical Physics, **21**, pp. 375–+ (1965).

VASSILIEV, V.V.
Extragalactic background light absorption signal in the TeV gamma-ray spectra of blazars.
Astroparticle Physics, **12**, pp. 217–238 (2000).

WEINBERG, S.
Gravitation and Cosmology: Principles and Applications of the General Theory of Relativity (Gravitation and Cosmology: Principles and Applications of the General Theory of Relativity, by Steven Weinberg, pp. 688. ISBN 0-471-92567-5. Wiley-VCH , July 1972., 1972).

WEISSKOPF, V.
Über die elektrodynamik des vakuums auf grund der quantentheorie des elektrons.
Kongelige Danske Videnskabernes Selskab. Math.-fys. Meedelelser, **14**, p. 6 (1936).

WILTSHIRE, D.L.
Black holes in string-generated gravity models.
Phys. Rev. D, **38**, pp. 2445–2456 (1998).

YAJIMA, H. AND TAMAKI, T.
Black hole solutions in euler-heisenberg theory.
Phys. Rev. D, **63**, p. 064007 (2001).

ZELDOVICH, Y.B. AND POPOV, V.S.
Electronic Structure of Superheavy Atoms.
Soviet Physics Uspekhi, **14**, pp. 673–+ (1971).